Narrow Vertical Mortar Connections for Precast Concrete Shear Walls

van Keulen, D.C.

Important note
To cite this publication, please use the final published version (if applicable).
Please check the document version above.

Narrow Vertical Mortar Connections for Precast Concrete Shear Walls

D.C. van Keulen

September 2023

Narrow Vertical Mortar Connections
for Precast Concrete Shear Walls

Dissertation

for the purpose of obtaining the degree of doctor
at Delft University of Technology
by the authority of the Rector Magnificus, Prof.dr.ir. T.H.J.J. van der Hagen,
chair of the Board of Doctorates

to be defended publicly
on
Wednesday 13 September 2023 at 5:30 pm

by

Dirk Christiaan VAN KEULEN

Master of Science in Architecture, Building and Planning, Eindhoven University of
Technology, The Netherlands
born in Vlaardingen, The Netherlands

This dissertation has been approved by the promotors.

Composition of the doctoral committee:
  Rector Magnificus,   chairperson
  Prof.dr.ir. M.A.N. Hendriks   Delft University of Technology, promotor
  Dr.ir. D.A. Hordijk   Delft University of Technology, promotor

Independent members:
  Prof.dr. L.C. Hoang   Technical University of Denmark
  Dr.ir. W. Jansze MBA   Consolis VBI
  Prof.dr.ir. P.C. Louter   Delft University of Technology
  Prof.dr. M. Overend   Delft University of Technology
  Em.prof.dipl.-ing. J.N.J.A. Vamberský   (formerly) Delft University of Technology

Reserve member:
  Prof.dr.ir. J.G. Rots   Delft University of Technology

Summary

The thixotropic properties of contemporary mortars allow the insertion of mortar in small vertical seams by using a mortar pump without the need for traditional formwork. In such a seam, a vertical mortar connection for the transfer of shear forces can be created by simply adding a profile to the mortar-to-concrete interfaces. In this way a constructible continious vertical shear connection can be constructed between storey-high precast concrete wall elements. Due to the absence of horizontal reinforcement like hairpins distributed over the height of the wall elements, the resistance against lateral dilation has to be taken by the concentrated tying reinforcement in the slabs. One of the things missing is an evaluation of the shear stiffness and the shear capacity of such a vertical connection. Therefore, the main objective of this research is to develop and model vertical mortar connections that perform optimally for the transfer of shear forces in precast concrete stability structures with tying reinforcement in the slabs. They should preferably transfer considerable shear forces in a reliable way and should behave with high shear stiffnesses. At the same time, the connections should preferably cause low dilation forces and should take full advantage of the lateral stiffnesses.

The co-called "Shear key" is a known profile for a shear connection with intermediate joint concrete or mortar. The Aligned shear key connection (with the indentations at both sides opposite to each other) is the most investigated and applied version. Structural information on the functioning of this connection is widely available. However, the earlier investigated connections have rather wide seams, are mostly filled with concrete instead of mortar and are applied with horizontal reinforcement like hair pins. Little information is found for profiled shear connections with narrow seams of around 25 mm wide, filled with contemporary mortar and without lateral reinforcement distributed over the height of the wall.

In this thesis work five different profiled or roughened interfaces are investigated for the transfer of shear forces. With these (profiled) interfaces, five different vertical mortar connections are created. The **Aligned shear key connection** is usually applied and therefore taken for examination. The **Staggered shear key connection** has shifted shear keys. This variant has a slightly steeper diagonal mortar bar and therefore possibly the potential to transfer even better the shear forces. The **Aligned small shear key connection** is proposed for researching the effect of more shear keys over the same height. To investigate the effect of roughened waterjetted interfaces in an

application with mortar instead of concrete, the **Plain waterjetted shear connection** is selected for examination. Finally, the **Serrated waterjetted shear connection** is selected because a combination of a rough waterjetted interface and a serration as a profile could provide a high shear capacity and significant shear stiffness.

As part of the research program, a contemporary pumpable type of mortar is selected as joint material. Alternatively, improved structural behaviour of the connection could be expected from a Steel Fibre Reinforced Mortar (SFRM). Both types of mortar are taken as joint material in the research program for investigation.

The profiled mortar connections are constructed in push-off type of specimens for performing shear test. The connections have a height of 600 mm. The horizontal and vertical forces and displacements are registered in each load step. To investigate the lateral interaction with the surrounding precast concrete structure, the lateral stiffness and the size of lateral compression are varied.

In the thesis all experimental results are presented and discussed, while the shear behaviour of the Staggered shear key connection is analysed in detail. The principal stages through which it goes during the shear test are explained. The debonding, the arise of diagonal cracks and the appearance of the failure crack are discussed. A diagonal resultant force inside the mortar filling is identified. It was found to be decisive for the functioning of this connection and is modeled with the help of a diagonal bar model. The test results are compared with the numerical results from a finite element model simulation. An analysis of both results explains the operation of the resultant diagonal force inside the Staggered shear key connection.

The shear behaviour of the five mortar connections are mutually compared and assessed on their performance for functioning as a vertical mortar connection. It shows that the Aligned and Staggered shear key connection and the Serrated waterjetted connection provide comparable **secant shear stiffnesses** which makes them equally usable. Also, the comparison reveals that the Staggered shear key connection and the Serrated waterjetted shear connection transfer the highest **ultimate shear forces**. The latter only does so under the condition that the failure crack runs through the mortar. This cannot be guaranteed which makes the Staggered shear key connection the best performing vertical mortar connection. It behaves with a significant high secant shear stiffness and provides the highest reproducable ultimate shear capacity with the least dependency on the lateral stiffness and lateral compression. It is determined that this performance is attributable to the diagonal resultant force that develops steeper inside the mortar filling of this connection than in the mortar filling of the other profiled connections.

Tiksomortar K70 as well as SFRM are applied as mortar filling in the connections. There is no significant positive effect of applying steel fibres in the mortar observed for the shear capacity and the shear stiffness of the Staggered shear key connection. Since pumping SFRM also requires additional handling and has some risks in execution, the Tiksomortar K70 appears to be preferrable for the mortar.

A diagonal bar model is proposed for simulating the behaviour of the diagonal resultant force of the Staggered shear key connection. By constructing the bars between two wall elements, a modeling method for the representation of this connec-

tion in a precast concrete structure is created. It is called the "**inclined compression strut model**" and its functioning is proven to be suitable via calibration on the shear test results. The compression forces that arise in the inclined truss elements must not exceed the values that represent the **shear capacity** of the Staggered shear key connection. The analysis of the shear tests results shows that the shear capacity depends on the occurring lateral displacements $\delta_{lateral}$. An equation for predicting the shear capacity including this lateral dependency is proposed.

The inclined compression strut model is developed based on the three-keyed Staggered shear key connection. Horizontal cracks in the mortar between the diagonal mortar bars show that the Staggered shear key connection can be considered as a set of individually functioning inclined compression struts. This means it does not matter how many struts are applied in a row. So, the inclined compression strut model and the equation for prediction of the shear capacity can be used for a storey-high application of the Staggered shear key connection.

The case studies show that the **storey-high Staggered shear key connection** functions excellently when applied in cantilever shear walls in versions with and without window openings. They demonstrate that for such commonly applied real precast concrete structures there are negligibly small differences in the force distributions in the precast concrete wall elements and displacements at the top compared to the monolitic concrete version of the same structure. The lateral displacements at the top only increase slightly in exceptional cases of cantilever shear wall designs and lateral loads. The shear capacities prove to be more than sufficient and the force distributions hardly changed.

Samenvatting

Door de thixotrope eigenschappen van hedendaagse mortels is het mogelijk smalle verticale voegen te vullen met behulp van een mortelpomp zonder dat daar een traditionele bekisting voor nodig is. In een dergelijke voeg kan eenvoudig een afschuifverbinding worden gecreëerd door een profilering in de aansluitvlakken tussen de mortel en het prefab beton aan te brengen. Op deze manier ontstaat een bouwbare continue verticale afschuifverbinding tussen verdiepingshoge prefab betonnen wandelementen. Door de afwezigheid van horizontale wapening zoals bijvoorbeeld haarspelden verdeeld over de hoogte van de wandelementen, moet de weerstand tegen zijdelings wijken worden geleverd door de trekbandwapening ter plaatse van de vloeren. Een van de zaken die ontbreekt is een beoordeling van de afschuifstijfheid en de afschuifcapaciteit van een dergelijke verticale afschuifverbinding. Het hoofddoel van dit onderzoek is dan ook het ontwikkelen en modelleren van mortelverbindingen, die optimaal presteren bij het overdragen van afschuifkrachten in geprefabriceerde betonnen wandschijven met trekbandwapening in the vloeren. Zij moeten bij voorkeur aanzienlijke afschuifkrachten kunnen doorgeven en een hoge afschuifstijfheid hebben. Tegelijkertijd moeten de verbindingen bij voorkeur lage wijkende krachten veroorzaken en de zijdelingse stijfheid die daar weerstand aan biedt, optimaal benutten.

De zogenaamde "Shear key" is een bekende profilering voor een afschuifverbinding met een verticale voeg die is gevuld met beton of mortel. De Aligned shear key connection (met de inkepingen aan beide zijden tegenover elkaar) is de meest onderzochte en toegepaste variant. Informatie over de wijze waarop deze verbinding constructief functioneert, is ruim voor handen. De eerder onderzochte verbindingen hebben echter vrij brede naden, zijn meestal gevuld met beton in plaats van mortel en zijn voorzien van horizontale wapening zoals bijvoorbeeld "haarspelden". Er is weinig informatie gevonden over geprofileerde afschuifverbindingen met smalle voegen van circa 25 mm breedte, gevuld met hedendaagse mortel en zonder over de hoogte van de wandelementen verdeelde horizontale wapening. In dit promotieonderzoek zijn vijf verschillende, geprofileerde of opgeruwde, aansluitvlakken onderzocht op de overdracht van schuifkrachten. Met deze (geprofileerde) aansluitvlakken zijn vijf verschillende verticale mortelverbindingen samengesteld. De **Aligned shear key connection** wordt meestal toegepast en is daarom geselecteerd voor het onderzoek. De **Staggered shear key connection** heeft verschoven inkepin-

gen. Deze variant heeft een iets steilere diagonale drukstaaf in de mortelvulling en daardoor mogelijk de potentie om de dwarskrachten nog beter over te dragen. De **Aligned small shear key connection** is voorgesteld om het effect van meer shear keys over dezelfde hoogte te onderzoeken. Om het effect van opgeruwde aansluitvlakken in een toepassing met mortel in plaats van beton te onderzoeken is de **Plain waterjetted shear connection** onderzocht. Ten slotte is gekozen voor de **Serrated waterjetted shear connection** omdat een combinatie van een ruw aansluitvlak en een profilering een hoge afschuifcapaciteit en een aanzienlijke afschuifstijfheid zou kunnen opleveren.

Voor het onderzoek is voor de vulling van de voegen een hedendaagse verpompbare thixotrope mortel gekozen. Een verbeterd constructief gedrag van de verbinding zou kunnen worden verwacht met een staalvezel versterkte mortel, de zogenaamde Steel Fibre Reinforced Mortar (SFRM). Beide mortelsoorten zijn in het onderzoek als voegvulling toegepast.

Voor het uitvoeren van afschuifproeven zijn de geprofileerde mortelverbindingen aangebracht in proefstukken van het type "Push-off specimen". De verbindingen hebben een hoogte van 600 mm. Na iedere belastingstap zijn de horizontale en verticale krachten en verplaatsingen geregistreerd. De zijdelingse stijfheid en voordruk zijn gevarieerd om de interactie met de prefab betonconstructie te onderzoeken.

In het proefschrift zijn alle experimentele resultaten gepresenteerd en besproken. Het afschuifgedrag van de Staggered shear key connection is in detail geanalyseerd. De belangrijkste stadia die het tijdens de afschuifproef doorloopt, zijn toegelicht. Het onthechten, het optreden van diagonale scheuren en het ontstaan van de bezwijkscheur zijn besproken. Een resulterende diagonale kracht in de mortelvulling is geïdentificeerd. Deze blijkt bepalend te zijn voor het functioneren van de verbinding en is gemodelleerd met behulp van een diagonaal staafmodel. De proefresultaten zijn vergeleken met de numerieke resultaten van een simulatie met een eindige elementen model. Een analyse van beide resultaten verklaart de werking van de resulterende diagonale kracht in de Staggered shear key connection.

Het afschuifgedrag van de vijf mortelverbindingen is onderling vergeleken en beoordeeld op hun functioneren als verticale mortelverbinding. Het laat zien dat de Aligned en Staggered shear key connection en de Serrated waterjetted shear connection vergelijkbare **secant afschuifstijfheden** hebben, waardoor ze even bruikbaar zijn. Ook blijkt uit de vergelijking dat de Staggered shear key connection en de Serrated waterjetted shear connection de hoogste afschuifkrachten overdragen. De laatste doet dat alleen onder de voorwaarde dat de bezwijkscheur door de mortel loopt. Dit kan niet worden gegarandeerd waardoor de Staggered shear key connection de best presterende verticale mortelverbinding is. Deze verbinding gedraagt zich met een significant hoge secant afschuifstijfheid en biedt de hoogst reproduceerbare afschuifcapaciteit met de minste afhankelijkheid van de zijdelingse stijfheid en zijdelingse drukvoorspanning. Vastgesteld is dat dit is toe te schrijven aan de resulterende diagonale kracht die zich in de mortelvulling van deze verbinding steiler ontwikkelt dan in de mortelvulling van de andere geprofileerde verbindingen.

Zowel de Tiksomortar K70 als de SFRM zijn als mortel toegepast in de verbindingen. Er is geen significant positief effect van het toevoegen van staalvezels in de mortel op de afschuifcapaciteit en de afschuifstijfheid van de Staggered shear key connection waargenomen. Aangezien het pompen van SFRM ook extra handelingen vergt en enkele risico's bij de uitvoering kent, lijkt het gebruiken van Tiksomortar K70 de voorkeur te hebben.

Een schuin staafmodel is voorgesteld voor het simuleren van het gedrag van de resulterende diagonale kracht in de Staggered shear key connection. Door drukstaven tussen twee wandelementen te construeren, ontstaat een modelleringsmethode om deze verbinding in een prefab betonconstructie te representeren. Dit wordt het "**inclined compression strut model**" genoemd en de werking ervan is met behulp van een kalibratie met de proefresultaten geschikt gebleken. De drukkrachten die ontstaan in de schuine staafelementen mogen niet groter zijn dan de afschuifcapaciteit van de Staggered shear key connection. De analyse van de proefresultaten heeft laten zien dat de afschuifcapaciteit afhankelijk is van de zijdelingse vervormingen $\delta_{lateral}$. Een vergelijking voor het voorspellen van de afschuifcapaciteit, inclusief de afhankelijk van de zijdelingse vervorming is voorgesteld.

Het schuine drukstaafmodel is ontwikkeld op basis van de Staggered shear key connection met drie diagonale mortelstaven. Horizontale scheuren in de mortel tussen de mortelstaven laten zien dat de Staggered shear key connection kan worden beschouwd als een samenstel van individueel functionerende schuine drukstaven. Hierdoor maakt het niet uit hoeveel mortelstaven boven elkaar worden toegepast. Als gevolg hiervan kan het schuine drukstaafmodel en de formule voor het voorspellen van de afschuifcapaciteit, worden gebruikt voor een verdiepingshoge toepassing van de Staggered shear key connection.

Met casestudies is laten zien dat de verdiepingshoge Staggered shear key connection uitstekend functioneert in verschillende in de fundering ingeklemde wandconstructies, in uitvoeringen met en zonder raamopeningen. Ze tonen dat voor dergelijke, veel toegepaste, prefab betonnen wandconstructies er verwaarloosbaar kleine verschillen zijn in de krachtverdelingen in geprefabriceerde wandconstructies en de horizontale verplaatsingen aan de top, in vergelijking met de monolithische betonnen variant. Slechts in uitzonderlijke gevallen nemen de horizontale verplaatsingen aan de top gering toe. De afschuifcapaciteit van de verbinding blijkt ruim voldoende en de interne krachtsverdelingen veranderen nauwelijks.

Preface

This thesis describes my PhD research into the shear behaviour of storey-high "narrow vertical mortar connections". Contrary to all other known connections, this connection has no horizontal reinforcement or other connecting means for joining precast concrete wall elements in the vertical seams. This challenges many structural engineers that are accustomed to immediate balancing of the lateral dilation forces, that arise with such a profiled shear connection, by using connectors. They feel compelled to apply for example horizontal hairpins in cast-in-place concrete interspaces. This thesis proves that it is quite possible to balance the sum of the lateral dilation forces only with concentrated tying reinforcement in the slabs. I greatly encourage structural engineers to consider the proposed mortar connection, which is friendly for precast concrete construction and patent free.

Conducting this PhD research has enriched me as an active structural engineer in the construction practice enormously. It was useful to observe the differences between conducting in-depth scientific research on one subject area and applying the more basic structural knowledge on the many structural subjects in engineering practice. Also, the insights that I gained from working with the promotors, colleagues and students from TU Delft are very valuable. They shaped my views on conducting research. The third enrichment that I want to mention is the possibility of collecting knowledge about the design and construction of precast concrete high-rise buildings in the margins of this PhD research. It was significant to co-write the state-of-the-art report *"fib* bulletin 101 Precast Concrete in Tall Buildings" and to have given some invited lectures on this subject during conferences and seminars.

Performing this PhD research was quite a challenge. I could not work full-time on this. I had to combine it with leading my engineering firm Ingenieursstudio DCK with ever larger projects and an increasing amount of staff that demanded the necesary commitment from me. I also regularly prioritized spending time with my family. So there where even periods that I could not work on it at all because I could not give it top priority. This is the reason why it took a little over 10 years for conducting the research and to complete this PhD thesis. However, it was a fascinating journey. I am happy and thankful that I was able to complete this job.

First of all, I would like to express my gratitude to my promoter, Dr. Dick Hordijk, who was the professor of concrete structures until March 2019. You enthusiastically welcomed me to your section concrete structures. I was very privileged that you de-

cided to remain my promotor after leaving TU Delft. I would describe your approach as always being sharp on the content and polite on the person. Your contributions have greatly helped me in conducting the research and in compiling this thesis. I thank you very much for your outstanding way of guiding. I was also privileged that Prof. Max Hendriks, the successor of Dr. Dick Hordijk, was willing to become my promotor. When you joined, you very quickly read up and came with many valuable recommendations. You took on the role as corresponding promotor as well. To avoid confusion for you on our equal first names, we had to define "Dick H" and "Dick vK" in our correspondences. I would like to thank you for the very pleasant cooperation and your meaningful contributions to the thesis.

At the time, I started my PhD research with Prof. Jan Vamberský. We discussed the intention to conduct an academic investigation on the precast concrete subject that I proposed. You offered to create an external part-time PhD position. When you became an emeritus professor, you had to pass on the promotorship. I am glad that you participate as a member of the doctoral committee. I would like to thank you and also the other researchers Dr. Roel Schipper, Dr. Karel Terwel and Sander Pasterkamp of the section Building Structures for their support and hospitality during the first stage of my PhD research.

A group of precast concrete companies became involved in the first stage of the PhD research. The representatives of these companies shared their valuable opinions. The five mortar connections were developed and tested in consultation with them. These companies were also prepared to make a significant financial contribution. It was not possible to conduct this research without the support of Rob Huijben (Hurks Delphi Engineering), Dr. Wim Jansze (Consolis), Toine Leijten (Cugla), Willem Welling (AB-FAB), Peter Wismans (Geelen Beton) and Marc van Zeijl (Bestcon). I would like to thank you all for your significant contributions.

Thirty-three shear tests were performed in the Structures laboratory of Eindhoven University of Technology. Special thanks go to the lab technicians Eric Wijen and Theo van der Loo for providing their expertise and support.

I spent a lot of time on working on this PhD research during the office times of Ingenieursstudio DCK. It sometimes reduced my availability for supervising my employees working on the projects or for coaching on their personal matters. I would like to thank the entire team of DCK for letting me do this research and taking responsibilities that I should have taken.

I would like to give my greatest gratitude to my family, Anneke, Joris and Nathan. You were affected the most by the everlasting necessity to work on my PhD research. I want to thank you very much for your endless and unconditional love, support and patience.

Dick van Keulen
July 26, 2023
Barendrecht, The Netherlands

Contents

Chapter 1

Introduction

1.1 Background

Reinforced concrete is the most used building material. This is also true for load-bearing stability structures of buildings, which is the topic of this thesis. Whereas in the past concrete and reinforcement were generally brought together at construction sites, nowadays, contractors increasingly use prefabricated concrete elements. These precast concrete elements are constructed in the concrete factory, transported across public roads and finally assembled at the construction site.

Precast concrete wall elements for load-bearing stability structures are stacked according to a pre-selected element lay-out. Figure 1.1 shows examples of such lay-outs for cantilever shear walls. Connections are used for acquiring structural co-operation between the individual wall elements. Precast concrete structures with connections behave structurally weaker than monolithic structures (without connections). Connections interrupt continuous concrete and reinforcement. They interfere with the transfer of internal forces throughout the structure and are structurally considered behaving with lower stiffness and lower capacity. To avoid a decrease in stiffness and capacity, load-bearing stability structures are preferably constructed with cast-in-situ concrete. However, despite this, concrete stability structures are increasingly constructed with precast concrete wall elements since their use can have important advantages in the construction processes at construction sites.

Horizontal and vertical linear interspaces are unavoidably present between the individual precast concrete elements. These interspaces are defined as "seams" in this thesis. Seams are essential for covering inaccuracies due to factory production and installation of the precast concrete elements on site. They are sometimes filled with non-structural building material. Seams filled with structural material can function as a precast concrete connection. Figure 1.2 shows the most used horizontal mortar connection. It is usually applied to the horizontal seams in the shear wall structures of figure 1.1. The mortar is able to transfer vertical compressive forces from the element above to the one below. Also, horizontal mortar connections can
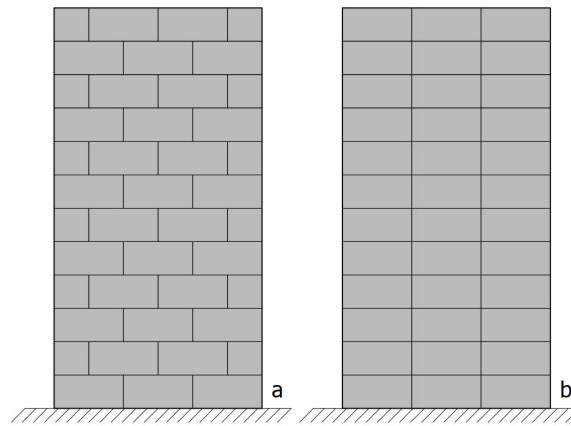
Figure 1.1: Cantilever shear wall structures; Element lay-outs with (a) and without (b) interlocking precast concrete wall elements

be reinforced with vertical projecting bars in grouted sleeves for transferring vertical tensile forces. Horizontal shear forces from the upper precast concrete element will be transferred via the mortar and reinforcement to the lower precast concrete element. This horizontal mortar connection has proven itself as the most suitable and has no serious competitors.
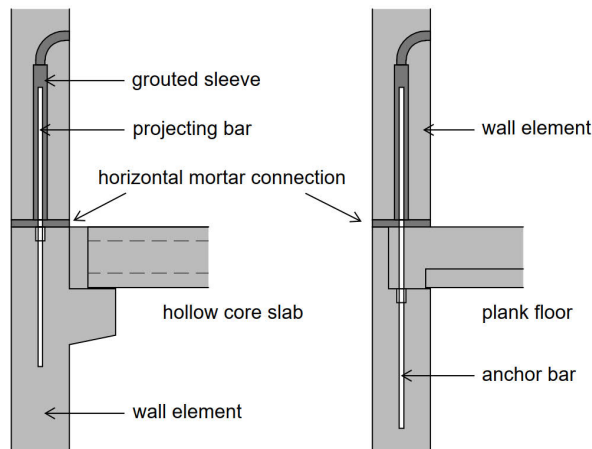
Figure 1.2: Traditional horizontal mortar connection

The shear walls in figure 1.1 have vertical seams as well. The vertical seams in shear wall 1.1a can be left open since the interlocking of elements are mostly able to provide sufficient cooperation between the precast concrete elements. If not, connections in the vertical seam can be applied to obtain more structural cooperation.

The shear wall of figure 1.1b requires so-called "vertical connections" in the vertical seams to obtain structural cooperation between the three vertical wall element stacks. A preferable structural composition can be obtained with the shear wall of figure 1.1b with simple vertical connections. The advantage is that less and less different types of precast concrete elements form the same concrete structure. It reduces the amount of moulds and handling in the concrete factory. Moreover, the precast concrete structure can be constructed with less handling during installation on site.

The role of vertical connections in the force distribution of horizontally loaded cantilever shear walls is illustrated in figure 1.3a. Their main task is to transfer shear forces (vertical arrows) from one precast concrete wall element to the adjacent one. Vertical connections possess a shear capacity and behave with a shear stiffness (k). Shear stiffness k=∞ represents an infinitely stiff shear connection. Customary connections do not behave with an infinite shear stiffness in shear wall structures. Shear stiffness k=∞ represents a fictitious shear connection in a monolithic concrete shear wall structure. This structure deforms according to the dotted line in figure 1.3a.

Vertical connections behave with a finite shear stiffness (0<k<∞). As a result, the precast concrete cantilever shear wall deforms horizontally more than the monolithic concrete version. Figure 1.3b shows the typical deformed shape of a shear wall with vertical connections. Furthermore, a cantilever shear wall without vertical connections (k=0) behaves similarly to three individual shear walls clamped into the foundation according to figure 1.3c. The ability to transfer shear forces is absent in the open seam and this shear wall deforms the most. Vertical connections with a finite shear stiffness (0<k<∞) possess a restricted shear capacity; the shear forces in the shear wall structure must not exceed the shear capacity of the vertical connection.
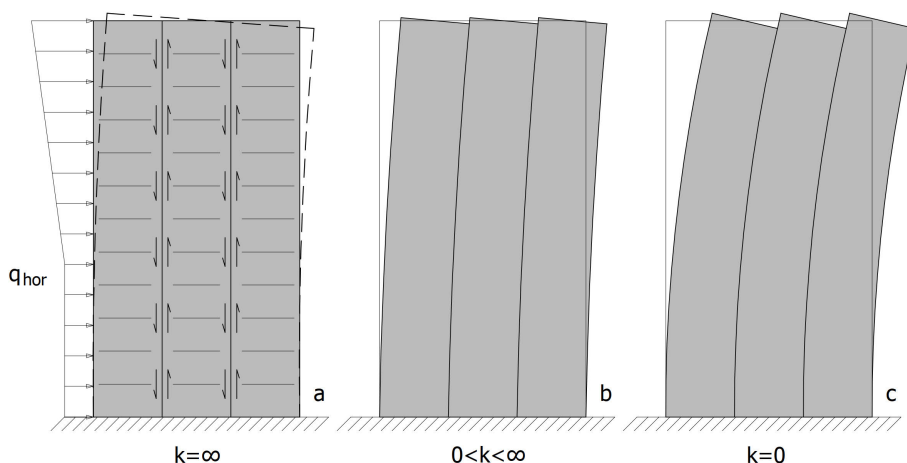
Figure 1.3: Shear wall structure with vertical connections (k = shear stiffness); Transfer of shear forces and monolithic deformation (a), typical deformed shape due to vertical connections (b) and deformed shape without vertical connections (c)

A frequently applied vertical connection is the "cast-in-place loop connection" as displayed in figure 1.4a. Horizontal protruding reinforcement combined with vertical reinforcement connect both precast concrete elements in the vertical cast-in-place joint concrete. It is a so-called "continuous" type of connection which means that the shear forces can be transferred along the entire height of the wall. Profiled interfaces (shear keys) between the joint concrete and the precast concrete elements can be applied to increase the shear capacity of this connection (see figure 1.4b).

A "welded connection" is drawn in figure 1.4c. An assembly of a steel plate with welded reinforcement is cast in the precast concrete element during production in the concrete factory. On site, a steel stitch plate is welded on the embedded steel plates and the precast concrete elements are connected. It is a so-called "discrete" connection since forces can be transferred only locally via the steel plates.

Interlocking corbels (see figure 1.4d) are used as discrete connection in precast concrete structures with low shear forces to be transferred. The horizontal mortar fillings between the elements are reinforced with protruding bars. They are able to connect both precast elements half way up the wall and just below each floor. There, the shear forces can be transferred from one to the other precast concrete element. Alternatives based on this principle exist. The corbels can be lower in such a way that they can be hidden above the ceiling. The alternative of "interlocking per storey" is frequently used as well. It possesses less connectivety but it provides an invisible solution for interlocking.
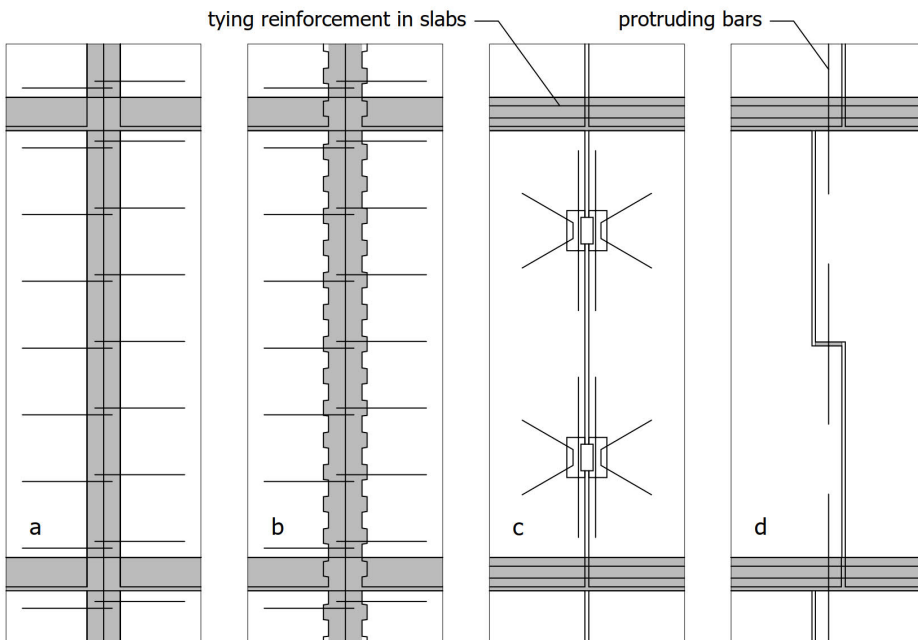
Figure 1.4: Vertical connections; Cast-in-place loop connections (a)+(b), welded connection (c), interlocking corbel (d)

1.2   Scope

Precast concrete construction should be the assembly of precast concrete elements without laborious cast-in-situ construction works. To achieve this, easy to install connections should be selected. A disadvantage of traditional cast-in-situ joints (figures 1.4a and 1.4b) is that laborious formwork, supplementary reinforcement and traditional casting are required on site. Construction of the connections displayed in the figures 1.4c and 1.4d are less laborious and therefore fit better in this assembly approach. However, they are discrete connections and behave with a substantial lower shear stiffness than continuous connections.

Nowadays, new types of mortar are available that make that continuous "narrow vertical mortar connections" can be constructed without using traditional formwork. The mortar can be inserted in the vertical seam with a hose. A mortar pump presses the plastic mortar through the hose into the vertical seam. The plastic mortar has sufficient stiffness to remain in place after injection (figure 1.5). This way of filling the vertical seams is made possible by the "thixotropic" and "swelling" properties of contemporary plastic mortars. With these thixotropic mortars, a continuous vertical mortar connection for shear transfer can easily be made by adding a profile to the mortar-to-concrete interfaces. One of the things missing is an evaluation of the shear stiffness and the shear capacity of such a vertical mortar connection when applied in precast concrete stability structures. Furthermore, how can the connection properties be optimized by selecting certain mortars and profiled or roughened mortar-to-concrete interfaces.

Figure 1.5: Testing the filling of vertical seams with a mortar pump

At first glance, a connection with two profiled old-to-new concrete interfaces next to each other might represent the behaviour of vertical mortar connections. NEN-EN 1992-1-1 (1992) and *fib* Model Code 2010 (2013) provide equations for approximating the shear strength of such profiled old-to-new concrete interfaces (see figure 1.6a).

These equations are proposed after decades of reseach on shear transfer via different types of old-to-new concrete interfaces. They led to the "Modified Shear Friction" theory by Mattock and Hawkins (1972) which is used for the equation in NEN-EN 1992-1-1 (1992) and the "Extended Shear Friction" theory by Randl (2013) which is included in *fib* Model Code 2010 (2013). However, these equations provide low shear capacities because the profiled old-to-new concrete interfaces must have indentations with a minimum depth of 5 mm (figure 1.6a) while the keyed vertical mortar connections are supposed to have shear keys of around 25 mm deep (figure 1.6b). This size difference makes that the known code equations do not cover the shear capacities of deep keyed interfaces.

Furthermore, a vertical mortar connection is not equal to two profiled interfaces since inclined compression struts in the mortar (figure 1.6b) play an important role in the transfer of shear forces. These struts have to be properly programmed to obtain well functioning profiled shear connections. The functioning of the inclined compression struts is not incorporated in the code equations for old-to-new concrete interfaces.
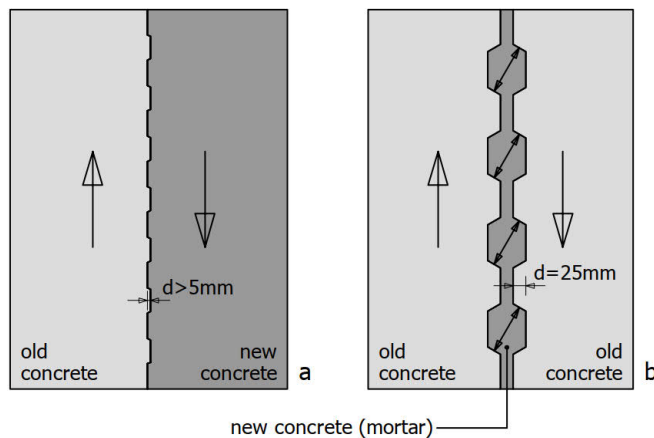
Figure 1.6: Old-to-new concrete interface according to NEN-EN 1992-1-1 (1992) (a) and one of the mortar connections (b) as investigated in this thesis

Research on vertical profiled cast-in-place connections with cement-based intermediate material could be found in literature: Hansen (1967), Bhatt and Nelson (1970), Cholewicki (1971), Fauchart and Cortini (1972), Backler et al. (1973), Hansen and Olesen (1976), Mehlhorn et al. (1977), Eriksson et al. (1978), Abdul-Wahab (1986), Chakrabarti et al. (1988), Abdul-Wahab (1992) and Chatveera and Nimityoungskul (1994). However, the profiled cast-in-place concrete and profiled mortar connections provided in the literature are not the same as vertical mortar connections because of the:

1. Traditional cast-in-place vertical connections are usually equipped with transversal reinforcement whereas there is no space for reinforcement, or other connectors, in the relatively narrow vertical seams of 20-30 mm wide. The absence of reinforcement changes the way of transferring shear forces.

2. Mortar is intended to be applied in smaller volumes than concrete. The reason is that concrete contains coarse aggregates while mortar is composed of smaller grained aggregates (sand). Mortar connections require probably other profiles for being effective.

A research on unreinforced profiled mortar connections was performed by Rizkalla et al. (1989). Six specimens were tested in shear and their behaviour was analysed. The researchers focussed on improving the shear capacity of compressed horizontal mortar connections by adding a profile. The difference between vertical and horizontal connections is that vertical mortar connections are usually not compressed. Also, connections with only one type of profile and with outdated (not thixotropic) mortar were tested. This research is rather limited and does not provide sufficient knownledge about the implementation of vertical profiled mortar connections in precast concrete stability structures.

The knowledge about the structural behaviour of vertical mortar connections is lacking to take full advantage of this innovative way of connecting precast concrete elements in stability structures. In order to achieve the required knowledge, research is needed in which the shear transfer mechanisms, the effect of profiles and the effect of material properties are studied. It is investigated in this thesis how vertical mortar connections can perform optimally in order to obtain the easiest way to install precast concrete connections for shear transfer. Furthermore, how precast concrete stability structures interfere structurally with vertical mortar connections is subject of this research.

1.3 Precast concrete concept

Figure 1.7a shows the way in which profiled (keyed) mortar connections principally transfer shear forces from one element to the adjacent element. Vertical shear forces are accompanied by an inclined compression strut in the mortar. A lateral clamping force is required to restrain horizontal dilation and to acquire local vectorial equilibrium. The local behaviour of one or a few shear keys is considered in this thesis as the research area on "Micro" level. The majority of the reseach performed on keyed connections with joint concrete as intermediate material has been performed at this level. Researchers proposed keyed shear connections and performed shear tests on just a few keys in a row.

The second research area can be defined on "Meso" level as displayed in figure 1.7b. It is a story-high vertical mortar connection between two precast concrete wall elements. The local shear forces to be transferred can possibly differ considerably over the height of the vertical connection. Also, more shear keys are placed in

a row and can possibly influence one another differently than compared to connections with just a few keys. If the test results obtained on Micro level can be taken for the storey-high application on Meso level is investigated. This is defined as an extrapolation step in this thesis work.

The lateral dilation forces displayed in figure 1.7a can be balanced by the surrounding precast concrete structure according to figure 1.7b. The bending resistance of the vertical "columns" in both wall elements and the horizontal tensile resistance of the tying reinforcement in the slab can be used for this purpose. This composition behaves with a non-linear distribution of the lateral stiffnesses over the height of the storey. This stiffness determines the size of the horizontal forces that are available for balancing the lateral dilation forces by the connection. This precast concrete concept is proposed in different precast concrete design books (e.g. *fib* bulletin 74 (2014), Steinle et al. (2019)). It is frequently called the concept of "vertical connections with concentrated tying reinforcement in the slabs". This concept is taken for the vertical mortar connections to be developed in this thesis. The lateral stiffness is explicitly part of the research because of its contribution to restraining the lateral dilation araising from the inclined compression strut in the mortar.

Finally, the entire precast concrete stability structure including the vertical mortar connections and tying reinforcement can be defined as "Macro" level (figure 1.7c). The figure shows the distribution of shear forces over the vertical connection of a cantilever shear wall. Internal shear forces will be transferred from the left to the right precast concrete elements and vice versa. It is investigated in this thesis how a vertical mortar connection functions when it is applied in shear walls.
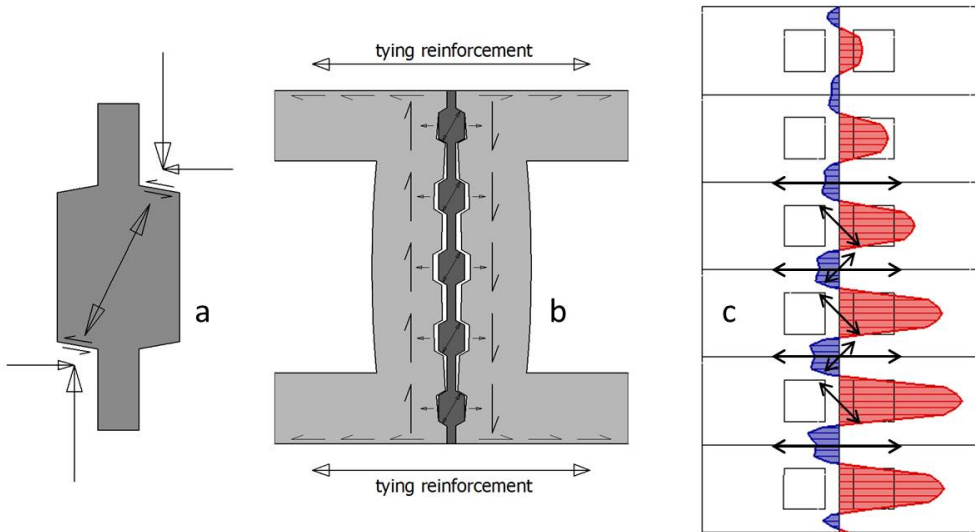
Figure 1.7: Vertical mortar connections at Micro (a), Meso (b) and Macro (c) level for the precast concrete concept of "vertical mortar connections with concentrated tying reinforcement in the slabs"

Lateral compression increases the shear capacity and shear stiffness of a vertical mortar connection. Internal compressive forces caused by external loads might be present in the precast concrete stability structure. Figure 1.8a shows an example of a cantilever shear wall with additional lateral compression available for the vertical mortar connection. Alternatively, compression can be obtained from horizontal pre-tensioning of the connection as well. However, this is usually not applied in practice for economical reasons. Insufficiently compressed vertical connections are sensitive to lateral dilation. Two examples of dilation are given in figure 1.8b and 1.8c. Figure 1.8b displays lateral dilation caused by the vertical point loads P that are unfavour-ably imposed to the cantilever shear wall structure constructed on a pile foundation with finite vertical stiffnesses (support springs). It will result in lateral dilation of the vertical connection. Another known example is the one of shrinkage of the joint material and shrinkage of the precast concrete element (figure 1.8c) leading to dila-tion. On the other hand, lateral compression which compensates lateral dilation can be beneficial for the vertical mortar connection. Therefore, the lateral compression is explicitly part of the research because of its contribution to restraining the lat-eral dilation and additional compression for probably raising the shear capacity and shear stiffness of the vertical mortar connections.
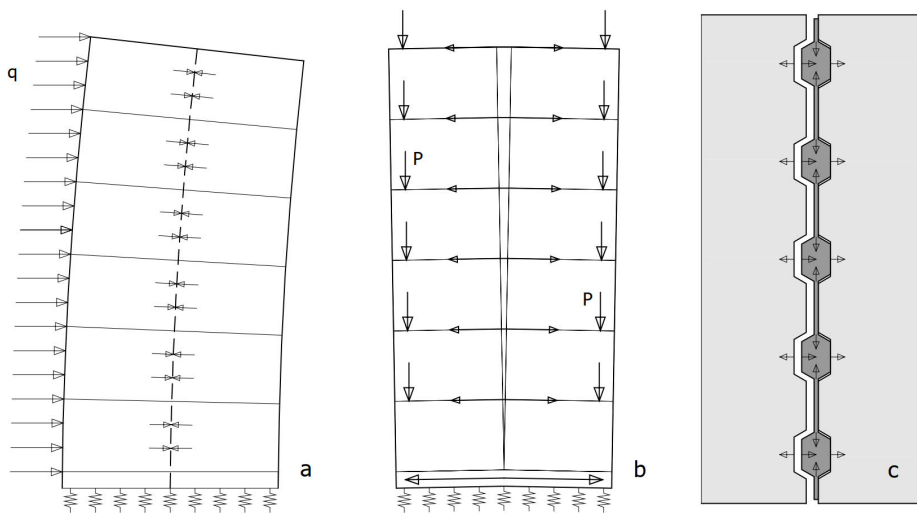
Figure 1.8: Precast concrete cantilever shear wall structure imposed with a dis-trubuted lateral line load q resulting in lateral compression forces on the vertical mortar connection (a), lateral tensile forces and dilation due to the point loads P (b) and shrinkage of the precast concrete and joint concrete (c)

1.4   Research objective and approach

The main objective of this research is to develop and model narrow vertical mortar connections that perform optimally for the transfer of shear forces in precast concrete stability structures with tying reinforcement in the slabs. They should preferably transfer considerable shear forces in a reliable way and should behave with a high shear stiffness. At the same time, the connections should preferably cause low dilation forces and should take full advantage of the lateral stiffness.

First, based on literature and structural design principles, the structural behaviour of connections with "joint concrete" is studied. With this knowledge, combinations of profiled mortar-to-concrete interfaces and mortars for shear connections are proposed. Shear tests on these mortar connections are performed. After a first series of experiments the findings are used to further optimize the connections. Their structural behaviour is studied in a second series of experiments. Next, the results of the first and second phase experiments are used for composing the third series of shear tests. Based on the experimental results, the structural behaviour of the developed and tested mortar connections is identified. Numerical analyses are performed to study the results of the shear tests. A model for the prediction of the shear behaviour of one vertical mortar connection is proposed. This model can be used to represent the connection behaviour in the composite precast concrete stability structures of the figures 1.7b and 1.7c. Also, a design equation for the prediction of the shear capacity of one of the vertical mortar connections is given.

1.5   Outline

Figure 1.9 displays an overview of the research presented in this thesis. The thesis starts with this introduction and succeeds with the literature review which is used to compile the research program. Next, the research continues with two methods of examination. The Physical examination refers to performing the experiments followed by explaining and analysing the test results. The Numerical examination refers to the simulation and modeling of the most suitable vertical mortar connection. This examination continues with the extrapolation of the test results to a storey-high application and succeeds with case studies. The final part of this thesis contains an retrospective view with the conclusions included and an outlook to the application of storey-high vertical mortar connections in precast concrete structures.

The present Chapter 1 Introduction presents a brief introductory description of vertical connections applied to precast concrete stability structures, the scope of the research, the proposed precast concrete concept and the research approach in this thesis. Chapter 2 is the literature chapter. It reviews and discusses the existing research on contemporary mortars, old-to-new concrete interfaces, connection design, structural behaviour of vertical connections, variables influencing the behaviour of connections, modeling and prediction. Chapter 3 describes the research program which includes the development of the five different mortar connections. The vari-

ables which were varied to study the connection behaviour are descibred in this chapter as well. Chapter 4 is the experiments chapter. It starts with the description of the pump test which allows the pumpability of (steel fibre reinforced) morter. Furthermore, the chapter provides information on the specimens in which the connections are included and the test setup in which the specimens are subjected to shear forces.

The test results are presented and explained in Chapter 5. The identified structural behaviour displayed in load-displacement diagrams, photos and videos of one example mortar connection is described in detail. Furthermore, the test results of the entire research program is given on their most relevant issues which are the principal stages identified during the shear tests, the observed failure cracks and their stiffnesses. The understanding of the connection shear behaviour requests closer analyses of the test results which is provided in Chapter 6. From these analyses, a modeling approach is proposed. This modeling method simulates the vertical and lateral displacements for a given shear force. Also, the chapter provides an equation for the prediction of the shear capacity. The next step is to investigate the shear behaviour of the connection in the storey-high application of shear walls with and without window openings in Chapter 7. The functioning of the proposed modeling method is identified and tested for application with the help of case studies. A retrospective view including the conclusions and an outlook to application in practice are drawn in Chapter 8.
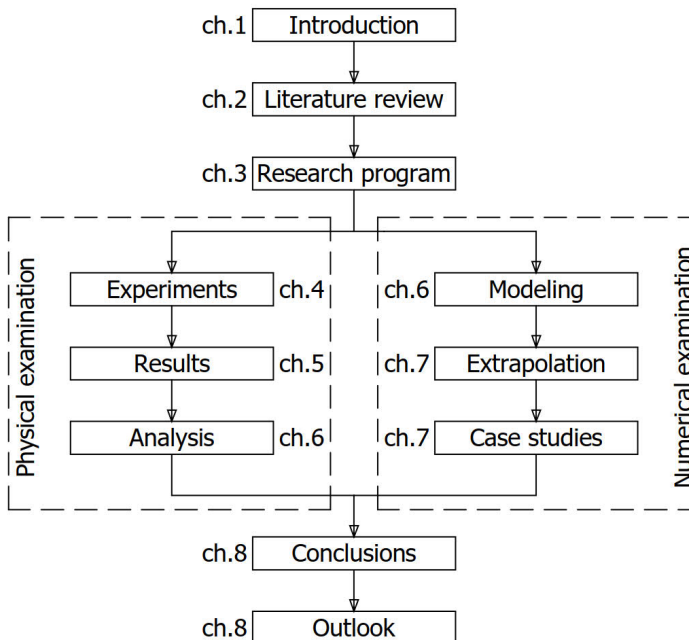
Figure 1.9: Overview of thesis outline

Chapter 2

Literature on Vertical Mortar Connections for Shear Transfer

2.1   Introduction

In this chapter a review is given for vertical connections with mortar or concrete as joint material. It starts in section 2.2 with an evaluation of mortar as joint material for the filling of narrow vertical seams. Section 2.3 explains the background on "interface shear transfer". It provides information about the transfer of forces via old-to-new concrete interfaces which are always present in mortar connections. The designs of known vertical connections are provided in section 2.4. They are reviewed on their appropriateness as vertical mortar connection. As reported at the end of this section, in some researches the "unreinforced profiled" type of connection was to some extent investigated before. This connection concept is identified as the version that could be adopted as profiled vertical mortar connection. It is determined the functioning of it requires further investigation.

Section 2.5 is dedicated to the shear behaviour of vertical connections. It discusses the characteristic shear behaviour of profiled connections using a general shear force-displacement diagram taken from previously conducted research. The transfer of shear forces is outlined and a general description of the basic structural shear behaviour of profiled connections with intermediate joint concrete is given.

Not just one connection lay-out is particularly suitable for the transfer of shear forces. Different types of profiles and roughnesses for the interfaces can be applied. They form a set of variables which influence the shear capacity and shear stiffness of vertical connections. Also, external forces and lateral stiffnesses imposed by the surrounding precast concrete structure interfere with the connection behaviour. These interferences form a set of variables as well. The influence of these variables was already studied in the previously conducted research. Section 2.6 provides a summary and the explanation on these works. The concept of storey-high vertical connections with concentrated tying reinforcement in the slabs is outlined in section 2.7.

2.2   Mortar for vertical seams

2.2.1   Contemporary mortars

Mortar is a cement-based construction material. It does not contain the large aggregates that are present in ordinary concrete mixtures. Mortar is intended to fill small spaces in which these large concrete aggregates do not fit. Mortars for narrow seams between precast concrete wall elements have typically maximum aggregate sizes of between 0,5 mm and 2 mm. CUR aanbeveling 24 (1991) defines mortar as "a factory-made mixture, composed of cement, fine aggregates, additives, possible filler material and an expansion-promoting additive for compensating the shrinkage in the plastic phase". Mortars of today are purchased as dry ready mixtures and are delivered in bags or silos to construction sites. Site workers have to add a prescribed amount of water for acquiring a workable plastic mortar and to initiate the hardening process.

The compressive and tensile strengths of contemporary mortars are in the same range as traditional concrete. Moreover, they have to achieve a significant compressive strength soon after applying in order to enable the continuation of the construction of precast concrete elements. Contemporary ordinary mortars reach compressive strengths of 45 N/mm^2 soon after applying.

Mortar shrinks due to the conversion of cement and water into cementstone and due to the evaporation of redundant water. Outdated mortars consist of just cement, sand and water. They shrunk considerably. To reduce the shrinkage, contemporary mortar mixtures contain an expansion-promoting additive. This additive maintains a volume increase of the mortar in the plastic phase. The mortar expands freely in an open space. Neppelenbroek (2004) calls this "free swelling". Mortar can be inserted in closed inner spaces where the swelling is restrained. A vertical seam between precast concrete elements can be considered as a closed inner space. The swelling is restrained by the edges of the precast concrete elements and the mortar presses itself against the concrete in the seam. As an example, a mortar with a K70 strength class (characteristic mortar compressive strength), the combination of free swelling and shrinkage results in a shrinkage of less than 0,75 mm/m after 7 days. It is a very small shrinkage and negligible for many applications. Because of this minimal shrinkage, these mortars are called "low-shrinkage mortars".

2.2.2   Insertion of mortar in seams

Mortars can be classified in accordance with their way of applying the mortar into the final place at the construction site. The so-called "fluidity" or "consistency" of the plastic mortar is the property that determines this classification. CUR aanbeveling 24 (1991) defines three principal groups of insertion methods; "casting mortars" with a high fluidity, semi-plastic "trowel mortar" and "underpinning mortar" with more stiff consistencies. The different types of mortar will be discussed for the application of filling narrow vertical seams between precast concrete wall elements.

Casting mortar is very fluid and requires formwork that prevents outflow. Leakage of mortar through holes and chinks in the formwork is a serious issue that must be prevented. The precast concrete industry considers the construction of formwork and additional taping as laborious and risky. The alternative with underpinning mortar in narrow vertical seams is laborious as well since the mortar has to be inserted and compressed with a trowel manually in order to get the right compaction. However, this approach is less risky and less laborious than working with casting mortar. Hence, the precast concrete industry does not prefer casting mortar and will choose for underpinning mortar out of these two options for narrow vertical seams.

The alternative is to inject the mortar in the vertical seam. This can be done by using a mortar pump as displayed in figure 2.1a. Figure 2.1b shows a view inside the hopper for mortar storage. It contains an auger which is able to screw the mortar into the hose. This screw in tube mechanism forces the mortar to flow through the hose. At the end of this hose, the plastic mortar can be injected into a vertical seam.

Figure 2.1a displays a hard plastic PVC pipe connected to the end of the hose for injecting the mortar into the seam. Figure 2.1c shows another type of nozzle. This tool facilitates the injection of the mortar into small and linear seams even in corners as displayed on the photo of figure 2.1d.

a

b

c

d
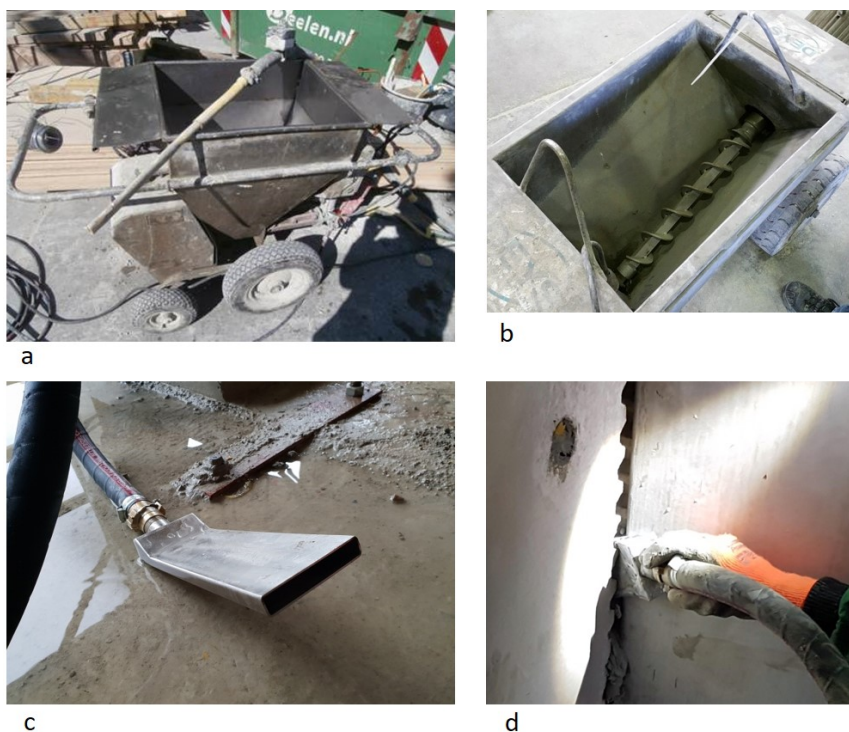
Figure 2.1: Insertion of mortar with pump into a vertical seam

Trowel mortar is the type of mortar that has the correct consistency to be pumped. It has a semi-plastic consistency and behaves thixotropic. The thixotropic properties causes the mortar to flow when stirred by the pump. A little moment after injection the thixotropic properties cause the mortar to change into a stiffer mortar paste. Then, the mortar remains in place. As a result, the mortar is pumped in a more liquid state while it remains in place after injection due to the stiffer viscosity. Also, the plastic mortar swells in the seam which provides bonding against the profiled surface of the precast concrete elements.

The injection of the mortar into the narrow vertical seam can be explained with the help of figure 2.2. The injection requires a temporary closure of the seam at the backside of a wall element. Otherwise, the injected mortar outflows the seam. The closure can be arranged with traditional wood functioning as formwork. A less laborious way is the use of pipe insulation displayed in the figure. The insulation is impressed in the seam. It remains in place because of the friction resistance between the insulation and precast concrete elements. The mortar will be pressed against the closure via the nozzle. After that, the nozzle slides to the frontside while injecting the mortar according to the red arrows in the figure.
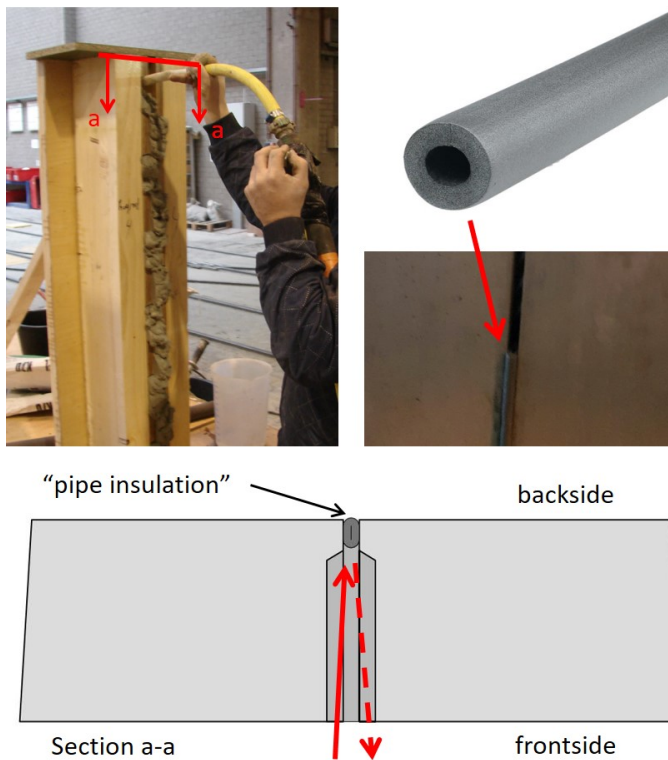
Figure 2.2: Injection of mortar into a vertical mortar connection between two precast concrete elements

2.3   Interface shear transfer

2.3.1   Old-to-new concrete interfaces

Vertical connections have two "old-to-new" concrete interfaces through which shear forces are transferred. They are named so because the new plastic joint concrete is poured against the old hardened concrete surfaces of the precast concrete wall elements. The interfaces do not only transfer shear forces because they transfer compressive forces at the same time. Furthermore, horizontal hairpins crossing the interfaces (see figure 1.4) transfer shear forces and lateral tensile forces.

"Interface shear transfer" is a well known research topic. Santos and Julio (2012) and Randl (2013) provide overviews on this topic in state-of-the-art articles. They are reviewed to the extent that they provide information about the interfaces of vertical connections applied between precast concrete wall elements.

Many types of roughness and profiles are tested and discussed in the research conducted in the past. A concrete surface will be very smooth when the concrete is cast against plain steel formwork. Adhesion between such very smooth old concrete surfaces and the joint concrete already breaks at low tensile or shear stresses. The interface properties can be improved by roughening the old concrete surface for the transfer of higher shear and tensile forces. Known roughening methods (among others) are high-pressure-water-jetting (HPW), milling, shot-blasting and sand-blasting. The different treatments do not result in the same structural improvement of the concrete surface roughness. The shear and tensile capacities will usually be higher for the coarser concrete surfaces.

Hordijk et al. (2005) published the results of shear tests on interfaces with several roughening methods used by the precast concrete industry in The Netherlands. Their roughening methods were (a) no treatment, (b) roughening with rake or trowel, (c) breaking cement fleece with air pressure, (d) addition of relief pattern in formwork and (e) exposing the aggregates with a surface retarder. These methods can be considered for the roughening of the interfaces of the vertical mortar connections.

The usability of the roughening is of utmost importance for the transfer of forces. Many unintended events can harm the concrete surface which results in the deterioration of the interface shear capacity. Contamination of the concrete surface before casting the new concrete is something that can happen easily at construction sites or in concrete factories. In particular, horizontal concrete surfaces are sensitive to contamination because dust and dirt can easily fall down on it. The use of an inappropriate roughening method is the second threat. The concrete surface can be damaged to an extent that it hinders adhesion or interlock. The third (often unavoidable) occurance is shrinkage of the precast concrete wall elements or the joint concrete. Shrinkage can be reduced by using low-shrinkage joint concretes or mortars.

Different methods for the quantification of surface roughnesses were developed. The Sand Patch Test depicted in figure 2.3 is a well-known and simple to execute method. A calibrated volume of fine sand is circular spread over the roughened concrete surface. The circle is measured after spreading the sand. A small circle diameter is measured in case of a very coarse surface. The diameter is larger for less rough concrete surfaces. The roughness can be estimated as the Mean Texture Depth (MTD) of the sand cylinder (four times the sand volume divided by circle area) as displayed in the figure. This is defined as the Mean Surface Roughness R_t in *fib* Model Code 2010 (2013) and Randl (2013). *fib* Model Code 2010 (2013) distinguishes the following four types of roughness for concrete surfaces: very smooth (R_t not measureable), smooth ($R_t < 1,5$ mm), rough ($R_t > 1,5$ mm) and very rough ($R_t > 3,0$ mm). Other more sophisticated methods exist. Santos and Julio (2013) reviewed sixteen different roughness quantification methods.
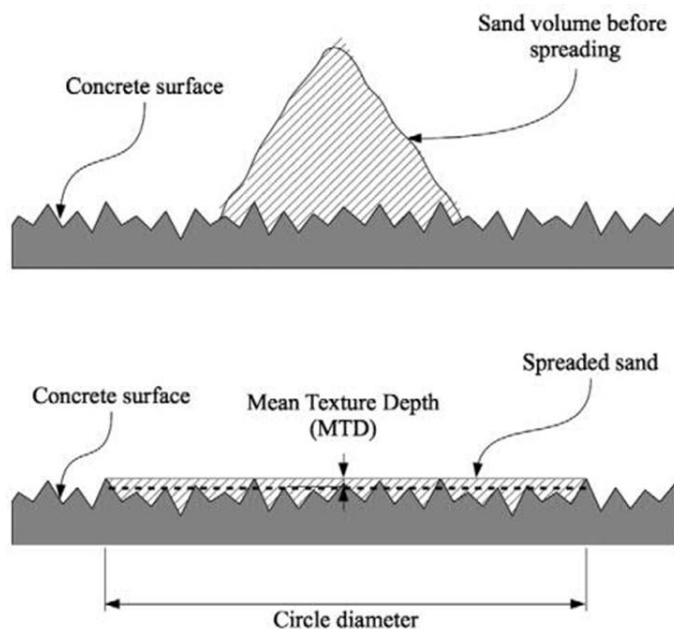
Figure 2.3: Sand Patch Test, Santos and Julio (2013)

Other roughness classification systems are invented for linking the measured roughnesses to the design codes. The International Concrete Repair Institute published the ICRI Technical Guideline (2013) with a Concrete Surface Profile (CSP) classification. Figure 2.4 displays in the table a substantial number of Surface preparation methods in the vertical column. The horizontal axis is the CSP classification 1 to 10. The concrete surfaces above the table display the roughness grades represented by the CSP classification. The table indicates which CSP number can be selected for the different Surface preparation methods.

| CSP 1 | CSP 2 | CSP 3 | CSP 4 | CSP 5 |
| CSP 6 | CSP 7 | CSP 8 | CSP 9 | CSP 10 |
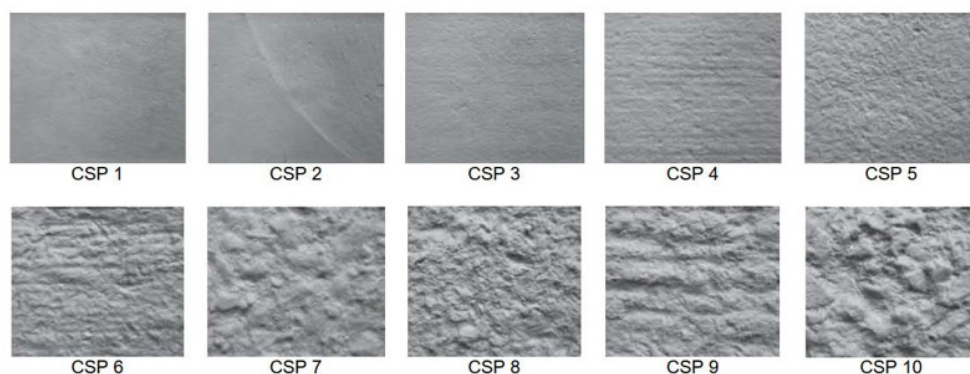
Surface preparation method	Concrete Surface Profile									
	CSP 1	CSP 2	CSP 3	CSP 4	CSP 5	CSP 6	CSP 7	CSP 8	CSP 9	CSP 10
Detergent scrubbing	■									
Low-pressure water cleaning	■									
Grinding	■	■								
Acid etching	■	■	■							
Needle scaling		■	■	■						
Abrasive blasting		■	■	■	■	■	■			
Shotblasting		■	■	■	■	■	■	■	■	
High- and ultra-high-pressure water jetting			■	■	■	■	■	■	■	■
Scarifying				■	■	■	■			
Surface retarder (1)					■	■	■	■	■	■
Rotomilling						■	■	■	■	
Scabbling							■	■	■	
Handheld concrete breaker							■	■	■	■

(1) Only suitable for freshly placed cementitious materials

Figure 2.4: Concrete Surface Profile (CSP) classification of the International Concrete Repair Institute, Henry (2018) and Winkler (2014)

2.3.2   Modeling interface shear transfer

The Saw-tooth model displayed in figure 2.5 is often used for the explanation of the structural behaviour of interfaces. It is used for the proposal of the first Shear Friction theory (SF) by Birkeland and Birkeland (1966). The sliding teeth are a representation of the rough interface providing shear friction capacity. The interface is subjected

to a shear stress (τ) and a compressive stress (σ) at the same time. The shear stress (τ) causes a shear displacement (s). The interface opens with a displacement (w) as a result of the resistance provided by the interlocking teeth. The steel bar crossing the interface is forced to deform to the displayed state in the Saw-tooth model and its resistance to deform contributes to the shear friction capacity of the Saw-tooth assembly.
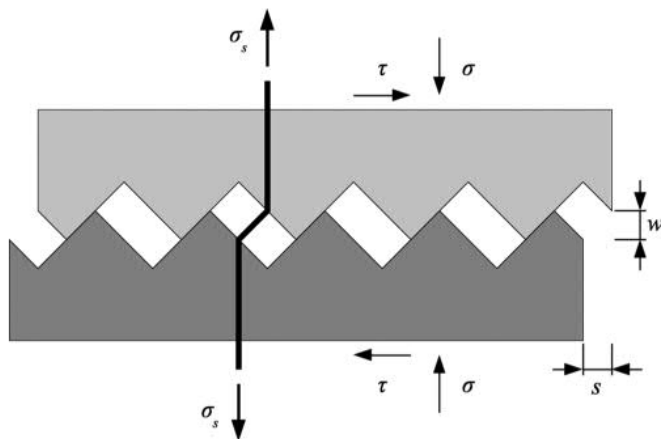
Figure 2.5: Saw-tooth model proposed in Birkeland and Birkeland (1966)

The different load carrying mechanisms active in an interface are usually discussed separately in literature. They are often presented as Adhesive bonding and Mechanical interlock, Friction and Dowel Action according to Zilch and Reinecke (2000), Randl (2013) and Santos and Julio (2014). Figure 2.6 displays the principles of these mechanisms, which will be explained below.

Adhesive bonding and Mechanical interlock. Adhesion and Cohesion provide bonding between two different particles. Adhesion is defined in literature as the attraction between dissimilar particles. Cohesion is determined as the attraction of similar particles. Santos and Julio (2014) and other researchers defined Cohesion as the combination of Adhesive bonding and Mechanical interlock within the research area of Interface shear transfer.

Figure 2.6a is used for discussing the mechanisms Adhesive bonding and Mechanical interlock. Adhesive bonding is the chemical and physical bonding between two different aged concrete layers placed against each other in an interface. The Adhesive bonding is provided by Van der Waals forces which allow the transfer of shear forces through the interface. The bond strength is controlled by the surface preparation, weakest concrete strength, shear reinforcement, differential shrinkage and differential stiffness according to Santos and Julio (2014). Rough surfaces possess more contact area than smooth surfaces. The more surface contact area available the more adhesion contributes to the shear and tensile capacity. The contribution of adhesive bonding to the shear capacity terminates after small shear displacements

(s = 0,05 mm) arise in figure 2.5 according to Randl (2013). Mechanical interlock is the load-bearing mechanism and closely related to adhesion. Figure 2.6a shows an interface with old and new concrete that interlock. This interlock contributes to the shear capacity as well. It is explained as "keying and intercutting effects" by Randl (2013). Mechanical interlock is not present in plain old-to-new concrete interfaces. Aggregates must protrude considerbly from the surface for being effective.

Adhesive bonding and mechanical interlock transfer shear forces at the same time. However, it is useful to study them separately. Shear capacities from both mechanisms can be identified from shear tests. A known method for acquiring the component mechanical interlock is by canceling adhesive bonding with a bond separator. This bond separator will be lubricated on the concrete surface before casting the new concrete against it. Then, the contribution of adhesion is excluded and the shear capacity of only mechanical interlock can be measured in a shear test. Shear tests on specimens without a bond separator will provide a shear capacity for both mechanisms together. Then the part of only adhesion can be determined by taking the difference between the results of both measurements.

Friction provided by external compression of an interface is the second main mechanism that contributes to the shear capacity of old-to-new concrete interfaces. Figure 2.6b$_1$ displays weight G that compresses the interface perpendicular to the surface. It represents a few possible causes of compressive forces through the interface like self weight of the structure, pre-tensioning or compressive forces imposed by the internal force distribution of a precast concrete structure.

Figure 2.6b$_2$ displays the contribution of steel bars (e.g. reinforcement) to the shear friction capacity. Displacements (w) perpendicular to the interface arises as a result of the shear displacement (s) over the rough old concrete surface. The displacements (w) and (s) together stress the steel bar with a tensile force N. This force presses the old and new concrete components against each other causing a compressive state in the interface. This is called the "clamping" effect of steel bars. These can be reinforcement bars or other type of connectors crossing the interface.

The amount of shear friction capacity depends on the interface roughness and the size of compressive forces. A more rough interface provides more shear friction capacity. Also, a more compressed interface provides more shear friction capacity.

Dowel action. Figure 2.6c displays the third main mechanism being active in an interface with a crossing steel bar that contributes to the shear capacity. The first drawing shows bending (M) of a steel bar while loaded with a shear force (V). The bending capacity of the steel bar allows the transfer of shear forces and provides resistance against shear displacements. The transfer via bending is generally called "dowel action" in literature. The second drawing in the figure shows the transfer of shear forces (V) through "kinking" of the steel bar. As soon as the bending stress in the steel bar reaches its maximum with yielding, this kinking mechanism remains and is still able to transfer shear forces V. The transfer of shear forces via kinking can become relevant at relatively large shear displacements (s).
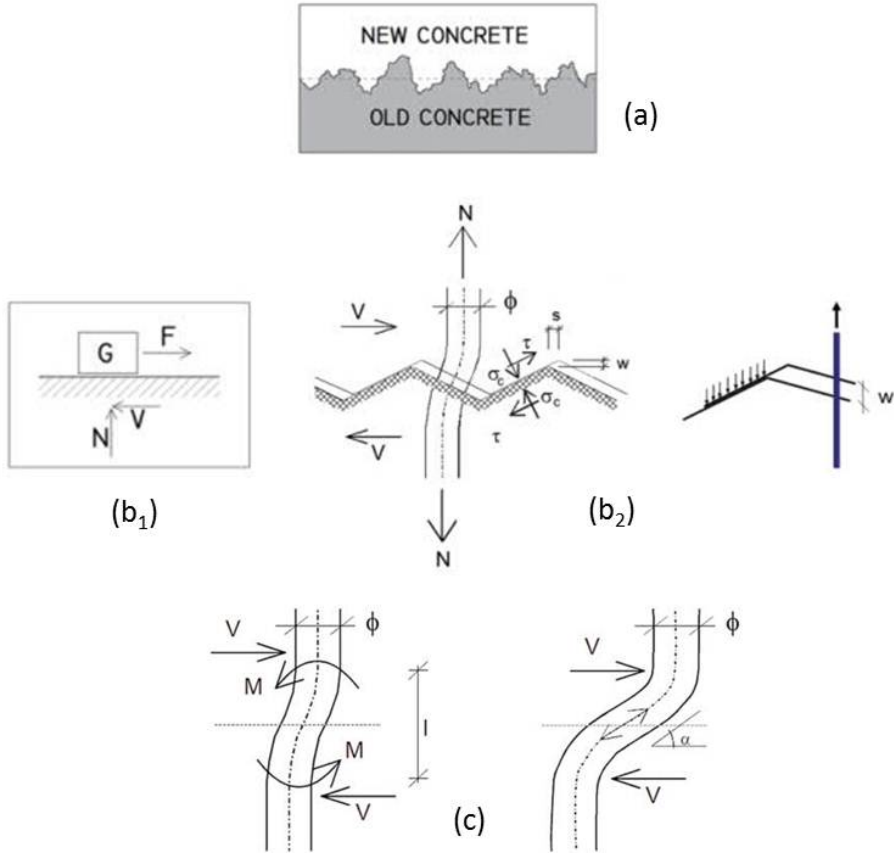
Figure 2.6: Adhesion + Mechanical interlock (a), Friction provided by compression due to external actions (b_1) or due to clamping forces (b_2), and Dowel action (c), Randl (2013)

Interaction. The three main mechanisms just discussed interact with one another during transferring a shear stress through an old-to-new concrete interface. Figure 2.7 shows a diagram with a shear stress $\tau_{(s)}$ as function of shear displacements (s) according to Zilch and Reinecke (2000). The shear-displacement developments of the separated three mechanisms defined are displayed in the diagram. It shows that the mechanisms affect one another depending on the displaced state (s) of the interface.

Cohesion takes the majority of the shear stresses in the initial stage. The diagram shows a significant decline for cohesion after the interface slips. The decline occurs after adhesive bond breaks and aggregates crush in the interface. Measurements taken from shear tests show that adhesion breaks at shear displacements of approximate s = 0,05 mm. Furthermore, the diagram shows that friction increases quickly from the origin of the diagram in the initial stage. The diagram demonstrates that the

shear friction capacity in the phase up to $s = 0,05$ mm is provided by the mechanisms Cohesion and Friction. *fib* Model Code 2010 (2013) and Randl (2013) define the shear behaviour of interfaces in this stage of the diagram as "Rigid bond-slip" behaviour. The dominant mechanism for this behaviour is cohesion and the interface behaves with a high shear stiffness. This interface fails brittle in case it is not equipped with reinforcement or other connections.

The diagram displays that dowel action starts transferring shear forces after the interface has undergone a certain displacement (s). The mechanism friction provides the transfer of considerable shear forces at the same time. The contribution of cohesion is rather limited in this stage. Cohesion is not available for (very) smooth interfaces according to *fib* Model Code 2010 (2013). The combination of cohesion, friction and dowel action contributing to the shear capacity is referred as "Non-rigid bond-slip" behaviour because of the larger shear displacements (s) which are in the range of 0,5 mm to 1,5 mm. In that case, the interfaces behave ductile during transferring shear force which is usually preferred in concrete structures.
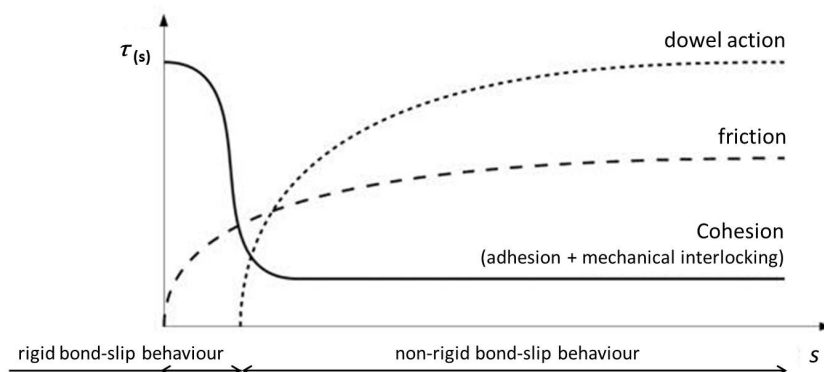
Figure 2.7: Diagram with interaction of Cohesion, Friction and Dowel action proposed by Zilch and Reinecke (2000)

2.4 Vertical connections

2.4.1 Basic connection designs

Vertical connections were subject of investigation in many research programs since the sixties of the last century. These studies were usually structured as indicated in the following. New connections with certain profiles or surface roughnesses for the old-to-new concrete interfaces were proposed. Destructive laboratory shear tests were performed with the goal to indentify the shear behaviour. A number of them have been modeled numerically for further studying the structural behaviour of the physically tested connections. The structural behaviour was analysed and empirical equations for the prediction of the shear capacity and secant stiffnesses were

proposed. The obtained knowlegde was brought together in a number of state-of-the-art articles provided by for example Cholewicki (1971); Olesen (1975); Hansen and Olesen (1976); Mehlhorn and Schwing (1977).

For the literature review in this thesis the vertical connections are brought together into four basic designs. Figure 2.8 displays them in an order leading to a vertical mortar connection (d). The first is the traditional cast-in-place loop connection (a) without a profile. Connection (b) is keyed in the direction out of the plane. (perpendicular to the wall). These keys are just used for making room for hairpins and the vertical bar. Connections (c) and (d) have horizontal keys as well as vertical shear keys. Horizontal hairpins are absent in connection (d). The four basic designs will be reviewed in next subsections.
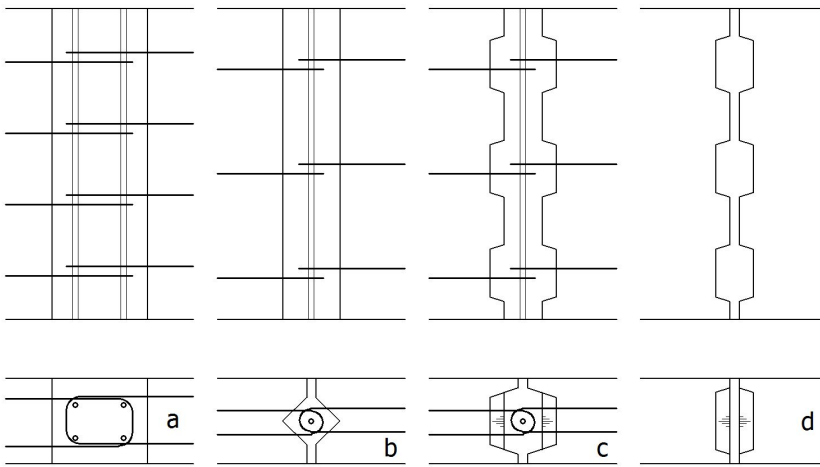
Figure 2.8: Vertical connections; plane interfaces (a), horizontal profiled interfaces (b), vertical and horizontal profiled interfaces (c) and unreinforced vertical profiled interfaces (d)

2.4.2   Reinforced unprofiled connections

The reinforced cast-in-place vertical connection displayed in figure 2.8a is the most applied vertical connection between precast concrete wall elements. Various studies are dedicated to this connection or variants on this connection (e.g. Abdul-Wahab and Sarsam (1988)). Also, this vertical connection is frequently proposed in precast concrete design books (e.g. Elliott (2011); Steinle et al. (2019); *fib* bulletin 43 (2008); *fib* bulletin 74 (2014)).

Forces will be transferred through two vertical reinforced concrete interfaces of a cast-in-place loop connection. The mechanisms Cohesion, Friction and Dowel Action are available for the transfer of shear forces through these interfaces. However, a little lateral dilation in the vertical connection of a precast concrete shear wall structure can affect the adhesion in an uncompressed or poorly compressed state of

the vertical connection. Also, mechanical interlock will be absent in case of (very) smooth shaped concrete interfaces. Therefore, it is questionable if Cohesion (Adhesion and Mechanical interlock) contribute to the shear capacity of a traditional cast-in-place loop connection with smooth concrete surfaces displayed in figure 2.8a. It is recommended to assume that the transfer of shear forces only relies on Friction and Dowel action in this type of vertical connection. Furthermore, uncompressed vertical interfaces should be classified behaving with non-rigid bond-slip behaviour according to *fib* Model Code 2010 (2013) as discussed in the previous section.

The manufacturability of such a vertical connection should be evaluated as well. Traditional hairpins protrude the edge formwork in the concrete factory according to figure 2.9a. This can be considered less suitable since the construction and demoulding of steel bars through wooden formwork is difficult. This can be prevented by applying a "Rebend connection" (figure 2.9b) which can be shaped with a profile or roughness for the concrete surface as well. The reinforcement stays temporarily within the edge formwork in the concrete factory and will be bent into the cast-in-place concrete interspace at the construction site.

Traditional cast-in-place loop connections require traditional concrete construction work. Additional reinforcement has to be installed at the construction site and formwork is required for keeping the plastic concrete in place. A precast concrete connection should be preferably less laborious to construct than a traditional cast-in-place loop connection is. Attempts have been made to improve and simplify the manufacturability of this connection. The connection discussed in the next subsection is one of them.

Concrete factory   Construction site
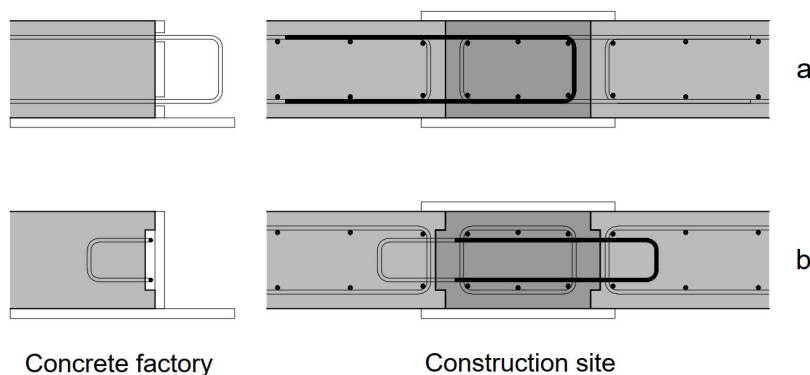
Figure 2.9: Cast-in-place loop (a) and Rebend connection (b) in the factory and on the construction site

2.4.3   Reinforced profiled (keyed) connections

The precast concrete industry is very familiar with mortar as joint material between precast concrete elements. Connection (b) in figure 2.8 is such a vertical mortar con-

nection intented for filling with mortar. This connection is called "grooved joint" in Cholewicki (1971), Abdul-Wahab (1992) and Bhatt and Nelson (1970). It cannot be filled with traditional concrete because of the lack of sufficient volume for the larger aggregates present in concrete mixtures. To position the hairpins and the vertical steel bar an inner space is created. As a result, the amount of interface surface is increased. It can increase the shear capacity provided by the mechanisms Cohesion or Friction in a compressed state. Also, it requires more simple formwork for closing the vertical seam at the construction site when compared to the traditional formwork needed for the previously discussed connections.

The applicability of this connection as narrow vertical mortar connection can be questioned. The starting point in this thesis is filling the vertical seams with thixotropic mortar by using a mortar pump. The reinforcement and the accesibility of the inner space hinders the filling with mortar inserted with a hose. This connection requires casting mortar. As stated before, reinforcement hairpins through the edge formwork in the concrete factory is laborious and therefore obstruct the production process. These considerations are the reason for not selecting this reinforced horizontally keyed connection for research in the current thesis.

Figure 2.8c displays a reinforced keyed mortar connection. It is the previously discussed horizontal keyed connection extended with vertical shear keys. The joint material can be a concrete mixture with limited aggregate sizes or a mortar. The shear keys are able to provide additional shear capacity to the vertical connection. However, the hairpins crossing the edge formwork can be considered again as less suitable for a precast concrete connection. The selection leads to the narrow "unreinforced profiled mortar connection" drawn in figure 2.8d which is discussed in the next subsection.

2.4.4   Unreinforced profiled (keyed) connections

The unreinforced profiled mortar connection (figure 2.8d) fits to the assumptions proposed in this thesis. The profile can be constructed with a simple addition to the edge formwork in the concrete factory. This connection has a smaller inner space which can be filled with the hose of a mortar pump. This vertically keyed mortar connection can be used for the precast concrete concept of vertical mortar connections with concentrated tying reinforcement in the slabs (displayed in figure 1.7).

Four basic designs for the unreinforced profiled mortar connection can be identified from research conducted in the past (see figure 2.10). The connection in figure 2.10a is the most used and is frequently called "Aligned shear key" connection or "Castellated joint". Shear forces flow via diagonal compression struts in the joint material from one precast concrete element to the adjacent one. The struts press against the interlocking ribbings (the shear keys), which have a sloped abutment surface roughly perpendicular to the diagonal strut. The keyed connection is designed for transferring positive as well as negative shear forces since the direction of the shear force in precast concrete stability structures can change due to e.g. wind loads from either sides of a building. The "Staggered" profiled connection in figure

2.10b, suggested in Elliott (2011), is an alternative shear key connection. A "continuous sinusoidal waved joint" has been proposed by Menegotto and Monti (2005) for the shear force transfer between two hollow core slab elements. The waved profile has been proposed for its favorable ductile behaviour. Mehlhorn and Schwing (1977) and Beck et al. (1973) proposed connection 2.10d as a profile for a vertical connection.
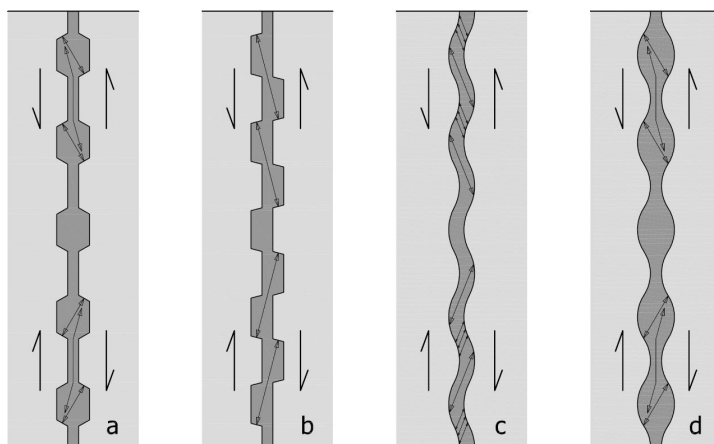
Figure 2.10: Basic profiles for mortar connections; Traditional aligned shear key (a), staggered key (b), waved keys (c + d)

Bringing together these profiles does not directly lead to the most suitable vertical mortar connection for current research. Researchers in the past had other goals to achieve and developed their profiles for other applications. Also, the profiles were subject in different research programs conducted by different researchers which makes a simple mutual comparison impossible. However, despite this, Hansen and Olesen (1976) state that "there has been a large degree of conformity between the observations made during tests" and collected it in their state-of-the-art report. This information was useful for selecting the vertical mortar connections for the current research. Also, understanding of the mechanisms involved in the transfer of shear forces is required. Therefore, in the next section the structural behaviour of these type of connections is discussed.

2.5 Shear behaviour of vertical connections

2.5.1 Shear tests

Physical shear tests are usually performed for the identification of the shear behaviour of shear connections. Researchers used different types of shear test specimens. Figure 2.11 displays the known lay-outs in which the shear connection can be constructed. They are primarily designed for the transfer of shear forces. The presence

of bending moments in the connection should be avoided. They cause non-uniform shear stress distributions over the height of the joint. Specimens that are able to transfer just shear forces do not exist. The non-uniformity is usually accepted since the transfer of shear forces dominates the force distribution in the shear connection.
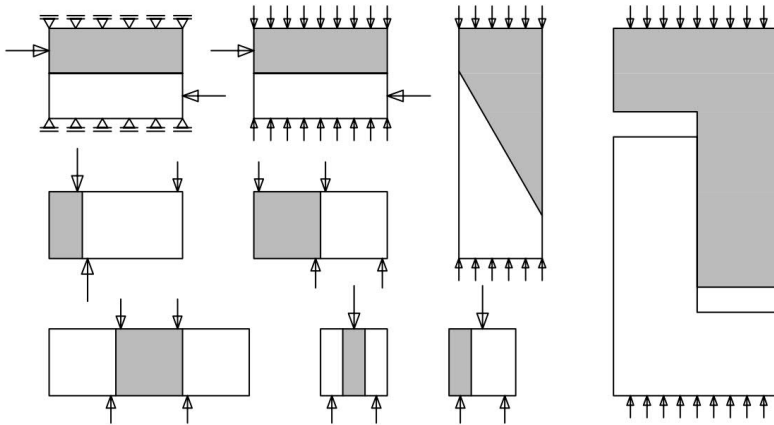
Figure 2.11: Various types of test specimens for to investigate the transfer of shear forces through an interface or connection, Espeche and Leon (2010)

Figure 2.12 displays in a drawing and a photo an example of the shear tests on an unreinforced keyed mortar connection performed by Rizkalla et al. (1989). The profiled connection was constructed in a specimen. The specimen was installed in a test setup. This connection was laterally compressed with an "applied preload" by tensioning the horizontal steel bars. A vertical load is imposed to the top of the specimen. This load is transferred via the vertical mortar connection as shear force. The shear force and lateral forces are known values since they are imposed to the specimen. The vertical slip of the shear connection was measured. These properties provided the shear force versus displacement behaviour from which the shear stiffness can be observed.

Figure 2.12 indicates four "independent post-tensioning systems" represented by small arrows in the drawing. The photo underneath displays these systems with steel bars and steel end plate assemblies. They were used for compensating the internal bending tensile stresses that arose in the L-elements during loading the specimen on top. An alternative for taking these stresses is applying embedded reinforcement in the L-elements. Then, the post-tensioning system is not required.
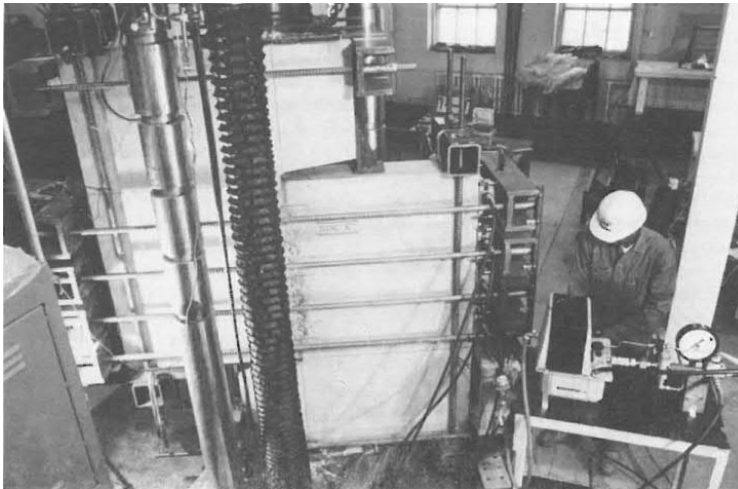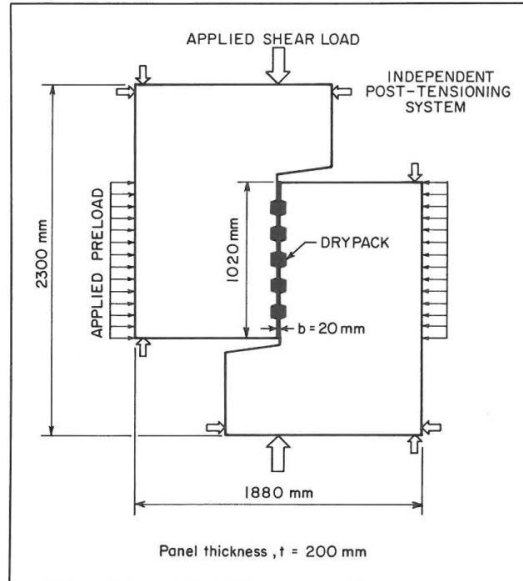
Figure 2.12: Specimen and shear test setup of Rizkalla et al. (1989)

2.5.2 Load-displacement behaviour of keyed connections

The profiled connections go through a number of principal stages during a shear test. These stages are displayed in the diagram of figure 2.13. It is a shear stress (τ) versus shear displacements (δ_v) diagram. The applied load on top of the specimen is divided by the connection surface area which equals the connection height multiplied by the panel thickness. This is defined as the shear stress (τ).
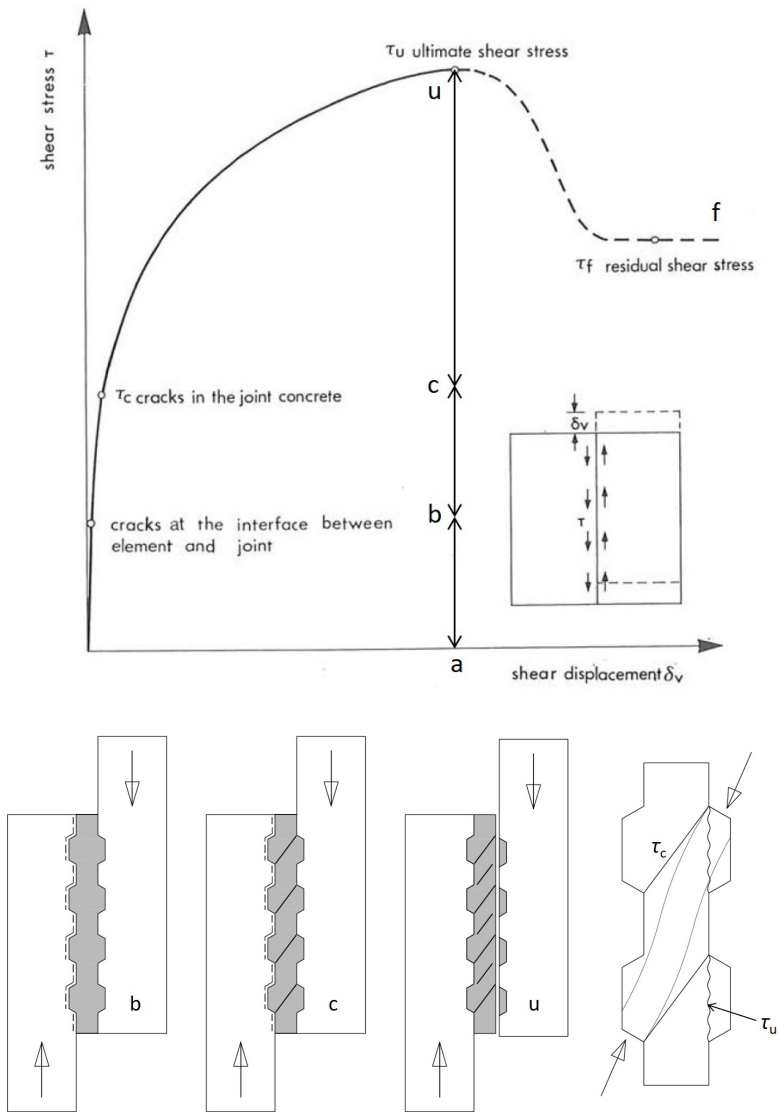
Figure 2.13: Shear behaviour of a profiled connection, stress-displacement diagram taken from Hansen and Olesen (1976), drawings with compression struts taken from Cholewicki (1971)

The connection is loaded increasingly with small shear stresses in stage (a-b) of the diagram. Adhesive bonding in the profiled interfaces transfer the shear stresses distributed over the entire interface of the connection in this stage. Also, the precast concrete and the joint concrete transfer shear stresses distributed and remain uncracked.

Adhesive bonding breaks in one of the two interfaces at the end of the first stage in point (b). The dotted lines near the interfaces in the front view of figure 2.13b indicates this broken adhesion. The gap between the precast and joint concrete does not allow the transfer of forces anymore. Then, the connection enters stage (b-c) in the diagram. In this stage only the inclined struts displayed below-right in figure 2.13 are able to transfer shear forces from one precast concrete element to the other.

The first diagonal cracks appear with shear stress τ_c in the diagram. It is the start of stage (c-u) in the diagram. More cracks appear in this stage up to the top of the diagram where the connection fails. There, the connection reaches its ultimate shear capacity τ_u. The joint material of the indentations are sheared off as can be seen in the front view figure 2.13u. Finally, the horizontal branche (f) in the diagram displays a constant residual shear resistance τ_f which is provided by the shear friction capacity of the main vertical crack displayed in the front view of figure 2.13u.

2.5.3 Failure mechanisms of keyed connections

At the instant of reaching the ultimate shear capacity τ_u in the diagram of figure 2.13, the vertical mortar connection fails. Figure 2.14 shows the known failure mechanisms of shear keyed connections with deep recesses. The picture (a) represents the failure of the connection due to the appearance of a dominant inclined crack. This mechanism at failure often arises in single keyed connections where the interaction between multiple keys in a row lacks. In picture (b) the connection fails due to shearing off the joint concrete in the corner of the indentation. This type of crack arises in cases with more lateral displacements and sufficient shear friction capacity in the sloped interface between concrete and the joint concrete or mortar.
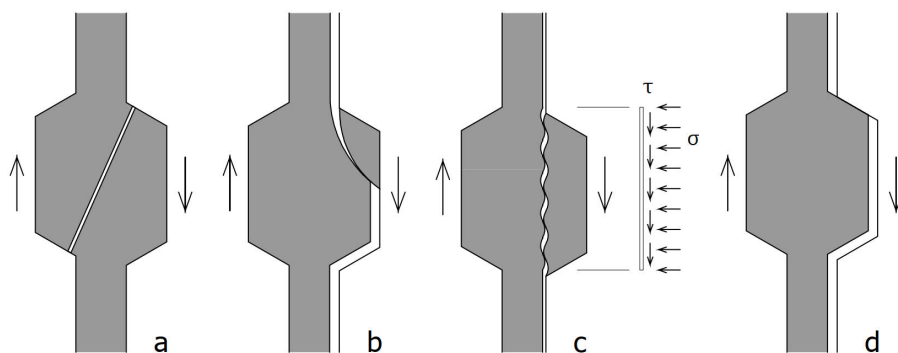
Figure 2.14: Failure mechanisms, presented in literature by e.g. Rizkalla et al. (1989), Hansen et al. (1974), Eriksson et al. (1978)

The third picture (c) in the figure displays the mechanism of the vertical shearing off of the shear key indentation. The shear stress τ combined with the lateral stress σ cause a stress state in the joint concrete or mortar that has exceeded its capacity in the vertical failure plane. This causes the vertical crack.

The mechanism of picture (d) occurs when the joint concrete slides off at the sloped compressed surface under a significant lateral displacement. This relates to the shear friction capacity of the sloped interface which will be explained. Figure 2.15 displays the force transfer via an inclined compression strut F_{strut} and shear friction $F_{friction}$ in the joint material. The steepness of this strut is varied in the three polygons of forces (a), (b) and (c). The angle between the compression strut F_{strut} and the interface is $90°$ in (b). The friction force $F_{friction}$ represents the shear stress present in the interface. This force arises for acquiring equilibrium in the polygon of forces. The friction force $F_{friction}$ is smaller in case of a steeper diagonal force F_{strut} as can be seen in picture (a). It requires less shear friction capacity of the interface. In the case of the flatter diagonal force F_{strut} in (c) it requires more shear friction capacity in the interface than it can provide. As a result, the concrete slides off the interface according to the mechanism of figure 2.14d. The force H is required for acquiring equilibrium in the polygon of forces which has to be provided by the lateral reinforcement. Cholewicki (1971) states that if the angle β in figure 2.15 is smaller than $56°$, the friction capacity of the interface will be lower than the force $F_{friction}$. In that case, the lateral force H is required to acquire equilibrium and a functioning vertical connection.
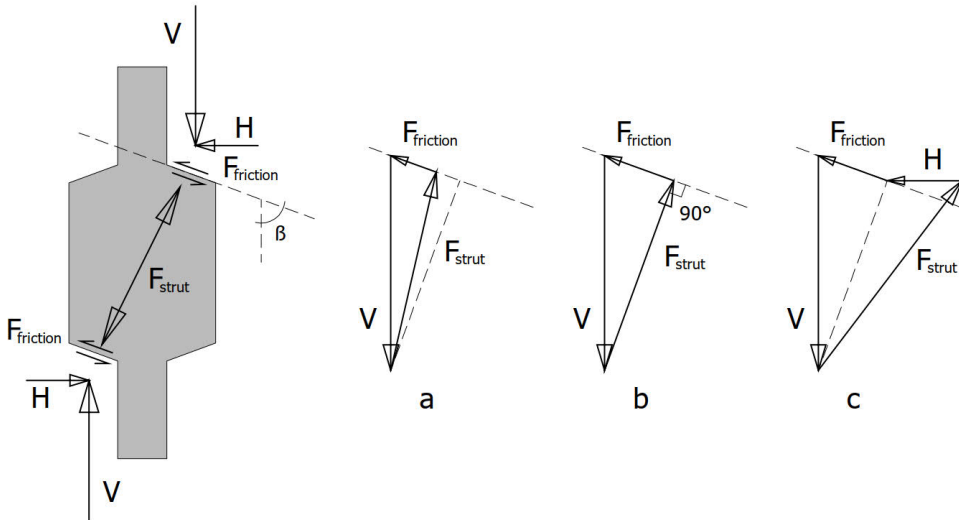
Figure 2.15: Shear friction capacity of compressed sloped interface, Cholewicki (1971) and Van (2019)

2.5.4   Shear stiffness

The shear stress-displacement diagram displayed in figure 2.13 provides a shear stiffness for the connection. The tangent stiffness changes along the shear stress-displacement relationship. The shear stiffness k is often simplified by a linear or

multi-linear approximation of the connection behaviour displayed in figure 2.16. The mortar connection is seen as a square piece of mortar that displaces with a displacement δ into a parallelogram because of the shear stress τ. Then the secant shear stiffness k [typically N/mm^3] is defined as:

$$k = \frac{\tau}{\delta} \tag{2.1}$$
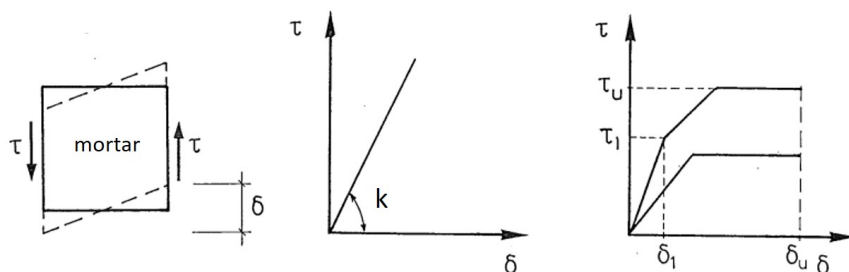
Figure 2.16: Modeling the shear stiffness of a shear connection, pictures taken from Straman (1988)

2.6 Variables affecting the connection behaviour

2.6.1 Variables

The shear behaviour of a narrow profiled mortar connection depends on its lay-out and material properties. The shear key with its shape, size and number in a row influence the transfer of shear forces. Also, the mechanical properties of the joint material, the amount of transversal reinforcement and external compression are influencing variables affecting the transfer of shear forces. Research on these variables was conducted by different researchers. Hansen (1974) compiled in one table an inventory collection of the research programs conducted by different researchers. It is displayed in table 2.17. Research within this collection can be found in the following publications: Hansen (1967), Hansen and Olesen (1976), Bhatt and Nelson (1970), Cholewicki (1971), Fauchart and Cortini (1972), Backler et al. (1973) and Mehlhorn et al. (1977). The test results of newer research can be found in Eriksson et al. (1978), Abdul-Wahab (1986), Chakrabarti et al. (1988), Abdul-Wahab (1992) and Chatveera and Nimityoungskul (1994).

In the table 2.17 provided by Hansen (1974) the variable "type of joint" is defined as if the connections in the research program are tested with or without "floor joints". The floor joints refer to the precast concrete concept with concentrated tying reinforcement in the floors. The table reveals that the majority of the research is about only "wall joints". The "geometry of the joint" is subdivided in "trapeziodal", "other" and "no" shear keys. The first refers to the traditional aligned shear key lay-out

while the waved keys in figure 2.10 and others belong to the group "other". The table shows that the majority of the research is dedicated to trapeziodal shear keys. The reinforcement can be "concentrated in the floor" or "distributed over the wall joint" or can be absent. The final variabele is "loading of the joint". The joints were loaded during the tests with only a shear force or with a combination of shear and normal forces. A number of joints were loaded cyclically. The total amount of shear tests included in this table equals 654.

		R. Halasz, G. Tantow	H. Hansen	D. Pume	K. Hansen, S.Ø. Olesen / see Part 3	A.H. Mattock et al	P. Bhatt, H.M. Nelson	A. Cholewicki	B. Foure	C. Harrysson	M. Pommeret	J. Fauchart, P. Cortini	M. Pommeret	A.P. Backler, M. Baylik, M.J. Dill	G. Mehlhorn, H. Schwing et al
Reference		1	2	3	4	5	6	7	8	9	10	11	12	13	14
Type of joint	Wall joint	●	●	●	●		●	●	●	●	●	●	●		●
	Wall joint + floor joint				●					●				●	
	No joint, monolithic					●					●				
Geometri of joint	Trapeziodal shear keys	●	●	●	●		●	●		○	●	●	●	●	
	Other shear keys								●		●				●
	No shear keys	●		●			●			○	●	●			●
Arrange-ment of reinfor-cement	Concentrated in floor joint		○		●	○					●			●	
	Distributed over wall joint	●			●	●	●	●	●		●	●	●	●	
	No rein-forcement	●		●		●		●			●	●			●
Loading of joint	Shear force	●	●	○	●	●	●	●	●	●	●	●	●	●	
	Shear and normal force				○	●						●			●
	Cyclic loading				●		●						●	●	
Number of tests		27	19	36	36	66	41	30	9	35	210	15	8	32	90

Figure 2.17: Collection of research on the shear behaviour of precast concrete connections with joint concrete or mortar in by Hansen (1974)

A number of variables affecting the shear behaviour are discussed. The first variable is the shape of the keyed connection explained in next subsection. Subsequently the variables joint material, reinforcement and external compression are discussed in the following subsections.

The different types of reinforcement for vertical connections used in literature have to be clarified. Reinforcement can be internally present in the connection. Figure 2.18a displays reinforcement with the shape of hairpins crossing the connection interfaces. This type of reinforcement influences the shear behaviour by clamping forces and dowel action according to figure 2.6. The second type of reinforcement is called external reinforcement accoording to figure 2.18b. This reinforcement refers to the steel bars which do not cross the connection interfaces. These steel bars are used for laterally compressing specimens in shear tests.
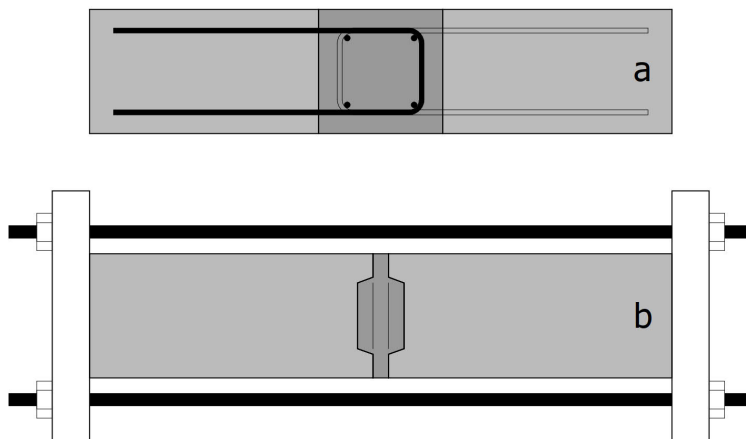
Figure 2.18: Examples of connections in specimens with "Internal" (a) and with "External" (b) reinforcement

2.6.2 Shape of the keyed connection

The influence of the angle β displayed in figure 2.19 was subject of investigation in the research of Eriksson et al. (1978). The shear behaviour of ten connections with different β-values was taken from shear tests and studied. Internal reinforcement was absent. External steel bars were slightly post-tensioned and used for keeping the connection together. Authors identified the main forces through the keyed interface as can be seen in the cutout of the front view (above, right). Shear force T and normal force N together balance the combination of N_c and T_c dependent on the angle β of the inclined interface.

The influence of the β-angle of the shear keys was investigated with the help of the shear stress-displacement diagram of figure 2.19. It shows the initial shear stiffness decreases when the angle β increases. Secondly, the researchers found different failure mechanisms at the ultimate shear stress τ_u. Specimens with $\beta \leq 55°$ (4 specimens) failed due to "cracking of the joint concrete". However, specimens with $\beta \geq 60°$ (6 specimens) failed due to "sliding of the key". In case of sliding, the shear stress T_c exceeds the shear friction resistance of the sloped interface. Finally, the diagram shows residual capacity is higher for connections with larger β-angles.
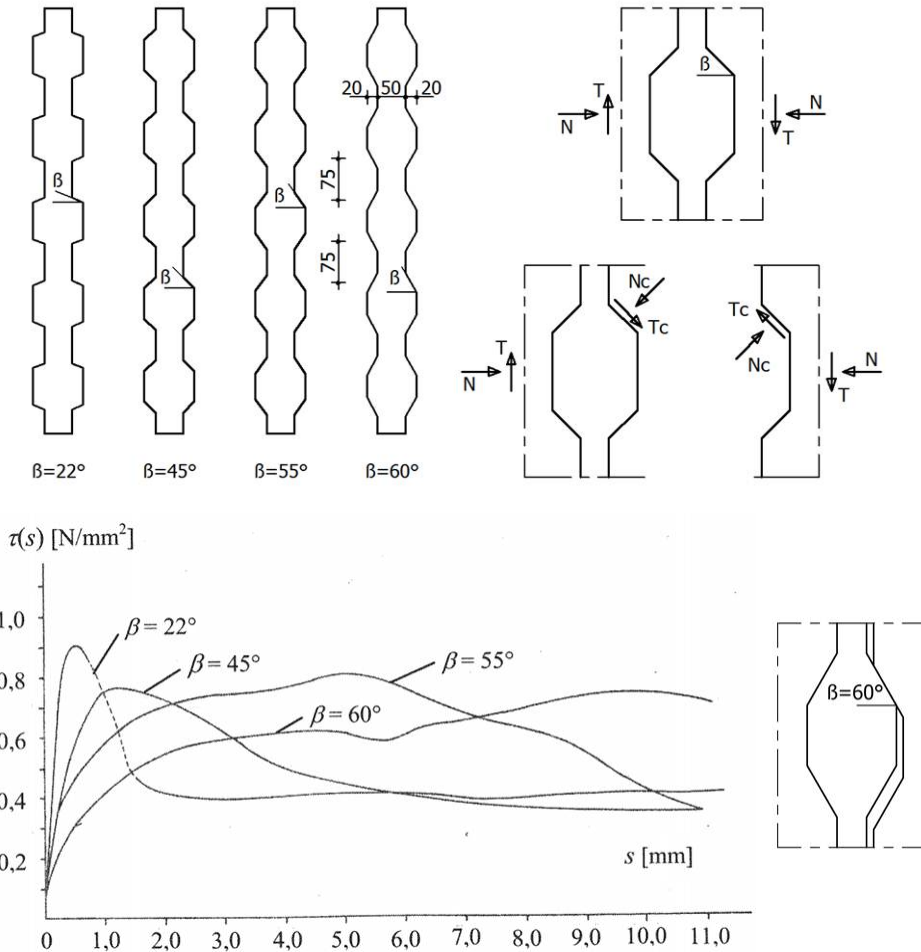
Figure 2.19: Lay-out of profiled connections (above), shear stress-displacement
            diagrams (below, left), failure mechanism "sliding of the key" (be-
            low, right) for the connections tested by Eriksson et al. (1978)

The Width (B) of the seam and the Height (D) and Depth (t) of the shear keys
displayed in figure 2.20 are relevant variables as well. Shear tests on profiled con-
nections, without internal reinforcement and changing the dimensions (B), (D) and
(t) were not found in literature. Abdul-Wahab (1986) studied these variables for pro-
filed connections with protruding lateral hairpins. Figure 2.20 displays the lay-out
of the connection and varied dimensions. The influence of the transversal reinforce-
ment on the shear behaviour of profiled connections is significant. Therefore, the
findings from this research of Abdul-Wahab (1986) are regarded to be less relevant
for the current research.

B =55-130mm (70)
t =15-50mm (25)
D =50-125mm (75)
H = 375-975 mm (825)
No. = 2-6 keys (3/5)
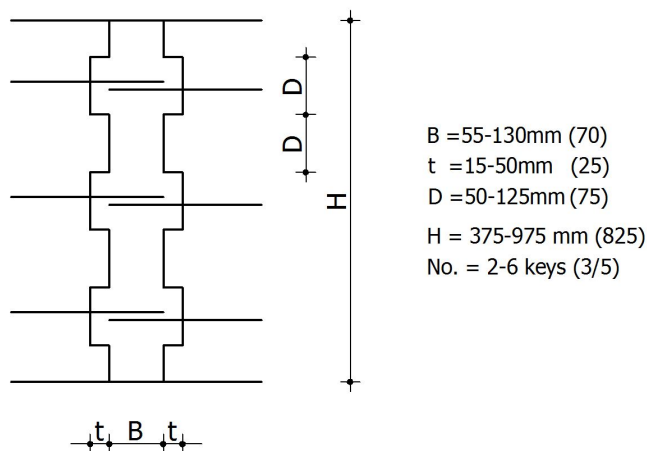
Figure 2.20: Vertical profiled connection with dimensional variables tested by Abdul-Wahab (1986)

The number of shear keys in a row of a profiled connection influences the shear behaviour. More keys can change the shear capacity and shear stiffness. Three basic different ways of increasing the number of keys were found in literature. Figure 2.21a shows the increase of shear keys by increasing the heigh h of the specimen to h1. The second way of increasing the number of shear keys is by adding shear keys within the same height h as can be seen in figure 2.21b. The third found method of increasing the number of keys is programming more and smaller shear keys in the same height 2.21c.

Abdul-Wahab (1986) studied the effect of the increase of the total height H (figure 2.21a). It was found that with an increase of the number of keys, the shear capacity of the joint increases.

In the research of Chakrabarti et al. (1988), the variable number of keys was tested as well. This variable is called "area of shear keys" in the paper according to the principle in figure 2.21b. All specimens had a height of 1,2 meter. The number of tested shear keys was 3 or 6, covering "50 or 25 percent of the overall shearing surface" as defined in this paper. This research showed the increase of 20-50% of the failure load for 6 keys compared to 3 keys.

The third way of varying the number of keys (figure 2.21c) can be found in the research of Rizkalla et al. (1989). The change in number of keys was created by changing the size of the shear key (figure 2.22). Smaller keys allow for more keys per unit of length. The idea is that smaller keys have more diagonal compression struts per meter and that it can be advantageous. However, the authors concluded that "the difference in shear key configurations considered had an insignificant effect on the behaviour or capacity of the connection".

The increase of the number of shear keys in the three different studies led to different changes of the shear capacity. It shows that the results of these studies are

incomparable because of the many mutual differences. However, the increase of keys for the connections of figure 2.21a and 2.21b results in higher shear capacities. This was demonstrated for (a) as a result of the additional connection length. Connection (b) has unused space for additional keys in the same connection height h for which the use causes an additional shear capacity. Connection (c) has to be considered as a refining the vertical connection without a clear advantage.
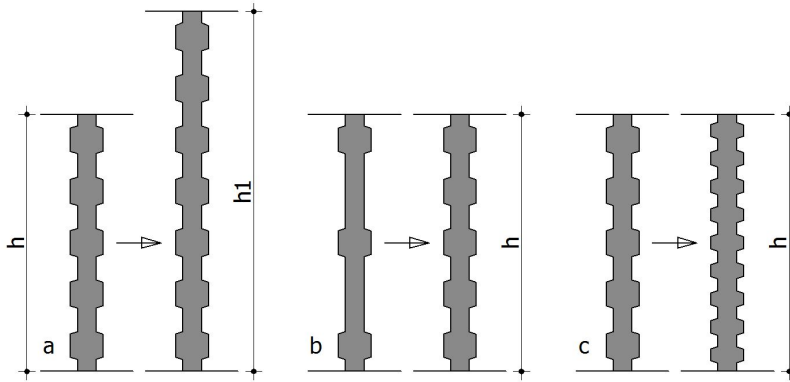
Figure 2.21: Three ways of increasing the number of keys in different research programs; increase of height of specimen from h to h1 (a), addition of identical shear keys in the same height (b), addition of smaller shear keys in the same heigth (c)
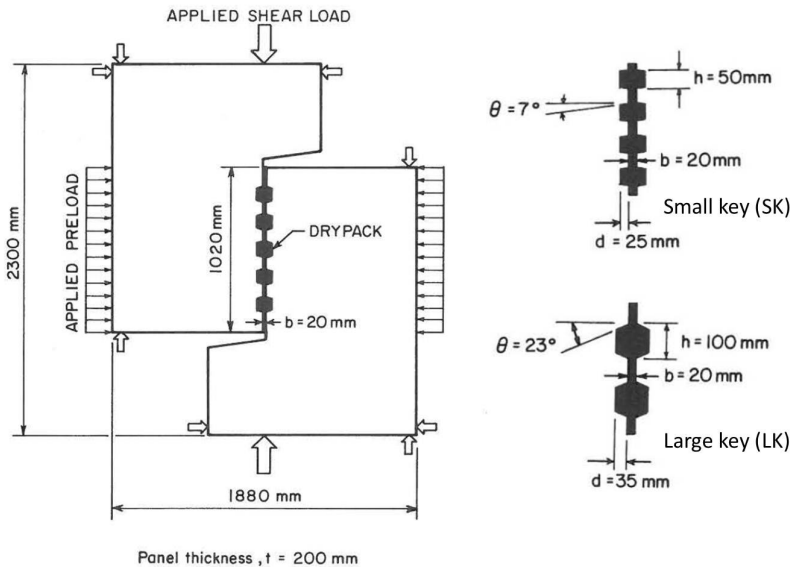
Figure 2.22: Specimen and profiled connections by Rizkalla et al. (1989)
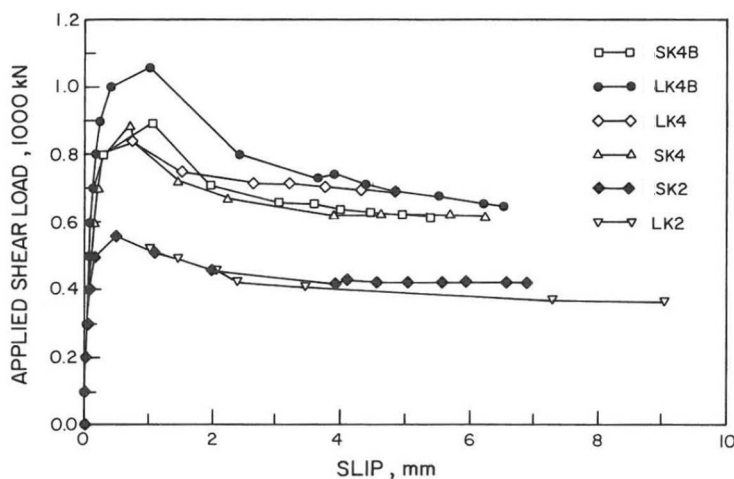
Figure 2.23: Load-displacement diagram for the research of Rizkalla et al. (1989)

2.6.3 Joint material

Chakrabarti et al. (1988), Chatveera and Nimityoungskul (1994) Cholewicki (1971), Hansen et al. (1974), Hansen and Olesen (1976) and many others studied the influence of the mechanical properties of the joint concrete on the shear behaviour of a profiled connection. They found that these material properties are decisive factors for the structural capacity of a profiled connection. Connections with higher joint concrete strength cracked and eventually failed at higher values of shear forces.

Figure 2.24a displays schematically the effect of shrinkage cracks. The joint concrete shrinks and the surrounding precast concrete deforms which may cause a crack between the joint material and the precast concrete element. Shrinkage is certainly a point of concern for outdated mortars. They shrink considerbly because of the rather simple mixtures of just sand, cement and water. Contemporary mortars shrink less as explained in subsection 2.2.1. The photos in figure 2.24(b + c) display the surface of a vertical profiled mortar connection in a real building with a mortar filling at an age of 63 days after pouring. Dilation is visually not observable in these pictures. However, dilation can occur in a precast concrete shear wall structure after these 63 days. Therefore, shrinkage cannot be neglected and has to be taken into account.

Research is published in literature on the shear behaviour of profiled connections in specimens with and without shrinkage cracks. Researchers were aware of shrinkage and defined the variable "shrinkage cracks" in their research programs. They had two options for incorporating the effect of shrinkage in their specimens. One way was that they applied a bond breaking agent to the concrete part of the interface before casting the joint concrete. This was done in the specimens of Rizkalla et al. (1989). The same shear behaviour was observed for the unbonded and bonded small key connection in this research.
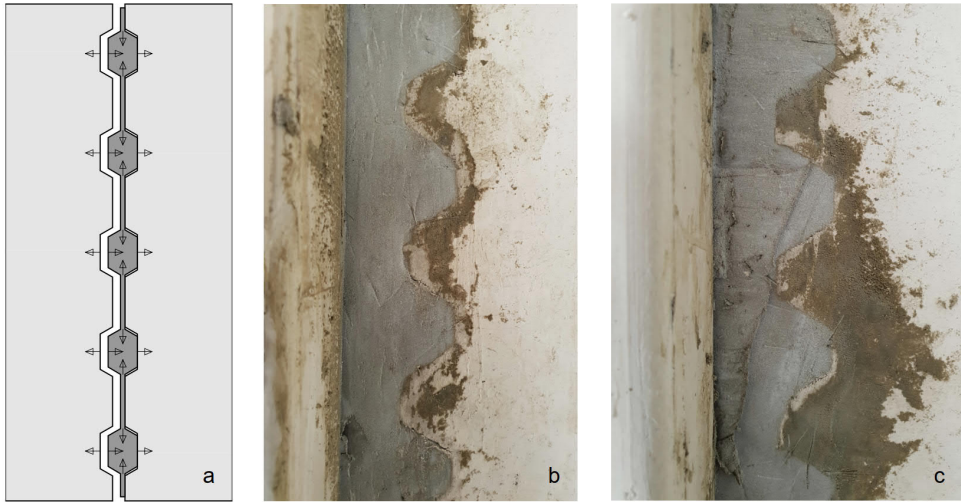
Figure 2.24: Effect of shrinkage (a) and a vertical profiled mortar connection, 63 days after pouring the mortar (b + c)

Another way is to introduce "artificial cracks" in the interface by separating both parts of the specimen a little before starting the shear test. Hansen (1967) used this method. The cracks were made by applying a coating to the joint interface area with a lime slurry before pouring the mortar. After the mortar was installed and had hardened, the elements were forced apart so that crack widths of 0,2 mm were created before testing the connection. Figure 2.25 displays the specimen, lay-out of the connection and the test results. The table shows results for connections without cracks (series 2A) and with cracks (series 2B and 2C). It shows higher failure loads per joint for the joints with artificial cracks. The joints with artificial cracks started to deform in shear just after imposing the connection to a shear force because of the interspace in the interface. The shear displacements remained initially zero for the joints without artificial cracks. At the same time, the forces in the four horizontal steel bars were substantially higher for the joints with cracks according to Hansen (1967). These forces did not increase significantly during the shear test for the un-cracked joints. Also, the precracked joints deform horizontally and vertically more. The cracked joint behaves as a more ductile shear connection.

The review of this research provides methods for representing shrinkage present in precast concrete structures in test specimens. Also, it shows to a certain extent how shrinkage effects the shear behaviour of a profiled vertical connection. A bond breaking agent did not change the shear behaviour in the research of Rizkalla et al. (1989). However, the application of artificial cracks by Hansen (1967) did influence the shear behaviour of a profiled connection.
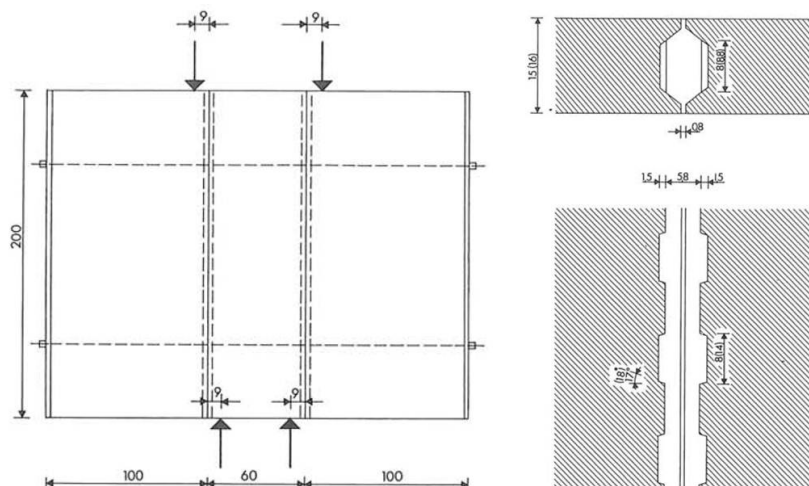
Joint	Horizontal ties	Test number	Force per joint, tons	Force per key, kg	τ_{mean} [1], kg/cm²
without crack	Ø 16 mm	2A/1	22,5	1770	7,5
		2A/2	25,5	2130	8,5
		2A/3	22,5	1770	7,5
		Mean	23,5	1970	7,8
with cracks	Ø 50 mm	2B/1	45,0	3750	15
		2B/2	40,5	3370	13,5
		2B/3	38,5	3210	12,8
		Mean	41,3	3450	13,7
with cracks	Ø 16 mm	2C/1	27	2250	9
		2C/2	29	2450	9,65
		2C/3	29,2	2440	9,45
		Mean	28,4	2370	9,45

Figure 2.25: Shear tests performed by Hansen (1967)

Fibres can be added to a cement-based joint material with the goal to improve its structural capacity. The research of Abdul-Wahab (1992) shows the effect of fibre reinforced joint concrete in castellated joints. Figure 2.26 displays an illustration of the tested specimens, a shear load-displacement diagram and the failure patterns. Four identical specimens were tested in shear. The steel fibres were "smooth drawn wires with hooked ends, high tensile steel, 30 mm long and 0,5 mm in diameter with an aspect ratio of 60". Each specimen was tested with another quantity of fibres in the mixtures. The steel fibre content (by volume) of the joint concrete was varied from 0%, 0,5%, 1,0% and 1,5% as can be seen in the diagram of figure 2.26. The researcher found a significant increase of the ultimate shear load when the amount of fibres in the joint concrete was increased.

Based on tests with control specimens, the researcher found that the amount of steel fibres had little effect on the compressive strength of the concrete. However, based on the increase of load-carrying shear capacity of the connections, Abdul-Wahab (1992) concluded that steel fibres cause an increase of the tensile strength of the joint concrete. Therefore, it can be concluded that the higher the steel fibre content used, the greater is the increase in the shear resistance of the joints.

Specimen	Fibre content	Increase of ultimate shear load V_u
B1	0,0 %	0,0 %
B2	0,5 %	26,6 %
B3	1,0 %	53,8 %
B4	1,5 %	87,3 %
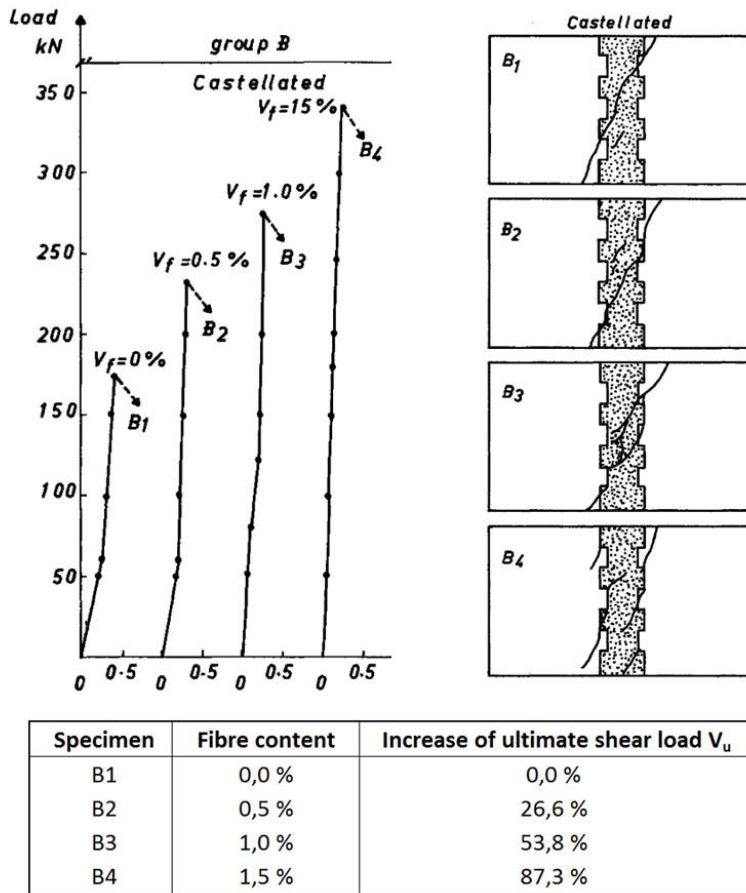
Figure 2.26: Castellated joint with fibre reinforced concrete as joint material by Abdul-Wahab (1992)

2.6.4   Reinforcement

As explained before, the transfer of shear forces via inclined compression struts goes with lateral dilation forces. These forces have to be compensated by internal or external reinforcement for acquiring vectorial equilibrium. In literature, this is called passive "confinement" in the case of external reinforcement around the specimens

clamping the connection. Research has been performed on connections without internal reinforcement and with external reinforcement by Hansen (1967), Bhatt and Nelson (1970) and Cholewicki (1971). Figure 2.25 displays the lay-out of the test specimen, the connection and measured failure loads for the research program reported in Hansen (1967). Fluid casting mortar was used as joint concrete. In the specimen drawing, the single dashed lines represent the horizontal external steel bars on both sides of the specimen. The cross-sectional area of these steel bars was varied: 800 mm^2 (4ø16 mm) and 1960 mm^2 (4ø50 mm). The steel bars were prestressed with a tensile force of 10 kN per bar before starting the shear test. Then the forces in the steel bars were reduced to 1 kN per bar after which the actual shear test started. The forces in the steel bars were not kept constant during the shear test. As a result, the actual forces in the bars changed during the shear test. The table in the figure shows the failure loads for the tested specimens. It shows that the specimens confined with steel bars 4ø50 mm possess approximately 45% more shear capacity than the ones with steel bars 4ø16 mm. Also, the paper lists the "sum of forces in the 4 steel bars" measured during the shear test. It reveals larger forces in the 4ø50 mm steel bars compared to the 4ø16 mm bars. It shows that these bars additionally compress the profiled connection because of their higher stiffnesses.

Confinement can be secured with concentrated tying reinforcement in the slabs in case of vertical profiled connections without internal reinforcement. A review on this topic will be presented separately in section 2.7.

2.6.5   External compression

Figure 2.22 shows the specimen and two profiled mortar connections which Rizkalla et al. (1989) tested. In this research program the studied variables were the "configuration of the shear keys" and the "compressive load normal to the connection". Six tests with profiled mortar connections were executed. Three of them with the small key (SK) and three with the large key (LK) configuration, as shown in figure 2.22. Two levels of compressive stresses normal to the connection (applied preload in the figure) were applied. The prestress levels (2 N/mm^2 and 4 N/mm^2) were maintained constant during the entire test. The numbers 2 or 4 in the legend of diagram (figure 2.23) indicates the applied prestress level. Two specimens were coated with a bond breaking agent for studying the influence of a possible lack of bond between the mortar and concrete. The letter B in the legend of the diagram indicates which specimens were provided with this agent. The mortar (drypack) used for these tests consisted of "two parts sand, one part normal Portland cement (Type 10) and approximately 0,2 part water" according to the authors.

The shear-displacement diagram of figure 2.23 shows the most important differences between the six profiled connections. First, it shows the influence of the compression perpendicular to the connection. The ultimate shear capacity is, according to the authors, about 60% higher for the preload of 4 N/mm^2 when compared to 2 N/mm^2. This increase in shear capacity is, according to the authors, caused by the increase of confinement and a postponed reaching of the mortar tensile strength.

Secondly, the shear behaviour of the small and large key connections display approximately the same shear load-displacement diagram when the connection is kept in a constant compressive state. Also, the ultimate shear capacity of the joint is approximately equal. The authors concluded that the key configuration had no effect on the shear capacity of the connection.

2.7 Vertical connections with concentrated tying reinforcement

2.7.1 Precast concrete concept

As stated before in chapter 1, for the vertical mortar connection to be developed, the precast concrete concept of unreinforced vertical connections with concentrated tying reinforcement in the slabs could be usable. Different precast concrete design books (e.g. *fib* bulletin 74 (2014), Steinle et al. (2019)) suggest the application of this concept. They refer to the research published by several researchers including Cholewicki (1971) and Mehlhorn and Schwing (1977). Figure 2.27 displays how it is suggested. This concept however, is still not frequently applied in practice. Structural engineers choose usually for the variant with distributed reinforcement like hairpins or wire loops over the height of a vertical connection.
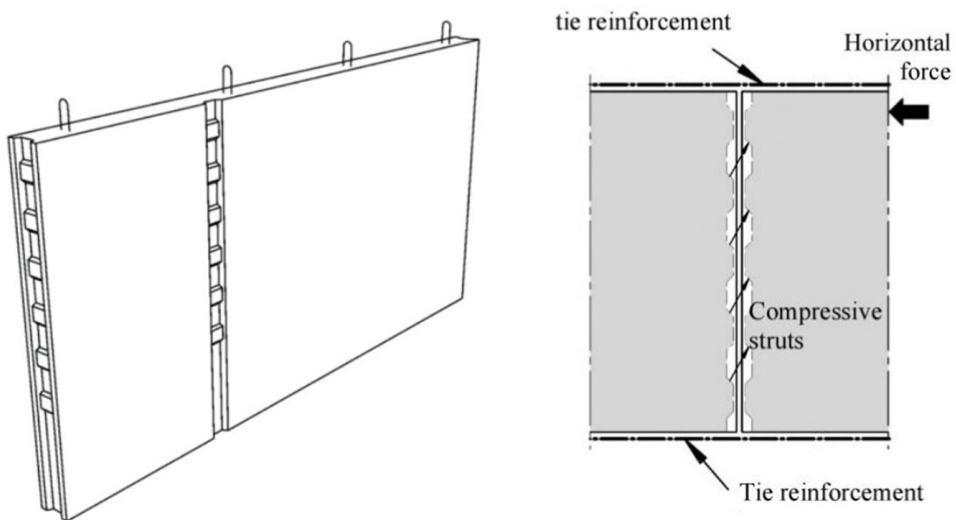
Figure 2.27: Concept of profiled vertical connections with concentrated tying reinforcement in the slabs, suggested in *fib* bulletin 74 (2014)

The design books comment on the precast concrete concept to instruct the readers. It is noticed that dowel action of the cast-in-place reinforced slabs is often neglected in structural design. Furthermore, it is warned that vertical connections without distributed hairpins tend to crack in the mortar-to-concrete interfaces. Figure 2.28a illustrates this for a T-connection between two walls. The left wall could bend to an extent that it disturbs the transfer fo shear forces between both walls. Figure 2.28b gives an instruction for the structural engineer to limit the functioning height next to a door opening to height L_w.
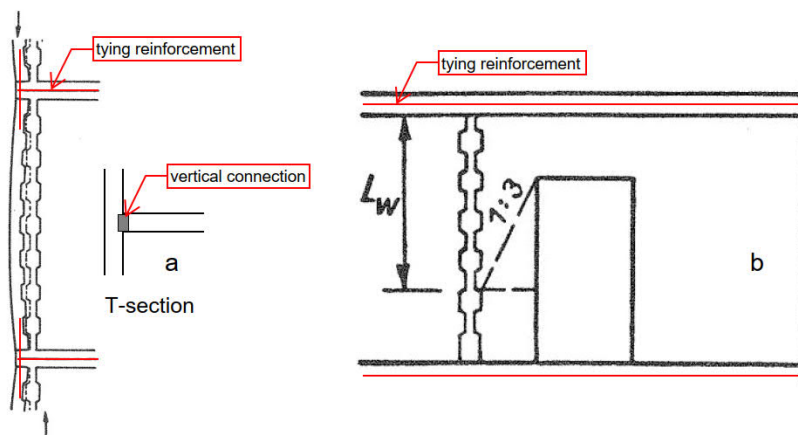
Figure 2.28: Lateral displacements at T-sections (a) and functioning length L_w near openings (b) according to Mehlhorn and Schwing (1977)

2.7.2 Research program Hansen and Olesen (1976)

The shear behaviour of vertical connections explained in previous sections is obtained from specimens that contain just a small part of the entire storey high vertical connection. The test results provide information of local shear behaviour on the Micro level. Information on the precast concrete concept can be taken from specimens with storey high connections including the concentrated tying reinforcement in the slabs. Shear tests on this type of specimen are performed in three research programs according to table in figure 2.17. The research presented by Hansen and Olesen (1976) is reviewed in this subsection. Figure 2.29 displays the specimen in a test setup used for performing shear tests. The specimens include a storey high "wall joint" and two "deck joints" in which the concentrated reinforcement is included. The vertical connections and the slabs were constructed half-scale (scale 1:2). The goal for the research was to test vertical connections as close as possible equal to conditions in actual Danish building practice. It is presumed that the lateral stiffness is provided mainly by the reinforcement of the deck joint.

Specimens including both, wall and deck joints, and specimens with only wall joints and specimens with only deck joints were tested. The goal of this collection

of tests was to identify the shear behaviour of the wall and deck joints separately as well as when they interact with one another. In case the deck joints were not programmed, still the concentrated reinforcement is required for clamping the wall joints together. In these specimens, the deck joint concrete was partly left out according to the detail in figure 2.29 where it is designated as "left open in tests with wall joints". It resulted in the elimination of dowel action of the reinforced concrete deck joint. In specimens for testing the behaviour of just deck joints, the joint concrete was left out in the wall joints.

Figure 2.29: Test setup for shear tests on vertical connections with tying reinforcement in the slabs by Hansen and Olesen (1976)

The concrete wall elements were constructed horizontally. The joint concrete was cast two days after casting the wall elements. The keyed surfaces of the wall joints received no treatment after demoulding. As a result, remains of formoil could have been left behind. Vertical loads from above this storey were simulated with stressed vertical steel bars around the test specimen as displayed in figure 2.29. The figure displays the supports of the specimen in the test setup as well. The authors stated that "no moment will occur in a vertical section through the wall joint. The supports ensure that horizontal forces cannot be transferred to the specimen through the load distributing beam or the test slab".

The researchers have chosen to keep the geometry of the wall joint the same for the entire research program. The variables included in the research program are displayed in table 2.1. The variables were selected from a practical range with the goal to remain close to Danish building practice in the year 1976.

Test no	Wall joint	Floor-wall joint	σ_b'			F_d			F_v			Horizontally prestressed σ_x	Shrinkage introduced	Repeated, alternating loads
			Low	Medium	High	Low	Medium	High	Low	Medium	High			
01	x				x	x								
04	x		x				x							
18	x			x			x							
02	x				x		x							
05	x				x		x							
03	x				x			x						
29	x		x					x						
14	x			x			x							
12	x			x			x							
13	x			x				x						
23	x			x					x					
25	x			x						x				
27	x		x								x			
29	x		x								x			
24	x			x					x					
26	x			x						x				
08	x		x									x		
07b	x		x									x		
07a	x		x									x		
72	x			x			x						x	
19	x				x		x						x	
22	x				x		x						x	
00	x				x		x						x	
20	x			x				x					x	
15	x			x			x							x
16	x			x			x							x
17	x			x			x							x
42		x		x			x							
43		x	x					x						
61	x	x		x			x							
71	x	x			x		x							
62	x	x		x				x						
70	x	x		x				x						
65	x	x			x			x				x		
66	x	x		x				x				x		
73	x	x		x				x					x	

Table 2.1: Research reported in Hansen and Olesen (1976)

The selected variables were:

- **Strength of the joint concrete** (σ'_b) for the wall and deck joint; three concrete strength levels were set:
  - low ($\sigma'_b < 20\,\text{N/mm}^2$),
  - medium ($20\,\text{N/mm}^2 < \sigma'_b < 30\,\text{N/mm}^2$) and
  - high ($\sigma'_b > 30\,\text{N/mm}^2$);

- **Reinforcement** of the wall joint (F_v) and deck joint (F_d); the wall joint reinforcement were hairpins protruding from the walls and distributed over the height of the wall joint according to figure 2.30a. The reinforcement of the deck joints were two or four straight steel bars as displayed in figure 2.29. Three "areas of reinforcement" ranges were defined and applied:
  - low ($F < 150\,\text{mm}^2$),
  - medium ($150\,\text{mm}^2 < F < 350\,\text{mm}^2$) and
  - high ($F > 350\,\text{mm}^2$) for the wall and deck joints.
  The reinforcement had plain, mild, steel surfaces with yield strengths between $250\,\text{N/mm}^2$ and $400\,\text{N/mm}^2$;

- **Horizontal prestress** (σ_x) of the wall joint; twelve horizontal steel bars (six on each side of the specimen) were distributed over the heigth of the wall joint according to figure 2.30b. They were used as external reinforcement for the application of a horizontal prestress. Three prestress levels σ_x applied to the specimens were $0{,}7\,\text{N/mm}^2$, $1{,}0\,\text{N/mm}^2$ and $2{,}7\,\text{N/mm}^2$. The steel bars were "furthermore prestressed through springs so that the prestressing force could be regarded as constant within the expected range of horizontal movements between the wall elements" according to Hansen and Olesen (1976). Five specimens of the entire research program were prestressed.

- **Shrinkage of the wall joint**; crack widths of between $0{,}5$ mm and $1{,}5$ mm were applied actively after casting and before testing to imitate shrinkage in the interfaces. This was done by separating the wall elements before the deck joint was cast. Five specimens were precracked for imitating shrinkage.

- **Effect of repeated shear loading with alternating direction**; The maximum shear load in each cycle was approximately 50% higher than the cracking load. After 20 cycles the shear load was increased to failure.

Figure 2.30: Internal reinforcement of the wall joint (a) and external steel bars for horizontal prestress (b) used by Hansen and Olesen (1976)
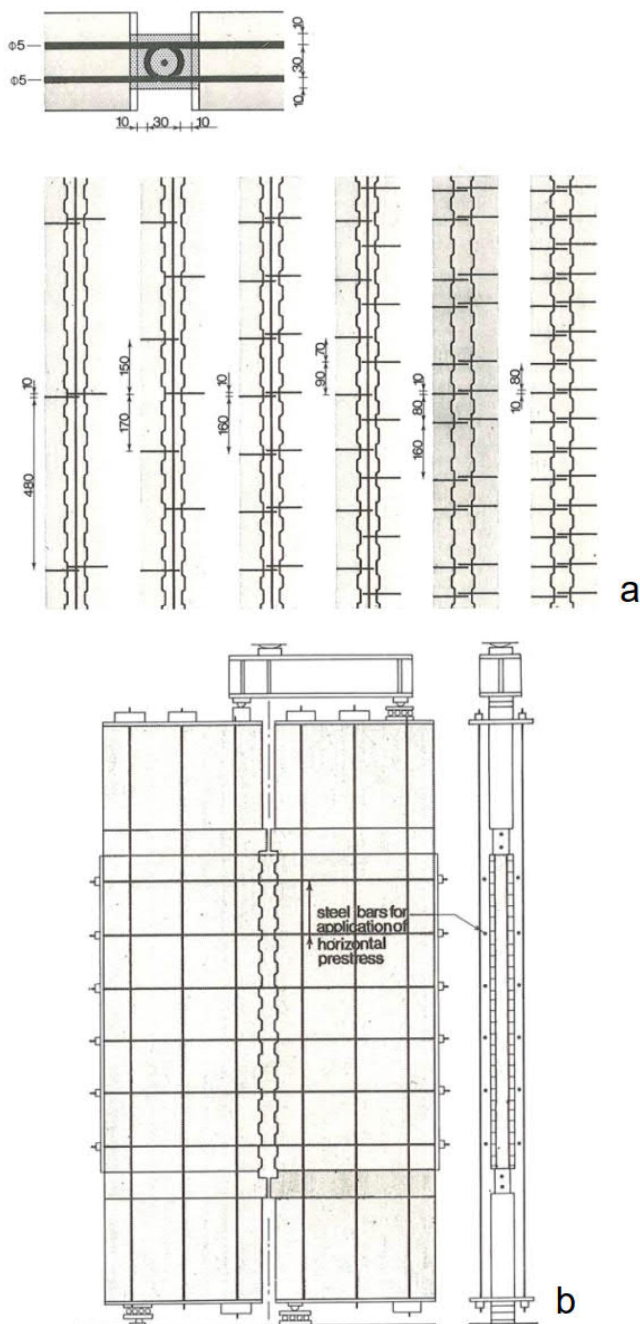
2.7.3 Evaluation research Hansen and Olesen (1976)

The research conducted by Hansen and Olesen (1976) will be reviewed. The test results of only wall joints, only deck joints and the combination of wall and deck joints including the relevant variables will be analysed. Also, the differences between distributed and concentrated tying reinforcement for wall joints will be discussed. Finally, the effect of the contribution of the concrete dowel to the transfer of shear forces via the wall joint will be identified.

Wall joints. Twenty seven shear tests were performed on specimens with only wall joints. A large number of load-displacements diagrams including the measurements are reported. The observed shear behaviour is in accordance with the principal shear behaviour explained in subsection 2.5.2 and the effects of the changed variables will be explained below.

The test results of four specimens (nr. 04, 18, 02 and 05) in table 2.2 are used for investigating the effect of the **strength of joint concrete** (σ'_b). For the concentrated tying reinforcement (F_d) in the deck joint were four steel bars ø8 ($F_d = 201$ mm^2) constructed in all four specimens. The increase of the joint concrete strengths σ'_b resulted in increasing shear force capacities Q_c (crack) and Q_u (ultimate). The table displays shear stiffnesses K2/3 which is defined as the secant shear stiffness at a shear force of 0,67Q_u . The stiffnesses K2/3 for three of the four tests did not change significantly.

The influence of the **amount of reinforcement in the deck joint (F_d)** on wall joints can be observed from the test results of specimens 01, 18, 02, 03 and 29 in table 2.3. These specimens were constructed without wall reinforcement. The table shows approximately a constant shear capacity up to the cracking load Q_c and increasing ultimate shear capacities Q_u for the first four specimens. The results of specimen 29 deviates. This has to be attributed to the substantial lower strength of the joint concrete σ'_b. The development of the shear stiffnesses K2/3 relates to this strength as well. A dependency on the amount of reinforcement F_d can barely be observed.

Specimens 08, 07b and 07a were used for investigating the effect of **horizontal prestress** (σ_x). Table 2.4 displays the test results. The cracking load Q_c of connection 07b would be expected to be higher than the of connection 08 because of the higher prestress. However, the level of compression stays close to one another which can easily result in such a deviation in the cracking load. The table shows an increase of the ultimate shear load Q_u for increasing compressed wall joints. It seems that the maximum load in the test setup in the structures laboratory equals 323 kN. It only shows that the connection was not cracked and did not reach the ultimate shear capacity. The effect of prestress on the shear stiffness can be observed in the table as well. The shear stiffnesses K2/3 are about ten times higher than for uncompressed wall joints. This analysis shows the beneficial effects of keeping vertical connections compressed. The shear capacities and stiffnesses of compressed vertical connections are higher.

Nr.	σ'_b	F_d	Q_c	Q_u	K2/3
	N/mm^2	mm^2	kN	kN	N/mm^3
04	**16**	201	39	78	7,2
18	**27**	201	69	110	15,0
02	**32**	201	73	171	13,0
05	**53**	201	107	203	15,0

Table 2.2: Results of specimens with increasing "strength of joint concrete"

Nr.	σ'_b	F_d	Q_c	Q_u	K2/3
	N/mm^2	mm^2	kN	kN	N/mm^3
01	16	**77**	78	104	8,4
18	27	**201**	69	110	15,0
02	32	**201**	73	171	13,0
03	32	**452**	78	188	13,0
29	17	**616**	58	130	9,7

Table 2.3: Results of specimens with increasing "concentrated reinforcement"

Nr.	σ'_b	F_d	σ_x	Q_c	Q_u	K2/3
	N/mm^2	mm^2	N/mm^2	kN	kN	N/mm^3
08	19	2413	**0,7**	196	196	108
07b	18	2413	**1,0**	171	217	250
07a	18	2413	**2,7**	>323	>323	180

Table 2.4: Results of specimens with increasing "horizontal prestress"

Table 2.5 displays the results of shear tests with and without **Introduced Shrinkage** (I.S.) as variable. The test data from specimens with approximately the same concrete strength and the same amount of concentrated reinforcement F_d are collected for comparison. The initially applied interface cracks were between 0,5 mm and 1,5 mm. The shear loads Q_c at cracking of the joint concrete were in the range between 53 - 78 kN. It seems that they crack at approximate the same shear force. Wall joints without "introduced shrinkage" possess a little more ultimate shear capacity Q_u. It shows only a small decline as a result of the interface cracks. The shear stiffnesses K2/3 are lower for the wall joints with initial cracks widths of between 0,5 mm and 1,5 mm.

Deck joints. Two specimens (42 and 43) were equipped with only reinforced concrete deck joints. Table 2.6 displays the test results of these joints. The shear capacities are about one third of the shear capacities of specimens with only wall joints (e.g. specimen 02 in table 2.5). Two amounts of reinforcement (F_d) were applied: 201 mm^2 and 452 mm^2. They influence the measured shear stiffness K2/3: 1,7 N/mm^3 compared to 3,6 N/mm^3.

Nr.	σ'_b N/mm^2	F_d mm^2	I.S. mm	Q_c kN	Q_u kN	K2/3 N/mm^3
18	27	201	-	69	110	15,0
02	32	201	-	73	171	13,0
03	32	452	-	78	188	13,0
72	23	201	**1,0**	69	139	2,2
19	30	201	**0,5**	73	147	7,7
22	33	201	**0,5**	53	147	7,7
20	31	452	**1,5**	69	131	2,9

Table 2.5: Results of specimens with and without "Introduced Shrinkage (I.S.)"

Nr.	σ'_b N/mm^2	F_d mm^2	Q_c kN	Q_u kN	K2/3 N/mm^3
42	21	201	16	49	1,7
43	19	452	16	49	3,6

Table 2.6: Results of specimens with "deck joints"

Wall and Deck joints. The number of specimens including both wall and deck joints equals seven. Table 2.7 displays the test results of this series. Internal reinforcement (F_v) was not present in the wall connection. The increase of deck joint reinforcement F_d results in an increase of the shear capacity compared to the same wall joints without concrete deck joints. The shear stiffnesses increase a little as well. It shows a modest contribution of the concrete in the deck joints. Cracks were introduced in specimen 73 for studying the influence of shrinkage. It revealed less shear capacity and a substantial less shear stiffness K2/3. The shear stiffness of specimen 73 (with Introduced Shrinkage) is about one tenth of the specimen without "shrinkage".

Distributed versus concentrated reinforcement for Wall joints. Table 2.8 displays the test results of wall joints with only distributed (F_v) or only concentrated (F_d) reinforcement. The concrete and reinforcement in the deck were absent in the

case of wall joints with distributed reinforcement. The concrete in the deck joints was interrupted for wall joints with only concentrated reinforcement according to the detail in figure 2.29. The amounts of reinforcement (F) in table are increasing from top down. This collection of joints allows the comparison of both reinforcements for wall joints.

The joint concrete strength (σ'_b) and the amount of reinforcement (F) both influence the shear loads Q_c and Q_u. It seams likely that the influence of the joint concrete dominates. At the same time, a higher amount of reinforcement increases the shear loads as well. However, the type of reinforcement (distributed or concentrated) does not change significantly the shear load capacity Q. This is not true for the shear stiffness K2/3. They are between 7,2 and 15,0 N/mm^3 for wall joints with concentrated reinforcement. They are approximately between 17,0 and 59,0 N/mm^3 for specimens with distributed reinforcement. The statistical spread is large for the latter and most of them remain below a shear stiffness of 20,0 N/mm^3. It shows that the shear stiffness is a little higher for wall joints with distributed reinforcement.

Nr.	Type joint	σ'_b	F_d	F_v	I.S.	Q_c	Q_u	K2/3
		N/mm^2	mm^2	mm^2	mm	kN	kN	N/mm^3
61	wall + deck	22	201	-		74	162	18,0
71	wall + deck	29	201	-		65	179	17,0
62	wall + deck	22	452	-		81	208	21,0
70	wall + deck	27	804	-		122	245	21,0
65	wall + deck	29	452	-		130	>173	<200
66	wall + deck	21	804	-		107	239	33,0
73	wall + deck	24	452	-	x	81	154	2,2

Table 2.7: Results of specimens with wall and deck joints

Nr.	σ'_b	F_v	F_d	Q_c	Q_u	K2/3
	N/mm^2	mm^2	mm^2	kN	kN	N/mm^3
01	29		**77**	78	104	8,4
23	31	**117** (6ø5)		77	139	31,0
24	26	**117** (6ø5)		60	105	59,0
04	16		**201**	39	78	7,2
18	27		**201**	69	110	15,0
02	32		**201**	73	171	13,0
25	24	**275** (14ø5)		103	216	17,0
26	24	**275** (14ø5)		141	167	190,0
27	15	**433** (22ø5)		53	179	18,0
03	32		**452**	78	188	13,0
28	13	**590** (30ø5)		152	>200	<120

Table 2.8: Comparison distributed and concentrated reinforcement

Additional contribution of Deck joints to Wall joints. In table 2.9 the test results of specimens with only wall joints and with both wall and deck joints transferring shear forces are presented. Only concentrated reinforcement (F_d) was installed in the deck joints. The distributed reinforcement in the wall joints (F_v) was absent. A comparison could reveal the influence of full deck joints when they are added to wall joints. Again, the amounts of reinforcement (F_d) in table are increasing top down.

The joint concrete strengths (σ'_b) differ a little. It influences the proposed comparison. The table shows that the shear loads Q and stiffnesses K2/3 are higher for specimens with both wall and deck joints. However, the deck joints do not significantly increase the overall joint properties. It shows the shear capacity and stiffness relies mainly on the wall joints. The contribution of the concrete deck joints is small.

Nr.	Type joint	σ'_b	F_d	F_v	Q_c	Q_u	K2/3
		N/mm^2	mm^2	mm^2	kN	kN	N/mm^3
18	wall	27	201	-	69	110	15,0
02	wall	32	201	-	73	171	13,0
61	wall + deck	22	201	-	74	162	18,0
71	wall + deck	29	201	-	65	179	17,0
03	wall	32	452	-	78	188	13,0
62	wall + deck	22	452	-	81	208	21,0
29	wall	17	616	-	58	130	9,7
66	wall + deck	21	804	-	107	239	33,0

Table 2.9: Results with increasing "amount of concentrated reinforcement"

2.8 Concluding remarks

This literature review demonstrates that the unreinforced version of a profiled vertical mortar connection fits to the assumptions proposed in this thesis. It could be incorporated in the existing precast concrete concept with concentrated tying reinforcement in the slabs. This concept was to some extent investigated on Meso level according to figure 1.7 by Hansen and Olesen (1976). Furthermore, the storey-high application on Macro level (e.g. shear walls) requires additional examination.

It appears that the profile of the interfaces, the joint material and lateral compression are important variables that determine the functioning of a vertical connection. These have to be included in the research program to the extent that they are relevant for a storey-high application of the vertical mortar connection in precast concrete shear walls. The specimen type that was used by Rizkalla et al. (1989) is often taken for performing shear test. This version is the preferred specimen for examining the shear behaviour of profiled mortar connections in this thesis.

Chapter 3

Mortar Connections and Structural Variables Examined

3.1 Introduction

This chapter describes the mortar connections selected for investigation in this thesis. In section 3.2 considerations for the selection are given. These are the starting points for the development of the intended vertical mortar connections. Section 3.3 outlines the actual five selected connections. A number of structural variables like the "type of mortar" are determined for the indentification of the shear behaviour in different applications or circumstances. They relate to the implementation of the storey-high vertical mortar connections in real precast concrete shear wall structures and are described in section 3.4. In the final section 3.5 it is described which variables are selected for investigation for each of the five mortar connections.

3.2 Considerations for the selection of mortar connections

A set of considerations for the mortar connections and structural variables is compiled in this section. They are used for composing the research program of mortar connections and variables to be investigated.

- The narrow vertical mortar connections have to be filled with thixotropic mortar which can be inserted with a mortar pump. This way of applying the mortar in vertical seams has important advantages over other insertion methods as discussed in the previous chapters.

- It is the intention to develop vertical mortar connections with considerable shear capacities and high shear stiffnesses at the same time. Therefore it is ex-

pected that they have profiled (shear keyed) shaped mortar-to-concrete inter-
faces. Reinforcement crossing the mortar-to-concrete interfaces is not allowed
because it hinders insertion with a mortar pump. The old concrete surfaces
could be roughened with one of the roughening methods available in concrete
factories. Fibres can be added to the mortar with the goal to improve the con-
nection behaviour.

- Prediction of the connection behaviour requires sufficient information to be
  taken from tests. Therefore, the shear capacity, shear stiffness, material proper-
  ties and cracking behaviour of the investigated vertical connections have to be
  identified.

- Information about the circumstances in which the vertical connections in pre-
  cast concrete structures function have to be incorporated in the research pro-
  gram. The lateral stiffness and lateral compression should be varied in order
  to study the connection behaviour under different external circumstances.

- The profiles and old-to-new concrete interfaces of the vertical mortar connec-
  tions should preferably be designed to function with minimal lateral com-
  pression and minimal lateral stiffness required for maximal functioning. The
  reason is that such boundary conditions may be limited available in precast
  concrete shear wall structures.

- Vertical mortar connections have to be installed in specimens for the identi-
  fication of their shear behaviour. The literature chapter has shown that shear
  tests can be performed with a limited number of shear keys in a row, clamped
  together with external steel bars in a small scale specimen.

3.3   Mortar connections for shear transfer

3.3.1   Overview of selected mortar connections

The five connections selected for the research are displayed in figure 3.1. They are re-
spectively called the Aligned shear key connection, the Staggered shear key connec-
tion, the Aligned small shear key connection, the Plain waterjetted shear connection
and the Serrated waterjetted shear connection. Each of these connections is outlined
and explained in the next subsections.

3.3.2   Aligned shear key connection

The Aligned shear key connection of figure 3.1a is for the generally applied wider
connections the most applied connection and therefore selected for the research pro-
gram. The Aligned shear key connection has two recesses opposite to each other and
is reshaped for a mortar version for this investigation. The manufacturability as well
as structural principles determine the lay-out of this connection. The narrow vertical
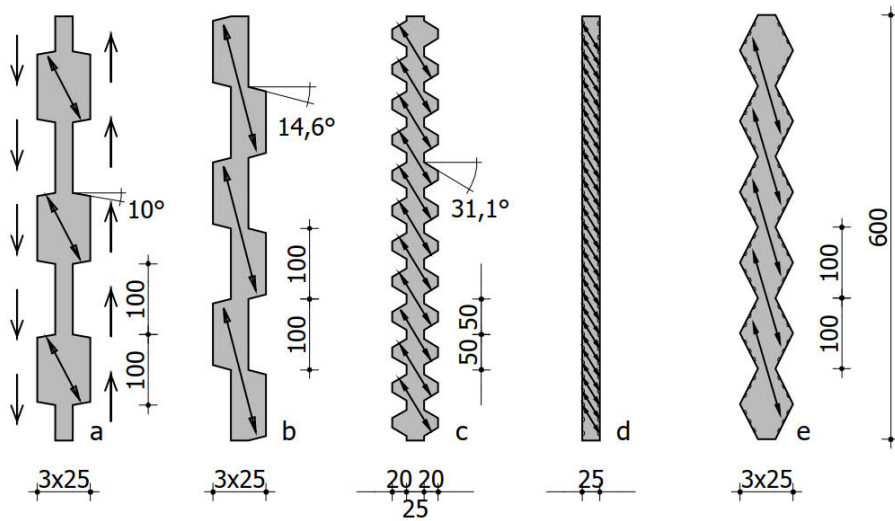
Figure 3.1: Selected vertical mortar connections (measures in mm); Aligned shear key connection (a), Staggered shear key connection (b), Aligned small shear key connection (c), Plain waterjetted shear connection (d), Serrated waterjetted shear connection (e)

seam has a thickness of 25 mm as can be seen in the figure. The depth of the key is 25 mm. The maximum thickness of the mortar in the seam is 3x25 mm=75 mm. The height of the key is 100 mm. Mortar with traditional a maximum aggregate size of between 0,5 mm and 2,0 mm can be used for this connection with these dimensions.

In subsection 2.5.2 the basic structural behaviour of profiled connections is explained. There it is shown that the main load carrying mechanism is the compression strut which transfers the shear forces via the mortar (figure 3.2a). The shear force direction can reverse in precast concrete stability structures. Therefore, the connection requires compression struts for positive as well as negative shear forces as can be seen in the figure. The compression strut has a cross-sectional area A_c (figure 3.2b). Diagonal cracks occur at a certain value of the shear force. The shear force at cracking can be postponed to a higher shear force by selecting a steeper compression strut (lower angle α in figure 3.2b). Also, a steeper compression strut reduces the horizontal force H that has to be compensated by the structure around the connection. However, steeper struts result in less shear keys per meter. This reduces the shear capacity since less keys per meter are available for transferring forces. Therefore, an optimal ratio between a small angle α and maximum number of keys per meter is selected for the Aligned shear key.

The influence of angle β in figure 3.2b-d is discussed in subsection 2.6.2. Connections to be developed and investigated in this research program are intended to behave initially stiff in shear and with a high shear capacity. This will probably not be reached with the profile of figure 3.2d (β ≥ 90°). This profile has the change to fail by the mechanism "sliding off the sloped abutment surface" according to figure 2.14d. The profile of figure 3.2b with β ≤ 90° is selected for this research program with the goal to prevent an early sliding off the sloped interface. The failure mechanism "shearing off the key" in figure 2.14c is espected for the aligned shear key connection. This shearing off can occur for the mortar as well as the precast concrete as displayed by the dashed line in figure 3.2e. The mortar used for this research program is approximately of the same grade as the concrete for the precast concrete elements. Thus, the material properties (compressive strength, tensile strength, etc.) are more or less the same. This is why the heights h1 and h2 in the figure are chosen approximately equal to each other. Different heights will result in an earlier shearing off of the lowest shear key.
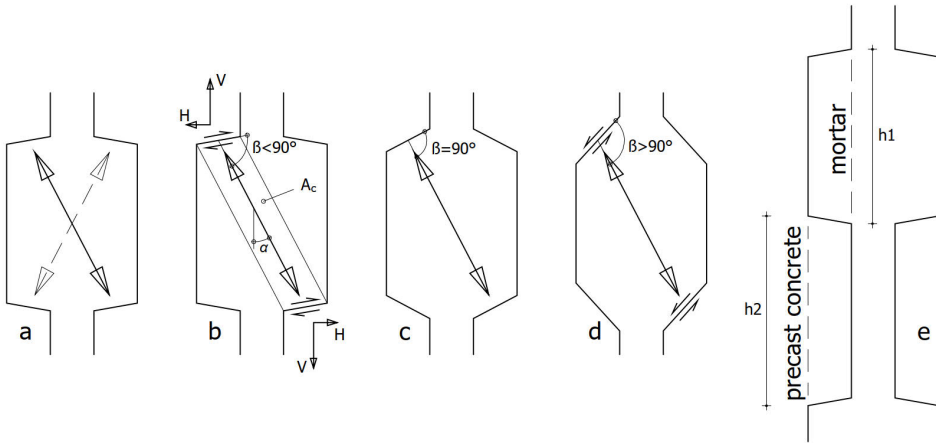
Figure 3.2: Aligned shear key connection

3.3.3 Staggered shear key connection

The Staggered shear key connection in figure 3.1b resembles the previous connection. This type of connection is suggested in Elliott (2011). The shear key recesses are now staggered instead of aligned positioned. Again, compression struts can arise for positive as well as negative shear forces (figure 3.3a). The main benefit of this connection is the steeper compression strut since angle α is smaller than present in the Aligned shear key connection. The benefit is further that the horizontal force H to be compensated by the surrounding precast concrete structure is lower for the same shear force to be transferred. An angle β = 90° was chosen for the abutment surface with the goal of to avoid the failure mechanism "sliding off the sloped abutment

surface". The failure mechanism "shearing off the key" is expected for the ultimate shear capacity. Again, heights h1 and h2 in figure 3.3c are chosen equal to each other because the mortar and the precast concrete are approximately of the same concrete strength for the same reasons as described in the previous subsection.
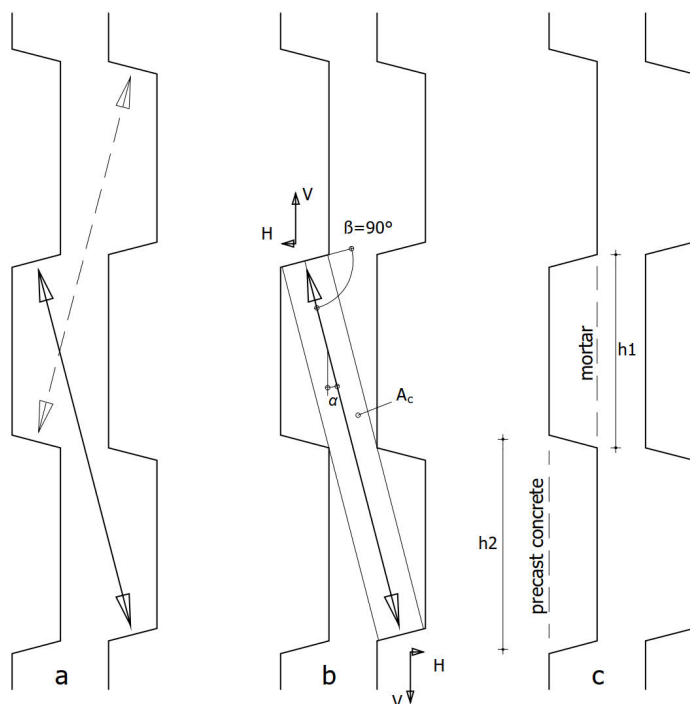
Figure 3.3: Staggered shear key connection

3.3.4 Aligned small shear key connection

Figure 3.4 shows the previously selected Aligned shear key connection (a) and the Aligned small shear key connection (b-c). The small key connection (b) has considerably more compression struts per unit of connection length compared to the one with large keys (a). There are more points of contact where the shear forces can be tranferred through the mortar. This profile may be able to enlarge the shear capacity and shear stiffness of the vertical mortar connection.

The three profiled keyed connections just presented can be constructed with ribbings of wood in the edge formwork of a precast concrete large panel element. Figure 3.5 shows the wooden ribbings of the Aligned small shear key connection. Figure 3.6 shows the constructed precast concrete element released from the formwork. Both figures show that the construction of this profile in common formwork is relatively simple. Alternatively, rubber concrete stamp mats including the profile, instead of wooden ribbings, can be constructed in the formwork for multiple use.
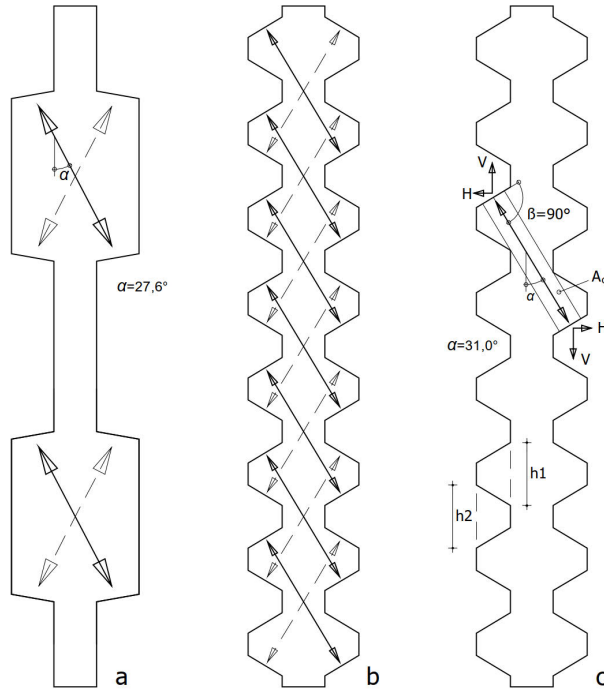
Figure 3.4: Aligned shear key connection (a), Aligned small shear key connection (b, c)

Figure 3.5: Wooden ribbings in the edge side formwork for the Aligned small shear key connection of a precast concrete large panel element

Figure 3.6: Precast concrete element with a profiled edge side for the Aligned
small shear key

3.3.5 Plain waterjetted shear connection

Figure 3.7a shows the Plain waterjetted shear connection. It consists of two plain roughened surfaces at the wall element edge sides with mortar in between. The surfaces of the edge formwork in the concrete factory are coated with a retarding agent before casting the concrete. This agent delays the concrete hardening process of the cast concrete next to the coated formwork. After casting and demouling the precast concrete element, the soft concrete at the surface is removed by waterjetting. In such waterjetted surface the coarse gravel remains in place while the cement paste and fine grained additives are disposed (figure 3.8). Fresh mortar connects very well to a waterjetted surface. The roughened surfaces are able to transfer shear forces along the entire length. In fact, there are an infinite number of diagonal struts present in the mortar and these are active in both opposite directions. This connection is likely to be able to transfer significant shear forces and behaves with a high shear stiffness. However, the application as vertical mortar connection has to be questioned. The reason is that possible small lateral displacements by the surrouding precast concrete structure can easily cause debonding of the plain interfaces and that can effect the transfer of shear forces. This connection is also selected for the research program because it relates to the vertical mortar connection discussed in the next subsection.
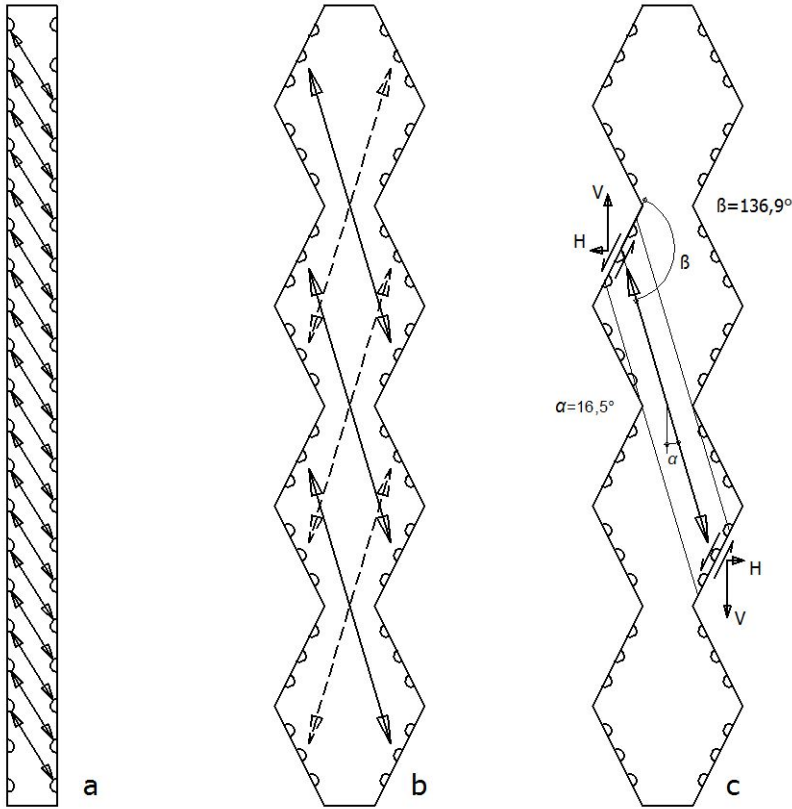
Figure 3.7: Plain waterjetted shear connection (a), Serrated waterjetted shear connection (b, c)

3.3.6   Serrated waterjetted shear connection

The profiled connection in figure 3.7b has waterjetted interfaces as in the plain waterjetted shear connection. This Serrated waterjetted shear connection combines a waterjetted interface with a profile. Compression struts can be identified (figure 3.7c). However, an infinite number of struts will be present analogous to the plain waterjetted connection. The sloped abutment surface and the compression strut are not orientated perpendicular to each other. The large angle β causes considerable shear stresses in the interface between the compression strut and precast concrete. However, the waterjetted interfaces are intended for the transfer of these large shear stresses. Because of the profile the Serrated waterjetted shear connection has approximately 10% more mortar-to-concrete interfaces are compared to the Plain waterjetted shear connection (see figure 3.8). This may result in postponing the instant of interface crack appearance in the diagram of figure 2.13. Also, the almost continuous transfer of shear stresses may result in a high shear capacity.

Figure 3.8: Shear keys for Staggered shear key connection (upper element), Serrated waterjetted shear connection (middle element) and Plain waterjetted shear connection (bottom element)

3.4 Variables affecting shear behaviour

3.4.1 Type of mortar

The influence of the type of mortar is investigated for a number of mortar connections. Two types of mortar were selected. They are a contemporary thixotropic mortar and a steel fibre reinforced mortar (SFRM) specifically designed for this research. The first one is a commonly used mortar provided by the Dutch firm Cugla BV. This mortar has the name "Cuglaton Tikso K70 mortar" which is called Tiksomortar K70 in this thesis. It is a trowel mortar according to CUR aanbeveling 24 (1991). The viscosity of this type of mortar is semi-plastic and it behaves thixotropic. A mortar with these properties can be pumped through a hose into the seam of a vertical mortar connection. The technical information of the supplier can be found in Cugla (2016). The reason for selecting this mortar is the fact that contractors use this mortar frequently for constructing mortar connections in precast concrete structures in the Netherlands. This mortar is approximately of the same strength grade (compressive strength is 70 N/mm^2) as the frequently used concrete strength grade (compressive strength is 67 N/mm^2) in precast concrete factories.

In the fibre reinforced mortar a certain amount of steel fibres is added to the same Cuglaton Tikso K70 mortar of Cugla BV. The goal of adding these fibres is in-

vestigating their influence on the mechanical properties of the mortar and the mortar connection. An improvement of the mortar properties is expected according to the research of Abdul-Wahab (1992). Moreover, an improvement of the shear capacity of a profiled vertical mortar connection with steel fibre reinforced mortar can possibly be expected. The type and amount of fibres are taken from the research conducted by Hobson (2014) which was part of this thesis work. His MSc research was initiated after the question arose which type and amount of fibres is suitable for the vertical mortar connections. With laboratory experiments the effect of different types and amounts of fibres on the mechanical behaviour of fibre reinforced mortar was investigated. Mixture S1 described in Hobson (2014) is selected for the research into the vertical mortar connections. This SFRM has a total steel fibre dosage of 30 kg/m^3. The applied steel fibres have a length of 13 mm, a diameter of 0,2 mm and a tensile strength of 2600 N/mm^2.

The ability of pressing the SFRM through a hose is tested in advance by performing a pump test. The test showed that the selected SFRM could be pumped through a hose into a vertical profiled seam. Subsection 4.2 discusses the pump test.

3.4.2 Lateral stiffness

The stiffness perpendicular to the connection will most probably to some extent effect the shear behaviour. Figure 3.9 shows the Aligned shear key connection constructed between precast concrete large panel elements as part of a precast concrete stability structure. Three fundamental assemblies are presented in this figure. Assembly (a) has two ordinary precast concrete elements positioned in line. Assembly (b) is similar but has openings for windows in the adjacent precast concrete wall elements. Assembly (c) represents a corner connection which can be part of a non-planar precast concrete stability structure.

The diagonal compression struts transfer the shear force to the adjacent precast concrete element. Lateral forces H will press against both precast concrete elements in order to acquire vectorial equilibrium in the connection. These dilation forces H operate in reversed directions and have to be compensated for keeping the vertical connection active in transferring shear forces. They find their equilibrium via the precast concrete elements and concentrated tying reinforcement present in the slabs above and below.

It is expected that the three assemblies in figure 3.9 offer different horizontal resistances for compensating the lateral forces H. The size of these resistances depends on the lateral stiffness provided by the precast concrete assemblies. The columns in assembly (b) deliver less lateral stiffness than assembly (a) because they deform more for the same force H. The corner connection possesses the lowest lateral stiffness since the transverse wall will deform horizontally the most. The concentrated tying reinforcement in the slabs influence the horizontal stiffness as well. The more amount of reinforcement the more the resistance against lateral forces H.

The lateral stiffness influences the shear capacity and shear stiffness of vertical mortar connections. Moreover, its contribution is essential for a well performing
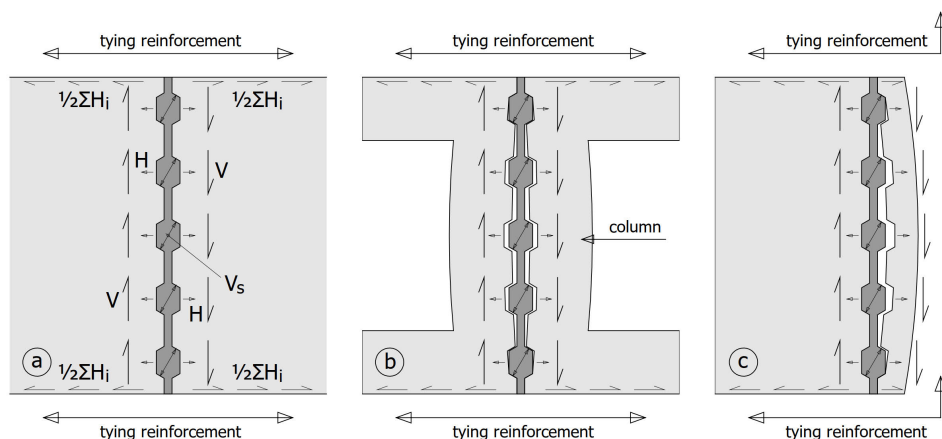
Figure 3.9: Horizontal stiffness of the surrounding precast concrete structure

vertical mortar connection. Therefore, the lateral stiffness is selected as a variable in this research program. Steel bars with three different diameters (4xM16, 4xM24 and 4xM38) were applied perpendicular to the connection around the specimen. They represent three different lateral stiffnesses which could be present in the precast concrete assemblies of figure 3.9. The lateral force in the steel bars and the horizontal deformations of the specimen are measured during the shear tests. The actual lateral stiffness can be calculated from these lateral forces and deformations afterwards.

3.4.3 Initial compression perpendicular to connection

Compression perpendicular to (profiled) mortar connections increases the shear capacity and shear stiffness as stated in the literature chapter. Horizontal mortar connections are compressed by gravity. Vertical connections are usually not compressed. They can be pre-tensioned horizontally but that is considered as less economic and generally not applied in the construction practice. However, structural engineers can select pre-tensioning as a measure for improving the structural capacity of vertical mortar connections. Therefore, compressed vertical mortar connections are relevant for less common applications. Furthermore, compression perpendicular to the connection relates to the variable stiffness perpendicular to the connection. Both variables provide compressive lateral forces for compensating the dilation forces H in figure 3.9. Studying the influence of both variables independently will reveal their individual contribution to the shear capacity. These were the arguments for selecting the variable initial compression perpendicular to the connection. Three levels of initial compression are selected. They are $0,1 \text{ N/mm}^2$, $1,0 \text{ N/mm}^2$ and $2,0 \text{ N/mm}^2$. These compressive stresses are adjusted before starting the test. The compressive stress changes due to the behaviour of the profiled mortar connection. It increases with an increasing shear force on the specimen.

3.4.4 Bonding agent in mortar-to-concrete interfaces

Profiled mortar connections transfer shear forces via adhesive bond over the entire length of the mortar-to-concrete interfaces. Figure 3.10a indicates this type of shear transfer in stage (a-b) of a shear stress-displacement diagram. The contribution of adhesive bond terminates as soon as cracks arise in the mortar-to-concrete interface of the joint. The shear desplacements in this first stage are small and the shear stiffness is high. The possibility of raising the bond strength in mortar-to-concrete interfaces is investigated with the application of a bonding agent.

Bonding agents are commonly used for old-to-new concrete interfaces in the field of repair and strengthening of concrete structures. A bonding adhesive can increase the bond strength in various types of old-to-new concrete interfaces. A bonding agent is selected in this research program for investigating its contribution to the shear capacity and shear stiffness of vertical profiled mortar connections. It is expected that the shear stress $\tau_{\text{deb};1}$ in figure 3.10a will raise to $\tau_{\text{deb};2}$ in figure 3.10b when the bonding agent is applied. The result is a higher shear stiffness ($k_{\text{con};2}$) and a higher shear capacity ($\tau_{\text{deb};2}$) at debonding.

The bonding agent Cuglacrete Hechtprimer Polymeer by Cugla B.V. is applied (Cugla (2015)). This agent can easily be nebulized with a sprayer after removing the cement skin of the precast concrete surface. This way of applying the agent can be considered as very suitable at construction sites.
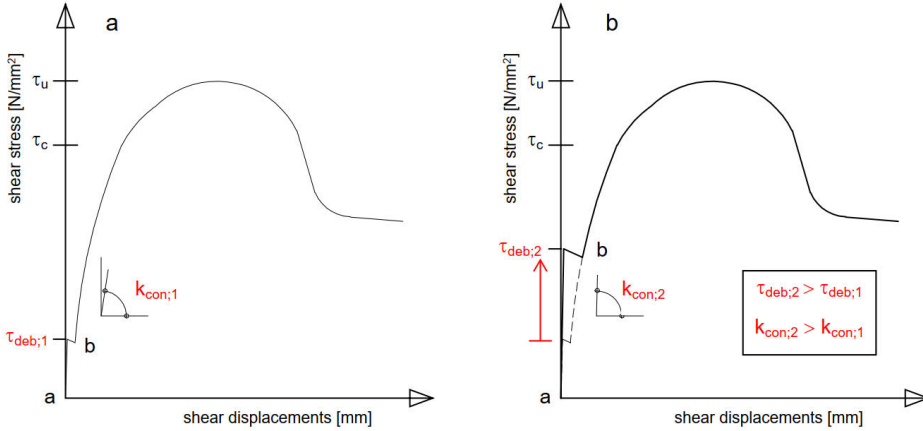
Figure 3.10: Shear stress-displacement diagram of a profiled connection

3.4.5 Variables not investigated

It is realised that there are also other variables that could have been varied in this research program. Among those, the following are mentioned:

- Height and thickness of the connection: all mortar connections in the specimens have a height of 600 mm and are 200 mm thick. The width of the seam is 25 mm;

- Grade of mortar and concrete: the mortar is a K70 mortar according to CUR aanbeveling 24 (1991) and the concrete has the grade of C55/67 according to NEN-EN 1992-1-1 (1992);

- Pre-cracking: the bond in the mortar-to-concrete interfaces could have been broken before testing the connection in shear.

3.5 Connections and variables selected for the research

In this research program a total of 33 specimens with vertical mortar connections are tested in shear. These tests are performed in three test phases. A study on the expected behaviour of the connections selected for testing is conducted prior to each phase. Furthermore, the acquired test results obtained in previous phases are analysed and used for selecting the connections for the next phase. This section contains a summarized description of the research program. In this thesis the tests of the three phases are discussed per connection. The shear tests conducted in the different phases are reported more extensively in Van Keulen (2013), (Van Keulen, 2014) and (Van Keulen, 2015).

3.5.1 Aligned shear key connection

Four shear tests are performed on the Aligned shear key connection as can be seen in figure 3.11. The variables type of mortar, lateral stiffness and initial compression are varied in this series.

The connection of specimen 1-1 is used as the reference Aligned shear key connection in this series. It contains ordinary thixotropic mortar and a lateral stiffness taken from four steel bars M24. The influence of the steel fibre reinforced mortar (specimen 1-2) and a lateral stiffness 4xM38 (specimen 1-3) can be identified from this series. Other comparisons can be made as well. However, these comparisons are different since two variables change at the same time (e.g. comparison 1-3 to 1-4). They can reveal additionally the influence of compressive stresses when taken into account the influence of lateral stiffness.

The behaviour of the Aligned shear key connection can be compared with the behaviour of the other vertical mortar connections presented in next subsections. A review later in this thesis on the shear behaviour of this Aligned shear key connection results in the conclusion that this connection is not the best performing. This is why only four shear tests of this type are performed. This connection is part of the first inventory test phase and reported more extensively in Van Keulen (2013).
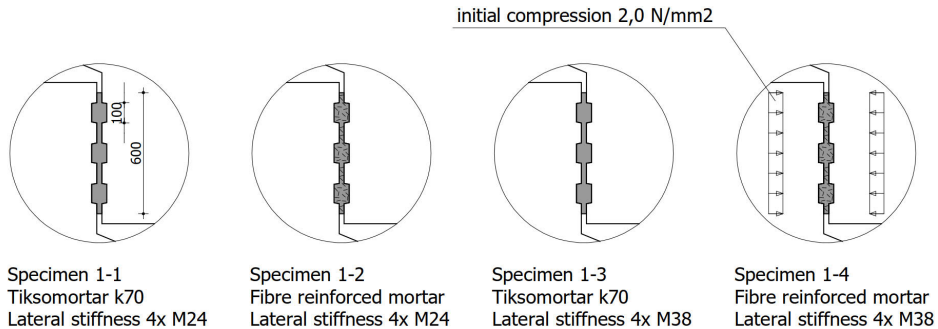
Figure 3.11: Tested Aligned shear key connections

3.5.2 Staggered shear key connection

The Staggered shear key connection is tested nine times as displayed in figure 3.12. The increased number of shear tests relates to the fact that this connection perfoms better as vertical mortar connection compared to the previous connection.

The same type of comparisons can be made as for the previously described connection. Besides the variables type of mortar, lateral stiffness and initial compression there are additional variables included. The lateral stiffness 4xM16 is added (specimens 2-1/2-2). Furthermore, the seam width of specimen 2-8 is 15 mm instead of 25 mm. It represents the influence of an unintended narrower seam caused by construction deviations. Also, the variable initial compression can now be compared without dealing with a second variable as it was in previous subsection. The shear behaviour of specimens 2-5/2-6 can be compared with specimen 2-9.

This Staggered shear key connection can be considered as an improved version of the Aligned shear key connection. The selection of mainly Tiksomortar K70 instead of SFRM is chosen for comparison purposes. A better performing vertical mortar connection with the same type of profile and regular mortar can be acquired with this vertical Staggered shear key mortar connection. Three connections with the same variables are tested two times.

initial compression 2,0 N/mm2

Specimen 2-1/2-2 (2x)
Tiksomortar k70
Lateral stiffness 4x M16

Specimen 2-3/2-4 (2x)
Tiksomortar k70
Lateral stiffness 4x M24

Specimen 2-5/2-6 (2x)
Tiksomortar k70
Lateral stiffness 4x M38

Specimen 2-7 (1x)
Tiksomortar k70
Lateral stiffness 4x M38

Specimen 2-8 (1x)
Tiksomortar k70
Lateral stiffness 4x M24

Specimen 2-9 (1x)
Fibre reinforced mortar
Lateral stiffness 4x M24

Figure 3.12: Tested Staggered shear key connections

3.5.3   Aligned small shear key connection

Nine shear tests are performed on the Aligned small shear key connection. Figure 3.13 shows this connection and the applied variables. Specimens 3-1 to 3-4 are tested with a lateral stiffness of four steel bars M16. The remaining specimens arre tested with 4xM24 or 4xM38 steel bars. Specimens 3-1 till 3-4 are the reference connections with regular Tiksomortar K70. The variable bonding agent in the mortar-to-concrete interfaces is added to specimens 3-3 till 3-8 with the aim of improving the bond strength and to postpone the shear stress level where the interface bond breaks according. Also, SFRM is inserted in the specimens 3-5 till 3-8 for investigating its effect on the connection behaviour.

Specimen 3-1/3-2 (2x)
Tiksomortar k70
Lateral stiffness 4xM16

Specimen 3-3/3-4 (2x)
Tiksomortar k70
Lateral stiffness 4xM16
Bonding agent

Specimen 3-5 to 3-6 (2x)
Fibre reinforced mortar
Lateral stiffness 4xM24
Bonding agent

Specimen 3-7 to 3-8 (2x)
Fibre reinforced mortar
Lateral stiffness 4xM38
Bonding agent

Specimen 3-9 (1x)
Tiksomortar k70
Lateral stiffness 4xM38
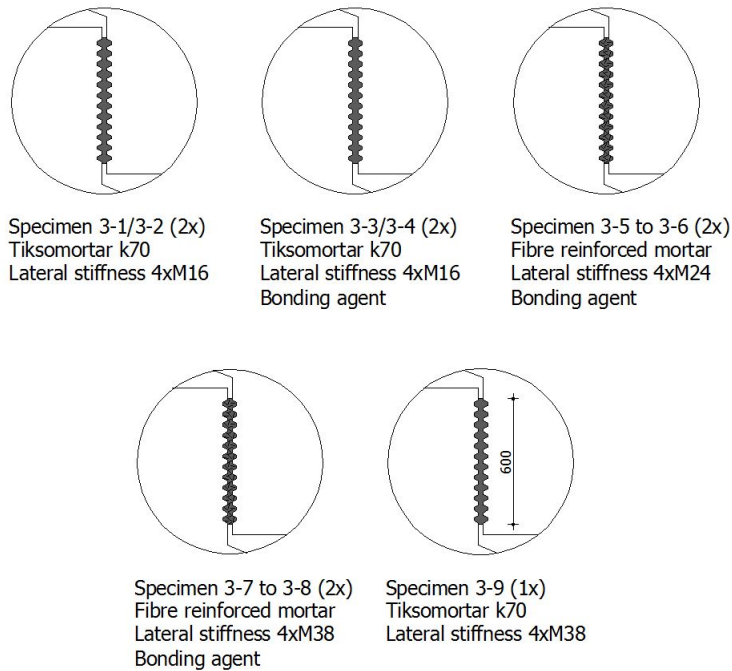
Figure 3.13: Tested Aligned small shear key connections

3.5.4   Plain waterjetted shear connection

Figure 3.14 shows the reserach program of the Plain waterjetted connection. Five connections with different variables are tested. Connections with a plain surface fail in debonding of the mortar-to-concrete interface. This failure does not depend on the type of mortar. This is the reason for not selecting SFRM for this connection. The variables used for this connection are lateral stiffness and initial compression.

This plain connection is able to transfer high shear forces and can be considered very suitable as horizontal mortar connection. The application of this connection for vertical seams is questionable. The reason is the absence of profiled interfaces according to the discussion in subsection 2.4.2. This series is tested for studying the influence of the selected variables on plain waterjetted interfaces compared to the Serrated waterjetted shear connection with the same interfaces in next subsection. Furthermore, a plain waterjetted mortar connection with two plain waterjetted interfaces close to each other is not tested in the past. Existing shear tests are only performed on a connection with a single waterjetted old-to-new concrete interface. It is relevant to study the shear capacity and stiffness of this new situation with two waterjetted interfaces close to each other. This is another argument for selecting this plain waterjetted connection in this research program for narrowvertical mortar connections.

Specimen 4-1
Tiksomortar k70
Lateral stiffness 4x M16

Specimen 4-2
Tiksomortar k70
Lateral stiffness 4x M24

Specimen 4-3
Tiksomortar k70
Lateral stiffness 4x M38

initial compression 1,0 N/mm2

initial compression 2,0 N/mm2

Specimen 4-4
Tiksomortar k70
Lateral stiffness 4x M24

Specimen 4-5
Tiksomortar k70
Lateral stiffness 4x M24
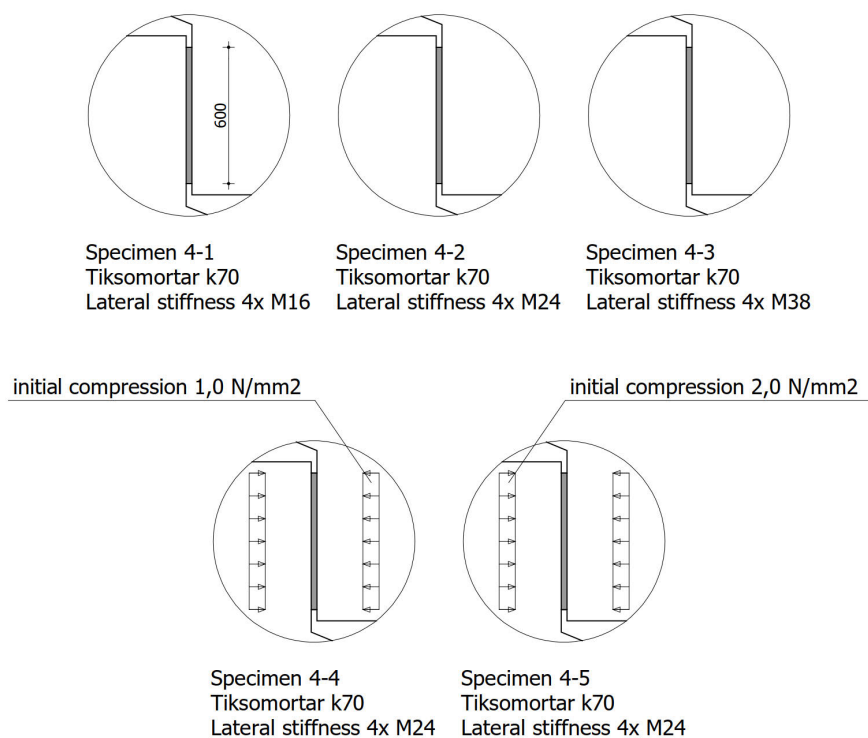
Figure 3.14: Tested Plain waterjetted connections

3.5.5 Serrated waterjetted shear connection

Figure 3.15 shows the test program for the Serrated waterjetted shear connection. This connection is developed after analysing the test results of the first inventory test phase of other connections. Subsection 3.3.6 discusses the arguments for this connection. It is expected to behave with a high shear stiffness and capacity and expected to be able to transfer the highest shear forces in precast concrete structures.

This connection is tested mainly with SFRM. Specimen 5-6 is the only one with Tiksomortar K70 and can be compared with specimen 5-3 where the mortar is changed into SFRM. The variables used for the connections with SFRM are lateral stiffness and initial compression according to the research program of the plain waterjetted connection. Identical comparisons can be made. Furthermore, both the plain and serrated connections tested with the same variables can be mutually compared.

Many precast concrete factories consider the treatment of waterjetting the concrete surface as less suitable than adding wooden ribbings in the side formwork according to figure 3.5. Waterjetting is considered laborious and difficult work. Keeping the level of roughness reproducible requires a constant amount of retarding agent. Moreover, acquiring the same level of roughness requires the same concrete

material grade for the moment of waterjetting. The depth of the removed cement paste and fine grained additives will be less if the waterjetting occurs one hour later than required. A shallower depth waterjetted surface results in less shear friction capacity and that results in the disapprove of the precast concrete element. Concrete factories try to avoid risking disapprovement by selecting an alternative connection.

Specimen 5-1
Fibre reinforced mortar
Lateral stiffness 4x M16

Specimen 5-2
Fibre reinforced mortar
Lateral stiffness 4x M24

Specimen 5-3
Fibre reinforced mortar
Lateral stiffness 4x M38

initial compression 1,0 N/mm2

initial compression 2,0 N/mm2

Specimen 5-4
Fibre reinforced mortar
Lateral stiffness 4x M24

Specimen 5-5
Fibre reinforced mortar
Lateral stiffness 4x M24

Specimen 5-6
Tiksomortar k70
Lateral stiffness 4x M38

Figure 3.15: Tested Serrated waterjetted connections

Chapter 4

Mortar Tests and Shear Test Setup

4.1 Introduction

In this chapter the experiments for the applied mortar as well as the setup for the shear tests on the narrow vertical mortar connections are described. It starts with an explanation of the pump tests in section 4.2. The pumpability of the thixotropic mortar and the steel fibre reinforced mortar are tested. The shear behaviour of the mortar connections is studied by shear tests. An explanation of the applied "push off" specimens is given in section 4.3. The lay-out and the assembly of the specimens are discussed in this section. Section 4.4 provides the test setup in which the shear tests are carried out. It contains a description of the used test setup, including a general description of the equipment, measurements and the testing procedure. The material tests for the applied mortars and concrete are explained in section section 4.5.

4.2 Pump tests

The process of inserting the mortar with a mortar pump in a vertical seam is rather critical since profiled seams have to be fully filled in order to acquire a well functioning connection. The thixotropic mortar may drain from the seam in case of an insufficient stiff plastic mortar. The feasibility of pressing the mortar via a hose into a vertical profiled seam and acquiring a sufficiently filled connection is tested. Two tests are done. The first test is the filling of vertical profiled seams with a thixotropic mortar. The second test is verifying the pumpability of Steel Fibre Reinforced Mortar through the hose of a mortar pump.

4.2.1 Filling test

Figure 4.1 shows the test setup applied for the filling test. Four upright wooden structures are constructed for simulating the vertical profiled seams to be filled with thixotropic mortar. The wooden structures function as the formwork for shaping the mortar fillings. They represent the sides of the precast concrete wall elements. Using a plain wooden surface for representing a concrete surface can be questioned. The adhesion of the mortar to a wooden or concrete surface can be different. However, the goal of this test is only to investigate if the recesses of the keys are sufficiently filled with mortar. The effect of adhesion is considered not a significant influencing parameter for this filling check. Therefore, a wooden surface is chosen.

Appendix A provides the drawing that is used for the construction of this test setup. The height of the mortar filling is 1,2 meter. The width of the seam and the depth of the indentations are both 25 mm. The profiled seams had a maximum horizontal width of 75 mm. Two mortar fillings with the profile of the Aligned shear key connection and two of the Staggered shear key connection are simulated.
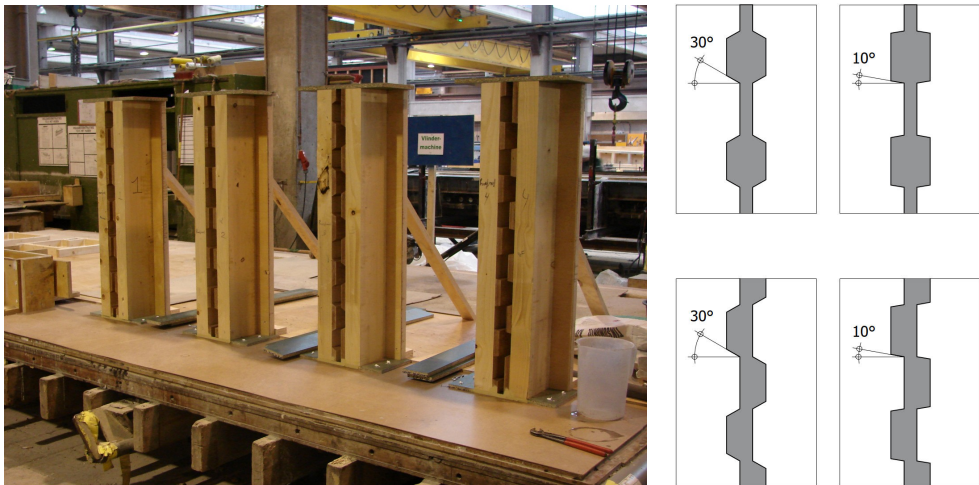
Figure 4.1: Test setup and profiles for pump test with thixotropic mortar

The angle α of the inclined surface in the profile is varied for both profiles according to the four drawings in figure 4.1. So, each profile is tested with an angle $\alpha = 30°$ and $\alpha = 10°$. The reason for changing this angle is checking if air inclusion between mortar and precast concrete will occur. The low angle $\alpha = 10°$ makes that the re-entrant corner of the formwork is close to 90°. This relatively sharp corner increases the risk of air inclusion. This has to be avoided since it may disturb the transfer of shear forces through the mortar.

The backs of the profiled seams are closed with plywood. The mortar is inserted from the front side. The mortar is pressed against the plywood at the back according to the principles explained in subsection 2.2.2. Figure 4.2 provides an overview of the work done for filling the seams. The mortar is inserted from the bottom to the

top. The mortar has sufficient stiffness to remain in place. The worker removes redundant mortar and smoothens the surface of the mortar filling with a trowel.

The filling, including the check for air inclusions, is verified by taking the wooden components apart from the mortar filling. Figure 4.3 shows one of the demoulded mortar fillings. Appendix A provides extra photos taken from these filling tests. This test has demonstrated the ability of filling sharp corners as can be seen on the photo. It has to be mentioned that the work of filling vertical mortar connections must be done by experienced site workers. The reason is that air inclusion can easlily occur and that has to be avoided. The profiled vertical seams have to be reproducibly well filled with mortar for acquiring good functioning connections.

Figure 4.2: Testing the filling of vertical seams with mortar pump

Figure 4.3: The mortar filling after demoulding

4.2.2   Pumpability of Steel Fibre Reinforced Mortar

Steel fibres added to thixotropic mortar changes the composition of the plastic mortar to be pressed through a hose. The pumpability of Steel Fibre Reinforced Mortar (SFRM) is tested in advance. The main threat is that steel fibres penetrate the rubber hose resulting in congestion of fibres. This test shows that congestion can be prevented by lubricating the hose with traditional mortar. This means that SFRM can be pressed through a 25 mm hose when a thin layer of traditional mortar is present on the rubber inside the hose. Cleaning the hose afterwards should be done by first pressing out the Steel Fibre Reinforced Mortar with traditional mortar. Then traditional mortar remains in the hose and can easily be removed with water. SFRM cannot be removed with water since it causes that the fibres remain present in the hose. They will penetrade the rubber hose. Then the hose becomes permanent unusable because the congested fibres cannot be removed from the hose.

4.3   Specimens for the shear tests

4.3.1   General description

The picture in figure 4.4 provides schematically the lay-out, the dimensions of the specimen and the way it is loaded during a shear test. Figure 4.5 shows a front view of the specimen in the shear test setup.
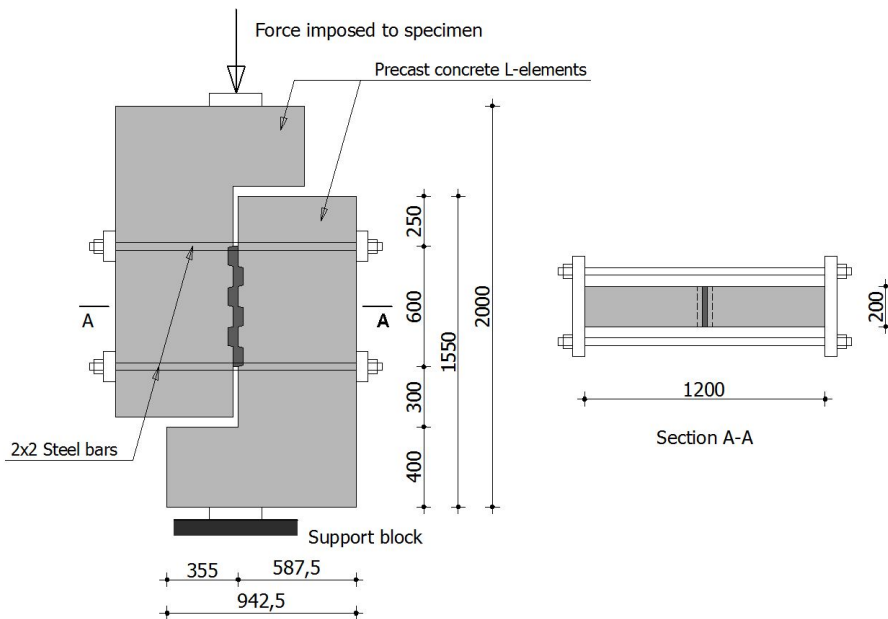
Figure 4.4: Test setup for the shear test (measures in mm)

Two precast concrete L-elements with the mortar connection in between form together the specimen. The specimen is positioned on a support block below and is loaded on top with a vertical compressive force. A ball hinge connection is installed at the top of the specimen. Four horizontal steel bars keep together the L-elements and prevent the specimen components from falling apart. The steel bars provide a lateral stiffness and are used for compressing in case of the mortar connection is pretensioned. Three sets (M16, M24 and M38) of four steel bars are used representing three lateral stiffnesses.
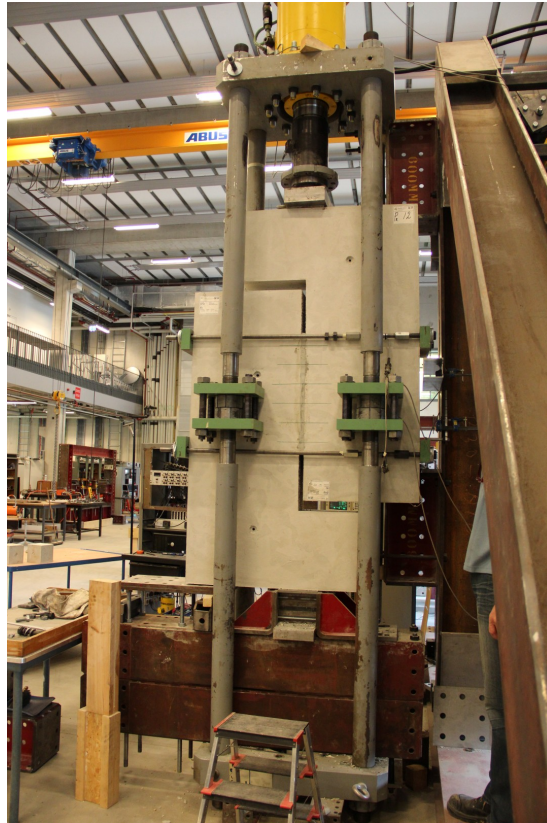
Figure 4.5: Overview of Test Setup in the Structures Laboratory of Eindhoven University of Technology

4.3.2 Precast concrete L-elements

The precast concrete L-elements for the specimens of phase 1 and 2 are constructed by the Dutch firm Hurks prefabbeton B.V. located in Veldhoven. The firm Bestcon B.V. produced the L-elements for the phase 3 series of specimens. Figure 4.6 shows the formwork with reinforcement in it in the concrete factory. The photo in figure 4.7 is taken after demoulding the L-elements.

Figure 4.6: Construction of L-elements in the concrete factory

An approximated force distribution in the elements is obtained from a structural model which has led to the applied amount of reinforcement in the L-elements. Starting point for the structural design of the precast concrete L-element is that failure or even excessive cracking in the reinforced concrete may not occur in the area outside the connection at all times. The specimen must fail in the mortar or the precast concrete close to the mortar connection. Therefore, the reinforced precast concrete L-elements are provided with more reinforcement than required according to the approximated force distribution from the structural model. Appendix B provides detailed the dimensions and reinforcement of the L-elements.
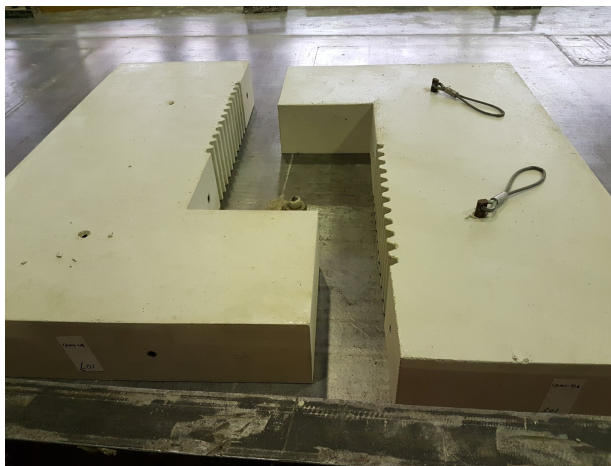
Figure 4.7: Finished precast concrete L-elements

4.3.3 Assembly of specimens

The assembly of the specimens started with laying down the precast concrete L-elements on a table according to the photo in figure 4.8. It has been chosen to fill the specimens in a horizontal position for reasons of workability. The bottom of the table functions as the mould and filling the connection is done from above. Filling the connection in a upright position requires temporary structures for fixation of the L-elements including formwork on the back side of the specimen. This is regarded as unnecessarily difficult. There are no significant differences expected for filling the thixotropic mortar in horizontal or vertical positioned specimens. Although the from bottom to top inserting procedure of the mortar in the seam is not followed, a 100% filling of the mortar connection is persued and satisfies the demands of this research. Potential differences may be expected for the SFRM since gravity load influences the distribution of the steel fibres in the plastic mortar. These differences are considered as not significant in this research.

Spacers taken from an insulation sheet with a thickness of 25 mm is positioned between the two L-elements (see figure 4.9). They are used for keeping the seam width 25 mm and the connection height 600 mm while casting the mortar in the seam.

Figure 4.8: Construction of specimens in the concrete factory of Bestcon

Figure 4.9: Spacers between L-elements

Figure 4.10 shows the filling of the Aligned small key connection by means of the hose. After inserting the mortar, plastic foils are placed on top of the mortar fillings for preventing fast dehydration. Figure 4.11 shows that two pre-tensioned steel bars are used for keeping the mortar fillings temporary in place. They are applied through the specimens as soon as the mortar had sufficient strength. The table on which the specimens are constructed is a so-called "tilting table". This table is tilted just before hoisting the specimens in a upright position as can be seen in figure 4.12. It prevents that the ready mortar connection is subjected to unacceptable stresses caused by tilting movements. The specimens are transported and stored in the upright position.

Figure 4.10: Inserting the mortar with a hose

2 Dywidag bars for compressing
the mortar filling during transport
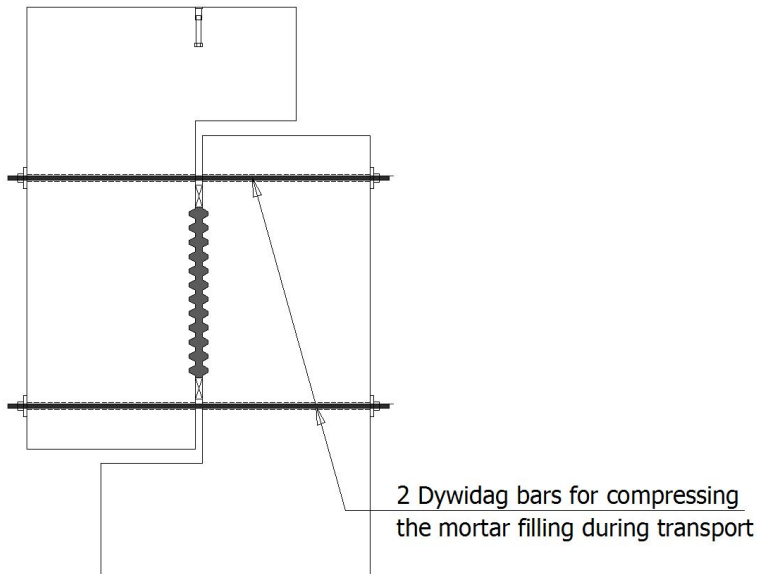
Figure 4.11: Dywidag bars through the specimen

Figure 4.12: Tilting the table just before hoisting the specimens

4.4 Test setup for the shear test

4.4.1 General description

The shear tests are performed in the Structures Laboratory of Eindhoven University of Technology. The photos in figure 4.5 show a steel frame with four columns, a support block below and a thick stiff steel plate on top. They form together a closed frame in which the specimens are positioned. A hydrolic jack with a capacity of 200 ton is fastened on top. The hydrolic jack presses on top of the specimen according to the vertical arrow in figure 4.13a. This force is displacement controlled imposed to the specimen by the displacements of the valve of the actuator. The specimen transfers the vertical force via the specimen to the support block. The specimens stand vertically upright and horizontally centered in the frame of the test setup to prevent excentricities causing other forces than shear forces in the mortar connection or even instability of the entire test setup. The two Dywidag steel bars shown in figure 4.11 are removed from the specimen after the 2x2 steel bars are installed.

4.4.2 Testing procedure

Testing of a mortar connection starts with applying an initial lateral compression to the specimen. The compressive stresses are applied by pre-tensioning the four steel bars with equal forces. These forces are applied by tightening the bolts at the sides of the specimen manually until the desired pre-tensioning is measured. The
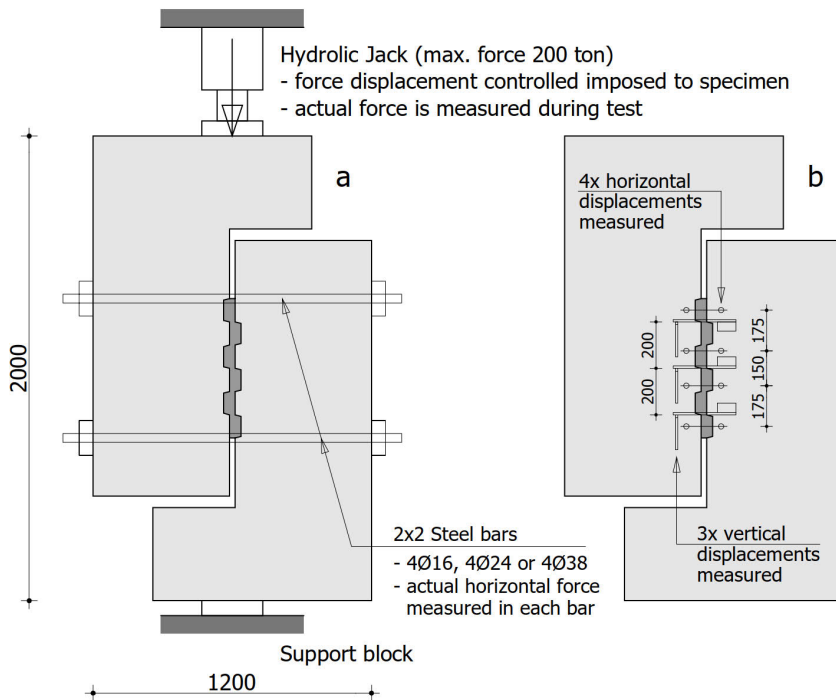
Figure 4.13: Overview of the test setup (a) and measurements (b), measures in
         mm

mortar connections are intended to be not compressed and are loaded with a very
small compressive stress of 0,1 N/mm². This is required for directly preventing the
L-elements to disconnect from the mortar filling. The level of pre-tensioning is not
varied during the test and is not adjusted. The increase of the forces in the steel bars
are caused by the dilation forces which arise in the mortar connection during loading
the specimen.

The next step is loading the specimen by means of the hydrolic jack at the top
of the test setup. The specimens are loaded displacement controlled with a speed of
0,2 mm per minute. The displacement controlled procedure is terminated as soon
as the shear displacements are in the range of 6 mm - 8 mm. It turned out that the
mortar connections are fully broken with shear deformations of this size.

The final step in this testing procedure is the inspection of the broken mortar
connections. The damaged specimens are taken out of the test setup and layed down
on the floor. Then, one L-element is detached from the mortar filling. After that, the
mortar filling is taken from the other L-element. Photos are taken during these works
in order to inspect and analyse the damaged mortar connection.

4.4.3 Measurements and observations

The drawing of figure 4.13b summarizes all displacement measurements performed during testing. They are registered in each load step. The vertical force imposed on top is measured with a load cell just below the hydraulic jack. The lateral forces perpendicular to the connection are taken from each of the four steel bars. All steel bars had calibrated strain gauges stuck on the bars for measuring the actual forces. Horizontal displacements are measured at four locations with LVDT sensors according to the dimensions provided in figure 4.13b. Vertical displacements are measured at three locations with LVDT sensors according to the same figure. The deformation measurements are taken on one side of the specimen (figure 4.14).

Photos and videos are taken from the specimen during the shear tests for observing both specimen surfaces. They show the cracks in the mortar or concrete element surfaces during the test. The cracks are signed by drawing a line with a marker as soon as the cracks became visable. The shear load at the instant of crack formation is noted on the specimen as well.
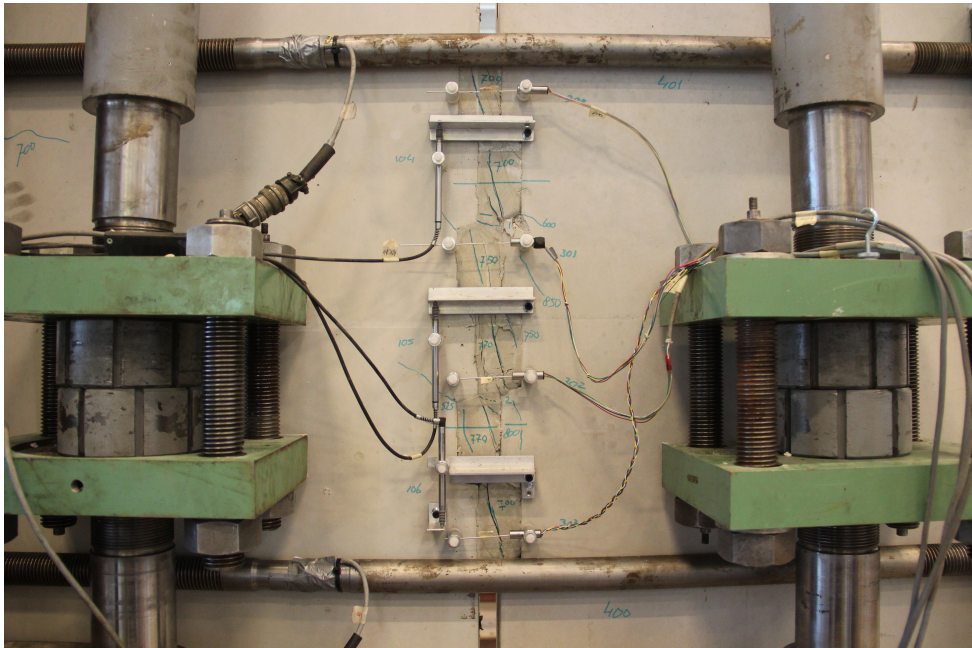
Figure 4.14: LVDT sensors and strain gauges stuck on the steel bars

4.5   Material tests

The concrete grade of the precast concrete L-elements is designed to be C55/67 according to NEN-EN 1992-1-1 (1992). The actual structural properties of the concretes at the moment of testing are measured with the test methods provided by the EN-12390 standards. Cube specimens are used for this research. The actual compressive strength of the concrete is tested according to NEN-EN 12390-3 (2009). NEN-EN 12390-6 (2009) is used for determining the tensile splitting strength. Three cube specimens are made for determining each type of strength. It has led to 6 concrete cubes of 150x150x150 mm^3 which are cast for each concrete batch. The Young's modulus of the concrete is taken from 3 prisms of 100x100x400 mm^3 for each concrete batch. The concrete cubes and prisms are stored near the specimens in order to represent the material properties of the precast concrete elements as good as possible.

The mortar is designed to be a K70 mortar grade. Again, the actual structural material properties are tested at the moment of testing the mortar connections. These tests are performed in accordance with the methods described in CUR aanbeveling 24 (1991). Small prisms of 40x40x160 mm^3 are used for determining the compressive strength, the bending tensile strength and Young's modulus. The material tests for the used mortars are reported thoroughly in the master thesis of Hobson (2014).

Chapter 5

Experimental Results

5.1   Introduction

This chapter presents the results of the mortar tests and the shear tests. In section 5.2 the research program is summarized in a table in order to provide an overview of the tested connections and variables. This section continues with a detailed explanation of how the measurements (forces and displacements) are taken from the mortar connections and specimens. In section 5.3 the results of the material tests on specimens taken from the used precast concrete and mortars are explained.

As an example the shear behaviour of one profiled mortar connection is extensively examined in section 5.4 (specimen 2-4). All measured data and observations of this connection are presented and analysed. For the remaining 32 connections not all of the measured data are used for further investigation. Therefore, section 5.5 discusses which of the data is selected to represent the shear behaviour of these connections in the remainder of the thesis. Also, this section presents the concept of the combined load-displacement diagram which is used for further representation of the connection behaviour.

In succession, sections 5.6 till 5.10 provide the test results for each mortar connection. They explain the most important measurements and observations. The shear stiffnesses and the lateral stiffnesses of all connections are summarized in a table in section 5.11, in which these results are discussed. Section 5.12 concludes this chapter by giving a number of summarizing remarks.

5.2   Overview of connections and measurements

5.2.1   Connections and variables

Table 5.1 displays the tested connections and variables. Each connection is tested with one of the two mortars: Tiksomortar K70 mortar or Steel fibre reinforced mortar. Three alternative sets of four steel bars, M16, M24 or M38, are attached to the

specimen representing the variable lateral stiffness. Lateral compression by adding an initial compression by means of the steel bars is the third variable. Compressive stresses of $0,1\,\text{N/mm}^2$, $1,0\,\text{N/mm}^2$ or $2,0\,\text{N/mm}^2$ are applied to the specimen prior to starting the shear test. The addition of bonding agent in the mortar-to-concrete interfaces is varied for the Aligned small shear key connection. Finally, the thickness of the seam is changed once for the Staggered shear key connection.
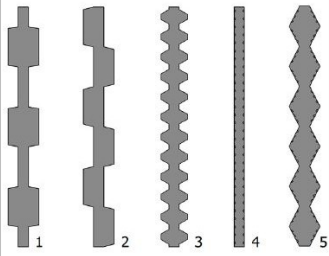
	Cuglaton Tikso K70 mortar	Steel Fibre Reinforced Mortar (SFRM)	Lateral stiffness 4xM16	Lateral stiffness 4xM24	Lateral stiffness 4xM38	Initial compression (0,1 N/mm2)	Initial compression (1,0 N/mm2)	Initial compression (2,0 N/mm2)	Bonding agent	Seam 15 mm (instead of 25 mm)
1. Aligned shear key										
Specimen 1-1	X			X		X				
Specimen 1-2		X		X		X				
Specimen 1-3	X				X	X				
Specimen 1-4		X			X			X		
2. Staggered shear key										
Specimen 2-1/2-2	X		X			X				
Specimen 2-3/2-4	X			X		X				
Specimen 2-5/2-6	X				X	X				
Specimen 2-7	X				X			X		
Specimen 2-8	X			X		X				X
Specimen 2-9		X		X		X				
3. Aligned small shear key										
Specimen 3-1/3-2	X		X			X				
Specimen 3-3/3-4	X		X			X			X	
Specimen 3-5/3-6		X		X		X			X	
Specimen 3-7/3-8		X			X	X			X	
Specimen 3-9	X				X	X				
4. Plain waterjetted shear connection										
Specimen 4-1	X		X			X				
Specimen 4-2	X			X		X				
Specimen 4-3	X				X	X				
Specimen 4-4	X			X			X			
Specimen 4-5	X			X				X		
5. Serrated waterjetted shear connection										
Specimen 5-1		X	X			X				
Specimen 5-2		X		X		X				
Specimen 5-3		X			X	X				
Specimen 5-4		X		X			X			
Specimen 5-5		X		X				X		
Specimen 5-6	X				X	X				

Table 5.1: Research program with connections and variables

Three series of shear tests are performed of which the results are reported in Van Keulen (2013), Van Keulen (2014) and Van Keulen (2015). For this thesis the codes to identify the different specimens is different from that in these reports. In table B.1 in Appendix B it is shown how the codes in this thesis and in the three reports relate to each other.

5.2.2 Measured forces and displacements

Figure 5.1 displays the codings for the measured forces and displacements. The LVDT1-0X series corresponds to the three vertical displacement measurements. Three pen-type of LVDT sensors are fixed to the specimen on the left side of the mortar filling as can be seen in the photo of figure 4.14. The second measuring point is on the right side of the mortar filling. There a bridge is fixed to the specimen that spans horizontally between the both points with a mutual distance of 115 mm. Figure 5.1 shows a vertical measuring length of 35 mm between the same measuring points. It is the length over which a change in length is measured by the LVDT sensors. This change equals the vertical displacement of the mortar connection loaded in shear.

The LVDT's with LVDT3-0X codings measure the horizontal displacements over the connection with a measuring length of 85 mm. The Strain4-0X measurements belong to the measurements taken from the steel bars. Forces are measured with strain gauges on every steel bar. The four forces together represent the full lateral force compressing laterally the profiled mortar connection.
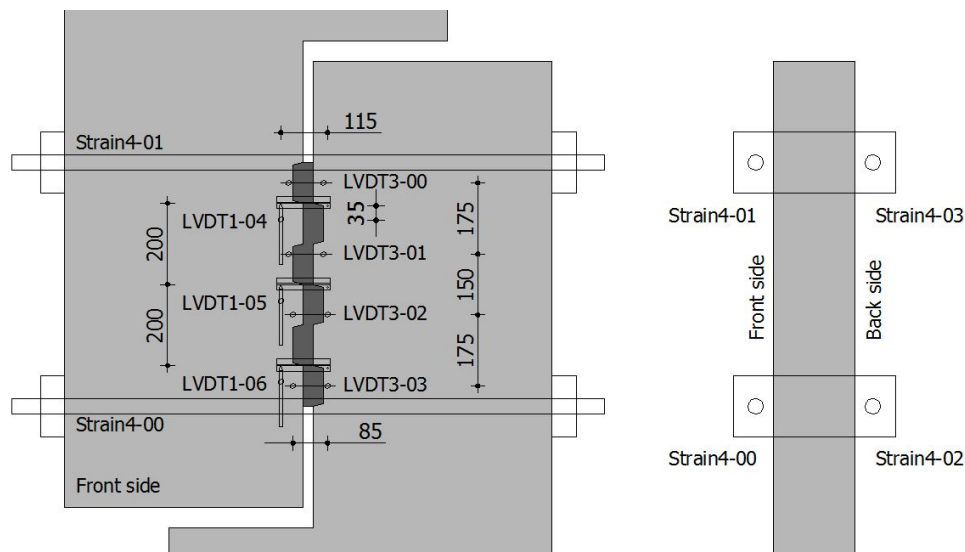

Figure 5.1: Instruments attached to specimen according to the photo diplayed in figure 4.14; 3x vertical displacements (LVDT1-0X), 4x horizontal displacements (LVDT3-0X) and 4x force in steel bars (Strain4-0X)

5.3   Material tests

5.3.1   Precast concrete L-elements

The same concrete grade for all precast concrete L-elements is used. This subsection reports about the actual measured material properties. Results for the compressive strength, tensile splitting strength and modulus of elasticity can be found in Appendix C. Concrete cubes (150x150x150 mm^3) and prisms (100x100x400 mm^3) are cast on the same day as the precast concrete L-elements. Also, the concrete material tests on the cubes and prisms are performed on the same day as the shear tests are performed. Therefore, the results of the concrete material tests link to the material properties of the precast concrete L-elements of the specimens. Six concrete cubes per concrete batch are used to determine the compressive strength (3x) and tensile splitting strength (3x). Also, three prisms per concrete batch are made for measuring the modulus of elasticity.

The Dutch firm Hurks Prefabbeton BV produced the precast concrete L-elements for the first two testing phases (Hurks 1 and 2) and Bestcon BV the L-elements for the third testing phase (specimens 3-1 till 3-8). The maximum gravel size of the concrete was 16 mm and the concrete grade of the elements was C55/67. Mean values for the compressive strength, tensile splitting strength and modulus of elasticity, taken from all measuraments reported in Appendix C, are listed in table 5.2.

	mean	standard deviation
compressive strength f_c [N/mm^2]	86,50	3,75
tensile splitting strength f_{ct} [N/mm^2]	4,90	0,32
modulus of elasticity [N/mm^2]	33.056	975

Table 5.2: Results of material tests of the precast concrete L-elements determined using NEN-EN 12390-3 (2009) and NEN-EN 12390-6 (2009)

5.3.2   Mortars

One of the variables in this thesis work is the type of mortar. Table C.4 shows the actually measured compressive strengths and flexural tensile strengths for the Tikso-mortar K70 and the Steel Fibre Reinforced Mortar (SFRM). These values are measured according to the test methods described in CUR aanbeveling 24 (1991). These tests are performed in the laboratory of supplier Cugla BV and are taken from prisms 40x40x160 mm^3. The testing procedure starts with a 3-point bending test on the prism for measuring the flexural tensile strength. Then the prism is broken into two parts. Then both parts are used for measuring two times the compressive strength.

The mean values of the compressive and flexural tensile strengths are presented in table 5.3. This table includes the age of the mortar, the strengths and the increase of compressive and flexure tensile strengths due to steel fibres. The measurements show increases of 23,9% and 21,2% respectively for the SFRM.

Table	Strength	Mean	Tikso K70	SFRM	Increase
		age (days)	N/mm^2	N/mm^2	%
C.4	Compressive (f'_{mk})	34	75,0	92,9	23,9
	Flexure tensile (f''_m)	34	9,9	12,0	21,2

Table 5.3: Increase of compressive strength and flexural tensile strength of the SFRM with respect to the Tiksomortar K70 type of mortar

5.4 Detailed view on the results of a shear test

Specimen 2-4 with a Staggered shear key connection has been selected for an in-depth study of a profiled mortar connection. The goal is to provide a thorough understandig of one profiled mortar connection. The structural behaviour of other connections relate highly to this example connection. The choice for this Staggered shear key connection is because it is one of the most varied connections with high potential for application in precast concrete stability structures. The characteristics of this connection are a lateral stiffness provided by 4xM24 steel bars, a minimal initial compression of 0,1 N/mm^2 and the traditional Tiksomortar K70 (see table 5.1). These variables represent common circumstances of vertical mortar connections applied in precast concrete stability structures.

5.4.1 Shear force - shear displacement relationship

The diagrams in figure 5.2 show the relationship between the shear forces and shear displacements of connection 2-4 in detail. Diagrams II and III are cutouts of diagram I. They all display the shear forces (V_F) on the vertical axis and shear displacements (δ_v) on the horizontal axis. In diagram I the LVDT1-04, LVDT1-05 and LVDT1-06 codings link to the three sensors for measuring the vertical shear displacements. The photos in the figure D.1 of Appendix D show the real sensors attached to specimen 2-4. In diagram I the letters A to E indicate a sequence of the specific events that occur in the connection during the shear test. Diagram II is a cutout of the upper part of diagram I. Diagram III shows a magnified view of the shear behaviour close to the origin of diagram I. They both contain only the measurements of the shear force set against the LVDT1-05 sensor. This is the middle sensor. The measured values are the dotted points in the diagrams. These points are coupled by connecting lines for acquiring a continuous representation of the load-displacement behaviour.

5.4.2 Principal stages

The shear force and shear displacements are set zero before starting the shear test. An initial horizontal compressive stress (initial compression is equal to 0,1 N/mm^2) is applied in advance with the goal of keeping the mortar filling only slightly pressed

between both the precast concrete L-elements. Imposing the vertical load on the specimen is performed by means of a displacement controled procedure. The hydraulic jack is set to a moving speed of 0,2 mm per minute.

Breaking adhesion $V_{F;B}$ (B)

After starting the test in A, the first observable event is breaking adhesion in the mortar-to-concrete interfaces. This is in point B at a shear force $V_{F;B}$ of 24,2 kN (see diagrams I and III). The lab technician wrote 22 kN on the specimen as can be seen in the second photo of figure D.1 in Appendix D. The diagram continues with a small drop of the shear force to 20,6 kN together with an increase of shear displacement of 0,083 mm - 0,037 mm = 0,046 mm.

Figure 5.3 illustrates in drawings the events A till E during shear test. Drawing A represents the transfer of shear forces via an infinite number of compression struts in stage A-B. These struts are able to continuously transfer forces because the adhesion in the interfaces is not broken. This way of transferring forces terminates in point B (dotted line in figure 5.3B). Adhesion in the mortar-to-concrete interfaces breaks when a certain combination of tensile and shear stresses exceeds the adhesive bond strength. Local debonding somewhere in the interface will cause immediately debonding of the entire interface. The reason is that local debonding results in a sudden increase of stresses in other parts of the interface. Then, the adhesive bond strength is suddenly exceeded along the entire interface just after local debonding.

The profiled mortar connection continuous to transfer shear forces via three diagonal compression struts as can be seen in figure 5.3B. The downturn in diagram III can be attributed to the takeover of the shear transfer from the infinite number of compression struts by the remaining three struts. This causes a sudden additional elastic shortening of the three struts and because of that a sudden increase of the slip δ_v with 0,046 mm. Also, the elastic shortening of the three struts results in a small relieve of the applied shear force V_F = 24,2 - 20,6 = 3,6 kN.

The third photo in figure D.1 shows the appearance of interface cracks at approximately 75 kN. Bond breaking behaviour at a shear force of 75 kN is not visable in the diagram. Therefore, it is reasonable to assume that adhesion is broken earlier at a shear force of 22 kN. The interface cracks are very small at that moment and therefore unobservable by the lab technician. They became visable at a shear force of 75 kN for the observer.

Cracks in the precast concrete or mortar $V_{F;C}$ (C)

The second visable event is the appearance of cracks in the precast concrete by a shear force $V_{F;C}$ of approximately 420 kN. This is observable in the fourth photo of figure D.1. The lab technician wrote 420 kN on the specimen. Also, this event is labeled in diagram I and in figure 5.3C.
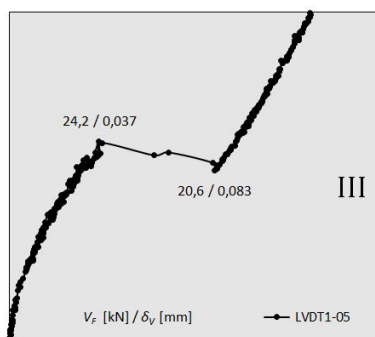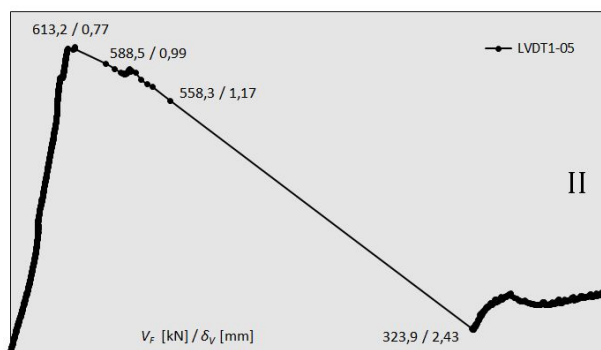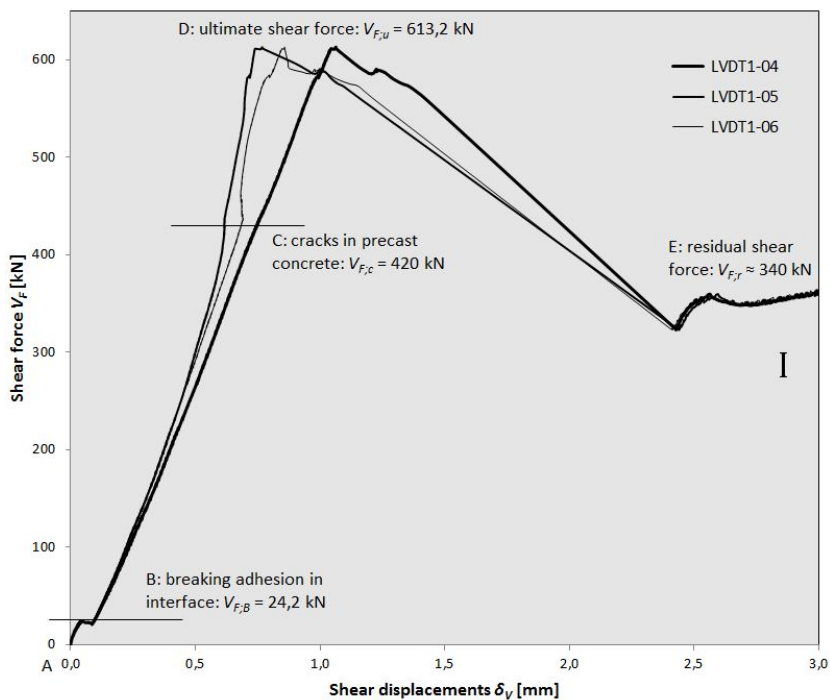
Figure 5.2: Shear force - shear displacements relationship of Specimen 2-4

Figure 5.3C suggests cracks in the precast concrete as well as diagonal cracks in the mortar (dashed lines). The photo in figure D.1 shows just cracks in the precast concrete. In this test only cracks appeared at point C in the precast concrete and not in the mortar. In a number of other Staggered shear key connections a combination of cracks in the precast concrete and mortar appeared in point C indicated by figure 5.3C. Figure 5.3C-1 displays the zones in the mortar and concrete that are stressed by the diagonal compression struts. This drawing shows with the sign "o" the parts of the concrete and mortar next to or in between the compressed zones. They are less stressed because they are not part of the compressed diagonals. The different stress states inside and outside the compressed zones cause a split of the different zones by means of a crack.
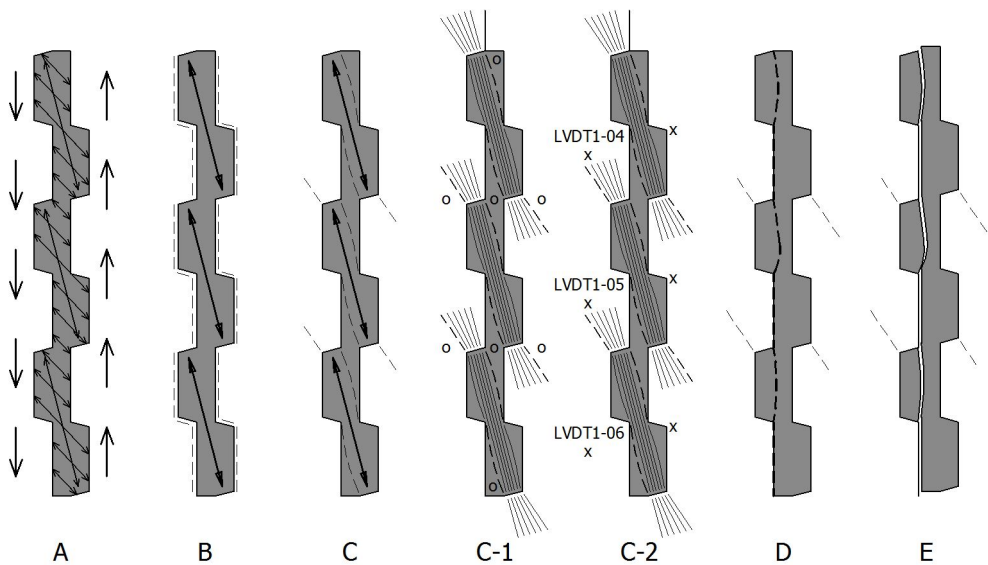
Figure 5.3: Principal stages in the mortar connection of specimen 2-4

The three relations in stage C-D of diagram I show somewhat different behaviour. The relation of the LVDT1-05 measurement develops steeper, appears a little curved for LVDT1-06 and continues with the same steepness as in the previous stage for LVDT1-04. A few issues relate to this irregular behaviour and are explained. The connection transfers diagonal forces via the cracked mortar and concrete. The cracks cause a new deformed state in the connection. It influences lateral displacement measurements at the specimen surface taken by the LVDT1-0X sensors. Figure 5.3C-2 shows with the sign "x" the fixation points of the sensors. The drawing shows the right fixation point of sensor 04 and left fixation point of sensor 06 are in a low-stressed zone. They are not in the diagonal compression struts. The remaining fixation points are glued to the specimen on the compression struts which are considerbly stressed. Having the fixation points in areas possessing different stress levels influences the measurements taken by the LVDT1-0X sensors. Then the cor-

responding sensors measure slightly more shear deformations because of this phenomenon. This is one of the issues that might cause the irregular measurements in stage C-D. Another issue can be the random crack pattern in stage C-D. New diagonal cracks appear during further compression the specimen in stage C-D. Also, existing cracks become wider or smaller after the appearance of new cracks. These cracks can be observed in the photos of figure D.2. These changes influence the measurements taken by the sensors as well.

Ultimate shear force $V_{F;u}$ (D)

Connection 2-4 finds its ultimate shear force $V_{F;u}$ at a jack force of 613,2 kN as can be seen in diagrams 5.2I and 5.2II. The last photo in figure D.2 shows the cracked surface of the specimen. The failure cracks seem to be diagonal cracks at the specimen surface in this photo. The photos in figure D.4 and D.5 show the dismantled connection. They indicate a rather vertical failure crack according to figure 5.3D. This crack is not visable when the specimen stands in the test setup. The cracks in the mortar are slightly curved. The failure cracks start on the top of the shear key via the diagonal cracks. However, they bend back to the left side in figure 5.3D. This observation proves that this connection fails according to the failure mechanism "vertical shearing off the indentation" drawn in figure 2.14c.

Stage D-E is enlarged in diagram II of figure 5.2. Again, the dots represent the measured points. The lines between the dots only connect these points. The ability to transfer increasing shear forces via the three inclined compression struts expires when the failure crack appears. The specimen is further vertically compressed and finds for a short time a new load carrying body in the mortar connection for shear transfer. This body fails at the point $V_F = 588,5$ kN and $\delta_v = 0,99$ mm (diagram II). The diagram continuous with a snap back to a substantial lower shear force of 323,9 kN and a very large displacement of 2,43 mm. The diagram draws a line between the 558,3 kN and 323,9 kN dots. This line does not represent actual measured points. It is a brittle and sudden change in the profiled mortar connection without measured points. The snap back has the shape of a V. The shear force climbs to the residual shear force after reaching the deepest point of 323,9 kN. An immediate downturn from the ultimate failure force $V_{F;u}$ to the residual force $V_{F;r}$ is to be expected. However, the sudden increase of the shear deformations cannot be tracked by the test setup. The finite stiffness of the test setup and the fact that deformations are controlled by displacements of the valve of the jack causes the V-shaped snap back.

Residual shear force $V_{F;r}$ (E)

The Staggered shear key connection is still able to transfer shear forces in the final stage E of the diagram in figure 5.3. This force is the residual shear force $V_{F;r}$. The shear friction capacity of the failure crack interface transfers shear forces as can be seen in figure 5.3E. The shear deformations are substantial in this stage according to the photos of figure D.3.

5.4.3 Shear force - lateral force relationship

The diagrams in figure 5.4 display the relationships between the shear forces and lateral forces of connection 2-4. Again, diagrams II and III in this figure are cutouts of diagram I. They all display the shear forces V_F on the vertical axis and lateral forces $F\sigma_n$ on the horizontal axis. The Strain4-00 till Strain4-03 codings correspond to the measured lateral forces taken by the strain gauges on the steel bars labeled in figure 5.1.

The initial compression of 0,1 N/mm^2 is added in advance to the mortar connection and that equals to a lateral force of approximately 2,0 kN per steel bar. Table 5.4 lists the measured initially applied lateral forces for each of the steel bars. Diagram I starts in "A: Initial compression" with these lateral forces $F\sigma_{n;A}$. The hydraulic jack begins vertically compressing the specimen from this point.

Steel bar (figure 5.1)	Strain4-00	Strain4-01	Strain4-02	Strain4-03
Position	Front below	Front above	Back below	Back above
Lateral force $F\sigma_{n;A}$	2,05 kN	2,10 kN	2,01 kN	2,11 kN

Table 5.4: Initial compression: lateral forces $F\sigma_{n;A}$

Shear force $V_{F;B}$ = 24,2 kN causes the breaking of adhesion in point B of the diagram (I and II). The same type of the downturn displayed in diagram III of figure 5.2 can be observed at this point. Suddenly, the lateral force $F\sigma_{n;B}$ increases from 2,04 kN to 2,15 kN and from 2,44 kN to 2,67 kN for respectively strain4-00 and strain4-01 as can be seen in diagram II. The same snap back explanation presented in previous subsection can be attributed to this connection behaviour.

The lateral forces in the two steel bars below increase less than in the two steel bars above in stage B-C. The lateral forces $F\sigma_n$ in the steel bars below increase from point B up to V_F = 90 kN without a significant increase of the lateral forces. The relations of the steel bars above bend almost immediately into the sloped line. Finally in the stage C-D the lateral forces in the upper bars are still higher than in the lower bars. This pattern is found in the test results of the other tested Staggered shear key connections as well. It is expected that the differences in the lateral forces between the upper and lower steel bars have no significant influence on the shear behaviour.

The shear force V_F further increases to point C where the first cracks in the precast concrete appeared. The diagram does not show any observable changes at the instant of first cracks at $V_{F;C}$. The connection is further loaded to the ultimate shear force $V_{F;U}$ = 613,2 kN. Diagram III shows the measured points around the instant of reaching the ultimate shear force. A downturn can be observed from the ultimate shear force (613,2 kN) to the residual shear force (323,9 kN). Again, this is the snap back discussed in previous subsection. The lateral force $F\sigma_n$ of Strain4-00 increases after $V_{F;U}$ is reached. However, the lateral force of Strain4-01 decreases. It shows scattered measurements of the lateral forces after the ultimate shear force is reached. This could indicate non-uniform behaviour over the mortar connection which cannot be proven from the measurements.
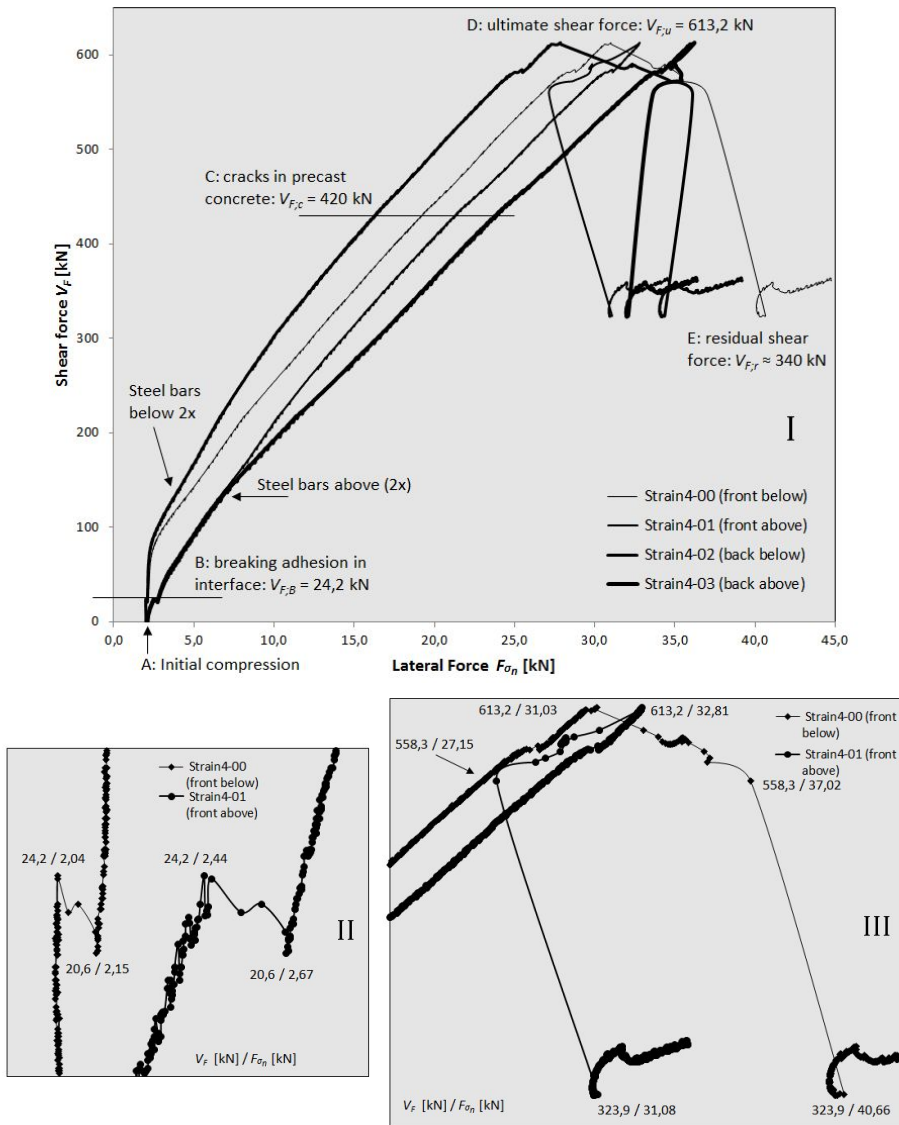
Figure 5.4: Shear force - lateral force relationship of Specimen 2-4

It can be concluded that during the shear test the lateral forces in the four steel bars show differences for which it is expected that it does not significantly effect the overall shear behaviour observed in the shear tests. As expected, the mortar connection tries to widen the vertical seam during transferring the increasing shear forces. The presence of the increasing lateral forces in the steel bars confirms this.

5.4.4   Shear force - lateral displacement relationship

In the diagrams I, II and III in figure 5.5 the relationships between the shear forces and lateral displacements are shown. The LVDT3-0X series of measurements correspond to the lateral displacements labeled in figure 5.1.
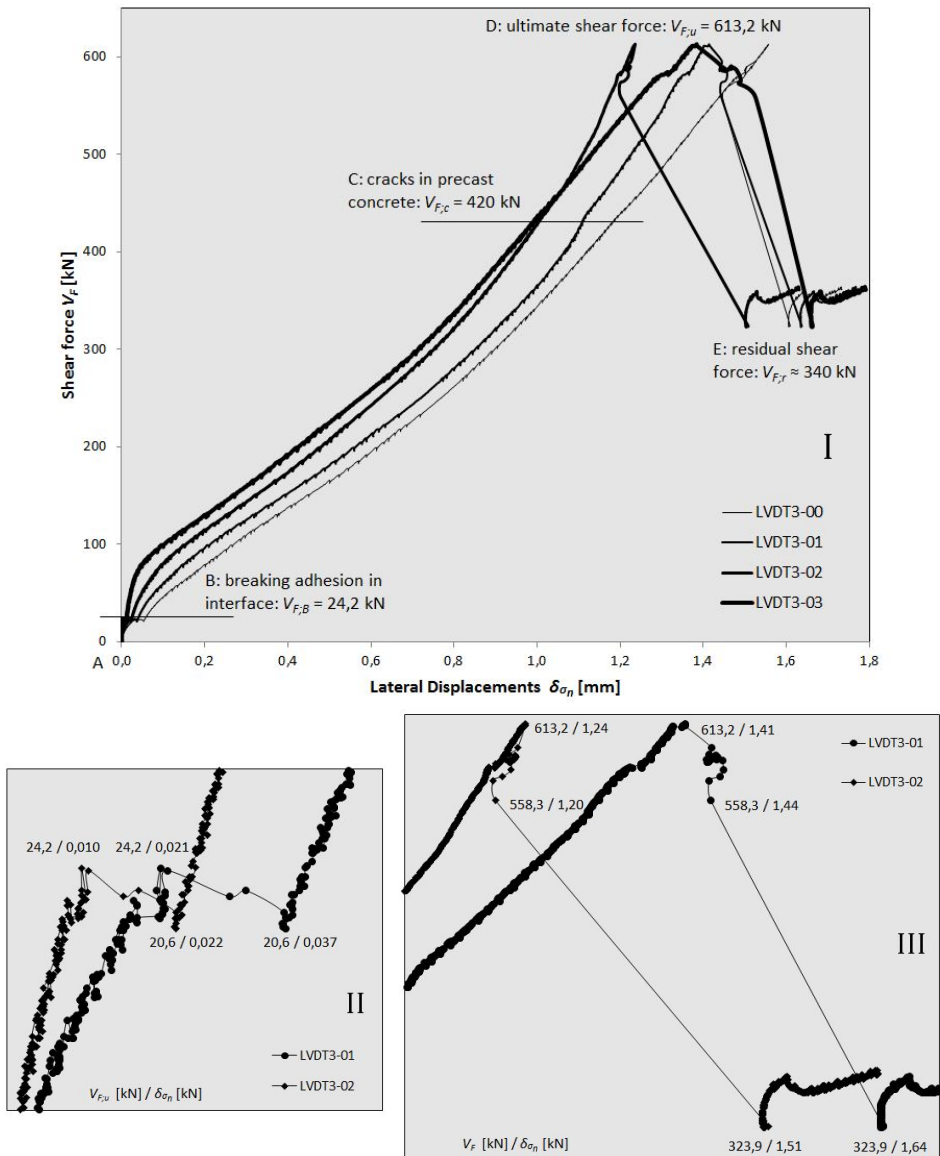
Figure 5.5: Shear force - lateral displacements relationship of Specimen 2-4

The relations develop, of course via the same stages A till E. The relations start in the origin of the diagram (A) where the shear force $V_{F;A}$ and the lateral displacements $\delta\sigma_{n;A}$ are both zero. The lateral displacements $\delta\sigma_n$ relate to the lateral forces $F\sigma_n$ since they both act perpendicular to the connection. If the lateral displacements increase the lateral forces also increase and vise versa. That this hold true can be proven with the next observation. Diagram I shows that the lowest sensor LVDT3-03 measures the lowest lateral displacement increase in stage A-C. The upper sensor LVDT3-00 deforms the most. The middle sensors develop in the same order. The lateral displacements development along the height of the connection can be visualised as a V-shaped deformation state. This observation can be linked to the lateral force developments in diagram I of figure 5.4. It shows the tensile forces in the steel bars below are lower than the tensile forces in the steel bars above according to the same V-shaped pattern. The lateral displacements of LVDT3-02 in diagram I show a steeper continuation from point C to D. The others change in this stage also a little. Causes for these changes are discussed in the previous subsection where diagrams revealed irregular behaviour in stage C-D as well.

5.4.5 Summed lateral force - lateral displacement relationship

The diagrams in figure 5.6 display the relationship between the summed lateral forces $F\sigma_{n;sum}$ and the lateral displacements $\delta\sigma_n$. The summed lateral force equals the summation of the four individual forces $F\sigma_n$ measured by sensors Strain4-00 till Strain4-03. The lateral displacements $\delta\sigma_n$ are the measurements from the four LVDT3-0X sensors.

Diagram I starts in A with a lateral force of $F\sigma_{n;sum}$ = 8,27 kN as a result of the slight initial compression. Adhesion breaks in B at a lateral force $F\sigma_{n;sum}$ = 8,97 kN. An increase of only 8,97 - 8,27 = 0,7 kN in stage A-B is measured. The diagram shows a similar trend for the four LVDT measurements till the instant of crack in C. Again, deviations from point C till D are observable in the diagram. The displacements development of the LVDT3-02 sensor stays behind. The summed lateral force $F\sigma_{n;sum}$ is 127,9 kN when the ultimate shear force equals $V_{F;D}$= 613,2 kN. Diagram II shows the measurements in detail. It shows the temporary resistance between 127,9 kN and 133,9 kN which is observed in diagram II of figure 5.2 as well. The snap back follows after this point leading to a lateral force of $F\sigma_{n;sum}$ = 138,2 kN. The relations in diagram I continue with an expected almost linear increase in the residual stage of the diagram.

A lateral stiffness can be read from this diagram. It is the lateral forces divided by the lateral displacement. This lateral stiffness is the combined stiffness of the steel bar assemblies with the steel plates, bolts and the concrete parts of the specimen. Diagram I in figure 5.6 shows curved force-displacement relationships representing the lateral connection behaviour. This demonstrates that this connection is tested with a non-linear lateral stiffness development. However, for the higher lateral forces a more linear lateral stiffness develops because the clearances in the stressed steel bar assemblies are disappeared.
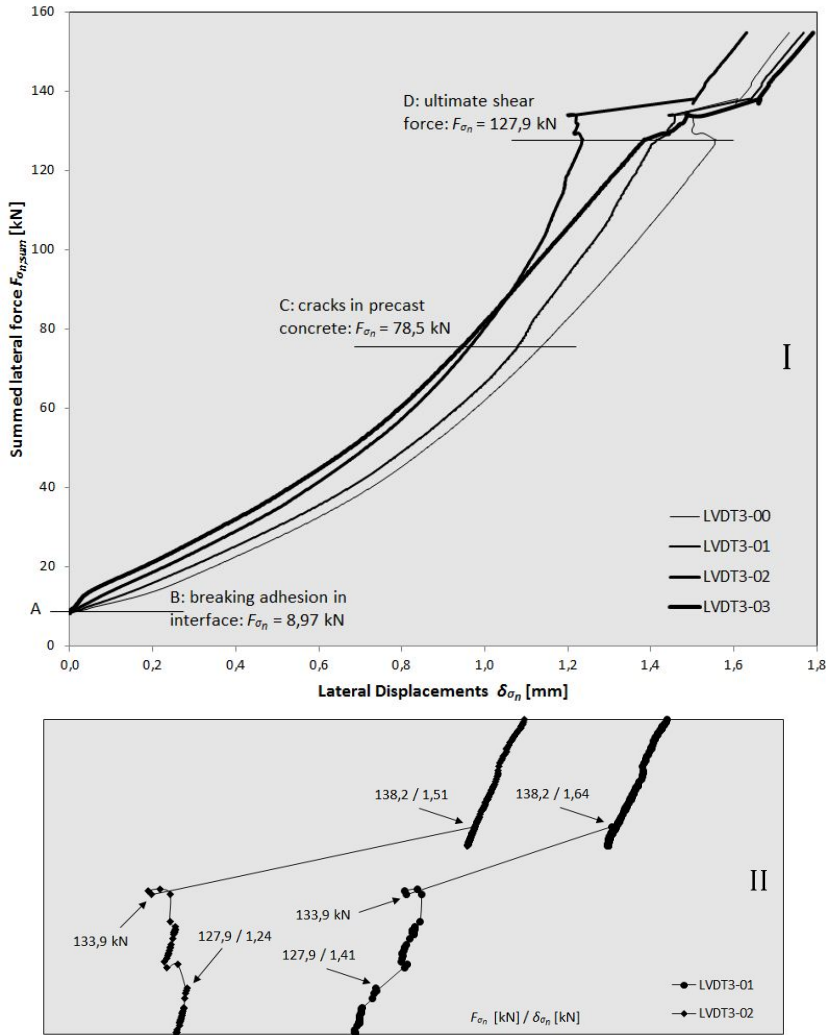
Figure 5.6: Summed lateral force - lateral displacements relationship of Specimen 2-4

5.4.6   Shear displacement - Lateral displacement relationship

Diagrams I and II in figure 5.7 display the relationship between the shear displacements and the lateral displacements. The lateral displacements $\delta\sigma_n$ taken from sensor LVDT3-01 (see figure 5.1) are set to the horizontal axis of the diagrams. This sensor is the upper of the middle two sensors measuring the lateral displacements. The vertical axis displays the shear displacements δ_V measured by sensor LVDT1-05. It is the middle of the three sensors LVDT1-0X. These diagrams display the distribution of shear and lateral displacements in the same diagram with the same scale.

Lateral Displacements δ_{σ_n} **[mm] - LVDT3-01**

A: breaking adhesion in
interface: $\delta_V = 0,037$ mm

C: cracks in precast
concrete: $\delta_V = 0,614$ mm

D: ultimate shear
force: : $\delta_V = 0,77$ mm

E: residual shear
force: $\delta_V \approx 2,43$ mm

I

0,77 / 1,41

1,17 / 1,44

2,43 / 1,64

II

δ_V [kN] / δ_{σ_n} [kN]

Figure 5.7: Shear displacement - lateral displacements relationship for Specimen 2-4

Diagram I shows that the shear displacements are dominant in stage A-B. The displacements bends to a more horizontal sloped development in stage B-D. It proves the larger increase of the lateral displacements than the shear displacements. This is different after the ultimate shear force is reached in point D. Then the displacements

bends to an almost vertical sloped relationship. The shear displacements increase the most in this part of the diagram. Again, diagram II shows the sudden large increase of the shear displacements δ_V in two steps from 0,77 mm to 2,43 mm.

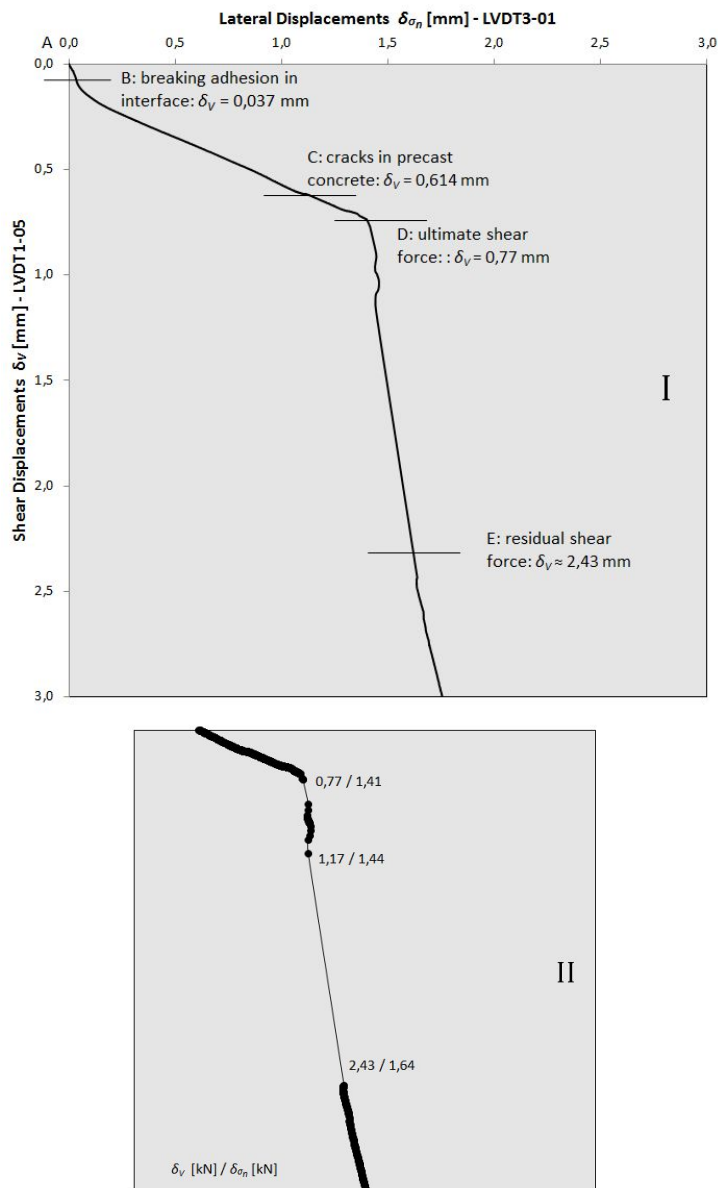The infinite number of diagonal compression struts in stage A-B according to figure 5.3A cause horizontal forces pushing both precast concrete L-elements apart. The initially applied lateral compression forces via the steel bars balance these dilation forces. As soon as the dilation force exceeds the initial compression force the connections starts to displace laterally. This causes a small rotation of the diagonal compression strut. For a short time, the tensile strength inside the vertical mortar-to-concrete interfaces offers lateral resistance against this rotation untill the adhesion breaks. After that the lateral forces in the steel bars increase substantially. The lateral stiffness of the steel bars assembly is lower than the shear stiffness of this connection. As a result, the lateral displacements grow faster than the shear displacements in stage B-D. It causes the more horizontally sloped displacement developments in the diagram. The sudden loss of shear stiffness at the ultimate shear force in point D changes the shear versus lateral stiffness ratio. The shear stiffness of the main crack in the residual stage E is very little relative to a mortar connection with three diagonal compression struts in stage A-D. It causes the faster growth of shear displacements relative to the lateral displacements in the final stage of diagram I.

5.5   Display of results in combined load-displacement diagram

The four diagrams discussed in previous section can be brought together in one combined load-displacement diagram. Figure 5.8 shows this diagram for the connection in specimen 2-4. The shear force (V_F) versus shear displacement (δ_V) relationship is displayed in diagram I. The shear displacements are taken from one of the three LVDT1-0X sensors displayed in figure 5.1. Sensors 04 and 06 register the shear displacements including the effect of the end keys at the top and bottom of the specimen. Sensor LVDT1-05 is the sensor that measures right in the centre of the connection. Measurements from this sensor are considered as the most accurate and used as shear displacements (δ_V) for diagram I. Diagram II shows the shear force (V_F) set against the summed lateral forces ($F\sigma_{n;sum}$). This summed lateral force is used for the representation of the lateral force on the connection from now on in this thesis because a separate display is less meaningful. Diagram III displays the summed lateral forces ($F\sigma_{n;sum}$) versus lateral displacement ($\delta\sigma_n$) diagram. The lateral displacements measured with sensor LVDT3-01 (see figure 5.1) are selected for this diagram. Again, this sensor measures close to the centre of the connection and away from the end effects. The final diagram IV presents the measured shear displacements (δ_V) versus lateral displacements ($\delta\sigma_n$) relationship. They all link to one another via the common horizontal and vertical axes.
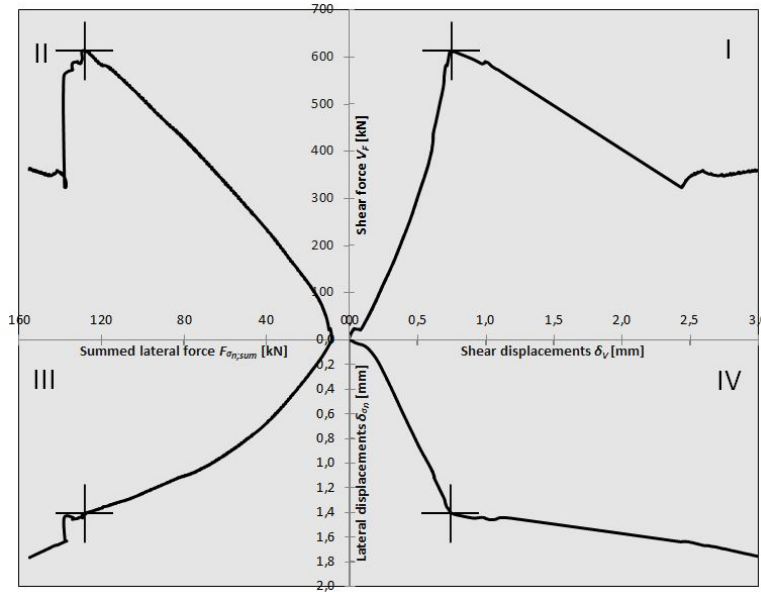
Figure 5.8: Combined load-displacement diagram (specimen 2-4)

5.6 Aligned shear key connection

5.6.1 Principal stages

Figure 5.9 shows in a diagram the relation between the shear force (V_F) and shear deformation (δ_V) of the Aligned shear key connection (specimen 1-4). It represents the principal shear behaviour of all Aligned shear key connections. Appendix E displays in E.1 photos of the cracked specimen 1-4 and provides photos taken during dismantling the specimens after the shear test. This connection is tested with Steel Fibre Reinforced Mortar, a lateral stiffness with M38 steel bars and an initial compression of 2,0 N/mm². The five drawings right in figure 5.9 show the principal stages A till E schematically.

Again, an infinite number of inclined compression struts transfer shear forces through the mortar in stage A-B according to drawing A. This is similar to the previously discussed mortar connection. Adhesion breaks at the instant of reaching $V_{F;B}$. Then the mortar connection enters stage B-C in which two types of compression struts continue the transfer of shear forces according to drawing B. The three struts span from one to the opposite key. The two other struts run from one key to the opposite key above or below as indicated in the same drawing B.

The first visible cracks appear in point C of the diagram. The cracks are visible on the photos in figure E.1. The shear force-shear displacement relation reveals that this point C is also the ultimate shear capacity ($V_{F;U}$) of this three-keyed connection. The

Staggered shear key connection discussed in previous section started cracking before the ultimate shear force is reached. It shows the Aligned shear key connection behaves different. The diagonal cracks displayed in figure 5.9C divide the mortar filling into two parts that are able to transfer forces. The two longer struts remain to be the dominant load-carrying bodies in stage C-D of the diagram. The appearance of a main crack in point D terminates the shear transfer via the the two long compression struts. The parameter "number of keys" determines if the ultimate shear force $V_{F;U}$ is equal to point C or D in the diagram. This phenomenon is explained and analysed in subsection 6.4.2.

The Aligned shear key connection continues to transfer shear forces via shear friction in the interface of the main crack. This residual shear capacity can be found in stage E of the diagram. Photos after dismantling the specimen are given in figure E.2. They reveal the main crack of this mortar connection.
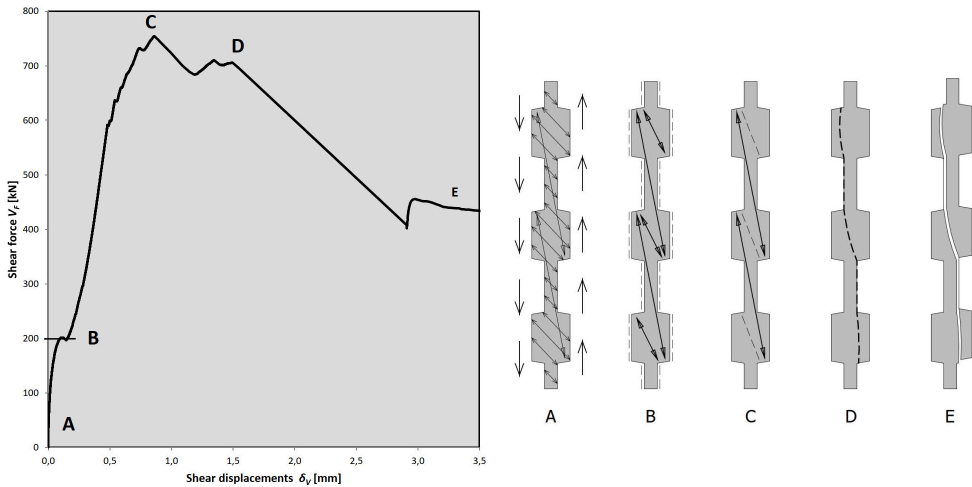
Figure 5.9: Principal stages of the Aligned shear key connection (Specimen 1-4)

5.6.2   Load-displacement diagrams

Figure 5.10 shows in the overall diagram the measured forces and displacements for the four Aligned shear key connections. The diagram incorporates the four subdiagrams (I to IV) according to the principles previously explained. The considered variables are pasted underneath the diagram.

Diagram I displays the relationships between the shear forces (V_F) and shear displacements (δ_V) for all Aligned shear key connections. The principal stages (A till E) addressed in previous subsection are labeled to the relations in this diagram. In the mortar-to-concrete interfaces adhesion breaks very fast in point B ($V_{F;B}$) for the specimens: 1-1 (37 kN), 1-2 (20 kN) and 1-3 (20 kN). However, adhesion breaks in the interfaces of specimen 1-4 at a considerable higher shear force $V_{F;B} = 200$ kN.

This is attributable to the larger compressive stress of 2,0 N/mm² (equals a summed lateral force of $F\sigma_{n;sum}$ = 240 kN) which is set prior to starting the shear test. The stress state in the vertical mortar-to-concrete interfaces is a combination of shear and compression. Lateral compression maintains the adhesive bonding and postpones the instant of debonding in the interfaces.

Figure 5.10: Diagrams for the Aligned shear key connection with a schematic representation of the applied variables underneath it

The mortar connections continue to transfer shear forces via the compression struts. The connections reach point C in the diagra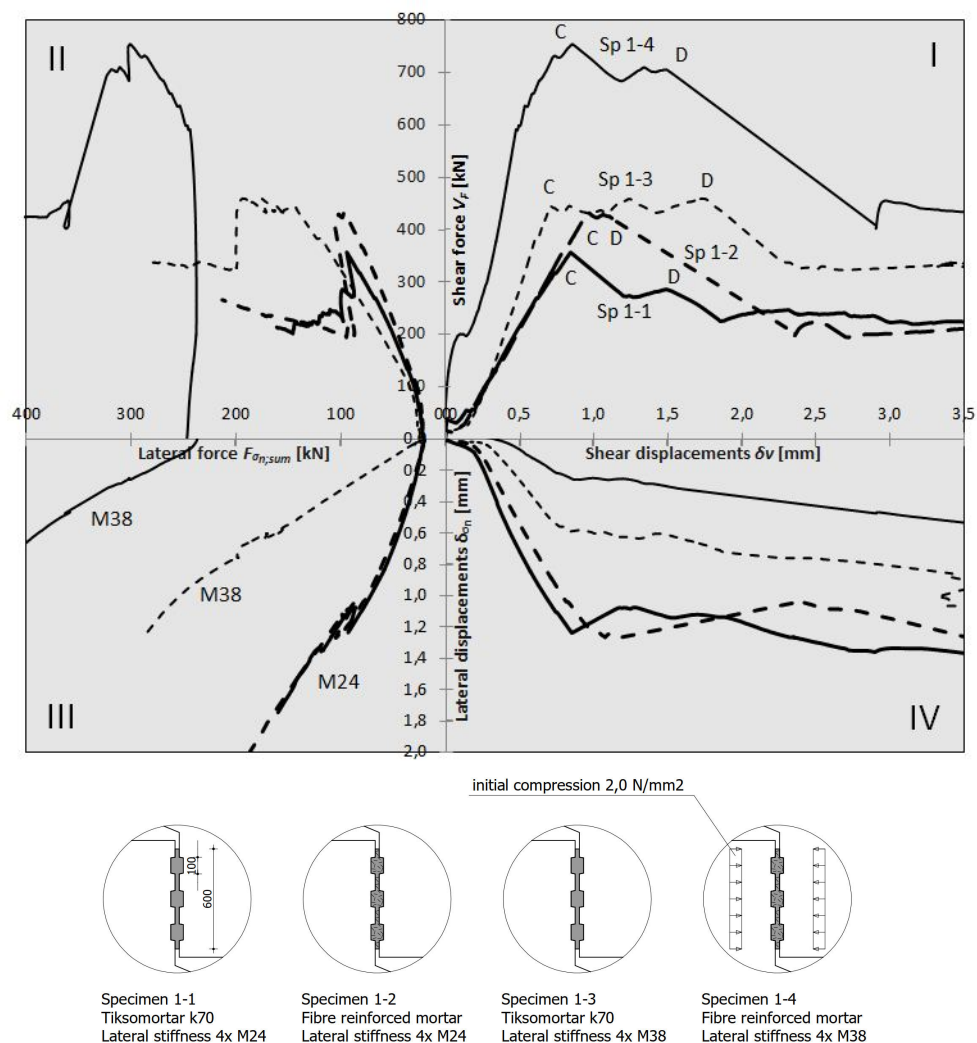m at different shear forces $V_{F;C}$: 1-1 (357 kN), 1-2 (433 kN), 1-3 (445 kN) and 1-4 (754 kN). This is the ultimate shear

force for three of the four connections ($V_{F;U} = V_{F;C}$). The ultimate shear force of connection 1-3 equals 459 kN in point D ($V_{F;U} = V_{F;D}$).

Diagram II displays the relationship between the shear force (V_F) and summed lateral force ($F\sigma_{n;sum}$). The pre-tensioning of the four steel bars with 20 kN (specimens 1-1 till 1-3) or 240 kN (specimen 1-4) can be identified in this diagram at the horizontal axis. The summed lateral force decreases slightly in stage A-B of specimen 1-4. This is observed for all of the four connections. However, it is less visible in the diagram for the other three.

Diagram III shows the summed lateral forces ($F\sigma_{n;sum}$) and lateral displacements ($\delta\sigma_n$) relationship. It shows the difference in lateral behaviour in case of respectively the M24 and M38 steel bars. The tangent stiffnesses for specimens 1-3 and 1-4 (both M38) in the diagram III develop approximately parallel to one another. This is true also for both the connections with M24 bars. The M38 tangent stiffnesses are less steep than the M24 tangent stiffnesses. It reveals the lower lateral stiffness of the M24 steel bars.

Diagram IV shows lateral displacements ($\delta\sigma_n$) set against the shear displacements (δ_V). The connections with M24 steel bars extend more than the connections tested with M38 bars. A higher lateral stiffness and a higher compressive stress reduce the lateral and shear displacements.

5.6.3 Failure cracks and residual shear capacity

Figure 5.11 shows the main cracks (dashed lines) observed in the four Aligned shear key connections. They all arise as soon as the shear force reaches point D in the diagram ($V_{F;D}$) and in all cases there is one diagonal crack and there are two vertical cracks. It demonstrates that the failure mechanisms of these connections are a combination of a dominant diagonal crack and shearing off the indentation of the shear key.
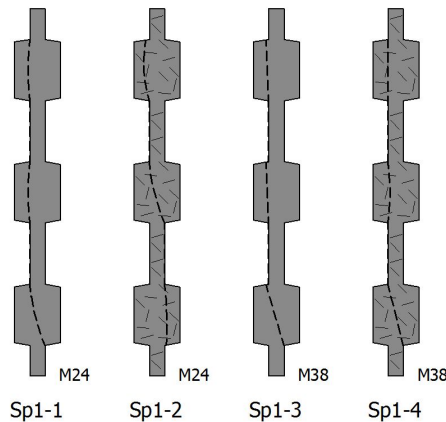

Figure 5.11: Failure cracks of the Aligned shear key connections

The residual shear forces $V_{F;E}$ of these connections are approximately 220 kN for connections 1-1 and 1-2. The residual force for connection 1-3 is approximately 327 kN and 424 kN for connection 1-4.

5.7 Staggered shear key connection

5.7.1 Load-displacement diagrams

Figure 5.12 shows in the overall diagram the measured forces and displacements of four Staggered shear key connections. These four are selected with the goal of providing understanding for the most important considered variables. The diagram in figure 5.13 displays the measurements of the remaining five connections by means of a shear force (V_F) versus shear displacements (δ_V) diagram. Appendix E displays in figure E.2 the photos of connection 2-7 as an example of this connection. The diagrams show incomplete load-displacement relations for connection 2-3 and 2-8 and that is caused by the detachment of the LVDT sensors at the instant of reaching the ultimate shear force. Also, the shear displacements taken from sensor LVDT1-04 instead of usually used LVDT1-05 sensor are used in order to make the measurements in the diagrams mutually comparable. The use of these other LVDT's will not change the overall assessment of this Staggered shear key connection.

The principal stages (A till E) addressed in figure 5.3 are found for all Staggered shear key connections. Table 5.5 provides the shear forces $V_{F;X}$ which belong to the points B till E. In the mortar-to-concrete interfaces adhesion breaks at shear forces ($V_{F;B}$) for specimens 2-1 (64 kN), 2-3 (16 kN) and 2-5 (10 kN). Shear forces with approximately the same values are found for the remaining connections in figure 5.13. Adhesion in the interfaces of specimen 2-7 breaks at a considerably higher shear force ($V_{F;B}$ = 174 kN). Again, this can be attributed to the larger summed lateral force ($F\sigma_{n;sum}$) which is the effect of the initial compression.

Shear force $V_{F;X}$	$V_{F;B}$	$V_{F;C}$	$V_{F;D}$	$V_{F;E}$
Connection	[kN]	[kN]	[kN]	[kN]
2-1	64	451	525	≈ 191
2-3	16	427	597	≈ 400
2-5	10	401	673	≈ 420
2-7	174	700	851	≈ 600
2-2	40	471	600	≈ 286
2-4	13	420	613	≈ 346
2-6	48	505	704	≈ 284
2-8	42	517	693	≈ 210
2-9	19	505	608	≈ 270

Table 5.5: Shear forces $V_{F;X}$ at points B till E for the Staggered shear key connection
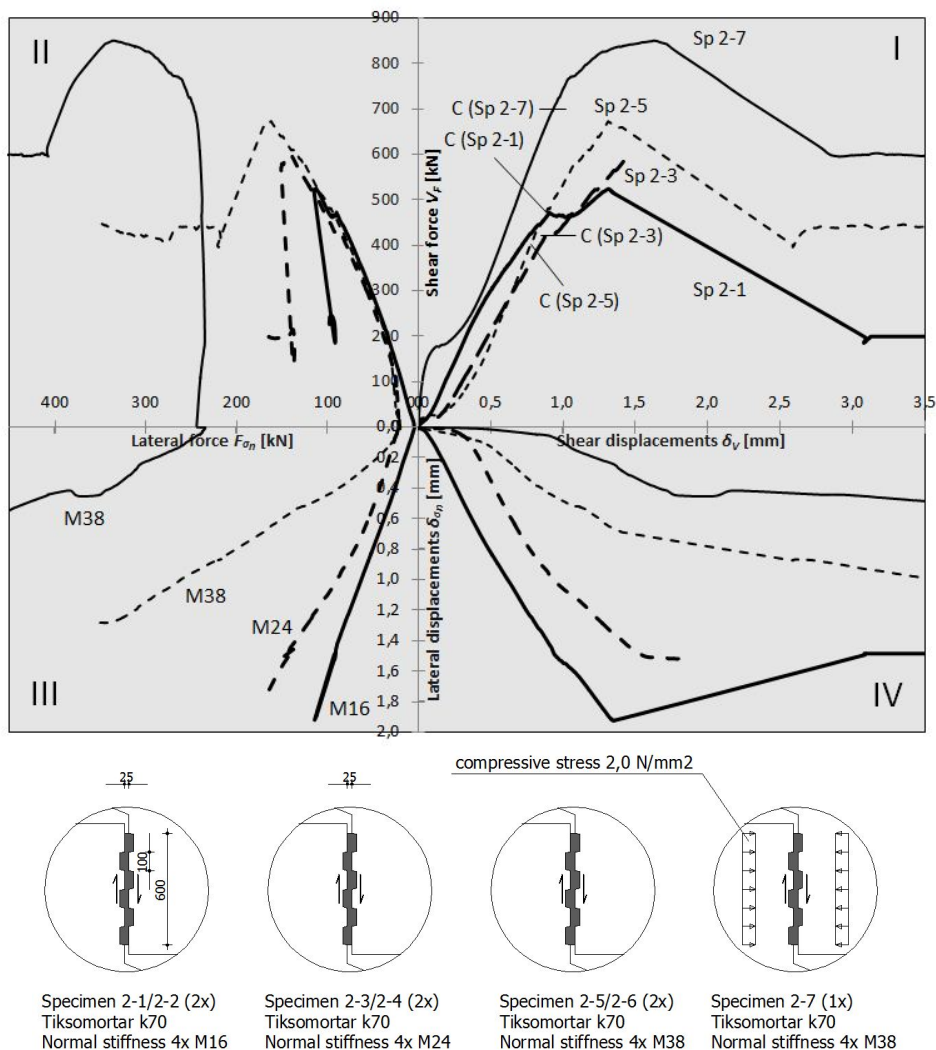
Figure 5.12: Diagrams for the Staggered shear key connection with schematic
representation of variables underneath it

The first diagonal cracks arise in point C at a shear force ($V_{F;C}$) for specimens
2-1 (451 kN), 2-3 (427 kN), 2-5 (401 kN) and 2-7 (700 kN). These points are marked
in the diagrams and listed in the table. After the appearance of the main crack in
point D ($V_{F;D} = V_{F;U}$), the shear force (V_F) drops to the residual stage E ($V_{F;E}$). Table
5.5 lists the corresponding shear forces at peak load ($V_{F;D}$) and the residual shear
forces ($V_{F;E}$). Diagram II, III and IV in figure 5.12 display the remaining forces and
displacements taken from the shear tests. The observations to be mentioned from
these diagrams are equal to the ones described for the Aligned shear key connection
in subsection 5.6.2.
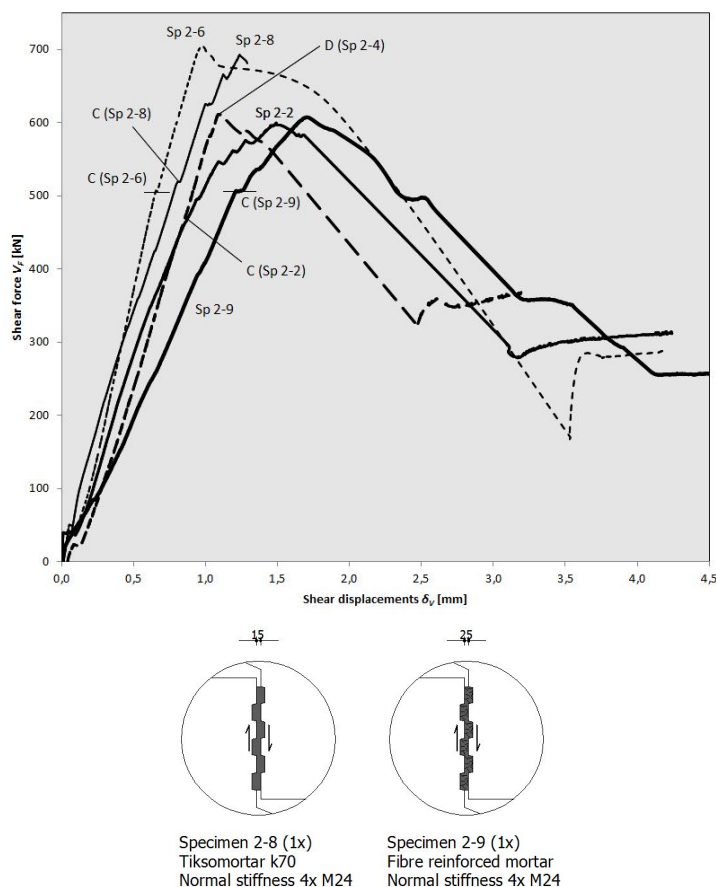
Figure 5.13: Diagrams for the Staggered shear key connection with schematic representation of variables underneath it

5.7.2 Failure cracks and residual shear capacity

Figure 5.14 displays the main cracks for all nine Staggered shear key connections. Different failure mechanisms can be identified. Shearing off the indentation is the most common one. Some diagonal cracks (as part of the main crack) are identified as well. The continuous vertical crack follows partly or fully the diagonal cracks which arose earlier in stage C-D. None of the connections fail ductile due to sliding off the sloped interfaces with significant lateral displacements. It proves that the Staggered shear key connection behaves as a rather stiff vertical mortar connection.
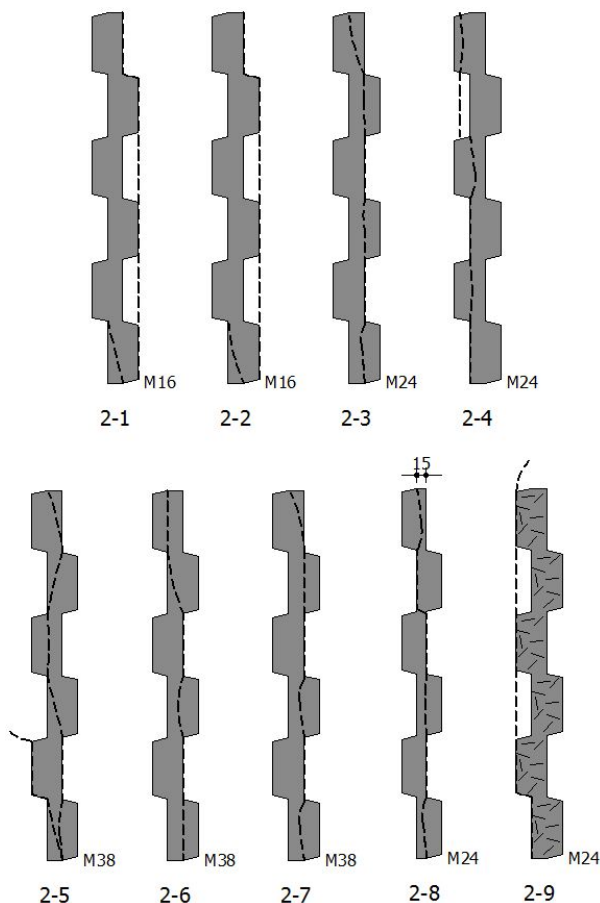
Figure 5.14: Failure cracks for all tested Staggered shear key connections

5.8 Aligned small shear key connection

5.8.1 Principal stages

The diagram in figure 5.15 displays the relationship between the shear force (V_F) and the shear displacements (δ_V) in case of the Aligned small shear key connection (specimen 3-9). Again, the drawings A till E next to the diagram represent the occurences during the shear test that are visable at the front or back side of the specimen. They are taken from the photos presented in section E.3 of appendix E. This connection is tested with Tiksomortar K70, a lateral stiffness supplied by 4xM38 steel bars and an initial compression of 0,1 N/mm^2.

Adhesion in the mortar-to-concrete interfaces allows a continuous transfer of shear forces through the mortar filling in stage A-B. Adhesion breaks at shear force ($V_{F;B}$) of 206 kN in point B of the diagram. Drawing B displays the breaking of

the adhesion with dashed lines. A few diagonal cracks arise in the mortar at the same time and drawing B displays these cracks as well. The shear force drops to point C ($V_{F;C}$ = 187 kN) immediately after the loss of adhesion in point B. Then, the connection continuous to transfer shear forces in stage C-D via mainly the eleven compression struts displayed in drawing A. The cracks in drawing C/D demonstrate that these struts transfer the forces between the cracks from one indentation to the opposite indentation underneath. It proves that the eleven struts are the main load carrying bodies in this connection. Additional diagonal cracks arise in the mortar and precast concrete later in stage C-D. They can be observed in the photos of section E.3. The cracked mortar filling terminates transferring shear forces via the eleven cracked diagonal struts as soon as the vertical failure crack arises in point D of the diagram ($V_{F;D}$ = $V_{F;U}$ = 710 kN). The dashed line in drawing D in figure 5.15 represents this failure crack. The photos in figure E.8 show this failure crack in the dismantled connection.
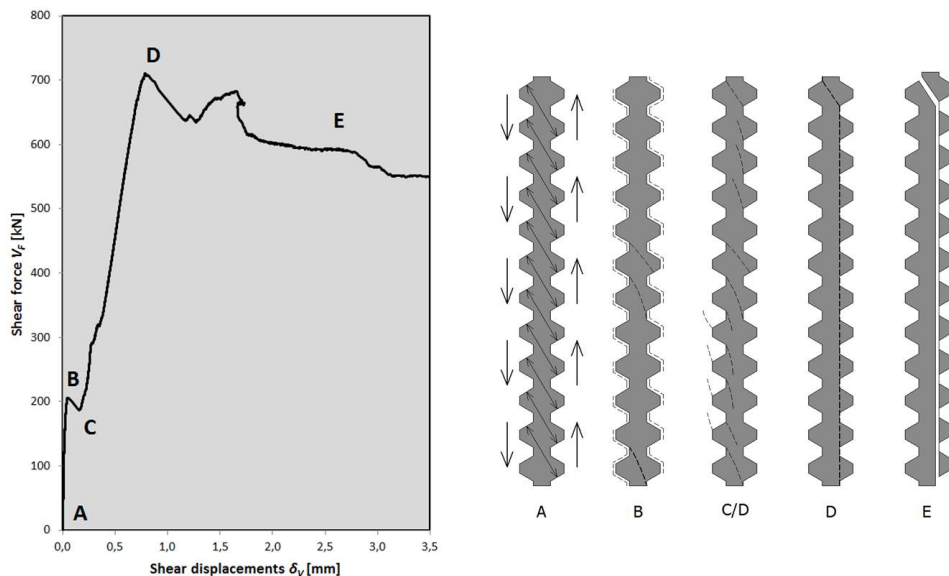
Figure 5.15: Principal stages of the Aligned small shear key connection in Specimen 3-9

Drawing E displays schematically the deformed crack in stage E of the diagram. This crack transfers the residual shear force ($V_{F;E}$) via shear friction. The drop from the failure load ($V_{F;D}$) to the residual load ($V_{F;E}$) processes gradually. There is a temporary increase of the shear force after the first drop in stage D-E. This connection found a new way of transferring forces via the cracked mortar filling. The cause of this observation cannot be extracted from the measurements and photos.

5.8.2 Load-displacement diagrams

The measurements for four Aligned small shear key specimens are selected for representation in this subsection. Figure 5.16 displays the combined load-displacement diagram with a schematic presentation of the applied variables underneath it. The considered variables are the lateral stiffness, the type of mortar and the use of bonding agent. All connections behave according to the principal stages A till E explained in the previous subsection.

Figure 5.17 shows a cutout of the load-displacement diagram. It displays a magnified view of the load-displacement behaviour of the connections in stage A-C of the shear tests. It allows the analysis of the connection behaviour in the stage where shear forces are transferred via adhesion of the mortar-to-concrete interfaces. This diagram shows the instants of debonding at different shear forces $V_{F;B}$. These forces are listed in table 5.6. Also, the diagram shows the absence of a clear instant in point C for specimens 3-1 and 3-5. The load-displacement relationships of these connections continues transferring shear forces after point B without a drop. Shear forces $V_{F;C}$ are observed for the remaining specimens 3-5 and 3-9 in the diagram. This phenomenon can be attributed to the applied steel bars. Specimens 3-1 till 3-4 are tested with M16 steel bars instead of M24 or M38 bars for specimens 3-5 and 3-9. The higher lateral stiffnesses of the M24 and M38 steel bars compress the connections and prevent the shear force V_F to drop to point C.

This Aligned small shear key connection is tested nine times. The diagrams and the table in current subsection belong to the measurements of four specimens. Appendix E provides the information about the remaining five specimens. Figure E.9 displays the shear force versus shear displacement diagram. Again, a cutout of this diagram has been made and is provided in figure E.10. Table E.1 gives the shear forces $V_{F;X}$ for these five connections. The appendix provides in figures E.11 and E.12 photos of the dismantled specimens 3-5 till 3-8.

Shear force $V_{F;X}$	$V_{F;B}$	$V_{F;C}$	$V_{F;D}$	$V_{F;E}$
Connection	[kN]	[kN]	[kN]	[kN]
3-1	109	–	278	≈ 263
3-3	125	–	314	≈ 260
3-5	164	120	431	≈ 385
3-9	206	187	710	≈ 600

Table 5.6: Shear forces $V_{F;X}$ (B till E) of the Aligned small shear key connection
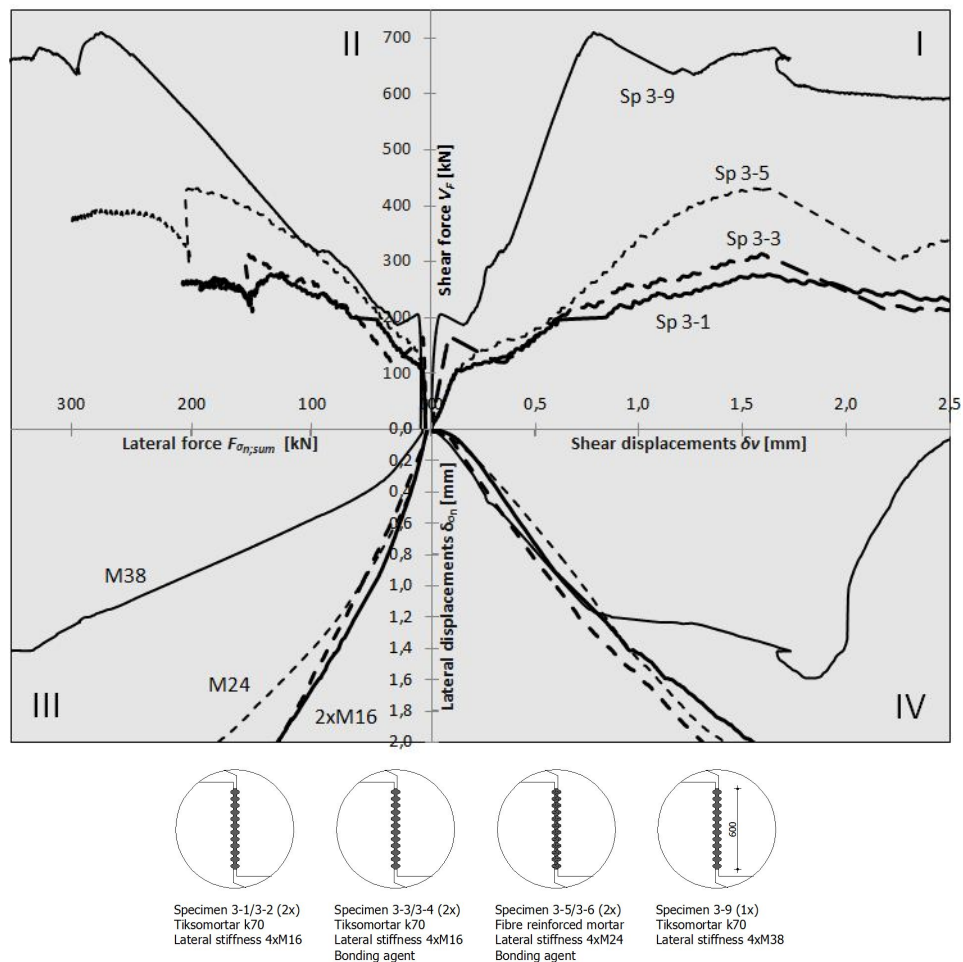
Figure 5.16: Diagrams for the Aligned small shear key connection
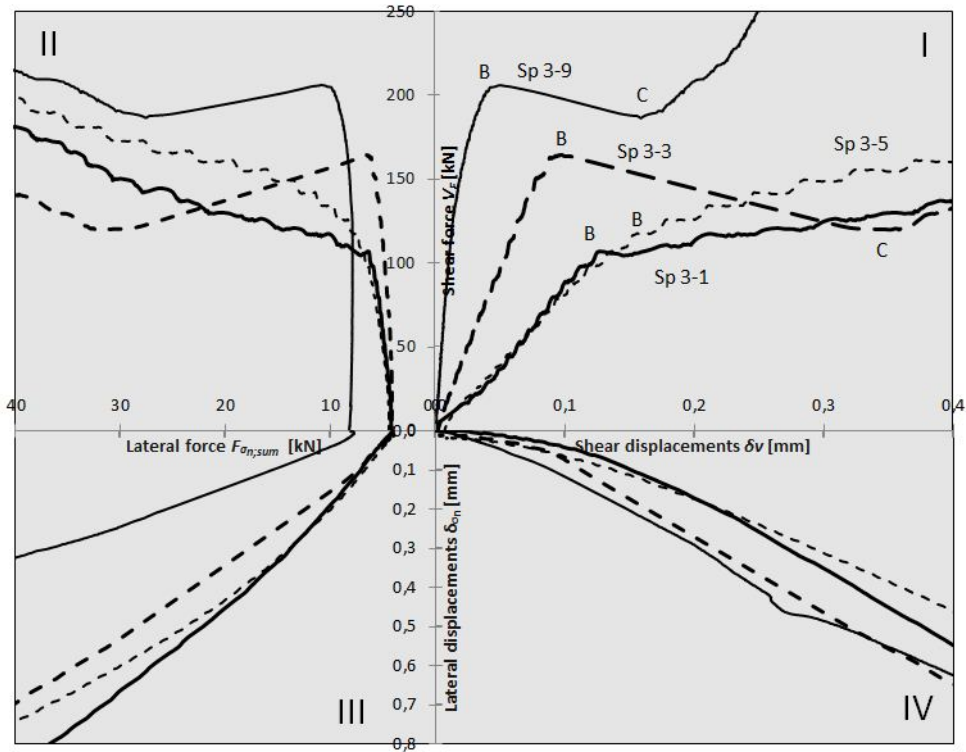
Figure 5.17: Enlarged diagram for the Aligned small shear key connection in the
traject from the origin till the first cracking (C)

5.8.3   Failure cracks and residual shear capacity

The failure crack of specimen 3-9 is discussed in the previous subsection (figure 5.15)
The photos of the dismantled specimens show that all Aligned small shear key con-
nections have a similar type of failure crack.

5.9   Plain waterjetted shear connection

5.9.1   Principal stages

The diagram in figure 5.18 displays the relationship between the shear forces (V_F)
and shear displacements (δ_V) of the Plain waterjetted shear connection of specimen
4-5. The drawings next to the diagram show the stages A-C during the shear test.
This behaviour is observed by using the photos presented in section E.4 of Appendix
E. This connection is tested with Tiksomortar K70, a lateral stiffness supplied by
4xM24 steel bars and an initial compression of 2,0 N/mm².

The diagram in figure 5.18 reveals that the Plain waterjetted shear connection goes through less stages than other connections in the research program. Stage A-B is the stage where the imposed shear force is transferred continously over the height of the 600 mm mortar filling. This force goes through two roughened mortar-to-precast concrete interfaces and the mortar filling. The shear connection reaches its failure force in point B of the diagram ($V_{F;B} = V_{F;U} = 568$ kN). Adhesion in one of the two mortar-to-concrete interfaces breaks at that point. The connection remains uncracked in the mortar or precast concrete as far as it is visible at the specimen surfaces up to the failure force. There are no shear keys present that are able to continue transferring shear forces via compression struts after the loss of adhesion. The failure force drops to the residual shear force $V_{F;C}$ which equals approximately 323 kN. A straight line between point B and C is to be expected. However, the sudden transition from failure force $V_{F;B}$ to residual force $V_{F;C}$ is measured via the same type of snap back which is already previously discussed.

The roughness of the interface and the actual summed lateral force ($F\sigma_{n;sum}$) determine together the residual shear capacity $V_{F;C}$ of this mortar connection. The photos in figure E.14 display the surfaces of the mortar filling and the waterjetted precast concrete which slide over one another in this interface. All five Plain waterjetted shear connections follow the stages just explained.
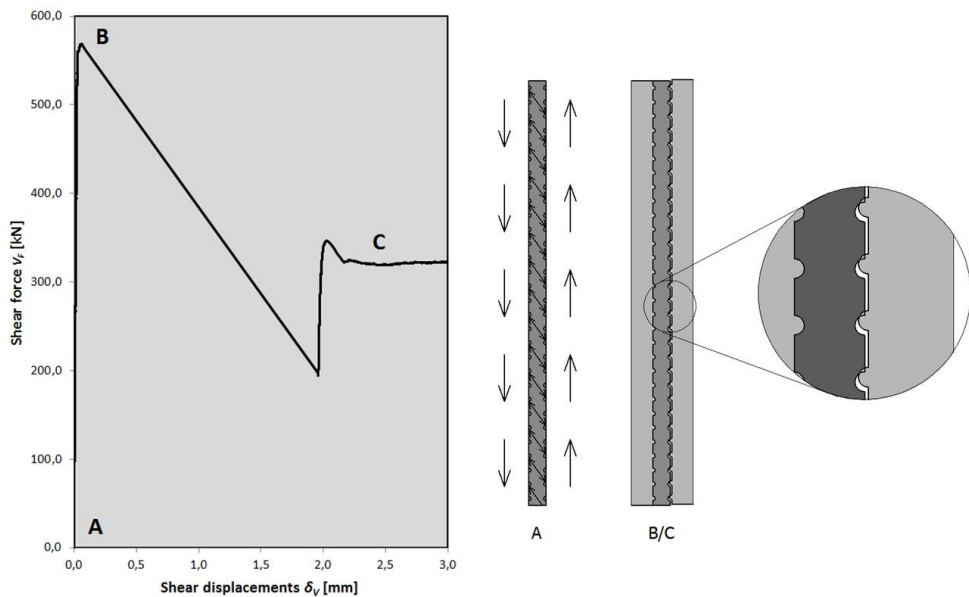
Figure 5.18: Principal stages of the Plain waterjetted shear connection (Specimen 4-5)

5.9.2 Load-displacement diagram

Figure 5.19 displays the combined load-displacement diagram of the five Plain waterjetted shear connections. The considered variables are given in the drawings below the diagram. The principal stages A till C found in previous subsection are found for all five connections. Table 5.7 provides the shear forces ($V_{F;X}$) that belong to the points B and C.
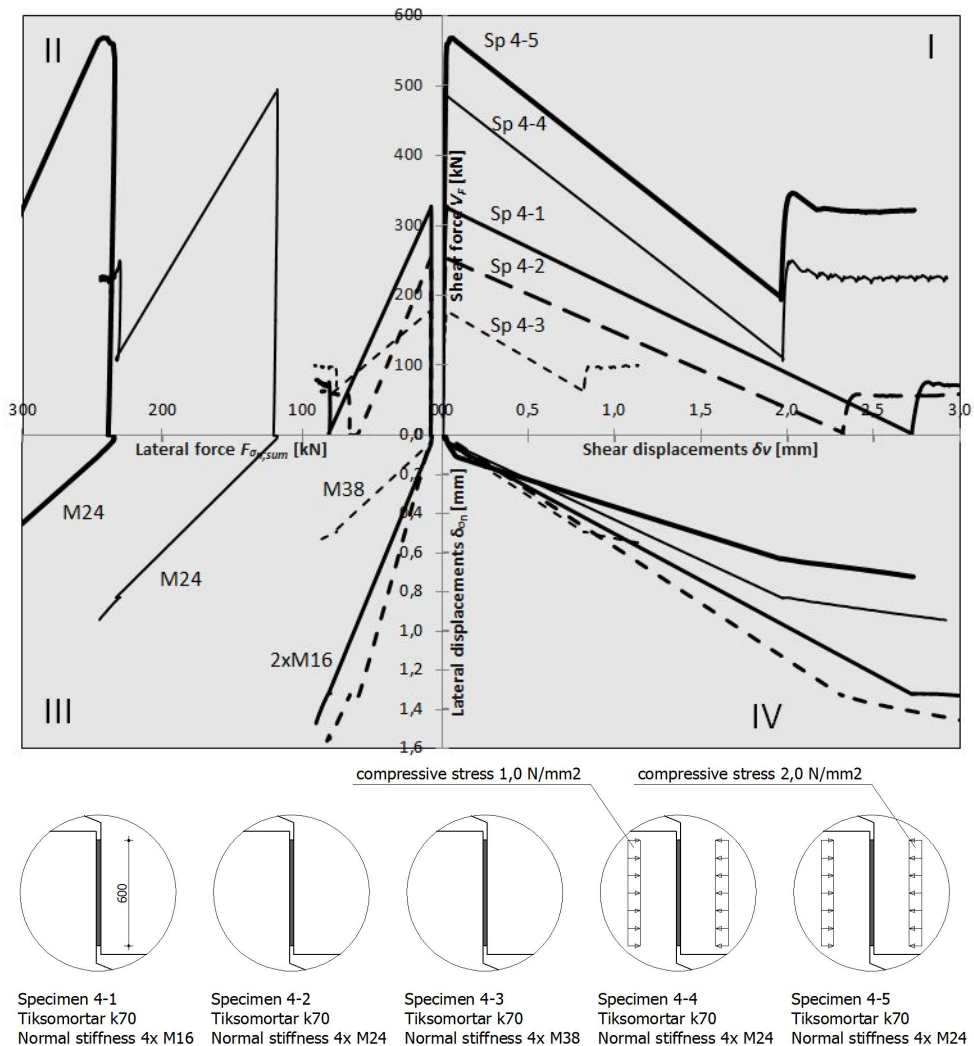
Figure 5.19: Diagram for the Plain waterjetted shear connection

The applied variables (lateral stiffness and initial compression) influence the value of the ultimate shear forces ($V_{F;B}$) and the residual shear forces ($V_{F;C}$) as can be seen

in both the diagram and table. It is barely visible but the summed lateral forces ($F\sigma_{n;sum}$) slightly decrease up to the ultimate shear force ($V_{F;B}$). Then, the shear forces drop to the residual stage C and the summed lateral forces increase significantly. They increase due to the appearance of the loss of adehesion in the rough interfaces that occurs in point B of the diagram. The rough interfaces dilate and that increase the lateral displacements, shear displacements and lateral forces in the steel bars to increase the lateral compression.

The summed lateral forces increase only a little after the start of the residual stage (C). They do not increase significantly while the shear displacements in diagram I do increase. The steel bars rotate a little because of the shear displacements (δ_V) causing a little extention and the small increase of the summed lateral forces ($F\sigma_{n;sum}$).

The summed lateral force ($F\sigma_{n;sum}$) versus lateral displacements ($\delta\sigma_n$) behaviour of the connections in stage A-B (up to $V_{F;B}$) is barely visable in diagram III. The instants at point B remain close to the horizontal axis and that has to be attributed to only little changes of the lateral forces and lateral displacements. After point B, the loss of adhesion cause the sudden increase of the lateral forces and lateral displacements which is clearly visible in diagram III. The different lateral stiffnesses provided by the steel bars (M16, M24 and M38) can be identified in this diagram.

Again, the shear displacements (δ_V) and lateral displacements ($\delta\sigma_n$) in stage A-B are barely visable in diagram IV because they are negligible small. They suddenly increase significantly to the values in the residual stage C. These changes from B to C dominate the diagram.

Diagram IV shows that the shear displacements increase more than the lateral displacements. The increase of the shear displacements is caused by the forced vertical deformations of 0,2 mm per minute by the hydrolic jack.

Shear force $V_{F;X}$	$V_{F;B}$	$V_{F;C}$
Connection	[kN]	[kN]
4-1	327	≈ 74
4-2	254	≈ 57
4-3	177	≈ 97
4-4	495	≈ 229
4-5	569	≈ 323

Table 5.7: Shear forces $V_{F;X}$ (B and C) of the Plain waterjetted shear connection

5.10 Serrated waterjetted shear connection

5.10.1 Principal stages

Two relations for the shear force (V_F) as function of the shear displacement (δ_V) are shown for the Serrated waterjetted shear connection in figure 5.20. The first belongs to specimen 5-1 and represents the four connections that are tested without signific-

ant initial compression. This connection is filled with Steel Fibre Reinforced Mortar and tested with a lateral stiffness imposed by the 4x M16 steel bars. The second diagram is representative for the two connections that are tested with an initial compression of 1,0 or 2,0 N/mm². The relation printed is the one of specimen 5-4 in which the initial compression was 1,0 N/mm², M24 steel bars were applied and was filled with Steel Fibre Reinforced Mortar. Section E.5 of Appendix E displays photos taken from specimen 5-3. The cracks as they can be seen on these photos are used for the drawings printed between the two diagrams in figure 5.20.
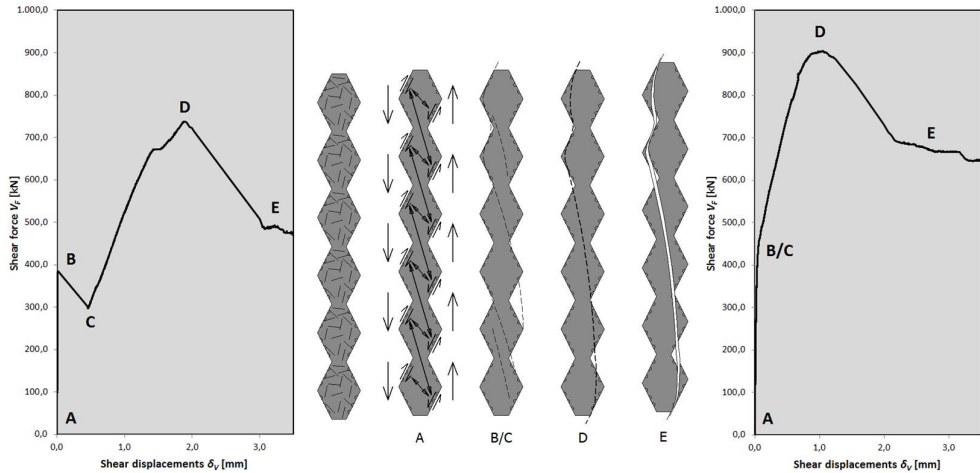
Figure 5.20: Principal stages of Serrated waterjetted shear connection for specimen 5-1 (left diagram) and for specimen 5-4 (right diagram)

Drawing A in figure 5.20 displays the compression struts that span between the both precast concrete L-elements in stage A-B. The compression struts press against the sloped and roughened mortar-to-concrete interfaces. The interfaces that are not compressed by the struts contribute to the transfer of shear forces as well. The reason is that the mortar-to-concrete interfaces are uncracked and able to transfer tensile forces from the precast concrete to the mortar. The connections transfer the shear forces without considerable shear displacements in stage A-B as can be observed in both diagrams. They remain uncracked up to point B with shear force ($V_{F;B}$). Point B marks the appearance of cracks in the mortar filling as well as the mortar-to-concrete interfaces as schematically shown in drawing B/C of the figure.

The connections behave differently after the first cracks appeared. The shear force $V_{F;B}$ drops to a shear force $V_{F;C}$ for specimen 5-1 in the left diagram of figure 5.20 whereas the relation of connection 5-4 a gradual transition to the a steep stage C-D displays. This different behaviour is due to the larger lateral compression present in connection 5-4.

The number of cracks in the mortar connection increases in stage C-D. Point D in both diagrams corresponds to the failure force ($V_{F;D} = V_{F;U}$). The first diagram

(specimen 5-1) shows a rather sharp transition in point D. The second diagram (specimen 5-4) displays a more gradual development when reaching the ultimate shear force. Again, this behaviour has to be attributed to the larger actual lateral compression stresses present at the instant of failure. It causes a gradual transition in point D. Drawing D and E in the figure show the failure crack of specimen 5-1 after which the residual stage of this connection is reached.

5.10.2 Load-displacement diagram

Figure 5.21 shows a load-displacement diagram with the measurements of connections 5-1 till 5-5. These five connections are tested with Steel Fibre Reinforced Mortar. The variables of all six Serrated waterjetted shear connections are displayed schematically in figure 5.22. Table 5.8 shows the shear force ($V_{F;X}$) values that correspond to the ones drawn in figure 5.20. Figure 5.23 shows enlarged a cutout of the full load-displacement diagram for analysis of the connection behaviour in stage A-B. Figures E.18 and E.19 in Appendix E display the measurement data of the remaining connection 5-6 together with the data of connections 5-1 till 5-3. The variables lateral stiffness and type of mortar can be analysed with the help of these diagrams.
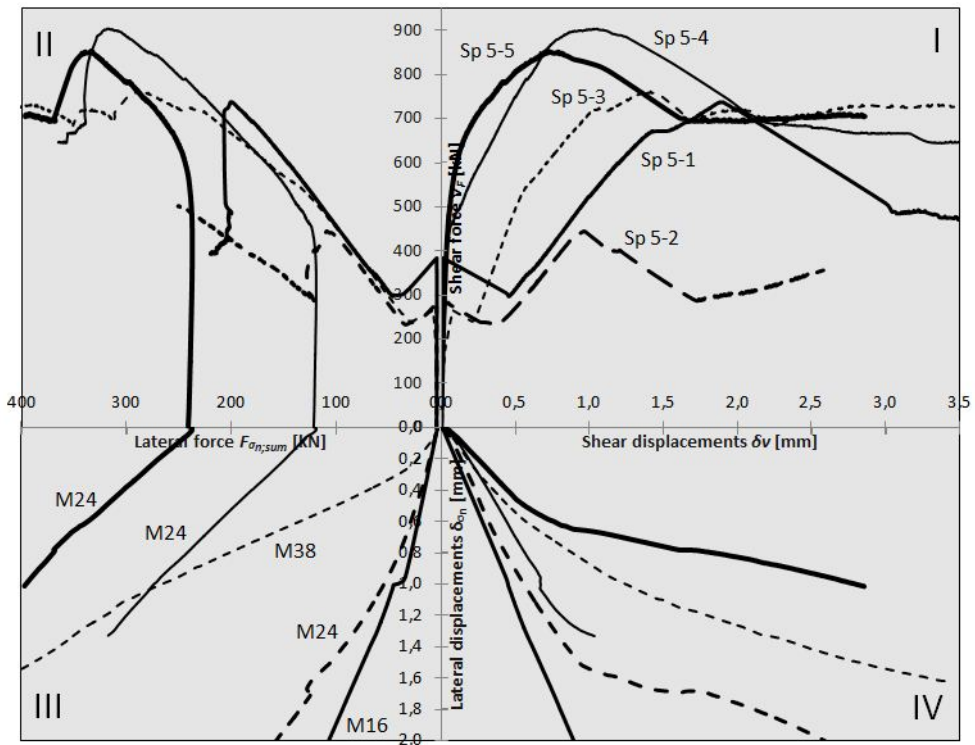
Figure 5.21: Diagram for the Serrated waterjetted shear key connection

Specimen 5-1
Fibre reinforced mortar
Lateral stiffness 4x M16

Specimen 5-2
Fibre reinforced mortar
Lateral stiffness 4x M24

Specimen 5-3
Fibre reinforced mortar
Lateral stiffness 4x M38

initial compression 1,0 N/mm2   initial compression 2,0 N/mm2

Specimen 5-4
Fibre reinforced mortar
Lateral stiffness 4x M24

Specimen 5-5
Fibre reinforced mortar
Lateral stiffness 4x M24

Specimen 5-6
Tiksomortar k70
Lateral stiffness 4x M38

Figure 5.22: Variables for the Serrated waterjetted shear key connection
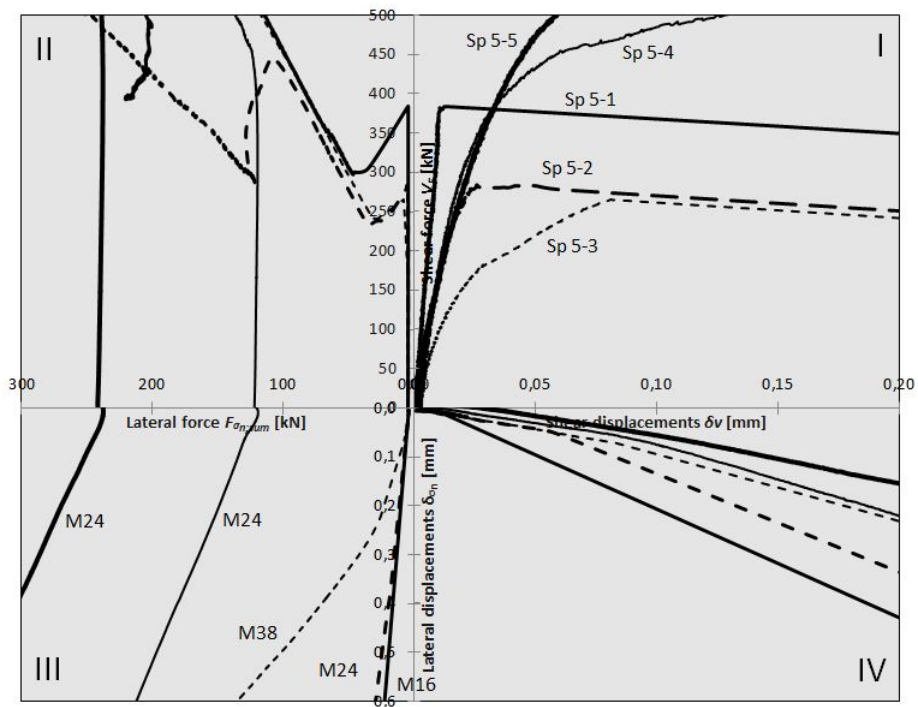
Figure 5.23: Enlarged diagram for the Serrated waterjetted shear key connection

Shear force $V_{F;X}$	$V_{F;B}$	$V_{F;C}$	$V_{F;D}$	$V_{F;E}$
Connection	[kN]	[kN]	[kN]	[kN]
5-1	384	297	738	≈ 489
5-2	283	235	445	≈ 592
5-3	265	241	762	≈ 725
5-4	442	–	904	≈ 668
5-5	620	–	853	≈ 695
5-6	260	231	817	≈ 682

Table 5.8: Shear forces $V_{F;X}$ of the Serrated waterjetted shear connection

5.10.3 Failure cracks

Figure 5.24 displays graphically the main failure cracks of the six Serrated waterjetted shear connections. These failure cracks arise in one of the two serrated mortar-to-concrete interfaces. A few of them are present in one interface and cross the mortar filling half way up the connection to the opposite interface. The failure mechanism of these connections can be classified as breaking adhesion of the mortar-to-concrete interface. Additionally, the tips of the serrated concrete and mortar shear off. They form together the shape of a vertical wave.
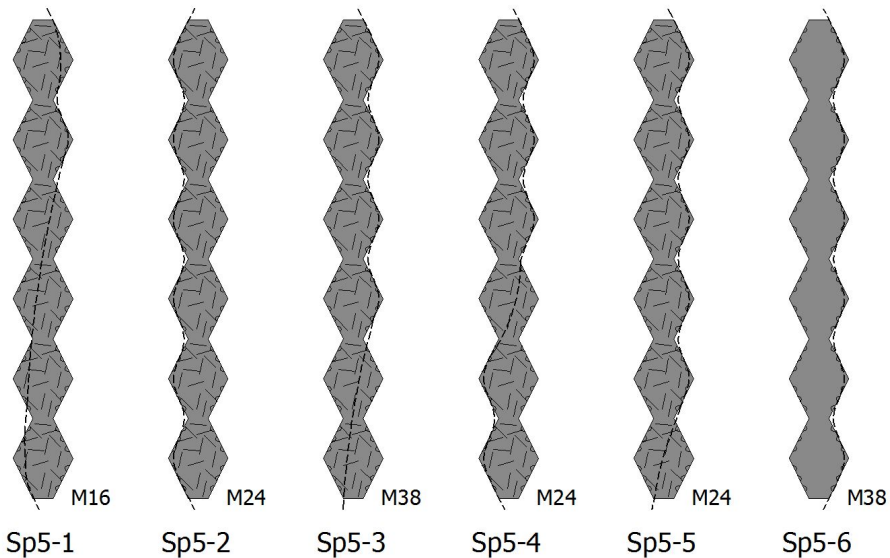
Figure 5.24: Main cracks of the Serrated waterjetted shear key connection

5.11   Stiffnesses of connections

5.11.1   Shear stiffness

The angle of the tangent lines along the shear force-displacement relationships represents the actual shear stiffnesses k_v. The shear stiffness is different in each of the principal stages and the highest in stage A-B. It becomes less high after the adhesion breaks in the interfaces in point B of the diagrams. However, the shear stiffnesses in stage B-C are still rather high. They are actually the most important because adhesion provided in the previous stage is normally unusable for vertical mortar connections. The final stage is the residual stage. The tangent line becomes alsmost horizontal which equals the absence of a considerbly shear stiffness.

The shear stiffness k_v can be defined as:

$$k_v = \frac{\Delta V_F}{\Delta \delta_V} \tag{5.1}$$

where:

k_v	shear stiffness	kN/mm
ΔV_F	difference between two shear forces on the tangent line $(V_{F;2} - V_{F;1})$	kN
$\Delta \delta_V$	difference between two shear displacements which belong to the two shear forces $(\delta_{V;2} - \delta_{V;1})$	mm

Table 5.9 shows the shear stiffnesses k_v of all tested mortar connections in the first (A-B) and second (B-C) stages. They are taken from the shear force-displacement relationships and calculated with equation 5.1. The slopes of the lines used for determining the shear stiffnesses approximate the angle of the mean tangent lines in both of the stages.

A number of mortar connections behave with a significant shear stiffness in stage A-B with a considerable shear force $V_{F;B}$. The column A-B in the table displays these stiffnesses. The stiffnesses present in stage B-C are rather high as well. They depend fairly on the lateral stiffness provided by the steel bars M16, M24 and M38. Therefore, the table displays them in separated columns for a quick overview on the effect of varying the lateral stiffness.

Tiksomortar k70 (T) / SFRM (S)		Shear stiffness k_v [kN/mm]				Lateral stiffness k_h [kN/mm]		
1. Aligned shear key		A-B	B-C (M16)	B-C (M24)	B-C (M38)	(M16)	(M24)	(M38)
Specimen 1-1	(T)			510			40	
Specimen 1-2	(S)			512			46	
Specimen 1-3	(T)				854			233
Specimen 1-4 --- (2,0 N/mm²)	(S)	2150			1265			271
2. Staggered shear key		A-B	B-C (M16)	B-C (M24)	B-C (M38)	(M16)	(M24)	(M38)
Specimen 2-1	(T)		591			53		
Specimen 2-2	(T)		570			51		
Specimen 2-3	(T)			557			52	
Specimen 2-4	(T)			653			45	
Specimen 2-5	(T)				727			215
Specimen 2-6	(T)				903			223
Specimen 2-7 --- (2,0 N/mm²)	(T)	1827			834			296
Specimen 2-8 --- seam 15mm	(T)			612			62	
Specimen 2-9	(S)			440			64	
3. Aligned small shear key		A-B	C-D (M16)	C-D (M24)	C-D (M38)	(M16)	(M24)	(M38)
Specimen 3-1	(T)	872	123			49		
Specimen 3-2	(T)	570	194			53		
Specimen 3-3 --- bonding agent	(T)	780	264			62		
Specimen 3-4 --- bonding agent	(T)	781	159			51		
Specimen 3-5 --- bonding agent	(S)	1843		158			68	
Specimen 3-6 --- bonding agent	(S)	1619		345			93	
Specimen 3-7 --- bonding agent	(S)	415			561			291
Specimen 3-8 --- bonding agent	(S)	1501			644			254
Specimen 3-9	(T)	4865			906			284
4. Plain waterjetted shear connection			A-B (M16)	A-B (M24)	A-B (M38)	(M16)	(M24)	(M38)
Specimen 4-1	(T)		16588			76		
Specimen 4-2	(T)			13596			59	
Specimen 4-3	(T)				8928			244
Specimen 4-4 --- (1,0 N/mm²)	(T)			84273			118	
Specimen 4-5 --- (2,0 N/mm²)	(T)			21790			96	
5. Serrated waterjetted shear connection		A-B	C-D (M16)	C-D (M24)	C-D (M38)	(M16)	(M24)	(M38)
Specimen 5-1 --- (M16)	(S)	38209	399			64		
Specimen 5-2 --- (M24)	(S)	13278		405			122	
Specimen 5-3 --- (M38)	(S)	6378			609			322
Specimen 5-4 --- (1,0 N/mm²) --- (M24)	(S)	11831		829			160	
Specimen 5-5 --- (2,0 N/mm²) --- (M24)	(S)	10074		432			168	
Specimen 5-6 --- (M38)	(T)	12713			1016			261

Table 5.9: Shear stiffnesses k_v and Lateral stiffnesses k_h

5.11.2 Lateral stiffness

The four steel bars, the steel transverse blocks with bolts at both bar ends and the precast concrete of the specimen (see figure 5.25) together are decisive for the lateral stiffnesses k_h present on the mortar connections. The steel bars are loaded with tensile forces, the transverse blocks with bending moments and the precast concrete L-elements are compressed by the lateral force equal to $F\sigma_{n;sum}$. All specimen components behave with a certain stiffness and are linked to one another as springs in series. The stiffnesses of each of the separate components can be measured in the

laboratory and combined to one lateral stiffness. However, the actual lateral stiffness k_h can be taken from the measured lateral force $F\sigma_{n;sum}$ in the steel bars and the lateral displacement $\delta\sigma_n$.

The lateral stiffness k_h can be defined as:

$$k_h = \frac{\Delta F\sigma_{n;sum}}{\Delta\delta\sigma_n} \tag{5.2}$$

where:

k_h	lateral stiffness	kN/mm
$\Delta F\sigma_{n;sum}$	difference between two lateral forces on the tangent line $(F\sigma_{n;sum;2} - F\sigma_{n;sum;1})$	kN
$\Delta\delta\sigma_n$	difference between two lateral displacements which belong to the two lateral forces $(\delta\sigma_{n;2} - \delta\sigma_{n;1})$	mm

Table 5.9 displays three columns with lateral stiffnesses k_h. Each of them belong to one of the used set of steel bars M16, M24 or M38. They are taken from the lateral force-displacement relationships (diagram III in the combined load-displacement diagram) previously provided in this thesis.

Figure 5.25: Lateral stiffness provided by steel bars, transverse blocks and precast concrete L-elements

5.12   Concluding remarks

The test results of all five vertical mortar connections has been reported and discussed in this present chapter. The analyses show that the shear force-diplacement relationships go through principal stages during the shear tests. These stages can be

linked to certain events in the mortar connections during the process of increasing the shear force on the specimens. The occurances are:

- debonding of the mortar-to-concrete interfaces;

- appearance of cracks in the mortar or precast concrete;

- reaching the maximum shear force when the failure crack appears;

- transfer of shear forces via shear friction in the post-peak failure crack in the mortar.

The five mortar connections behave to some extent differently. In this respect the following can be mentioned for the different type of connections, when compared to what in this thesis is seen as the standard connection behaviour:

- **Aligned shear key connection;** the instant of first diagonal cracks equals the ultimate failure force. The main crack appears later at a lower shear force than the ultimate failure force;

- **Staggered shear key connection;** this connection behaves in shear fully according to standard connection behaviour;

- **Aligned small shear key connection;** the instant of debonding takes place at a considerable higher shear force than for those mentioned above. A small drop occurs after debonding. At the same time, first cracks appear immediately after the instant of debonding in the mortar and concrete.

- **Plain waterjetted shear connection**; the instant of debonding equals the ultimate failure force. After that, this connection goes straight to the residual branch of the shear force-displacemnt diagram. There are no cracks in the mortar. The failure crack is right in the mortar-to-concrete interface.

- **Serrated waterjetted shear connection;** the instant of debonding takes place at a considerable higher shear force than for those mentioned above. A small drop occurs after debonding for the mortar connections without initial compression. At the same time, first cracks appear immediately after the instant of debonding in the mortar and concrete. The place of the failure crack is mainly in the mortar-to-concrete interfaces.

Chapter 6

Detailed Analyses of the Mortar Connections

6.1 Introduction

Using the test results provided in the previous chapter, the functioning of the connections and the influence of the various variables on the shear behaviour are analysed in this chapter. First, the Staggered shear key connection is studied in detail in section 6.2. How the connection functions and how the observed shear behaviour relates to a simplified analytical approach with an inclined compression strut is discussed. Also, the connection behaviour is simulated with a finite element model.

Section 6.3 provides analyses of the influence of various variables on the behaviour of the Staggered shear key connection. The effect of the lateral stiffness, the thickness of the seam, the type of mortar and lateral compression on the shear behaviour are analysed.

The Staggered shear key connection has its specific preselected profile of the mortar-to-concrete interface. The remaining four connections are constructed with other profiles and some have waterjetted concrete surfaces for getting roughened mortar-to-concrete interfaces. These interface properties are considered as a variable in this chapter. The effects of these varied interfaces are analysed in section 6.4.

Section 6.5 provides an assessment of the five mortar connections on their structural performance for application. One of them is judged as the best for use as vertical mortar connection between precast concrete elements in shear wall structures. For this connection, an equation for predicting the shear capacity is presented and a compression strut model for modeling its shear behaviour is proposed. Section 6.6 provides concluding remarks on the findings presented in this chapter.

To support the analyses, figure 6.1 displays a graphical overview of the specimens and variables. The framed specimens link to the test results provided in the diagrams of the different sections in this chapter.
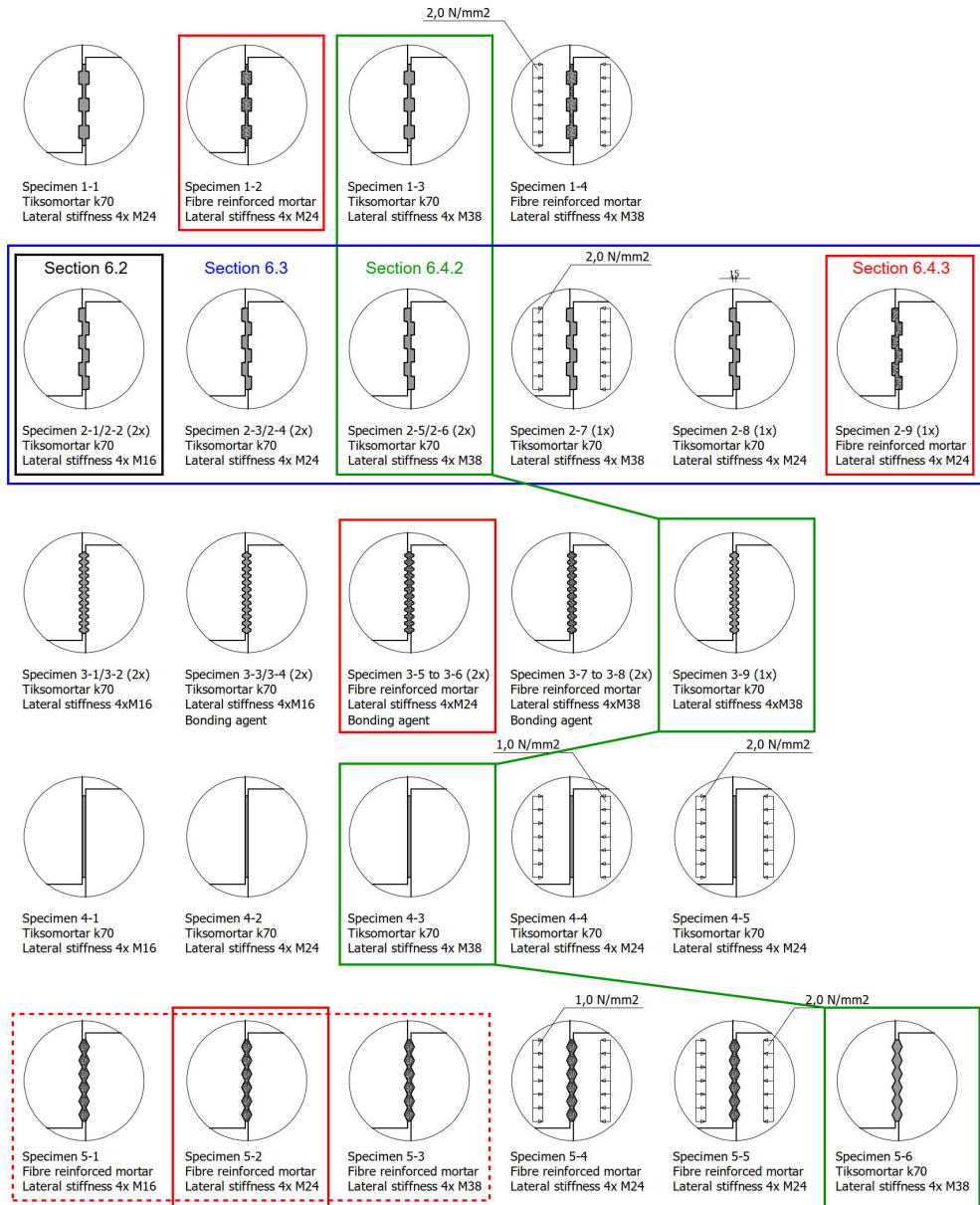
Figure 6.1: Graphic overview of specimens and variables

6.2 Staggered shear key connection

6.2.1 Analysis of connection behaviour

The two identical connections 2-1 and 2-2 are analysed first. The Tiksomortar K70 is applied as filling and they are clamped laterally by four external steel bars M16. Figure 6.2 displays the test results for the measured forces and displacements in vertical and lateral direction. In general they show approximately the same behaviour for both connections. It can be observed that with an increase of the shear forces V_F the shear displacements δ_v, the lateral forces $F\sigma_{n;sum}$ and the lateral displacements $\delta\sigma_n$ increase.

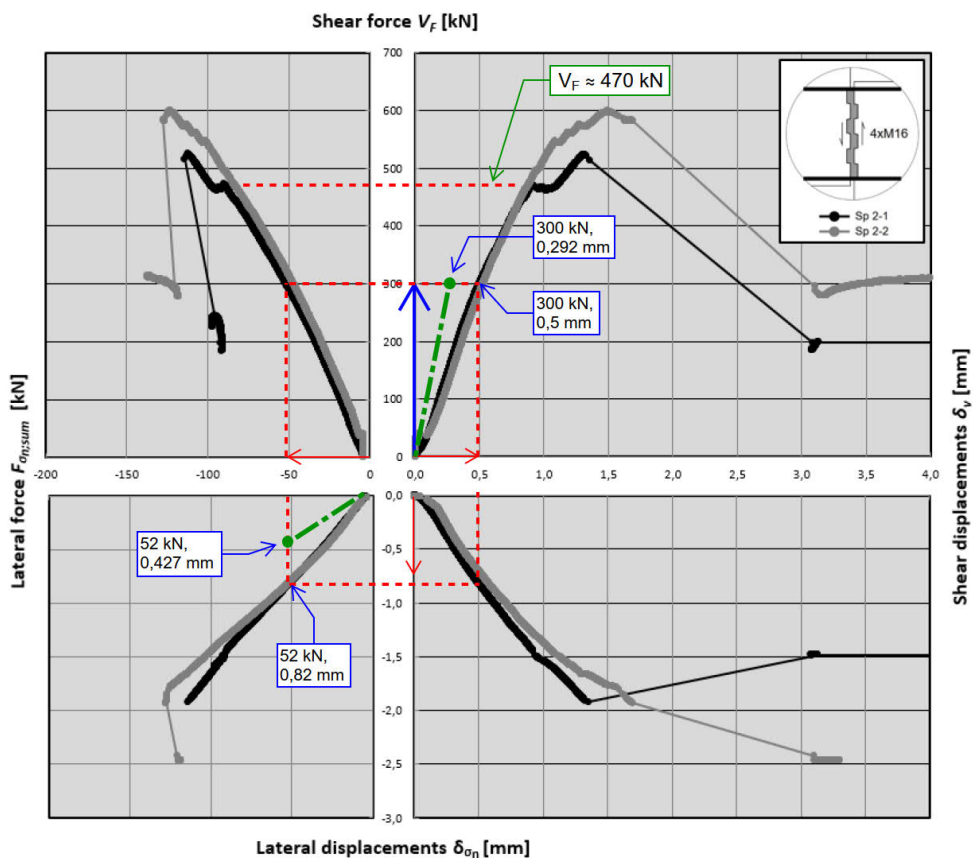

Figure 6.2: Experimental results for Specimens 2-1 and 2-2

The Staggered shear key connection transfers the shear forces primarily via the three inclined compression struts between the in figure 6.3 indicated sloped surfaces of the wall indentations. The three compression struts in fact function independently. Although they are initially part of one full mortar filling, the struts are separ-

ated at rather low shear force levels by cracks, that were initiated at a shear force of 65 kN and 40 kN in respectively Specimens 2-1 and 2-2 (see figure 6.3). These cracks span more or less horizontally between the sides of the compressed, sloped interfaces. The mortar filling is forced to crack at these locations because the compressed sloped interfaces at the right side moves upwards and the ones at the left side move downwards while transferring shear forces.
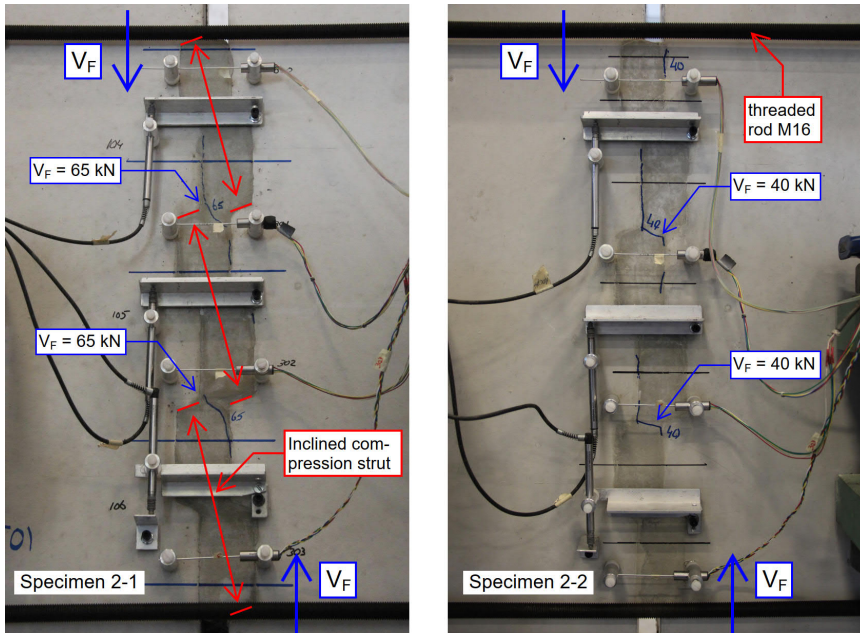

Figure 6.3: Separation of mortar filling into three parts (compression struts) by more or less horizontal cracks

More cracks arise parallel to the compression struts in the mortar and the concrete of the precast elements with an increasing shear force, as can be observed in figure 6.4. These inclined cracks resemble splitting cracks that are usually observed in compression tests on a concrete prism. Perpendicular to the direction of the compression strut tensile stresses occur that result in these type of cracks once the tensile strength is reached.

The connections fail as soon as the shear keys of the precast concrete L-elements at one side of the connection shear off vertically. Figure 6.4 displays these failure cracks in the front view. Figure 6.5 shows the dismantled mortar connection including a view on the fracture surface of the sheared shear keys. It is expected that the connections fail by shearing off the three shear keys. However, this was not entirely the case. The failure of the lowest shear key is caused by crushing of the mortar of the compression strut according to the photo and drawing in figure 6.5. The cause of this is attributable to the missing 100 mm high shear key underneath the lowest sloped interface which had to be sheared off. The absence of the recess (see figure)

provides much more resistance against the diagonal force than with only the shear key causing the crushing of the mortar.

The diagram in figure 6.2 shows a different shear force-displacement relation for the two connections from a shear force of $V_F \approx 470$ kN up to the failure load. The cracked mortar connection of specimen 2-2 is able to transfer higher shear forces with the same shear displacements leading to a higher shear capacity $V_{F;U}$. Specimen 2-1 is unable to continue the transfer of increasing shear forces just after reaching $V_F \approx 470$ kN. This is caused by new cracks that arise and develop at this shear force which can be seen in the photos of figure 6.6. The photos show the cracked connection before and after a shear force of $V_F \approx 470$ kN was imposed to the connection. As a result of these cracks, the vertical shortening of the specimen only causes additional shear and lateral displacements. After the connection has undergone some deformations a renewed resistance is found leading to an increasing shear force. Specimen 2-2 fails at a higher ultimate shear capacity than specimen 2-1 which is attributable to the more deformed state of the connection in Specimen 2-1.

In figure 6.2 it can be seen that specimen 2-2 has a higher residual shear capacity. The difference with specimen 2-1 is approximately 100 kN. This higher capacity has to be attributed to the higher lateral force combined with a coarser failure crack through which the shear forces are transferred in this stage.
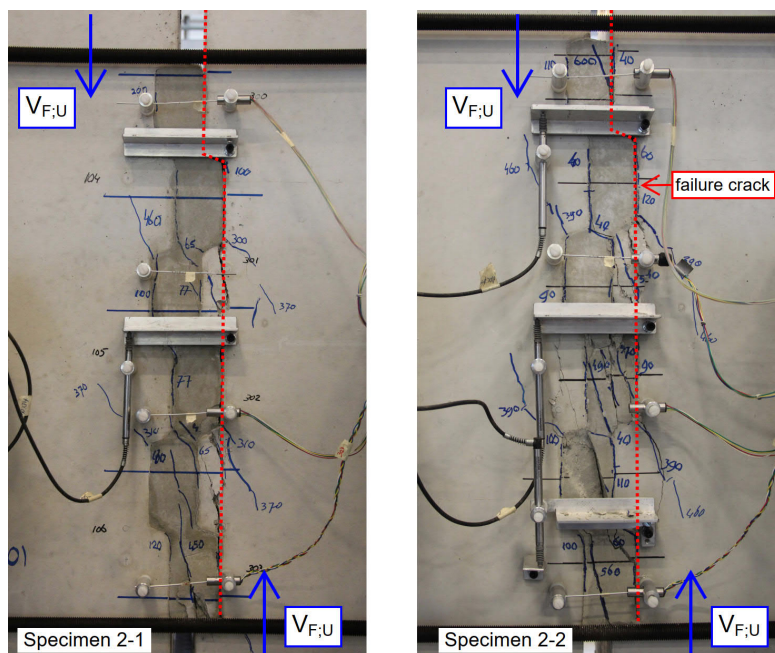

Figure 6.4: Inclined and vertical failure cracks in Specimens 2-1 and 2-2 at ultimate shear force $V_{F;U}$
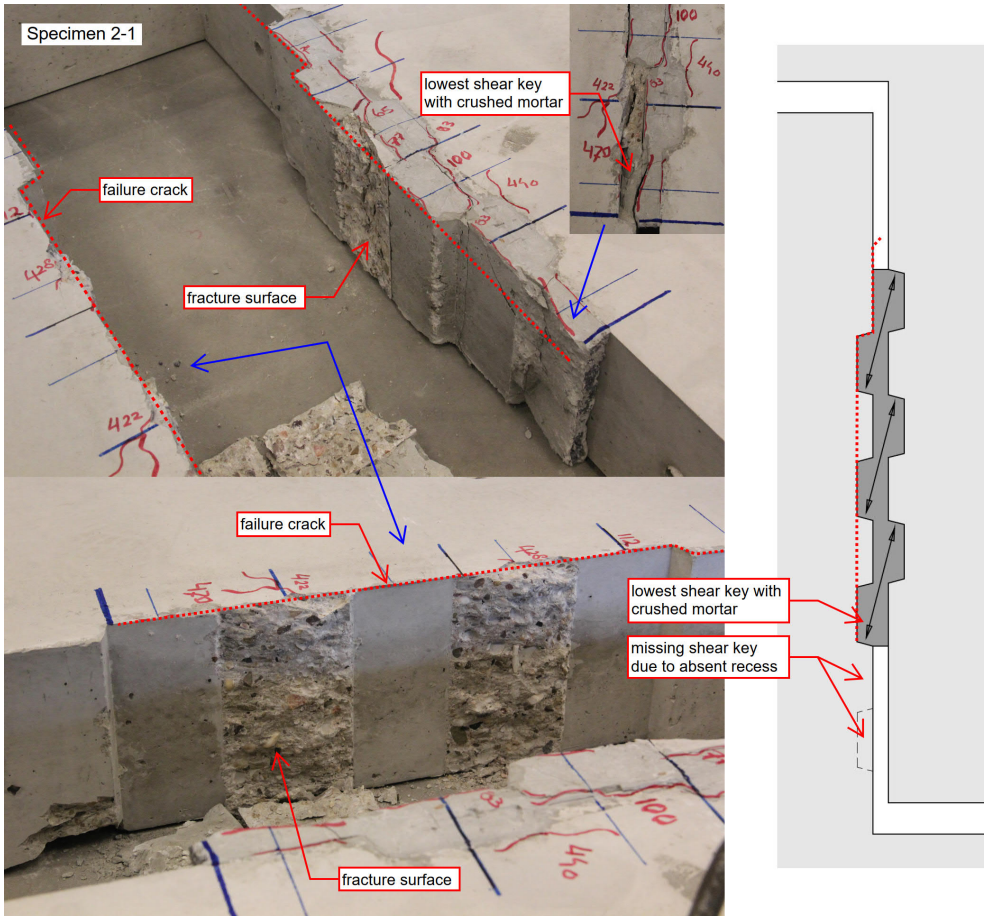
Figure 6.5: Fracture surfaces of Specimen 2-1 (viewed from the backside)
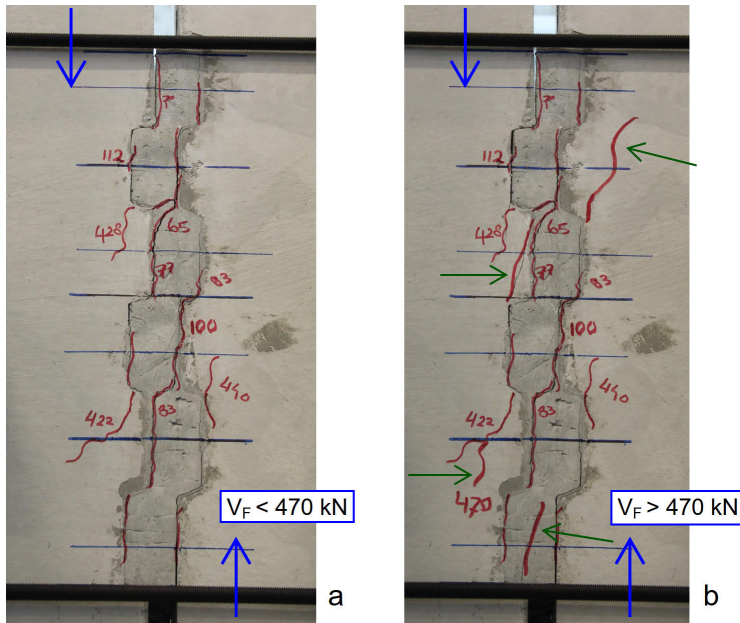
Figure 6.6: Specimen 2-1 just before and after shear force levels $V_F \approx 470$ kN

6.2.2 Analysis based on inclined compression strut

Figure 6.7a and 6.7b show the mortar filling of the Staggered shear key connection modeled as an inclined compression strut for transferring the shear forces V_F. The lateral force $F\sigma_n$ is determined by the shear force V_F and the inclination angle α. The drawn angle is representative for the compression strut when there is a uniform stress distribution where the strut presses on the sloped concrete surfaces or when the strut is hingely connected. In reality the stress distribution will be non-uniform. The resultant diagonal force is expected to transfer the forces via a slightly steeper compression strut. In fact, the mortar connection itself determines the position of the resultant force and the accompanying inclination angle α. The diagram in figure 6.2 displays for a shear force of $V_F = 300$ kN (0,5 mm) the corresponding lateral force of $F\sigma_n = 52$ kN (0,82 mm). Based on these forces, the inclination angle of the resultant force is approximately $\alpha = 9,9°$. The compression strut with this angle is drawn in figure 6.7c. As can be seen, the resultant force is located more towards the edges of the sloped surfaces of the shear keys.

Figure 6.7: Inclined compression strut for modeling the transfer of shear forces
through the mortar filling

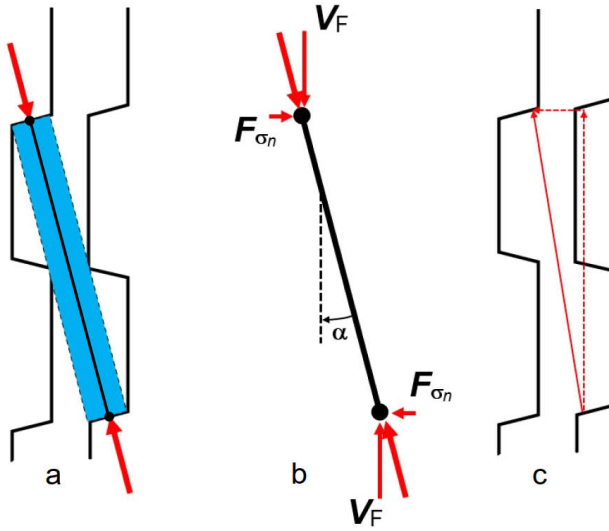The non-uniformity of the interface stresses can be understood as follows. The lateral reaction force $F\sigma_n$ is accompanied by a lateral dispacement $\delta\sigma_n$ as displayed in figure 6.8a. In figure 6.8b the inclined compression strut with the axial force N_c is drawn vertically for reason of simplicity. Besides the load transfer via normal forces, there is an imposed lateral displacement $\delta\sigma_n$ on the mortar-to-concrete interface. Figure 6.8c shows the effect of the axial force and lateral displacement on the interface stresses. The axial force N_c causes a uniform stress distribution. At the same time, the imposed lateral displacement $\delta\sigma_n$ causes a bending moment with compression and tensile stresses. As a result, for the combined stress distribution the resultant of the compression force is located more towards the edges of the shear keys. This explaines the observed steeper inclination angle $\alpha = 9{,}9°$ calculated from the measured shear and lateral forces as displayed in figure 6.7c.

Up till now the forces and the interface stresses of the compression strut are analysed. The next question is if the measured deformations can be explained with a simplified analytical approach. A rough estimation for the shear displacements can be found by adopting the elastic shortening of the compression strut. For this representation a cross-sectional area of 25 x 200 mm^2 is taken for the compression strut, which is the thickness of the seam times the thickness of the specimen. The compression strut has a length of 201 mm. A Young's modulus of 27.500 N/mm^2 is assumed for the mortar. The axial force N_C of the compression strut for a shear force of $V_F = 300$ kN and the corresponding lateral force of $F\sigma_n = 52$ kN is equal to:

$$N_C = \sqrt{V_F^2 + F\sigma_n^2} = \sqrt{300^2 + 52^2} = 304{,}5\,\text{kN} \qquad (6.1)$$

The elastic shortening $\delta\sigma_n$ of the three compression struts is calculated with Hooke's law of elasticity and is equal to:

$$\delta_{Nc} = \frac{N_C \cdot l_{strut}}{E_c \cdot A} = \frac{304.500 \cdot 201}{27.500 \cdot 3 \cdot 25 \cdot 200} = 0,149\,\text{mm} \tag{6.2}$$
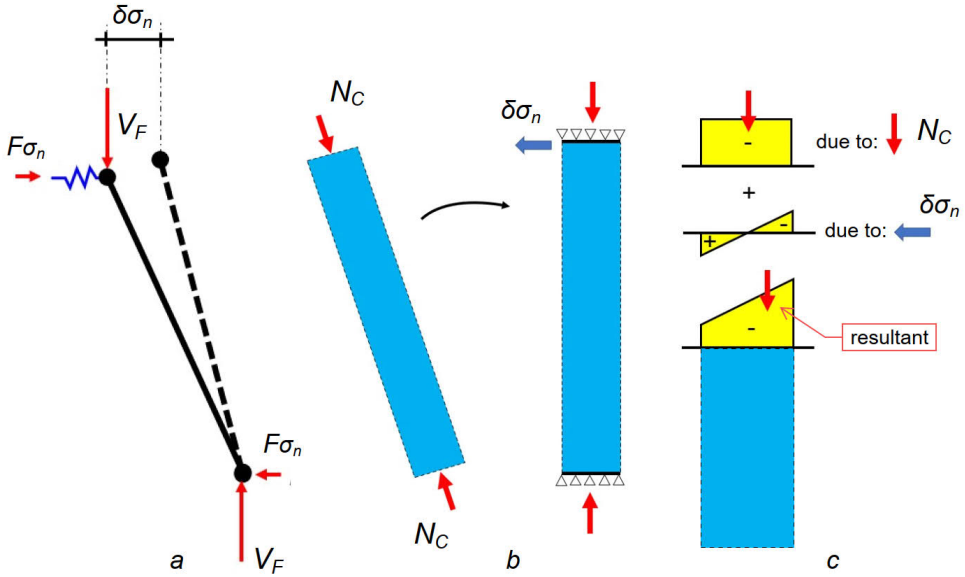
Figure 6.8: Effect of the lateral displacement $\delta\sigma_n$ on the stress distribution at the ends of the compression strut

The shortening $\delta\sigma_n$ is only 30% of the measured shear displacement of $\delta_v = 0{,}5$ mm at a shear force of $V_F = 300$ kN according to figure 6.2. There is another aspect involved in contributing to the shear displacement δ_v which is explained with the help of the model displayed in figure 6.9a. It shows the original and displaced compression strut including the shortening $\delta\sigma_n$ quantified above. This second aspect is the rotation of the compression strut over the angle β. The compression strut is forced to rotate because of the lengthening of the four steel bars M16 that allow the lateral displacement $\delta\sigma_n$. It rotates to where the end point at the top of the strut intersects the vertical line of the lateral displacement $\delta\sigma_n$. The polygons of displacements in figure 6.9b show how the shortening of the compression strut δ_{Nc} and the lateral displacement $\delta\sigma_n$ relate to the shear displacements $\delta_{v;x}$. This model is used for determining this shear displacement δ_v.
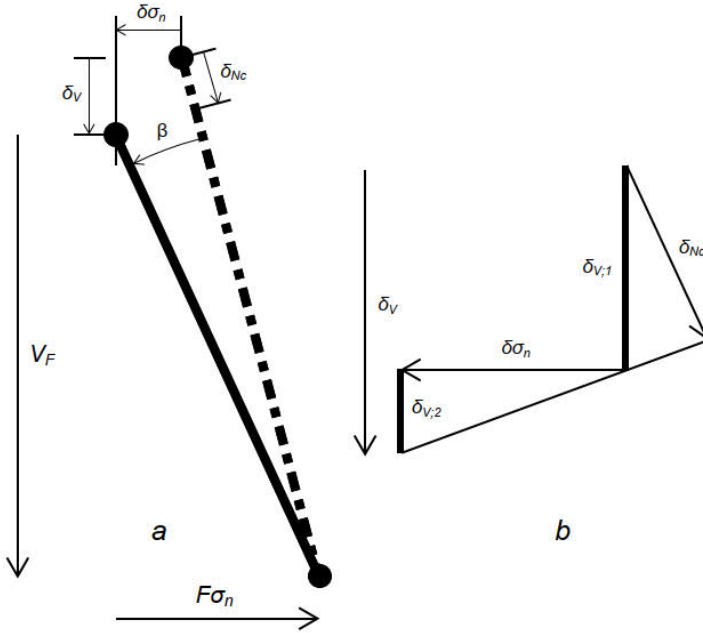
Figure 6.9: Shear displacement δ_v caused by shortening δ_{Nc} and rotation β of the compression strut in a model adopted from Van (2019) (drawings are not to scale)

The determination of δ_v requires the quantification of the lateral displacement $\delta\sigma_n$. The diagram in figure 6.2 shows a measured lateral displacement for Specimen 2-1 of $\delta\sigma_n = 0,82$ mm for a lateral force $F\sigma_n = 52$ kN and a shear force of $V_F = 300$ kN. Again, the question is if this value can be explained with a simplified analytical approach. Two elements of the specimen determine the lateral stiffness. These are the lengthening of the steel bars and the lateral deformation of the precast concrete L-elements. The first is a significant contributor to the lateral displacements while the second will hardly participate. The specimen was tested with four steel bars M16 with a length of 1,32 m. For a Young's modulus of steel of 200.000 N/mm^2 and a cross-sectional area of the steel bars of 201 mm^2 the calculated lengthening of the bars for a total lateral force of $F\sigma_n = 52$ kN is:

$$\delta_{4xM16} = \frac{F\sigma_n \cdot l_{bar}}{E_s \cdot A} = \frac{52.000 \cdot 1.320}{200.000 \cdot 4 \cdot 201} = 0,427 \, \text{mm} \tag{6.3}$$

A Young's modulus of 34.500 N/mm^2 is taken for determining the deformation of the concrete specimen being compressed by the lateral force of 52 kN. When a cross-sectional area of 200 x 600 mm^2 and a length of 1200 mm is assumed the deformation of the concrete elements is equal to:

$$\delta_{concrete} = \frac{F\sigma_n \cdot l_{bar}}{E_c \cdot A} = \frac{52.000 \cdot 1.200}{34.500 \cdot 200 \cdot 600} = 0,015 \, \text{mm} \tag{6.4}$$

As expected the deformation of the concrete specimen is negligible compared to the lengthening of the four steel bars. The diagram in figure 6.2 shows a greater lateral displacement ($\delta\sigma_n = 0,82$ mm) for the specimen 2-1 than the calculated 0,427 mm. In this context it should be noted that the real lateral displacement is larger than only the lengthening of the steel bars as calculated before. In this respect the following aspects can be mentioned. The assemblies of the steel bars M16 are connected to the specimen with end plates, washers and bolts. The photo in figure 6.10 displays this connection. In addition to the lengthening of the steel bars, there can be an additional deformation in these components. Furthermore, the steel bars are adapted locally for applying strain gauges to the bars. There they have a smaller cross-sectional area leading to an additional lengthening. Also, the stressed area of a threaded rod M16 is smaller than the cross-sectional area of a plain bar ø16. Anyhow, the lateral force and the lateral displacement are known, since these are measured. For the analysis it is chosen to apply a cross-sectional area of the steel bars of 201 mm^2 for the M16 and to calculate a fictitious Young's Modulus so that for the measured lateral force the also measured lateral deformation is found. The fictitious Young's Modulus is than 105.000 N/mm^2:

$$\delta_{4xM16} = \delta\sigma_n = \frac{F\sigma_n \cdot l_{bar}}{E_s \cdot A} = \frac{52.000 \cdot 1.320}{105.000 \cdot 4 \cdot 201} = 0,813 \, \text{mm} \tag{6.5}$$

For a shear load of 304,5 kN the shear displacement δ_v displayed in the model of figure 6.9 can now be calculated with the values for the shortening of the compression strut δ_{Nc} and the lateral displacement $\delta\sigma_n$:

$$\delta_{V;1} = \delta_{Nc} \cdot \frac{N_C}{V_F} = 0,149 \cdot \frac{304,5}{300,0} = 0,151 \, \text{mm} \tag{6.6}$$

$$\delta_{V;2} = \delta\sigma_n \cdot \frac{F\sigma_n}{V_F} = 0,813 \cdot \frac{52,0}{300,0} = 0,141 \, \text{mm} \tag{6.7}$$

$$\delta_V = \delta_{V;1} + \delta_{V;2} = 0,151 + 0,141 = 0,292 \, \text{mm} \tag{6.8}$$

As can be seen in figure 6.2 the calculated shear displacement $\delta_v = 0,292$ mm is significantly smaller than the 0,5 mm that is measured at a shear force of 300 kN. The difference is most probably caused by the deformation in shear keys of the precast concrete L-elements within the area of the applied LVDT's. This can be investigated with a finite element model of the full specimen and the results of such an analysis are elaborated in the next subsection.
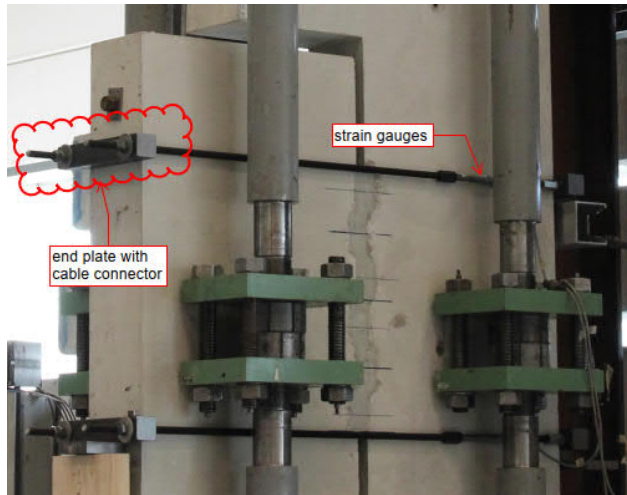
Figure 6.10: Specimen with steel bars M16 connected to the specimen

6.2.3   Simulation with finite element model

A numerical model is used for studying the behaviour of the Staggered shear key connection. The finite element program ATENA is selected for the simulation. This program is very suitable to simulate the real behaviour of reinforced concrete structures including concrete cracking, crushing and yielding of the reinforcement. It is chosen to use membrane elements with plane stress idialization for modeling the specimens. Figure 6.11a displays the applied finite element model for the Staggered shear key connection. The steel plate at the bottom of the specimen is connected to the base support which behaves fixed in the two directions. The steel plate at the top is only horizontally fixed. External reinforcement bars represent the 4 horizontal steel bars. They are fixed to the steel plates at the ends of the bars. Figure 6.11b shows the principal stresses (compression) and the deformed specimen. The stress distribution indicates that the vertically imposed force on the specimen transfers via an S-shaped track through the specimen.

A closer look at the connection itself is displayed figure 6.11c. The mesh generator generates the finite element mesh based on user defined prescribed element sizes. The element size for the mortar is related to the size of the mortar filling between the L-elements. An element size of 12,5 mm has been set for the mortar and the adjoining parts of the concrete L-elements. The element size of the remaining part of the L-elements is 50 mm.

For the analysis of which results are shown in figure 6.11 it was chosen not to connect the mortar to the concrete where debonding is expected to occur at a low shear force. So, only the sloped compressed mortar-to-concrete interfaces have connecting interface elements.

Furthermore, it was decided to skip the phase where cracking in the mortar filling makes that the three separated parts of the mortar filling (figure 6.3) can develop. This is done by creating a crack in the model at two locations in the mortar filling by modeling a separation (see figure 6.11c). By modeling in this way the mortar of the inclined compression struts can act directly, without first debonding between the mortar and the concrete and also without the horizontal cracking.

Figure 6.11c shows the four monitoring points that are used for measuring the displacements. The locations of the measuring points correspond to the locations of the LVDT sensors glued against the specimens and drawn schematically in figure 4.13. This allows the comparison of the test results and the numerical results in the load-displacement diagrams.

Table F.1 in Appendix F summarizes the selected material properties for the material models. The concrete of the L-elements is represented by two different material models. The model of concrete (1) indictated in figure 6.11a is provided with smeared reinforcement and behaves fully non-linear including cracking, while a linear elastic material model is selected for concrete (2). The reason is that the focus is on the structural behaviour of the connection parts mortar and concrete (1). The steel plates and steel bars (external reinforcement) are modeled with a linear elastic material model.

ATENA has a tool that calculates all material properties based on only the "MC strength value" of concrete. It uses the equations described in *fib* Model Code 2010 (2013) for this purpose. This tool is used as starting point for determining the material properties. The applied Cubic MC strength value for Concrete (1) was 67 N/mm^2 representing the used concrete grade C55/67. The MC strength value for the mortar was taken 70 N/mm^2 representing the Tiksomortar K70. This tool provided higher elastic moduli for these materials than measured for the used concrete or may be expected for the mortar. It was decided to use the measured Young's modulus of 34.500 N/mm^2 for the concrete (1) and (2). A Young's modulus of 27.500 N/mm^2 was taken for the mortar.

As explained in the previous subsection (with a fictitious Young's modulus for the external steel bar assemblies M16 of 105.000 N/mm^2 and a cross-sectional area of 201 mm^2) a lateral stiffness as measured in the experiments is taken because the same issue applies for the functioning of the external steel bars in the finite element simulation model. The same reduced fictitious Young's modulus is applied.

The loads on the numerical specimen model are applied in steps. In load step 1, the steel bars are slightly prestressed equal to the levels of prestressing in the experiments and the top plate is vertically displaced downwards by 0,1 mm. For the subsequent load steps the top plate is given a vertical displacement of 0,1 mm/step.

The results of the numerical analysis are displayed in figure 6.12 as well as the results of the two experiments. Figure 6.13 shows the corresponding stresses and inclined cracks of the numerical model.
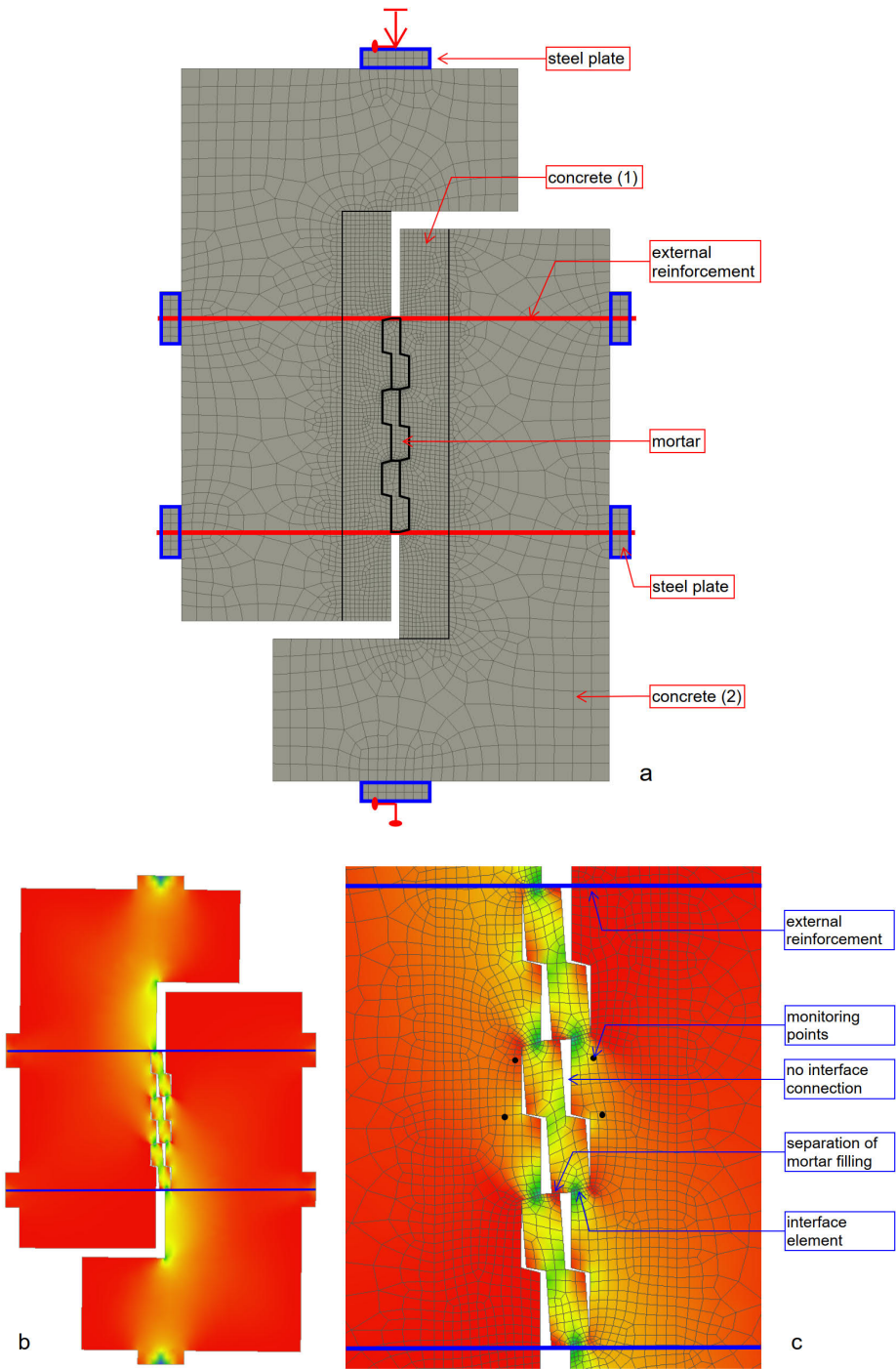
Figure 6.11: Membrane specimen model (a) and deformed models with principal stresses (compression) in (b) and (c)
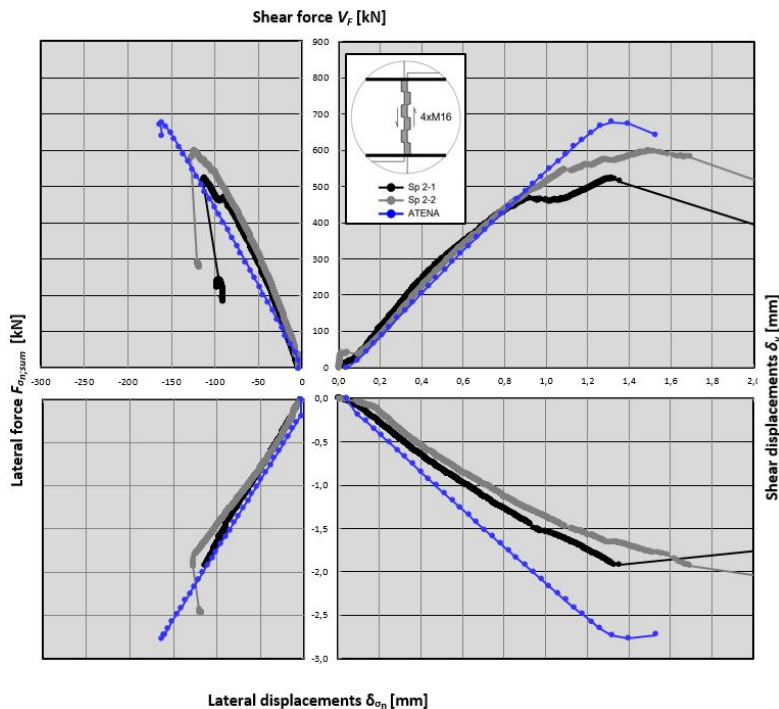
Figure 6.12: Results of the numerical analysis and experiments for the Staggered shear key connections

In this first numerical simulation the results are remarkably good, when compared to the experimental results. The shear displacements δ_v and the lateral forces $F\sigma_{n;sum}$ are slightly overestimated. Furthermore, a higher shear capacity is found compared to the experiments.

As explained before, the mortar connection itself determines the angle α of the resultant diagonal force. This force is traceable from the compressive stresses in the membrane elements of the numerical model which is indicated in figure 6.13a. The picture shows larger stresses at the edges of the shear keys as indicated by the arrows. Figure 6.13b shows the interface stresses perpendicular to the concrete surface. It displays the triangular distributions of compressive stresses at the interfaces that reaches their maximums near the shear key edges.

Figure 6.13c shows the diagonal cracks in the three compression struts at the failure force of 677 kN. The cracks arise and grow during increasing the shear force to the mortar connection. The middle shear key has the fewest cracks compared to the upper and lower. This indicates that this key transfers slightly less inclined forces than the other two. This is in accordance with the known phenomenon that in a welded lap joint the first and last parts of the weld take the most forces to transfer. The lowest shear key already has a vertical failure crack. As a result the transfer of forces through this key drops, as well as the total shear forces that can be trans-

ferred. In a load-controlled simulation this would mean that the specimen fails. In a deformation-controlled experiment or analysis often a new equilibrium is found at a lower load level and with increased deformations. Also in the numerical analysis a few more load steps could be performed. However, whether these represent real behaviour concerning the load-deformation relation cannot be said, since in the analyes the convergency criterion could not be reached.
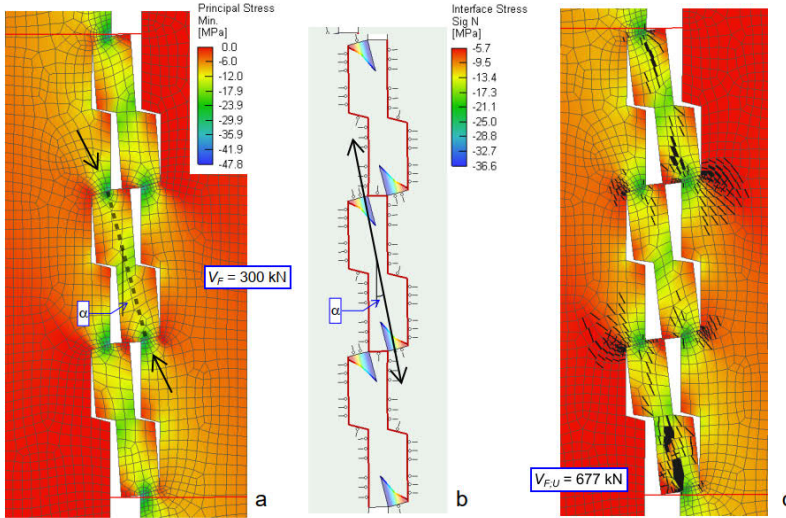
Figure 6.13: Principal stresses (a), interface stresses (b) for a shear load of 300 kN and cracks at a shear force of 677 kN (c)

Because of the cracks displayed on the photo's of figure 6.3, the three pieces of mortar filling were separately modeled in the first numerical model (ATENA (1) results in figure 6.14). However, despite the cracking there is most probably a minor structural interaction between the three parts in reality because the mortar filling is initially uncracked. Furthermore, the cracked mortar filling is probably able to provide lateral resistance against dilation. In the second numerical model (ATENA (2)), the mortar filling is modelled without the initial horizontal cracks simulated by separation. The results of this numerical analysis are shown in figure 6.14. As can be seen, the force and displacement relations even better fit with the experimental results. The picture next to the diagrams in figure 6.14 shows this numerical separation with cracks that initiate at very low shear force. As a result, the steel bars have to provide less lateral resistance, which leads to the lower lateral force $F\sigma_n$ in the diagram. At the same time, the lateral displacements $\delta\sigma_n$ become smaller. This causes the inclined compression struts to rotate less leading to a steeper compression strut with a higher axial force N_C for the same shear force V_F. This higher axial force V_F explains the lower failure load $V_{F;U}$ of model ATENA (2) because the compression strut probably fails at approximately the same axial force N_C. Finally, the steeper compression strut causes less shear displacements δ_v.
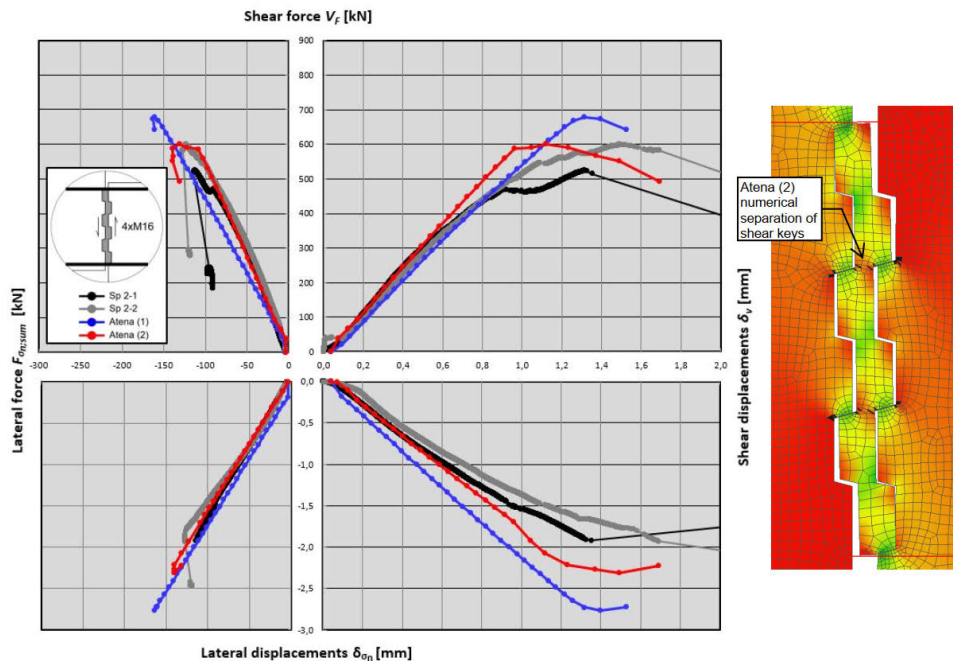
Figure 6.14: Numerical results compared with the experimental results

A shear displacement of $\delta_v = 0,292$ mm for a shear force of $V_F = 300$ kN was obtained from the compression strut approach in previous subsection. A similar shear displacement can be calculated by the ATENA (1) model with membrane mortar filling for the same shear force. Figure 6.15a displays the shear displacements at the top and bottom of each shear key for a shear force of $V_F = 305$ kN. The difference between those two values is the shear displacement of the shear key only. As indicated in the figure, the numerical program calculates a shear displacement of $\delta_v = 0,34$ mm for each of the membrane mortar fillings. This is quite close and considered approximately similar to the value obtained from the compression strut approach in previous subsection. It demonstrates the suitability of the compression strut approach.

Figure 6.15b displays the results provided by the ATENA (2) model for a shear force of $V_F = 294$ kN. The effect of the initially uncracked mortar filling can be identified from this figure when compared to figure 6.15a. It shows that the lateral forces in the steel bars and the shear displacements are lower than proposed by the ATENA (1) model. It demonstrates that resistance against lateral dilation is provided by the initially uncracked mortar filling. As a result, the connection behaves with less lateral displacements $\delta\sigma_n$. The resultant diagonal forces stayed more upright which caused less shear displacements δ_v. The shear displacement of middle shear key is the smallest because of the lateral restraining by the upper and lower parts of the mortar filling.
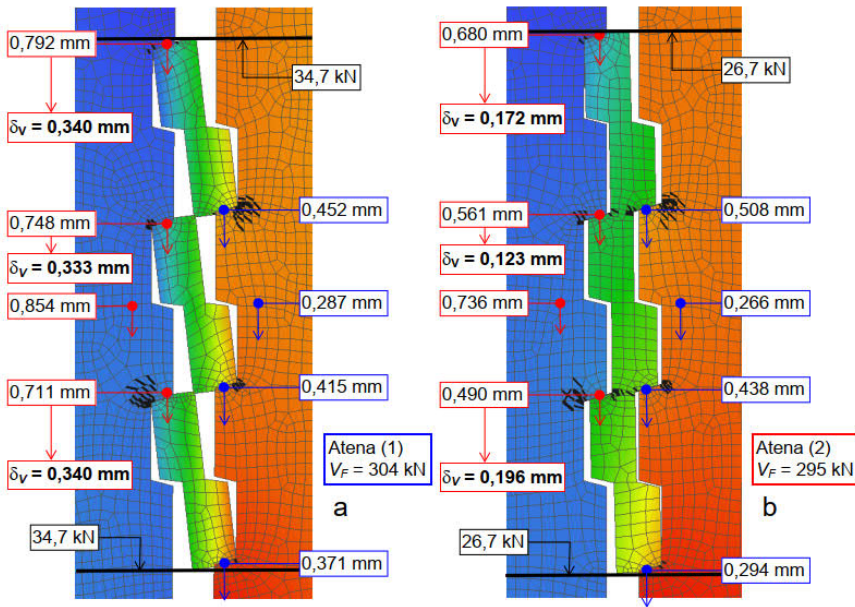
Figure 6.15: Vertical displacements (a) for model ATENA (1) and (b) for model ATENA (2)

6.3 Influence of variables on the Staggered shear key connection

6.3.1 Lateral stiffness

For investigating the influence of the lateral stiffness on the shear behaviour of the Staggered shear key connection, the test results of the tests Specimens 2-1 and 2-2 (M16 bars), Specimens 2-3 and 2-4 (M24 bars) and Specimens 2-5 and 2-6 (M38 bars) are used. The results of these experiments are plotted in the diagrams of figure 6.16.

Firstly, it can be seen in the diagram in the upper left corner of figure 6.16 that the lateral stiffness does not influence the relationship between the shear force V_F and the lateral force $F\sigma_n$. This is understandable, because the lateral forces are determined by the inclination angles α which are the same for these identically sized and shaped profiled mortar connections.

Secondly, it can be observed that an increase of the lateral stiffness results in an increase of the shear stiffness. This is especially the case for the higher shear forces. Also, the shear capacity $V_{F;U}$ appears to increase slightly with higher lateral stiffnesses. However, this increase is quite small. Thirdly, the residual capacities after shearing off the shear keys show a reasonable scatter and it is expected that the roughness of the cracked surfaces have more influence on the residual capacities than the lateral stiffness.
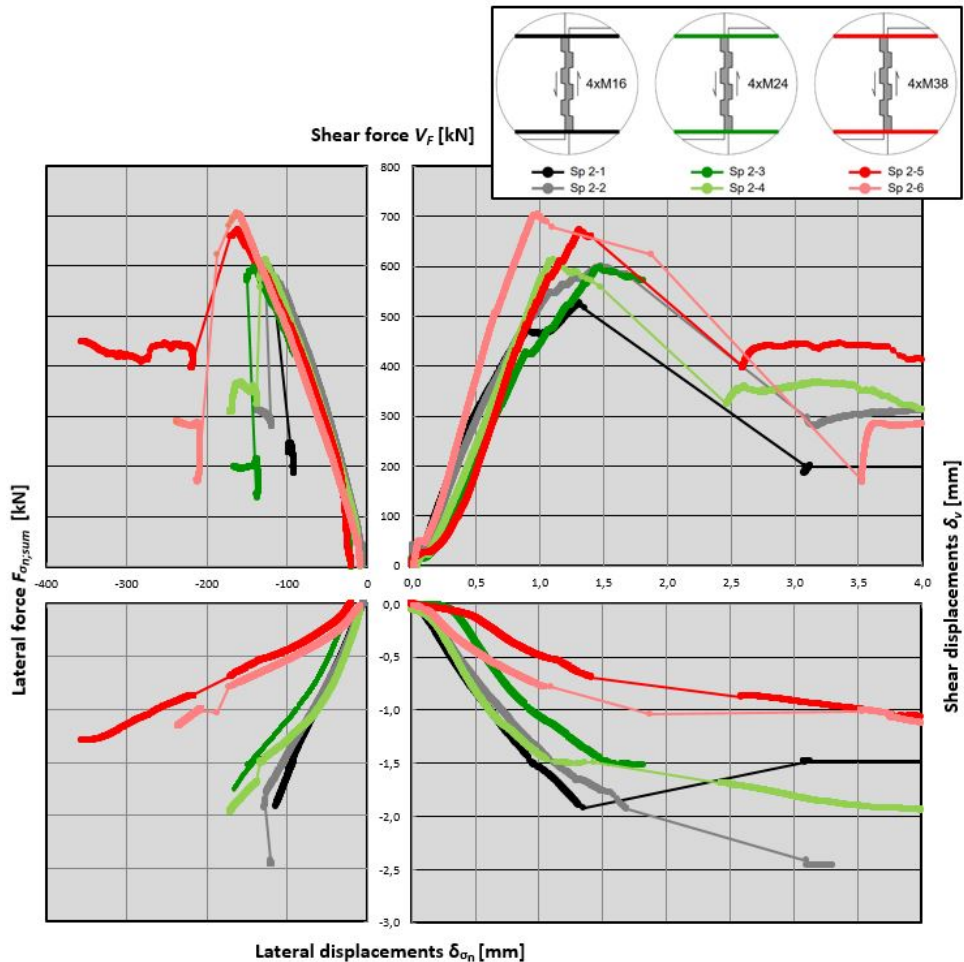
Figure 6.16: Test results of Specimens 2-1 till 2-6 for examination of the influence of lateral stiffness

Finally, the lateral force-lateral displacement diagram shows lower lateral displacements for the higher lateral stiffnesses. This is highlighted in the diagram of figure 6.17. It is clear that this is attributable to the dependency of the lateral displacements to the stiffnesses of the horizontal steel bars. It should be noted that for the lower shear forces the lateral displacements of the specimens with M16 and M24 steel bars do not differ significantly. For the specimen with M38 steel bars the lateral dilation is significantly less. The lateral force-lateral displacement relations bend after an initial higher lateral stiffness towards a more or less linear relation. This bending occurs earlier in case of the higher M38 lateral stiffness, compared to the other stiffnesses. The dashed lines in figure 6.17 represent the lateral stiffnesses for the linear branch of the developments. The corresponding lateral stiffnesses are:

- M16 - 60 kN/mm

- M24 - 110 kN/mm

- M38 - 270 kN/mm
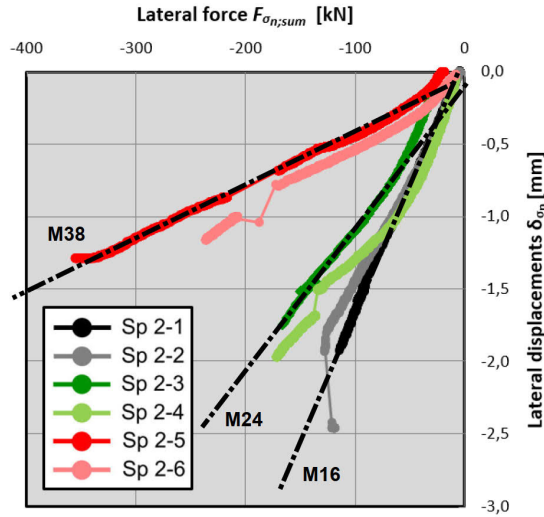
Figure 6.17: Lateral force-lateral displacement diagram for Specimens 2-1 till 2-6

The numerical model used for the specimen with M16 steel bars in the previous subsection did simulate the connection behaviour well. It is questionable if the same model, but with the M24 or M38 steel bars, approximates the specimen behaviour of specimens 2-3 till 2-6 also well. Therefore, the cross-sectional area, the level of pre-stressing and the material stiffnesses for taking into account the M24 and M38 steel bars are changed in the used numerical model. The other properties of the numerical models are kept the same. The results of the numerical analyses are displayed in figure 6.18 for the M24 connection and in figure 6.19 for the M38 connection. The connection behaviour for the three separated shear keys is called ATENA (1) and the one fully filled with mortar is marked ATENA (2). It was chosen to display the results of both models for verifying if they provide the same type of shear force-shear displacement relations for other lateral stiffnesses. This allows to use the numerical models for accurate simulation as well as simplified simulations for more than the tested lateral stiffnesses.

The diagrams show that the results obtained numerically approximate the test results of specimens 2-3 till 2-6 well, as it was found before for the experiments with M16 steel bars. Worth mentioning is that the three numerical ATENA (2) models provide approximately the same shear capacity $V_{F;U}$ (± 600 kN) for the three different lateral stiffnesses while the models (1) with separated shear keys all exceed the measured shear capacities about 10-15%.
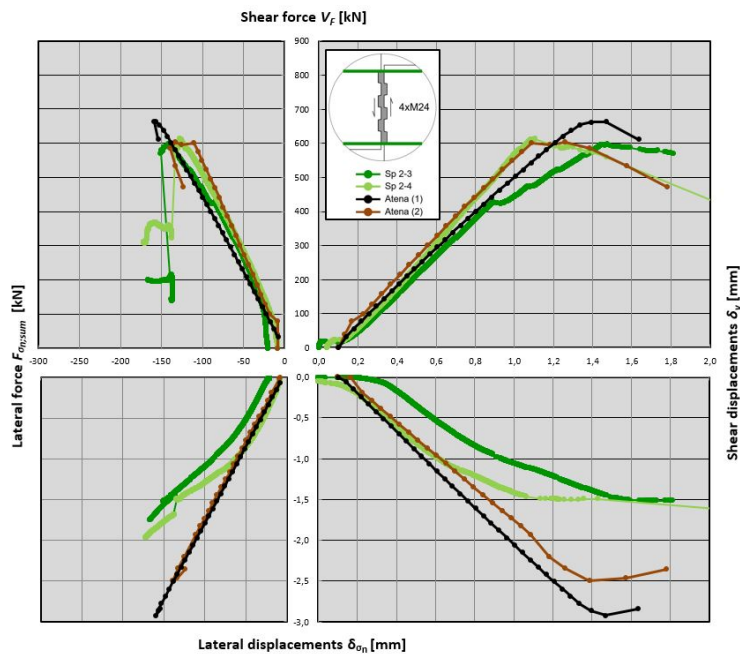
Figure 6.18: Numerical test results and Specimens 2-3 and 2-4 with M24 bars
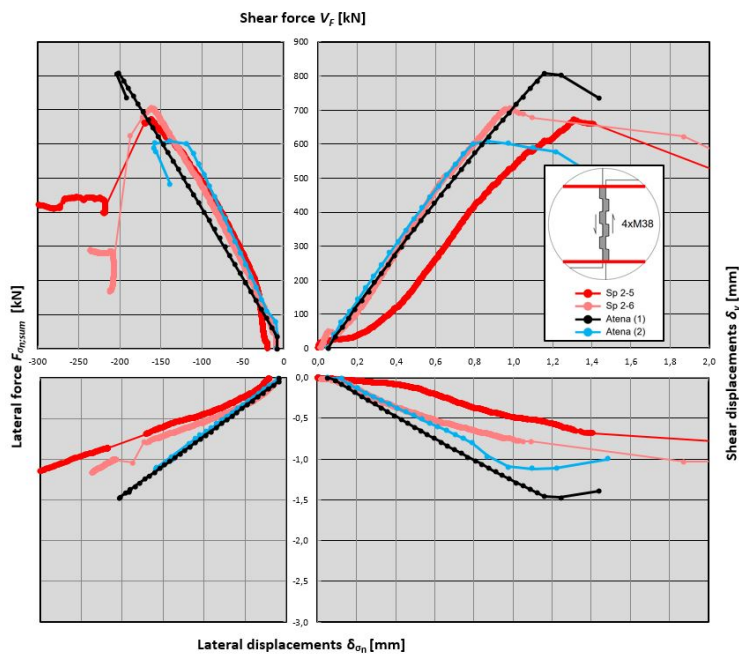
Figure 6.19: Numerical test results and Specimens 2-5 and 2-6 with M38 bars

6.3.2   Lateral compression

The effect of compressing the mortar connection laterally is investigated with the help of the diagrams in figure 6.20. Specimen 2-7 was clamped with an initial lateral compression of 2,0 N/mm^2 imposed by the 4 steel bars M38 ($F\sigma_n$ = 243 kN). Specimens 2-5 and 2-6 had the same M38 steel bars but were not prestressed laterally which make them comparable to Specimen 2-7 for examining the influence of the lateral compression. The results of the experiments are the first to be analysed below. After that the analysis of the numerical results follow.

The shear force-lateral force diagram shows clearly the effect of the initial compression in Specimen 2-7. This force remains approximately unchanged while the shear force increases up to V_F = 700 kN. This is understandable because the lateral compression forces compensate the lateral dilation forces. As a result of this, the M38 steel bars do not lengthen and the connection does not dilate. This is in contrast with the developments of the initially uncompressed connections. There the steel bars extend and provide lateral forces that are equal to the increasing development of the dilation forces.

The shear force-shear displacement diagram displays a steep curve for Specimen 2-7 up to a shear force of V_F = 175 kN. This is attributable to the shear friction capacity of the vertical mortar-to-concrete interfaces. Because of the higher lateral compression, the interfaces are able to transfer higher shear forces and the connection behaves with low shear displacements. The Specimens 2-5 and 2-6 are less compressed and debond at lower shear forces (10 and 48 kN). It explains that a compressed mortar connection behaves with a higher shear stiffness up to debonding of the interfaces. After debonding, the compressed connection of Specimen 2-7 continues to behave with approximately the same shear stiffness as provided by the remaining connections.

With Specimen 2-7 higher shear forces could be transferred compared to Specimens 2-5 and 2-6. Starting from around V_F = 700 kN the initially imposed lateral forces do not cover the dilation forces any more. As a result, the lateral forces and lateral displacements start to increase with the lengthening of the steel bars M38. From that point on, the additional clamping effect is provided by the resistance against lengthening of the M38 steel bars. In this stage, the connection is able to transfer increasing shear forces up to its failure. In the residual stage, the compressed mortar connection is able to provide more capacity. This is understandable because the higher level of lateral compression provides more shear friction capacity in the cracked mortar connection.

In the compression strut approach of subsection 6.2.2, an inclined resultant force was addressed to function in the mortar that determines the triangular interface stresses in the sloped surfaces. The angle of inclination of this force is affected by the lateral displacements resulting in bending of the compression strut. This effect does not occur when the initial lateral force compensates the dilation force. As a result, the inclined compression force transfers the shear forces with a more uniformly distributed interface stress.
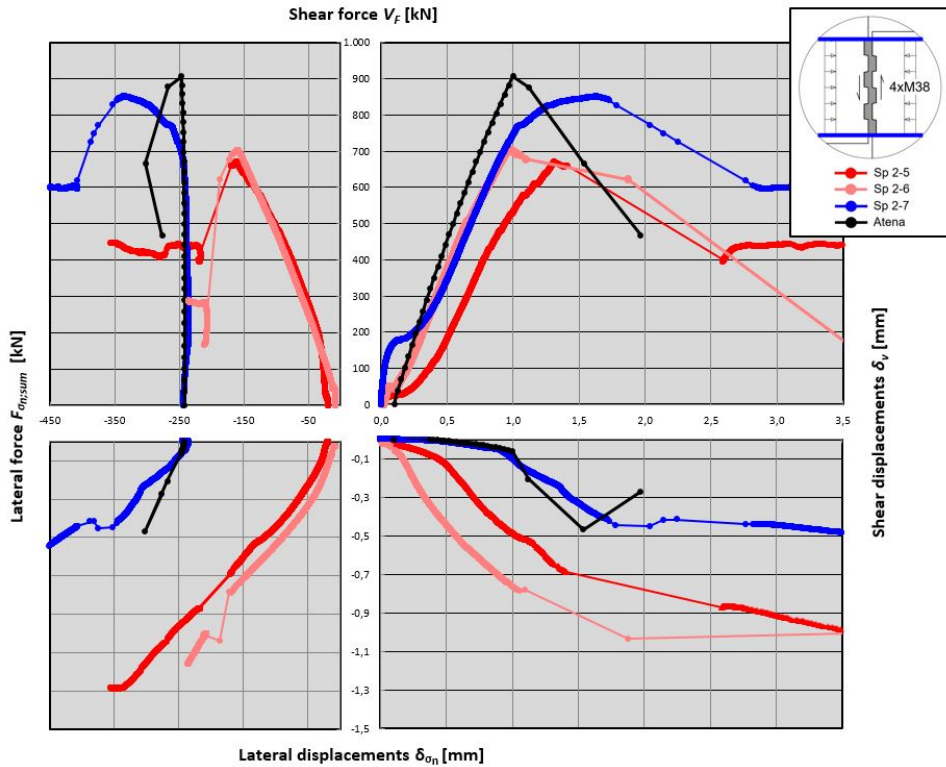
Figure 6.20: Test results of Specimens 2-5 and 2-6 (not prestressed) and Specimen 2-7 (prestressed) and results of numerical simulation for the prestressed experiment

Figure 6.20 shows the results of the numerical simulation of Specimen 2-7 as well. The model used is equal to the model used for the simulation of Specimens 2-5 and 2-6, apart from adding a lateral force of $F\sigma_n = 243$ kN. Also, interface elements are added to the vertical mortar-to-concrete interfaces which are not present in the previous models. These interface elements are able to transfer lateral compression forces. The ability to transfer shear forces and tensile forces are excluded in these interface elements. The reason for modeling compression capacity is that the initial lateral compression set by the steel bars would penetrate the precast concrete and mortar membrane elements into each other. This cannot happen in reality and would cause an unrealistic displaced mortar connection during the numerical analysis.

The diagrams show that the numerical model approaches the connection behaviour of Specimen 2-7 well. It provides a little more steep shear force-displacement relation. However, the shear stiffness from this development remains close to the ones measured in the specimens. The numerical model does not predict that the lateral force ($F\sigma_n$) exceeds the initial compression force of 243 kN before failure occurs. The stage of lengthening of the steel bars M38 is not reached. This is understandable

because the less shear displacements (δ_v) in the numerical model indicates a steeper resultant force in the mortar and that reduces the lateral forces ($F\sigma_n$) for the same shear forces (V_F) to be covered.

6.3.3 Thickness of the seam

For investigating the influence of the thickness of the seam, the test results of Specimen 2-8 and the results of the Specimens 2-3 and 2-4 are brought together in the diagrams of figure 6.21. The latter two had a seam thickness of 25 mm, while Specimen 2-8 was constructed with a narrower thickness of 15 mm.
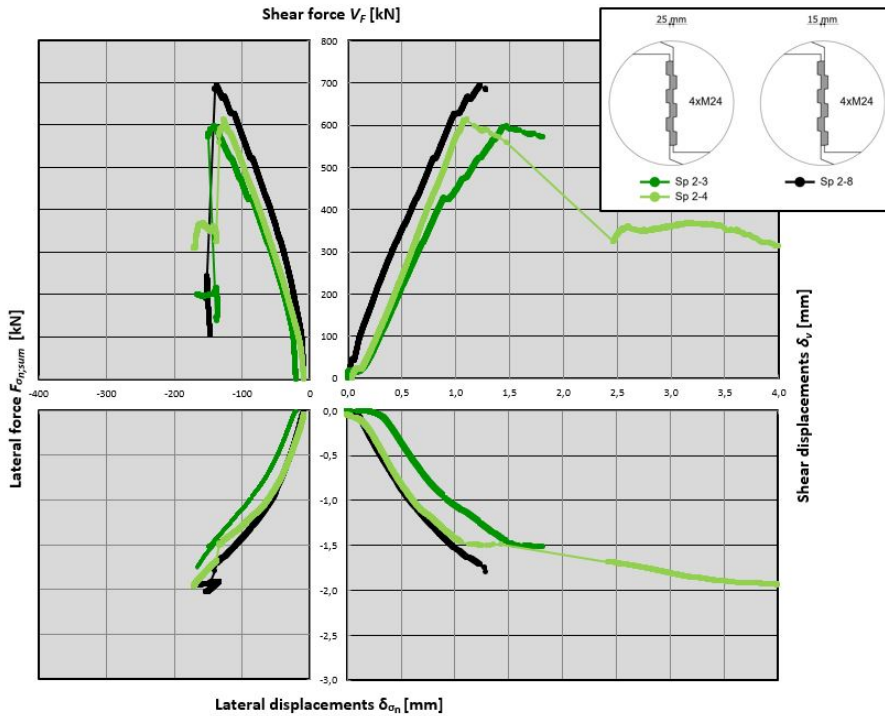
Figure 6.21: Test results of Specimens 2-3, 2-4 and 2-8 for examination of the influence of the seam thickness

The influence of the reduced thickness appears to be relatively limited. It can be expected that the slope of the inclined resultant force for transferring the shear forces will be somewhat steeper in case of a smaller seam thickness. The effect of this can be observed in the shear force-lateral force diagram. It shows a relation with somewhat smaller lateral forces for the specimen with the more narrow seam. The test results show insignificant differences for the shear stiffnesses in the shear force-shear displacement diagram. The relation of Specimen 2-8 is positioned left from those for the other two specimens. However, this is mainly attributable to the

initial displacement at the start of the test. The shear capacity $V_{F;U}$ of Specimen 2-8 (700 kN) is higher than of the other specimens with approximate 600 kN. It indicates that a higher shear capacity can be expected for this smaller thickness of the seam.

6.3.4   Type of mortar

The effect of applying Steel Fibre Reinforced Mortar (SFRM) instead of Tiksomortar K70 can be identified by comparing Specimen 2-9 to Specimens 2-3/2-4. Photos of Specimen 2-9 (with SFRM) are displayed in figure 6.22. The photos (a) and (b) show the front and rear views of this specimen. Photo (a) shows that the profiled mortar-to-concrete interfaces are not fully visable. This is caused by some crumbled concrete parts of the precast concrete L-elements. After dismantling, it turned out that the specimen has only a small damage at the surface of the specimen. The shear keys function almost completely between the surfaces of the specimen. It can be observed from the pictures (a) till (c) that the keys of one precast concrete L-element sheared off. This is in contrast with the crack development and the failure cracks of the Specimens 2-3/2-4 displayed in photos (d) and (e). These connections crack and fail with a lot more cracks in the mortar. It demonstrates that the SFRM causes the cracks to appear in the precast concrete L-elements instead of in the mortar filling. The less brittle SFRM material forces the precast concrete to crack significantly more in Specimen 2-9.
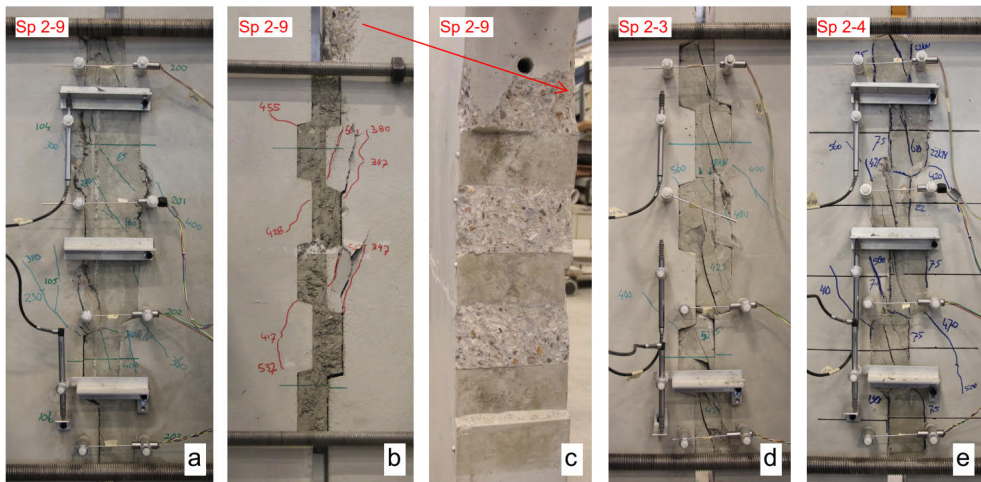
Figure 6.22: Specimens 2-9, 2-3 and 2-4 with cracked connection components

It is questionable if the use of SFRM instead of Tiksomortar K70 has a benefical effect on the shear behaviour of the mortar connection. This can be observed from the diagrams in figure 6.23 in which the test results of the three specimens are brought together. For Specimen 2-3 and 2-9 there is hardly any difference between the developments observed visible. The deviation with respect to Specimen 2-4 is slightly

larger. This is attributable to the smaller initial force of 8,0 kN instead of 20,0 kN applied to the four steel bars M24 for Specimen 2-4. This comparison demonstrates that despite the improved properties of the mortar the overall connection behaviour does not change significantly in this connection. For application, it could beneficial to use SFRM for getting less brittle behaviour and less visable cracks in mortar fillings. However, this is not required for a proper functioning mortar connection. The pumping of SFRM via a hose requires additional handling and material that is not paid off. As a result the Tiksomortar K70 can be seen to be advantegeous for this application compared to the SFRM in the Staggered shear key connection.
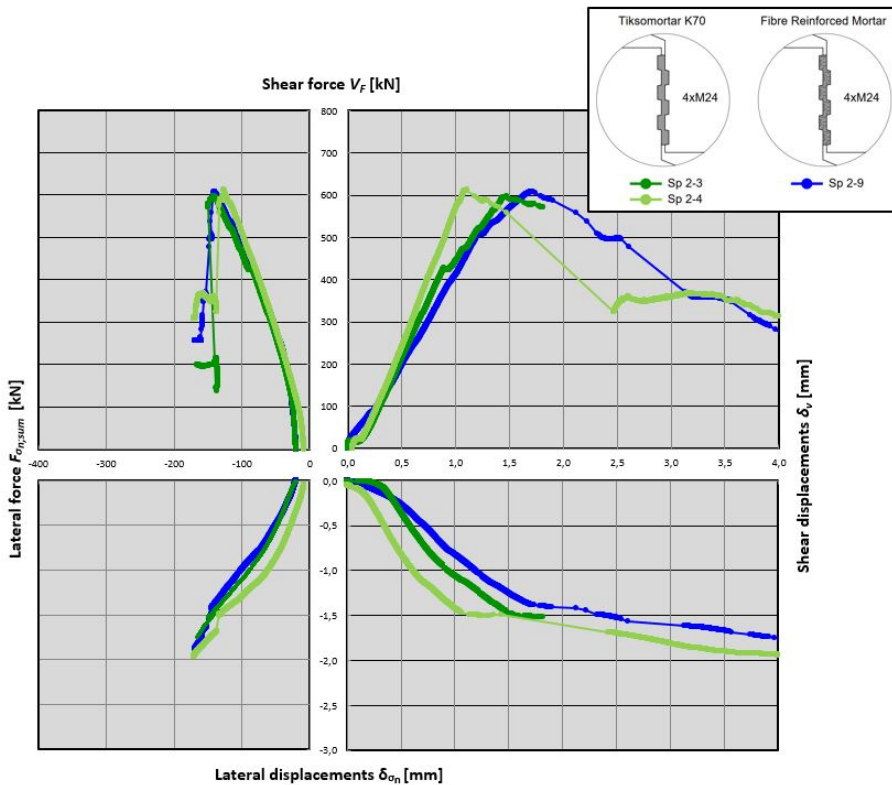
Figure 6.23: Test results of Specimens 2-3, 2-4 and 2-9 for examination of the type of mortar

6.4 Effect of the shape of the interface

6.4.1 General

The analysis of the shear behaviour of the connections with different profiles and in some cases a roughening of the precast concrete surface are performed by com-

paring mutually their test results. First it was chosen to study the behaviour of the five mortar connections with Tiksomortar K70 and steel bars M38 with the help of figure 6.24. This is followed by an analysis of the four connections with Steel Fibre Reinforced Mortar and steel bars M24. Their results are displayed in figure 6.28.

6.4.2 Tiksomortar K70 Connections - steel bars M38

It can be seen from the shear force-shear displacement diagram of figure 6.24 that the Aligned shear key connection (Specimen 1-3) and the Staggered shear key connection (Specimens 2-5/2-6) debond almost immediately in the vertical interfaces. This is to be expected because these interfaces are not provided with a roughening or profiling with the aim of improving the bonding behaviour between the mortar and the concrete. This is different for the other 3 connections with the result that the Aligned small shear key and the Plain waterjetted connections debond at higher shear forces. This occurs at 205 kN (Specimen 3-9) and at 177 kN (Specimen 4-3) respectively, as can be seen in the photos of figure 6.25. There is hardly debonding at the Serrated waterjetted shear connection (Specimen 5-6). Here a snap back occurs at 260 kN mainly as a result of the formation of inclined cracks in the mortar.
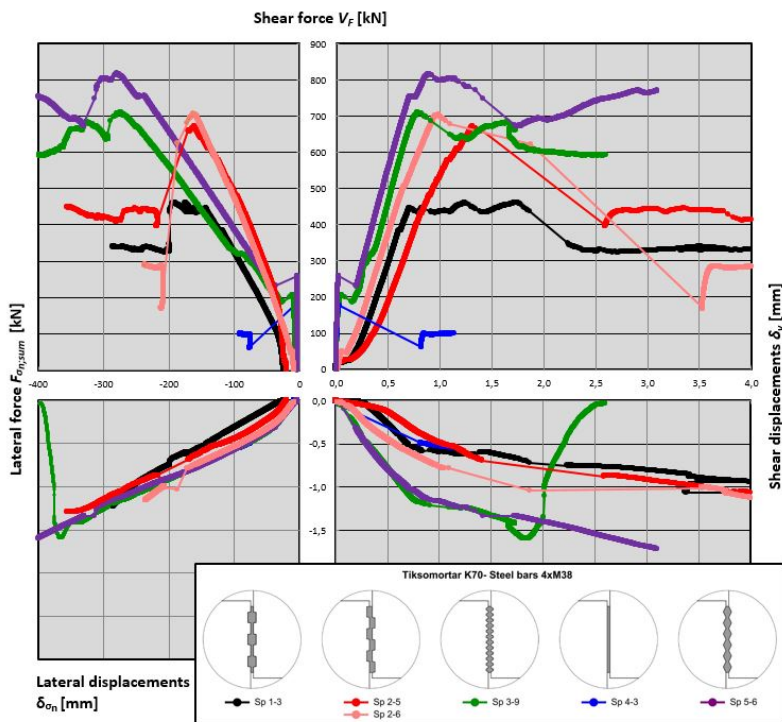
Figure 6.24: Test results of the five mortar connections with Tiksomortar K70 and steel bars M38

The effect of the selected profiles and roughenings for the 3 connections is that they can initially transfer higher shear forces without significant deformations due to the absence of debonding or cracks. Because of the lack of lateral displacements, the steel bars are not activated. This explains that in the shear force-lateral force relationships no increase in lateral forces can be seen until debonding or cracking.

By adding shear keys with smaller dimensions, there is more interlock between the concrete and mortar in the Aligned small key connection (Specimen 3-9) compared to the Aligned and Staggered shear key connections (Specimens 2-5 and 2-6). Over the same height of the joint (600 mm), more bonding surface has been created via the angled and vertical interfaces that can transfer shear forces along with the interlock without significantly deforming. This is because bonding in the interfaces enables the connection to resist the lateral dilation forces. For the Serrated water-jetted shear connection (Specimen 5-6), the same effect is achieved with a slightly different profile in combination with the roughening. The profile is less interlocking, but the precast concrete surfaces do receive a treatment (waterjetting) that improves the bond between concrete and mortar.

Sp 3-9   Sp 4-3   Sp 5-6
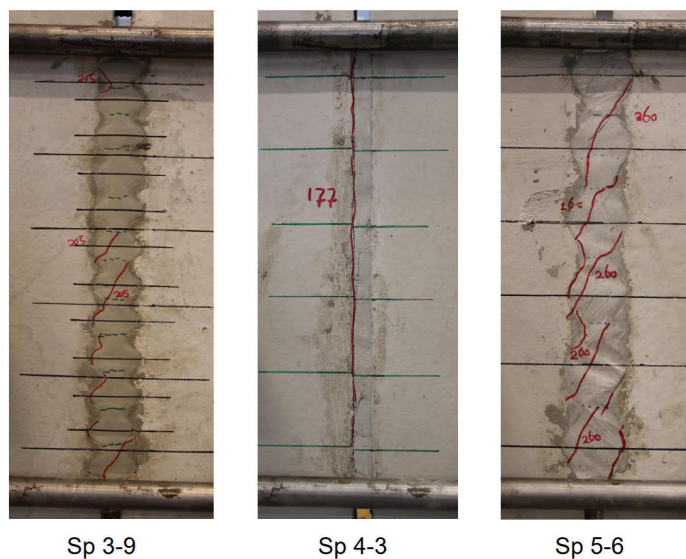
Figure 6.25: Aligned small key connection (Specimen 3-9, 205 kN), Plain water-jetted shear connection (Specimen 4-3, 177 kN) and Serrated waterjetten shear connection (Specimen 5-6, 260 kN) directly after debonding or cracking

Due to the lack of a profile, the Plain waterjetted shear connection (Specimen 4-3) also immediately reached the failure load when debonded. There is only the residual phase where shear friction capacity is provided via the debonded rough surface of the interface. It is characteristic for this connection that, apart from the displacements in one interface, no cracks appear in the mortar or concrete.

When the shear force increases further, the crack widths become larger and new cracks arise in the mortar of connections Specimens 3-9 and 5-6 (figure 6.26). These cracks eventually lead to failure through the main crack. The Aligned small shear key connection (Specimen 3-9) fails due to shearing off the shear keys of the mortar. The failure crack arises in the mortar because the cracks that arose earlier had already damaged its shear keys, while the keys of the precast concrete are still undamaged. The Serrated waterjetted shear connection (Specimen 5-6) fails through a main crack in the mortar-to-concrete interfaces. This crack crosses once from one side to the other (figure 6.26). Despite this crossing, this connection eventually reaches its ultimate capacity through the failure of the interface. This was also the case for the Plain waterjetted shear connection (Specimen 4-3). The influence of the serrated interface appears to be enormous because the failure load of the serrated connection (Specimen 5-6) is approximately 4 times that of the plain waterjetted connection (Specimen 4-3). This is again the effect of the interlock in combination with increasing the amount of bonding surface in the mortar-to-concrete interfaces.

The behaviour of the Aligned shear key connection (Specimen 1-3) is analyzed using figure 6.24 and the photos in figure 6.27. Figure 6.27a shows that a first crack is formed at a shear force of 380 kN. Two more cracks follow at about 433 kN. The shear force-shear displacement diagram shows that the shear force hardly increases after these cracks have formed. This is because the additional cracks (figure 6.27b) increase the displacements and as a result preventing the connection to provide more shear capacity. The connection fails due to the shearing off in 2 shear keys and 1 inclined crack in the mortar.

Sp 3-9   Sp 5-6
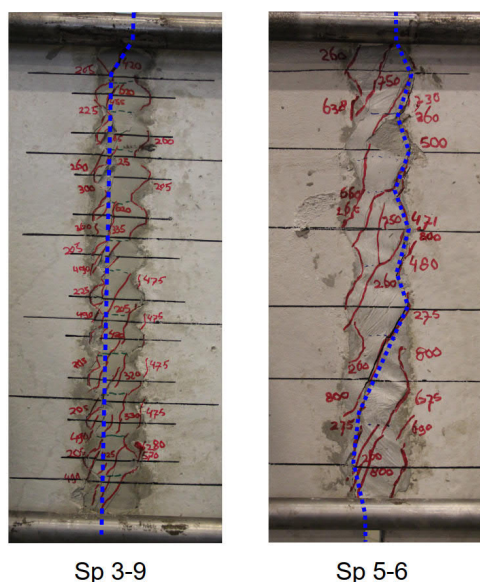
Figure 6.26: Aligned small shear key connection (Specimen 3-9) and Serrated waterjetten shear connection (Specimen 5-6) with failure cracks

The shear force-shear displacement diagram (figure 6.24) shows that the shear capacity of Aligned shear key connection (Specimen 1-3) is lower than provided by the other connections. This has to do with the number of pressure diagonals (n) as it is explained with the help of figures 6.27c and 6.27d. When a connection has n=1 shear key, it fails through one inclined crack similar to the one at the bottom in figure 6.27a. This crack is caused by the splitting or shear failure in the inclined compression strut. The shear force-shear displacement diagram would look like shown in figure 6.27d (n=1). After the formation of this crack in point C in the diagram, the connection would fail and the residual phase follows. When the connection consists of n=2 shear keys, with a certain shear force, two inclined cracks will occur as a result of the splitting or shearing off of the two short compression struts. However, the longer compression strut remains active after point C (fig. 6.27c, n=2). This happens at a lower shear force and the connection fails at point D in the diagram due to the shearing off of one shear key. The tested connection has n=3 shear keys with three short and two longer compression struts. In that case, in the phase C-D of figure 6.27d (n=3) two longer and one short (the middle) compression struts are still active. This shows that the first and last short compression struts collapse and the other struts still remain active. This effect is not present for the Staggered shear key connection because the three pressure diagonals remain active until failure at this connection. With the Aligned shear key connection, the influence of this effect becomes smaller as the number of shear keys increases. In that case the diagram n>5 in figure 6.27d arises, where after the failure of the two short compression struts the shear capacity will increase to point D.
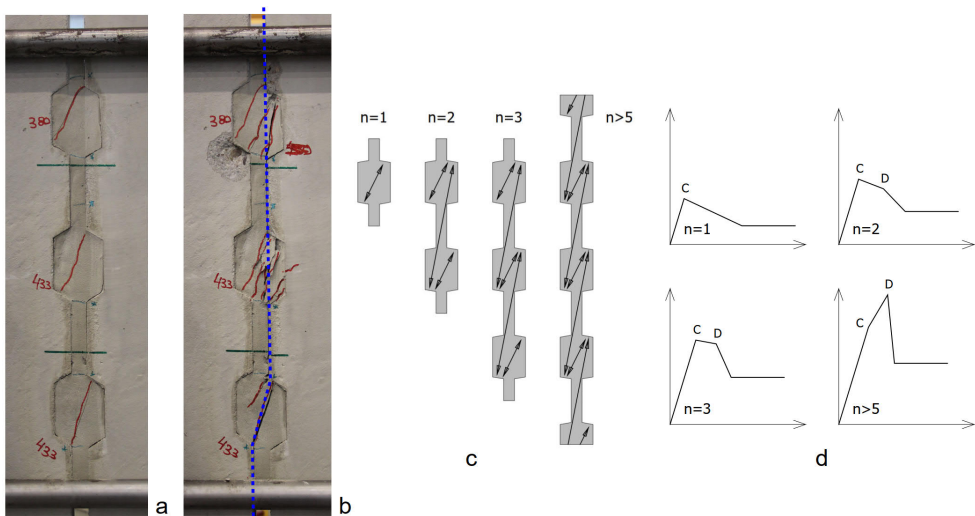
Figure 6.27: Structural behaviour of the Aligned shear key connection (Specimen 1-3)

6.4.3 Steel Fibre Reinforced Mortar Connections - steel bars M24

The shear behaviour of the four connections with Steel Fiber Reinforced Mortar and 4xM24 Steel bars is discussed using the graphs in Figure 6.28. First, a comparison is made between the Aligned (Specimen 1-2) and Staggered shear key connection (Specimen 2-9). Up to the instant of failure of connection Specimen 1-2, the diagram show relationships that are close to each other. The lateral forces and lateral displacements are slightly greater for Specimen 1-2 because the inclined compression strut sets itself a little less steeply due to the chosen profile. The shear force upon failure of the Staggered shear key connection (Specimen 2-9) is approximately 40% higher than that of the Aligned shear key connection. The reason is the aforementioned effect that the Staggered connection has 3 pressure diagonals until failure while the Aligned connection loses the short inclined compression struts in the first and last shear key allowing lower shear forces to be transferred.
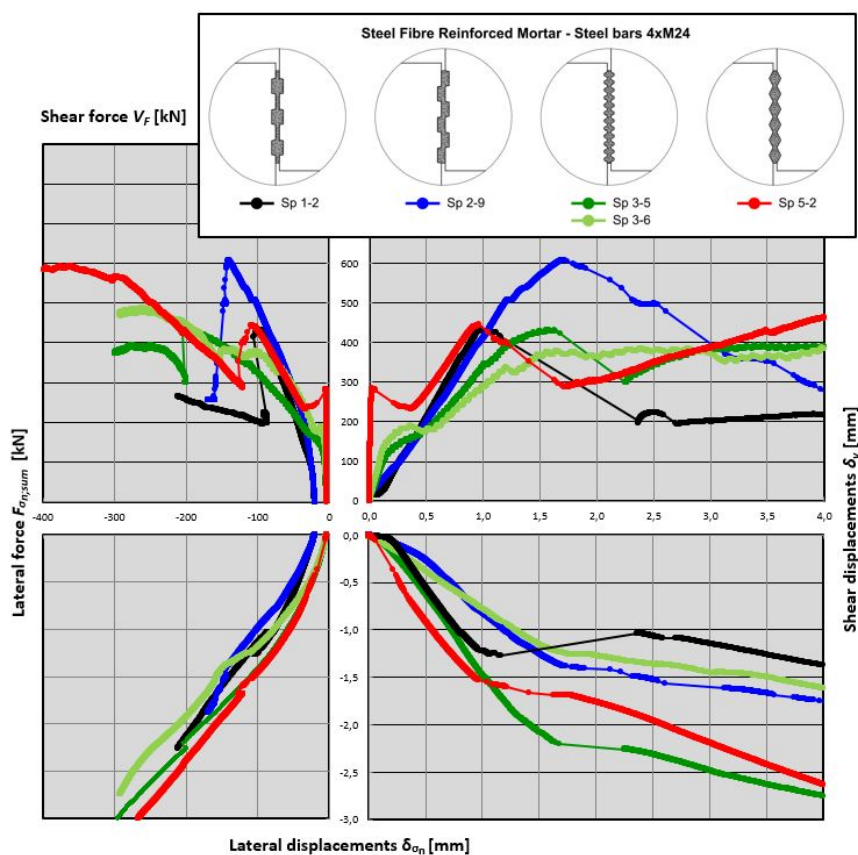
Figure 6.28: Test results of the four mortar connections with Steel Fibre Reinforced Mortar and steel bars M24

Figure 6.29 shows the failed Aligned shear key connection (Specimen 1-2) with a magnification of the middle key. This connection has failed in the mortar with two keys sheared off and one inclined crack. The photo with magnification shows the steel fibers in the inclined crack. During the experiment, the sound of the steel fibers snapping could be heard. The fibers in the direction perpendicular to the cracks have been pulled out of the mortar. Other fibers have been torn or sheared apart because of exceeding the tensile or shear strength of the steel.
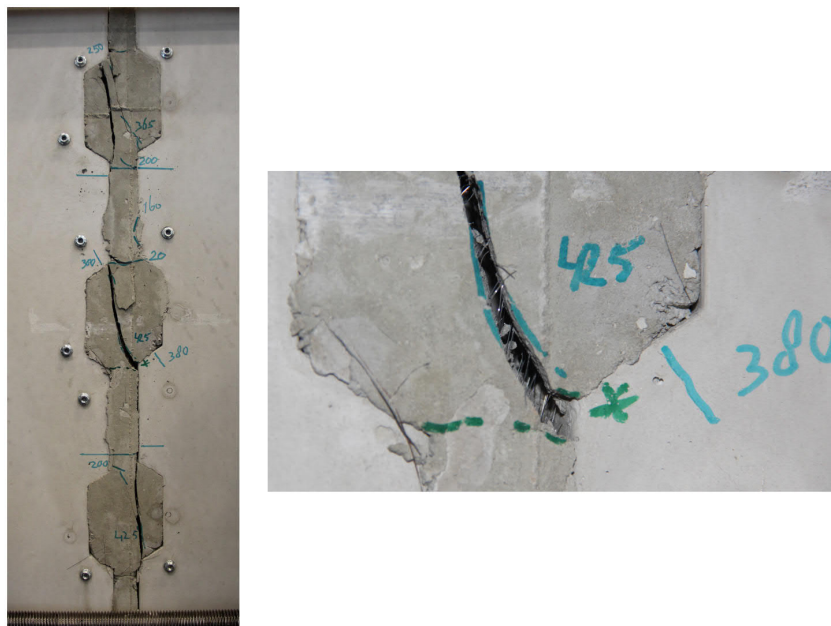
Figure 6.29: Aligned shear key connection (Specimen 1-2) in the residual stage

For the Aligned small shear key (Specimens 3-5 and 3-6) and the Serrated shear key connection (Specimen 5-2) again high shear capacities and shear stiffnesses for the first stage until debonding could be expected. However, the shear force-shear displacement diagram of figure 6.28 shows that the deformations in the Aligned small shear key connections increase quite quickly. Thus, this connection cannot hold the high shear stiffness. The reason is that the mortar-to-concrete interfaces in both connections debond quickly as can be observed in figure 6.30 (Specimens 3-5 and 3-6). No explicit explanation is found for this. It can be argued that the M24 steel bars provide less lateral confinement than M38 steel bars. However, with good bonding in the interfaces this should have little effect. There is also a difference between Steel Fiber Reinforced Mortar and Tiksomortar which could influence the bonding in the interfaces. This has not been confirmed.

It should be noted that in the connections Specimens 3-5 and 3-6 a bonding agent has been used with the aim of improving the bonding behaviour in the interface.

The effect of this can be determined by comparing the behaviour of the connections Specimens 3-1 to 3-4. The diagrams in figures 5.16 and 5.17 show an improvement of the shear capacity and shear stiffness at debonding from Specimen 3-1 (without bonding agent) to Specimen 3-3 (with bonding agent). However no effect was found for the other specimens. Therefore, that comparison did not show any significant effect by the bonding agent and so this cannot cause the difference as well.

The fact that the lower lateral stiffness also influences the behaviour of Specimen 5-2 is apparent from the photo in figure 6.30. Here too, the mortar-to-concrete interfaces debond, while this is hardly observed in Specimen 5-6 (figure 6.25).

Sp 3-5 (170 kN)   Sp 3-6 (130 kN)   Sp 5-2
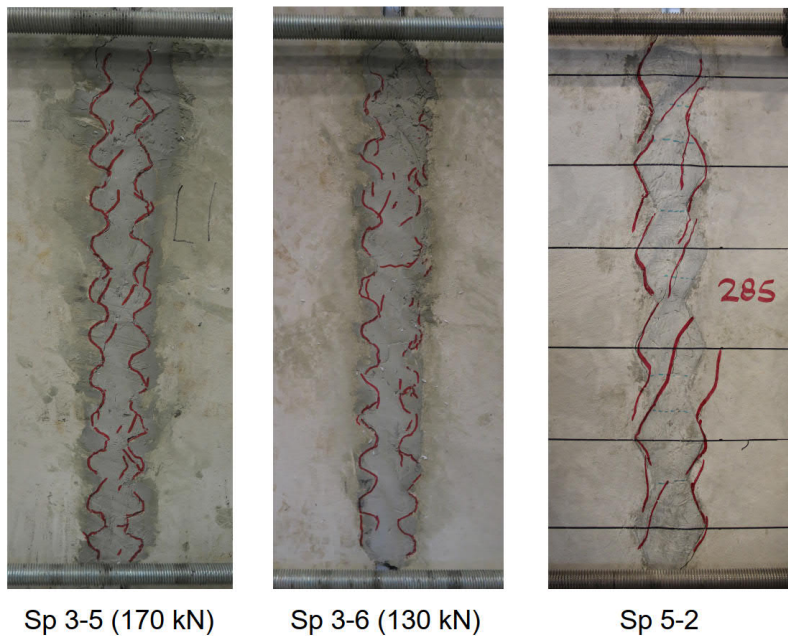
Figure 6.30: Aligned small shear key connection (Specimens 3-5, 3-6) and Serrated waterjetted shear connection (Specimen 5-2) immediately after debonding and cracking

The shear force-shear displacement diagram in figure 6.28 shows that with the Aligned small shear key connection (Specimens 3-5, 3-6) some debonding/cracking occurs at approximately 180 kN. Thereafter, the shear forces continue to increase until the connections fail. These relationships also develop with a lower shear stiffness compared to the other three connections (figure 6.28). From this it can be distracted that the lateral confinement via the stiffness of M24 steel bars is too little to achieve the shear stiffness of the other connections. This was not yet the case with the Aligned small shear key connection with steel bars M38 (Specimen 3-9). It has to be noted that this connection requires a minimal lateral stiffness to perform optimally.

The shear force at failure $V_{F;U}$ of the Serrated waterjetted shear connection (Spe-

cimen 5-2) with 4xM24 steel bars is 445 kN (figure 6.28). This is lower than would be expected based on the performance of the same connection, but with a lower lateral stiffness (Specimen 5-1, steel bars 4xM16). The shear capacity at failure of this connection was less than 738 kN. The reason for this lower capacity can be explained by comparing the shear behaviour and cracking pattern of the connections Specimens 5-1 to 5-3. Figure 6.31 shows the test results of the three connections. Figure 6.32 shows the cracking behaviour of these connections. The lateral force – lateral displacements diagram shows that the lateral stiffness of the steel bars 4xM24 (Specimen 5-2) lies between that of 4xM16 (Specimen 5-1) and 4xM38 (Specimen 5-3). It is then to be expected that the relation of Specimen 5-2 in the shear force – shear displacements diagram lies between Specimens 5-1 and 5-3. This does not appear to be the case. The photos in figure 6.32 show that the main crack at failure of Specimens 5-1 and 5-3 goes partly through the mortar filling and partly through the mortar-to-concrete interface. In Specimen 5-2, the main crack goes entirely through the serrated mortar-to-concrete interface. The mortar filling has sheared off the sloping and roughened concrete surface. The more the extent of the main crack goes through the mortar filling, the better the connection performs.
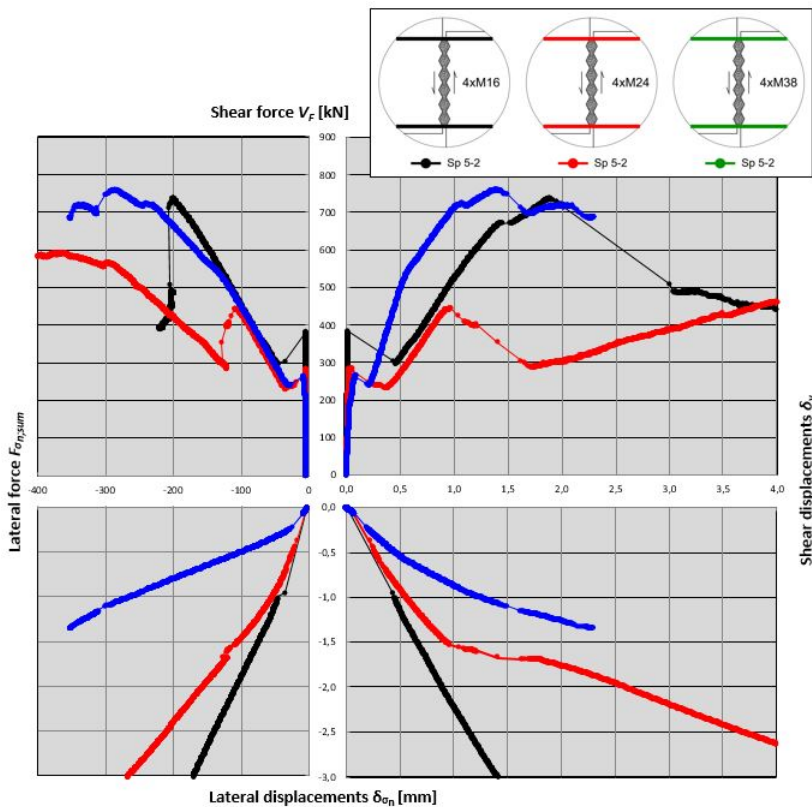
Figure 6.31: Test results of the Serrated waterjetted shear connection

Sp 5-1   Sp 5-2   Sp 5-3
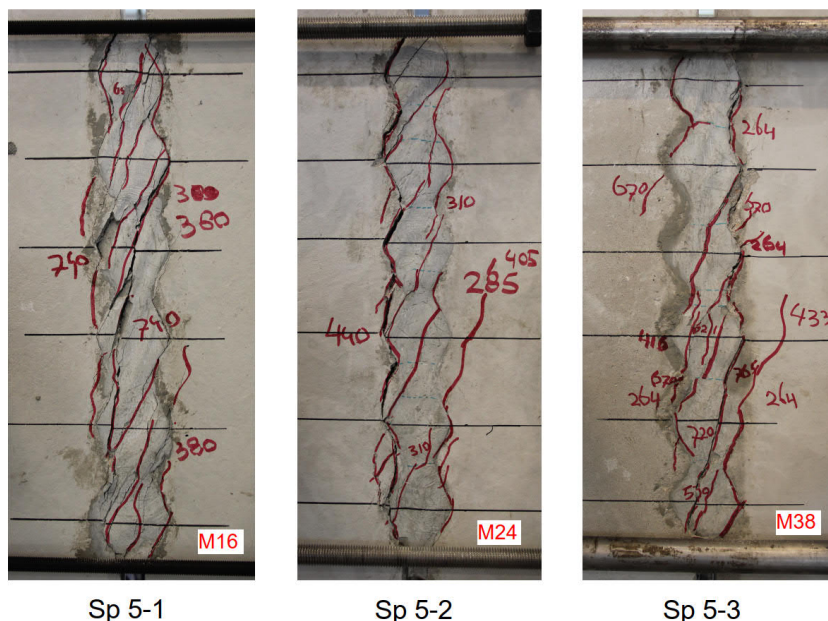
Figure 6.32: Cracked Serrated waterjetted shear connections

6.5 Modeling the vertical mortar connection

6.5.1 Assessment of the connections

The shear behaviour of the five mortar connections are assessed on their performance for functioning as a vertical mortar connection. This is done by discussing the relevant shear stiffnesses and shear capacities with the help of the simplified representation of the shear force-shear displacement relations displayed in figure 6.33.

Initial shear stiffness; The use of the initial (high) shear stiffness up to debonding (figure 6.33) is limited for initially compressed mortar connections. The initial compression prevents the interfaces to debond which might be initiated by shrinkage of the mortar or lateral displacements by the surrouding precast concrete structure. Lateral pre-tensioning is usually not designed for vertical mortar connections that makes the use of this initial shear stiffness for vertical mortar connections unlikely. Furthermore, the use of the Plain waterjetted shear connection for vertical seams has to be questioned because it fails brittle which has to be avoided in a structural application. The use of the initial high shear stiffness is more likely to be used for horizontal mortar connections with favorable dead weight of the building structure on top as a compressive loading on the connection. Then the permanent compression ensures that the interfaces remain uncracked in this horizontal application.

Sp 1-x Aligned shear key
Sp 2-x Staggered shear key   Sp 3-x Aligned small shear key   Sp 4-x Plain waterjetted connection
                                  Sp 5-x Serrated waterjetted connection
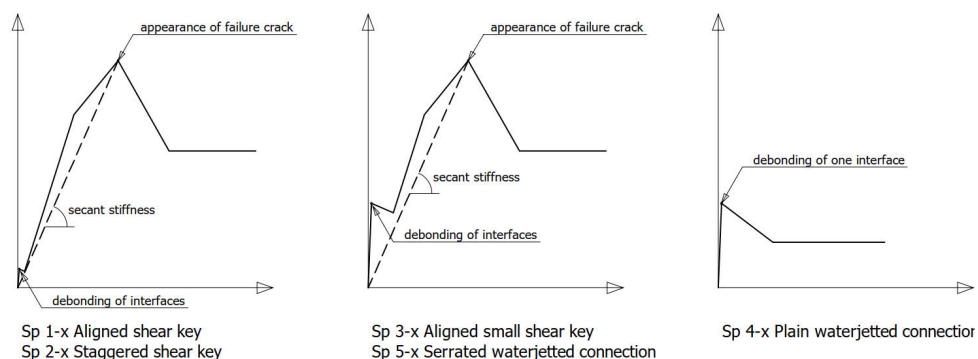
Figure 6.33: Simplified representation of the shear force-shear displacement re-
lations

Secant shear stiffness; The usual approach for modeling the shear stiffness of
a vertical mortar connection is taking the secant shear stiffness from a shear force-
shear displacements relation. Figure 6.33 indicates this stiffness in the simplified
shear force-shear displacement diagrams. Table 6.1 lists these stiffnesses for the
initially uncompressed connections. The table shows rather low stiffnesses for the
Aligned small shear key connections 3-1 till 3-6 (M16 and M24 steel bars). These are
lower than found for the remaining connections. The connections 3-7 till 3-9 (M38
steel bars) behave with stiffnesses that are comparable to the other connections. Be-
cause of the lower stiffnesses for the M16 and M24 steel bars, the application of this
connection is not preferred. The remaining connections all show a secant stiffness
in the range of 400 kN/mm till 900 kN/mm. No preference for the remaining three
mortar connections can be appointed on the basis of this comparison.

Spec.	Steel bars	Shear stiffness [kN/mm]	Spec.	Steel bars	Shear stiffness [kN/mm]
1-1	(M24)	420	3-1	(M16)	166
1-2	(M24)	451	3-2	(M16)	205
1-3	(M38)	626	3-3	(M16)	197
			3-4	(M16)	204
2-1	(M16)	401	3-5	(M24)	264
2-2	(M16)	403	3-6	(M24)	350
2-3	(M24)	406	3-7	(M38)	530
2-4	(M24)	552	3-8	(M38)	645
2-5	(M38)	514	3-9	(M38)	910
2-6	(M38)	718	5-1	(M16)	388
2-9	(M24)	356	5-2	(M24)	464
			5-3	(M38)	548
			5-6	(M38)	908

Table 6.1: Secant shear stiffnesses of the connections

Ultimate shear capacity (depending on lateral forces); The next connection property to be discussed is the shear capacity. Figure 6.34 displays in a diagram the ultimate shear forces $V_{F;U}$ as function of the corresponding lateral forces $F\sigma_{n;sum}$ for all mortar connections. A trendline (linear) is taken from the point results of each connection. The lateral dilation forces should be as little as possible in order to minimize the lateral compensation by the tyings in the precast concrete structure. The diagram clearly shows that the Staggered shear key connection (Specimen 2-x) provides the highest ultimate shear forces for the lowest lateral forces.
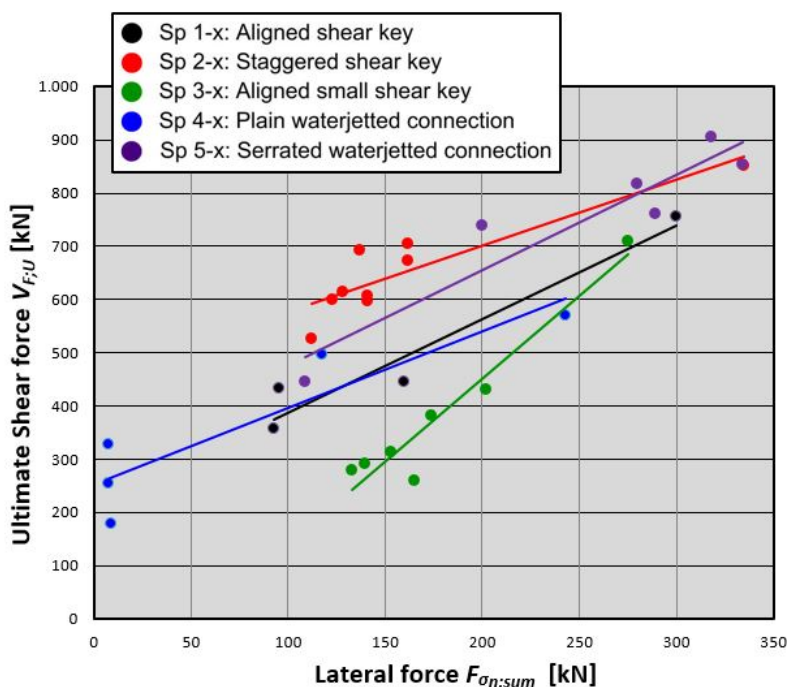
Figure 6.34: Ultimate Shear force-Lateral force relations

Ultimate shear capacity (depending on lateral stiffness); The ultimate shear capacity depends on the lateral stiffness present in the surrounding precast concrete structure. The lateral stiffnesses k_h the connections require from the surrounding structure for getting a certain shear capacity has been made visible in the diagram of figure 6.35. The ultimate shear forces are plotted as function of the tangent lateral stiffnesses k_h as presented in table 5.9. Again, trendlines are added to the point results of each connection. The best performing connection should provide the highest shear force with a low need for lateral stiffness. This diagram shows the Serrated waterjetted shear connection (Specimen 5-x) provides the highest ultimate shear forces. The close second is the Staggered shear key connection.
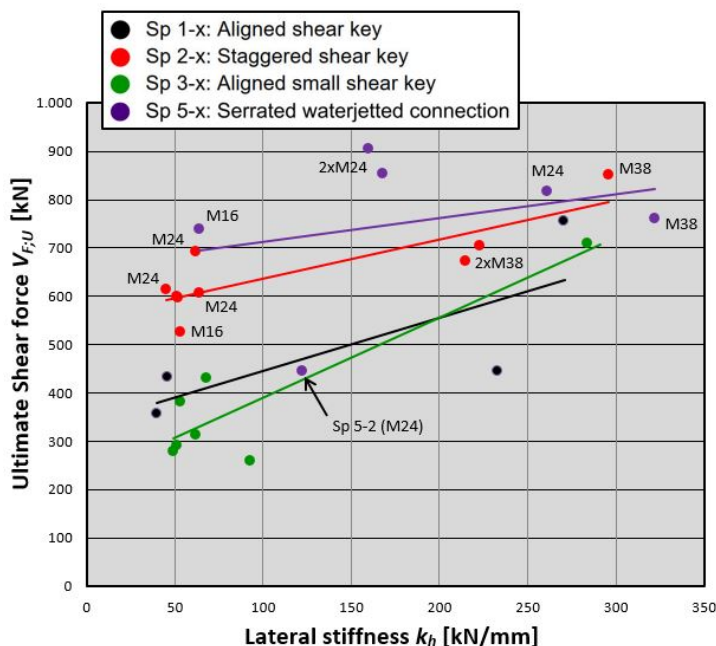
Figure 6.35: Ultimate Shear force-Lateral stiffness relations

The considerations above show that the Serrated waterjetted shear connection (Specimen 5-x) seems to be one of the most promising connections. However, a few comments should be made for the application of this connection. First, it turned out that the high ultimate shear forces were only found when the main crack runs through the mortar filling. In Specimen 5-2 the main crack appeared to run only through the interface (figure 6.32) with the result that the ultimate shear force was significantly lower (figure 6.35). It cannot be guaranteed that with a storey-high Serrated waterjetted shear connection the main crack runs through the mortar once every 600 mm because of shrinkage of the mortar or the precast concrete wall elements. In addition, roughening with retarder and waterjetting is an additional process that only gives a reproducible roughening with precise work. The third point is that the mortar in the connection will visibly crack when the initial high stiffness is lost. The fact that the mortar cracks is not a problem in itself. However, with the other promising connection (Staggered shear key connection), the first visible cracks in the mortar appear at a considerably higher shear force. It can be concluded that despite the fact that this connection provided high shear capacities in the test specimens, this connection is ultimately less attractive for application because of the arguments just mentioned.

From this assessment it can be stated that the Staggered shear key connection transfers the vertical shear forces in the most effective way. The force distribution can be approximated with a clear and relatively simple compression strut model. It

delivers high shear capacities for relatively low lateral forces and lateral stiffnesses. It also appears that the secant shear stiffness is not less than provided by the other connections. The Staggered shear key connection is taken for investigating its application and modeling in a storey-high situation in the next chapter.

When applying this connection, one can choose for the Tiksomortar K70 or the Steel Fibre Reinforced Mortar. The investigation shows that SFRM causes the cracks to appear in the precast concrete L-elements instead of in the mortar and that no significant improved shear behaviour was found. The secant shear stiffness was somewhat lower (Specimen 2-9, table 6.1), but that is only based on one observation. Based on the measurements, there is no argument for applying SFRM. The pumping of SFRM via a hose requires the additional handling, which means that the application of Tiksomortar K70 is preferred for reasons of manufacturability and costs.

6.5.2   Shear capacity of the Staggered shear key connection

In this subsection the shear capacity of the Staggered shear key connection is specified for application in practice. It is considered to be dependent on the lateral effects that can be revealed by contemporary structural calculation programs. From the foregoing, it appeared that the size of the ultimate shear force $V_{F;U}$ depends on the lateral stiffness k_h and the initial compression σ_n. Both variables determine the dilation of the seam and thus how large the lateral displacements $\delta\sigma_n$ become. The dependency of the shear force $V_{F;U}$ on the lateral stiffness and initial compression can be expressed both at the same time in the lateral displacement $\delta\sigma_n$ which is defined as $\delta_{lateral}$. With this approach it can be said that a larger lateral displacement $\delta_{lateral}$ causes the arise of the failure crack for a lower shear force $V_{F;U}$. This can be observed in the diagram of figure 6.36 where this relationship is plotted for the nine measured shear forces $V_{F;U}$ of the Staggered shear key connection (Specimens 2-x). This overview of test results underscores that the connection fails at a lower lateral stiffness (M16 steel bars) with a larger lateral displacement $\delta_{lateral}$ and vice versa. Also, the initial compression hinders the increase of the lateral displacements up to significant shear forces $V_{F;U}$, after which the connection fails with a rather small displacement as can be observed for the measurement M38 with initial compression in the diagram. A linear mean (trendline) is calculated for the nine test results.

Because the lateral displacements $\delta_{lateral}$ can easily be measured in a structural calculation model with inclined compression struts for the Staggered shear key connection, the design value of the shear capacity V_{Rd} has been determined from the mean value of the measured shear capacities. This was done by using the "Annex D Design assisted by testing" method provided in NEN-EN 1990 (1992). With this method for achieving the level of reliability required for design, it can be determined that the design value for the shear capacity V_{Rd} depending on the lateral deformation $\delta_{lateral}$ [mm] and for a three keyed Staggered shear key connection can be calculated by using the equation[1]:

---

[1]The equation applies to the used Tiksomortar K70 and concrete with strength grade C53/65.

$$V_{Rd} \left[\text{kN/3 shear keys}\right] = 524 - 138 \cdot \delta_{lateral}, \quad \delta_{lateral} < 2,0 \text{ mm} \qquad (6.9)$$

This equation will be used for the verification of the shear capacity of the Staggered shear key connection applied in the case studies of the next chapter.
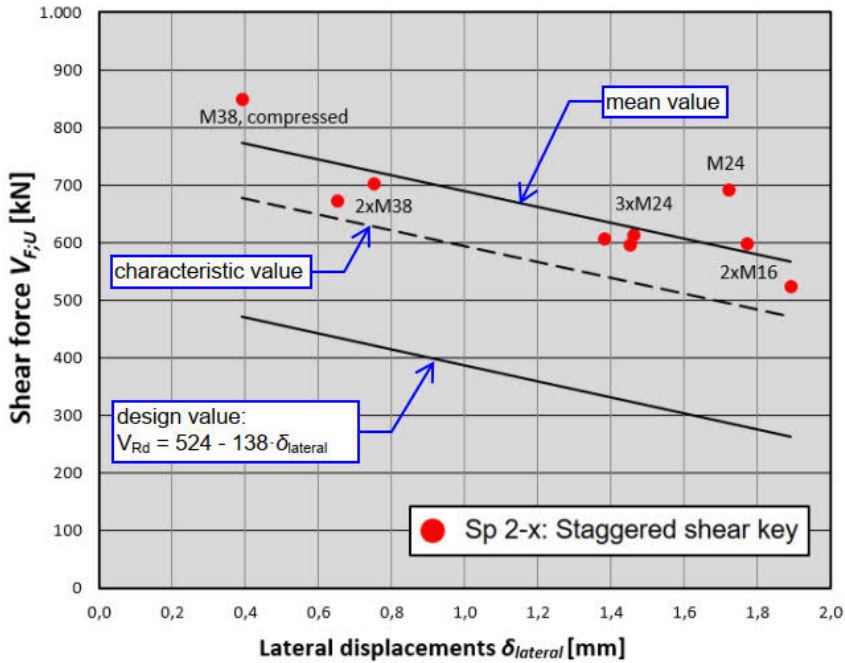
Figure 6.36: Ultimate Shear force-Lateral displacements relations for the 3-keyed Staggered shear key connection

6.5.3 Compression strut model for Staggered shear key connection

The previously discussed inclined compression strut way of modeling can also be used for modeling the Staggered shear key connection without explicitly modeling the indentations of the shear key. To represent the diagonal resultant force, it is required that the strut sufficiently approximates the real (measured) connection behaviour for the three lateral stiffnesses 4xM16, 4xM24 and 4xM38 applied in the experiments. If that is the case, it can be assumed that the model is able to simulate the connection behaviour for various lateral stiffnesses.

Figure 6.37 displays a numerical specimen model with only the three inclined compression struts for the transfer of forces. They are hingedly connected to the wall elements. To find a suitable inclined bar, the three truss elements are given a height (200 mm), width (30 mm) and size (25x200 mm^2), close to what was found for

the resultant diagonal force in the mortar filling earlier in this chapter. The displacements in this specimen model are obtained from monitoring points that are located where the displacements on the real specimens were taken.
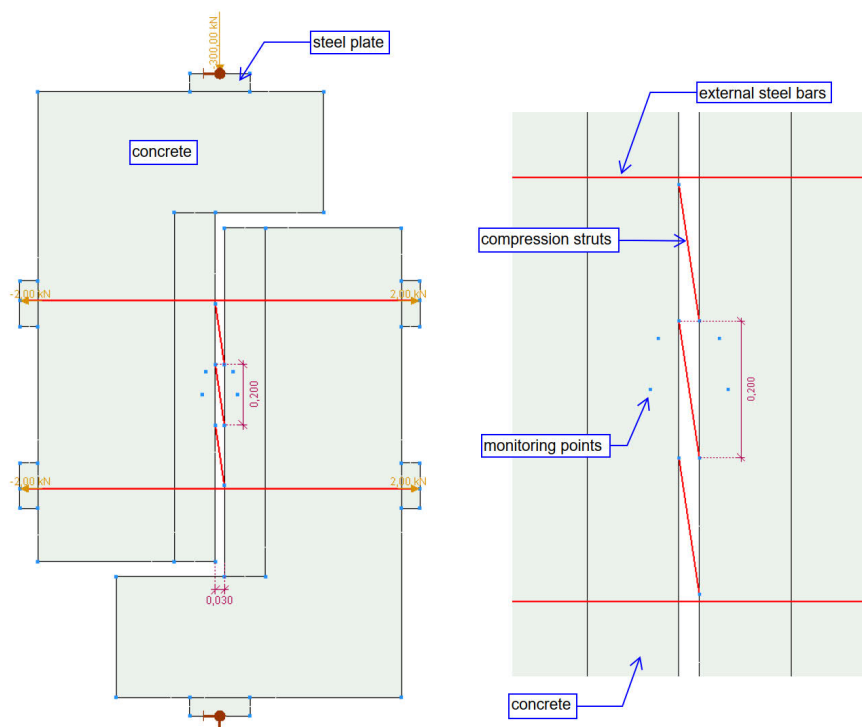
Figure 6.37: Compression strut specimen model

A vertical (shear) force of 300 kN was imposed to the numerical specimen. A Young's modulus[2] of 9.000 N/mm^2 for the diagonal bar was chosen after a number of iterations for matching the numerical vertical displacements to the real (measured) shear displacements. The remaining model properties are listed in table F.2.

It was found that the selected Young's modulus provided a good approximation for the three sets of steel bars M16, M24 and M38 representing three different levels of lateral stiffness (k_h). This can be observed in the load-displacement diagrams of figure 6.38 where the numerical results are plotted as a dot. They are located sufficiently close to the measured forces and displacements of the real specimens. It demonstrates that the selected compression strut model is able to behave under shear and for various lateral stiffneses close to the ones of the real connections. It allows the model to represent the Staggered shear key connection in this numerical specimen model.

---

[2]The Young's modulus applies to the used Tiksomortar K70 and concrete with strength grade C53/65.
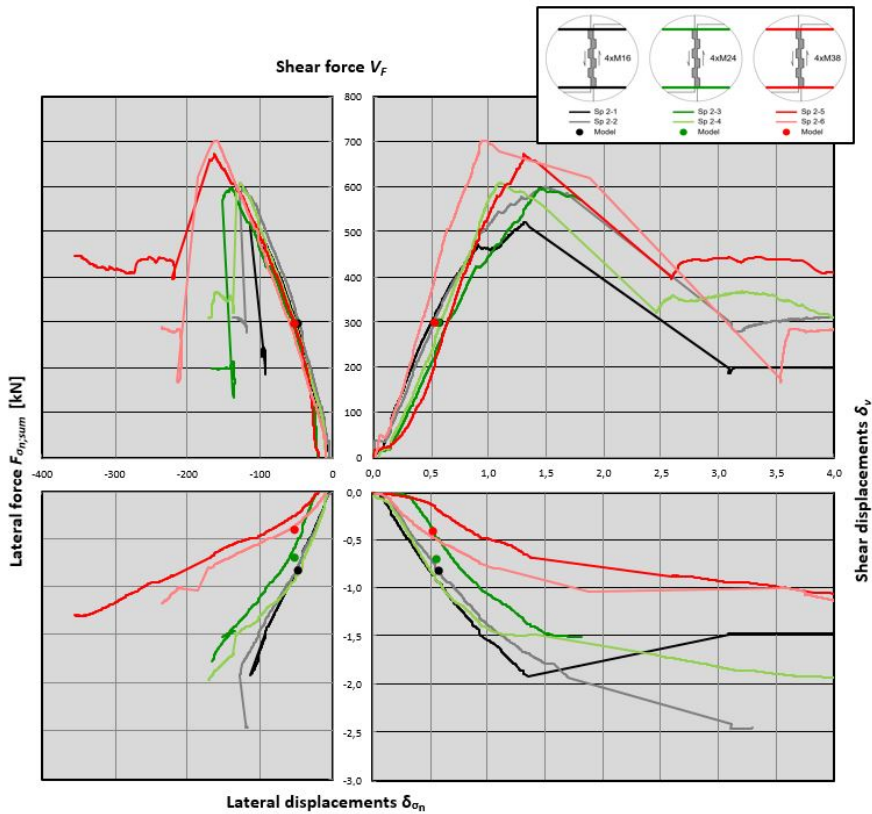
Figure 6.38: Test results of Specimens 2-1 till 2-6 and results of the proposed
compression strut model (dots)

6.6 Conclusions

The analysis of the Staggered shear key connection demonstrates that the imposed shear forces are transferred via three diagonal forces through the mortar filling. The transfer of one diagonal force is modeled with an inclined compression strut. The functioning of this strut with its force distribution and interface stresses is analysed. It turned out that the lateral displacements mainly determine the slope of the resultant force of the compression strut. It is a steeper angle than can be distracted from the geometry of the connection. As a result, this resultant diagonal force causes a nonlinear stress distribution in the sloped mortar-to-concrete interfaces.

The compression strut model is also used for simulating the vertical displacements δ_v. It turned out from a polygon of displacements that the vertical and horizontal displacements are caused by the shortening and rotation of the compression strut. In addition, the full deformations of the connection also include the displaced shear keys of the precast concrete L-element. In order to simulate the displacement

field of the entire Staggered shear key connection, the full specimen is modeled with a finite element program. It turned out that the shear displacements δ_v of both the compression strut model and the mortar filling in the finite element model are approximately equal to each other. It demonstrates that the forces and deformations of the mortar filling can be simulated with the proposed compression strut model.

The finite element model is also used for studying the behaviour of the whole Staggered shear key connection. In this model, triangular interface stresses were found in the sloped compressed interfaces of the shear keys. This supports the finding that the inclined resultant force develops more steeply than the geometry suggests. In addition, the numerically calculated forces and deformations were compared with the real values measured on the specimens. This comparison was made for the two identical Staggered shear key connections (Specimens 2-1 and 2-2) with Tiksomortar and steel bars 4xM16. The results from the numerical simulation appeared to approximate the measured values quite closely.

The effect of varying the lateral stiffness, the lateral initial compression, the thickness of the seam and the type of mortar are studied. The analyses shows that a higher lateral stiffness (4xM24 and 4xM38) leads to an increase of the shear stiffness and shear capacity. In addition, lateral displacements are lower for connections with a higher lateral stiffness. The effect of varying the lateral stiffness has also been investigated numerically. A comparison of the numerical results with the measured results for three lateral stiffnesses demonstrates that the numerical models have approximated the real behaviour quite accurate.

The analysis also shows that increasing the initial lateral compression causes the debonding of the vertical interfaces to take place at a higher shear force. In addition, the lateral displacements do not increase because the steel bars do not lengthen until the lateral dilation force exceeds the initial compression force. No significant higher shear stiffness is found for the initially compressed connection after debonding. At the same time, the ultimate and residual shear capacities do increase. A finite element model simulation of the connection with initial compression has also been performed. For this variant, too, it appears that the numerical model approaches the measured behaviour of the initially compressed Staggered shear key connection sufficiently accurate.

An analysis of the test results of the connection with a reduced thickness of the seam (15 mm instead of 25 mm) demonstrates an insignificant influence of the seam thickness in this range. The next variable investigated is the application of Steel Fiber Reinforced Mortar instead of Tiksomortar for the Staggered shear key connection. The comparison shows that the cracks mainly arose in the Tiksomortar, while the connection with SFRM shows the cracks in the precast concrete. Apart from this, a mutual comparison of both connections demonstrates that despite the improved properties of the SFRM the overall connection behaviour do not significantly change.

Apart from the Staggered shear key connection the remaining connections are constructed with four other interface profiles and in some cases waterjetted precast concrete surfaces for getting roughened interfaces. The effects of these connection variants are analysed. With simplified representations the shear force-shear dis-

placement relations of the five connections are represented. The comparisons show different behaviour for the initial stage up to debonding of the interfaces. It turned out that both the Aligned and Staggered shear key connections debond almost immediately at very low shear capacities. For the Aligned small shear key connections (Specimen 3-x) compared to the other the shear capacities and the shear stiffnesses are higher as a result of adding smaller sized shear keys with additional interlock and an increased amount of bonding surface. The Serrated waterjetted shear connection (Specimen 5-x) with its profiled and roughened interfaces provides the highest shear capacity in the initial phase. The combination of this profile and the roughened interfaces turns out to be very effective. Finally, the Plain waterjetted shear key connection (Specimen 4-x) with its unprofiled roughened interfaces provides significant high shear capacities and shear stiffnesses. The force at debonding is the ultimate shear capacity after which the shear force-shear displacement relation drops to the residual stage because of the absence of a profiled interface.

The ultimate shear capacity $V_{F;U}$ of the Aligned shear key connection turns out to be considerably lower than that of the other profiled connections. The reasing is that because after the formation of the first diagonal cracks in fact two inclined compression struts remain. The analyses show that this effect diminishes when more shear keys are present above one another. With the Aligned small shear key connection, it is found that at the lower lateral stiffnesses (4xM16 and 4x M24) develops with low shear stiffnesses and ultimately fails with lower shear capacities. However, this connection is effective with a high lateral stiffness (4xM38). In addition, the bonding agent for improving the bonding in the interfaces is found not to improve the shear behaviour of this connection. The Serrated waterjetted shear connection provides the highest shear capacity under the condition that the main crack also runs straight through the mortar. When it only runs via the interface (Specimen 5-2) the shear capacity turns out to be much lower.

The shear behaviour of the five mortar connections are assessed on their performance for functioning as a vertical mortar connection. This is done by discussing the relevant shear stiffnesses and shear capacities. From this assessment, it is concluded that the Staggered shear key connection transfers the shear forces in the most effective way for the use as a vertical mortar connection. Therefore, this connection is taken for investigating its modeling and application in a storey-high situation in the next chapter.

For the shear capacity of the three keyed Staggered shear key connection a relation is derived in which the shear capacity is dependent on the lateral displacements $\delta_{lateral}$. This is done because these displacements can easily be evaluated by contemporary structural calculation programs. For prediction purposes, a design equation (6.9) including this dependency is proposed for the verification of the shear capacity in the case studies in the next chapter.

Finally, an inclined compression strut model for a three-keyed connection without shear key indentations is proposed for the representation of the Staggered shear key connection. The shear behaviour is modeled with truss elements in a numerical specimen model. The selected bar model is adjusted for the simulation of the specimen

forces and displacements that approximate the measured values of the three lateral stiffnesses (M16, M24 and M38). This is found sufficiently accurate and the inclined compression strut model is considered suitable for simulation of the three-keyed Staggered shear key connection for different lateral stiffnesses.

Chapter 7

Behaviour of a Storey-high Staggered shear key connection in Cantilever Shear Walls

7.1   Introduction

In the previous chapters, the shear behaviour of various connections has been invest-igated and it turned out that these connections can potentially be used as storey-high vertical shear connection. In this chapter, the Staggered shear key connection is taken to investigate its shear behaviour in the storey-high application as part of a precast concrete cantilever shear wall structure.

It is found that the inclined compression struts are very suitable for transferring shear forces, provided that the resulting lateral dilation forces are balanced. These forces are taken by the external steel bars in the specimen with the 3-keyed Staggered shear key connection. As previously proposed, for the intended storey-high applica-tion, these lateral forces have to be balanced by the concentrated tying reinforcement in the concrete slabs. It is the question what this means for the shear transfer mech-anism and the shear stiffness of the storey-high Staggered shear key connection.

In section 7.2 the shear behaviour of the Staggered shear key connection applied in a cantilever shear wall is considered. Particularly attention is paid to the force effects at the location of the slabs and the distribution of the forces in the connection over the height of the storey. In practice, window openings can also be present in the shear walls. The effect that these openings have on the force distribution of the same storey-high connection in a cantilever shear wall is considered in section 7.3.

The cantilever shear walls in this chapter are representative for real precast con-crete structures in buildings. How the storey-high Staggered shear key connec-tion performs in such real applications is investigated by means of the case studies presented in section 7.4. In the final section 7.5 conclusions are drawn.

171

7.2   Storey-high shear transfer mechanisms

7.2.1   Modeling of the storey-high Staggered shear key connection

The way a storey-high Staggered shear key connection transfers shear forces is investigated with the help of the numerical cantilever shear wall model displayed in figure 7.1a. This structure has seven floors constructed with 2,80 meter high precast concrete wall elements and concrete slabs in between. The cantilever shear wall is clamped into the foundation and loaded with a lateral line load at the left side. The two vertical "stacks" of wall elements are jointed in the middle with the vertical Staggered shear key connection. Figure 7.1b displays the mortar filling including the compression struts representing the diagonal resultant force as considered in the previous chapter. The struts are modeled in the cantilever shear wall as inclined truss elements between the precast concrete wall elements according to figure 7.1c. Finally, horizontal truss elements (figure 7.1d) are modeled for connecting the both parts at the location of the slabs. It can be argued how to model the slabs in these numerical analyses. In reality the slab itself can possibly also contribute to the shear transfer. However, for these analyses it is chosen to model the connection of the shear wall elements at the level of the slab by truss elements that are hingedly connected. With the horizontal loading on the left part of the shear wall, the right wall is also activated via a horizontal compressive force in the truss elements to function as a composite shear wall for transferring the horizontal loading forces to the foundation.

The inclined compression struts should approach the correct connection behaviour in order to allow them to represent the Staggered shear key connection in the storey-high application. The analyses of the connection behaviour in the previous chapters demonstrates that the shear stiffness (k_v) depends on the lateral stiffness (k_h). In general, the profiled mortar connection provides a higher shear stiffness when it is clamped by a higher lateral stiffness. This dependency has to be taken into account by the inclined compression strut model. The bar model of figure 7.1c is capable to do this because a lower lateral stiffness allows the connection to displace laterally more and that results in additional vertical displacements due to the rotation of the truss element. This larger shear displacement for the same shear force lowers the shear stiffness of the connection. It demonstrates the inclined compression strut model is able to behave with a dependency on the lateral stiffness.

For a proper functioning, the compression strut model has to approach sufficiently accurate the real shear behaviour for different lateral stiffnesses. This was already verified for the specimens with three struts and different steel bars (M16, M24 and M38) in subsection 6.5.3. It demonstrates that the numerical specimen model (figure 6.37) with the given properties for the three struts simulates sufficiently accurate the shear behaviour for different lateral stiffnesses. The question is whether a storey-high shear connection with substantially more than three shear keys in a row behaves differently than from what was found in the three-keyed specimens. It has been established in the foregoing of this thesis that the resultant di-

agonal forces transfer the shear forces almost without influencing each other. As a result, the inclined compression struts function individually and respond to the shear forces applied locally with the same horizontal and vertical deformations as was found in the three-keyed specimen. Therefore, it is expected that a storey-high Staggered shear key connection will not behave differently. This allows the use of the earlier proposed compression strut element over the height of a storey for representing the behaviour of the Staggered shear key connection in the cantilever shear wall.
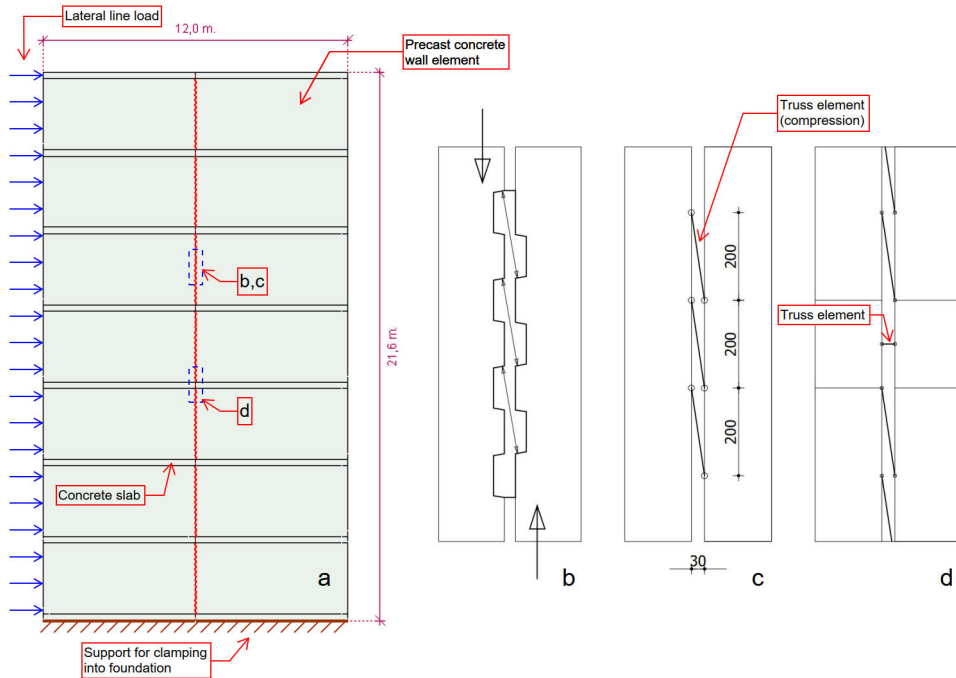
Figure 7.1: Precast concrete cantilever shear wall (a) with Staggered shear key connections (b), modeled inclined truss elements (c) and truss elements to represent the slabs (d).

7.2.2 Behaviour of a storey-high Staggered shear key connection

Figure 7.2a displays the distribution of normal forces in the inclined compression struts that are calculated with the numerical model for the lateral line load. The distribution of the normal forces over the height of the shear wall resembles the typical development of shear forces in such a structure. This implies that the shear forces increase from the top to the bottom of the cantilever shear wall. The distribution of shear forces over the height of one single storey is rather constant. It demonstrates the absence of changing lateral stiffnesses as would be expected by wall openings. In this case, the precast concrete wall elements behave in-plane very stiff and this does

hardly change the shear behaviour of a vertical mortar connection over the height of a single storey. A small increase of the strut forces just above and below the slabs can be observed. This has to be attributed to the inability to transfer shear forces over the height the slabs. As a result these shear forces are redirected via the adjacent compression struts causing a slight increase of the diagonal forces.

According to the proposed precast concrete concept, the summed lateral dilation forces have to be balanced by the tying reinforcement in the slabs. It can be expected that the horizontal truss elements representing the slabs can transfer these tensile forces. However, the shear wall in figure 7.2a is loaded with a line load at the left side causing these tensile forces to interfere with horizontal compression forces in the truss elements that load the right stack of the cantilever shear wall. The figure displays the normal forces N_x that were calculated in each of the slabs for this load. They are all compression forces. This demonstrates that horizontal compression at the location of the slabs dominates. The mechanism is that the summed lateral tensile forces are lower than the horizontal compression forces causing only a decrease of the compression forces. As a result, in this case the tyings in the slabs are not activated for transferring tensile forces and lateral dilation does not occur. In this specific case of the single line load at the left, the shear behaviour of the storey-high vertical mortar connection does not depend on the lateral stiffness provided by lengthening of tying reinforcement.

In reality, cantilever shear walls in buildings are not loaded with only a line load on one side. Applying line loads along the slabs according to figure 7.2b is supposed to better resemble the actual loading. They represent the reaction forces that are usually imposed by diaphragm force distributions. In the case of figure 7.2b, the line loads at the left and right side of the vertical connection are identical. As a result, an exchange of lateral forces via the slab connection does not occur. This is why the figure shows tensile forces in the horizontal truss elements being the forces due to lateral dilation. In this case they certainly have to be taken by the tying reinforcement in the slabs and probably influence the connection shear behaviour only a little. It is recommended to apply slab reinforcement as tying for covering the lateral forces due to dilation even when these tensile forces do not occur due to the compression force between the two stacks.

Figure 7.2: Connection behaviour of cantilever shear walls with lateral line load
at the left side (a) and with horizontal line loads along the slabs (b)

7.3 Application in cantilever shear wall with openings

7.3.1 Modeling the Staggered shear key connection in rigid frame

Wall openings can be present in the precast concrete cantilever shear wall as for
example in the case of a façade of a building. Figure 7.3a displays the numerical
model of this variant. This type of structure is to be considered as a rigid frame
system. In general, the shear force can reverse as a result of a change of the direction
of the lateral load. Furthermore, the force distribution in the rigid frame can cause a
reverse of the shear forces over the height of the vertical mortar connection. Figures
7.3b and 7.3c show that the Staggered shear key connection is capable to tranfer both,
positive and negative shear forces. Therefore, the compression strut model displayed
in figure 7.3d has truss elements (only for compression) allowing the connection to
tranfer reversed shear forces as well. These trusses are of the type of independent
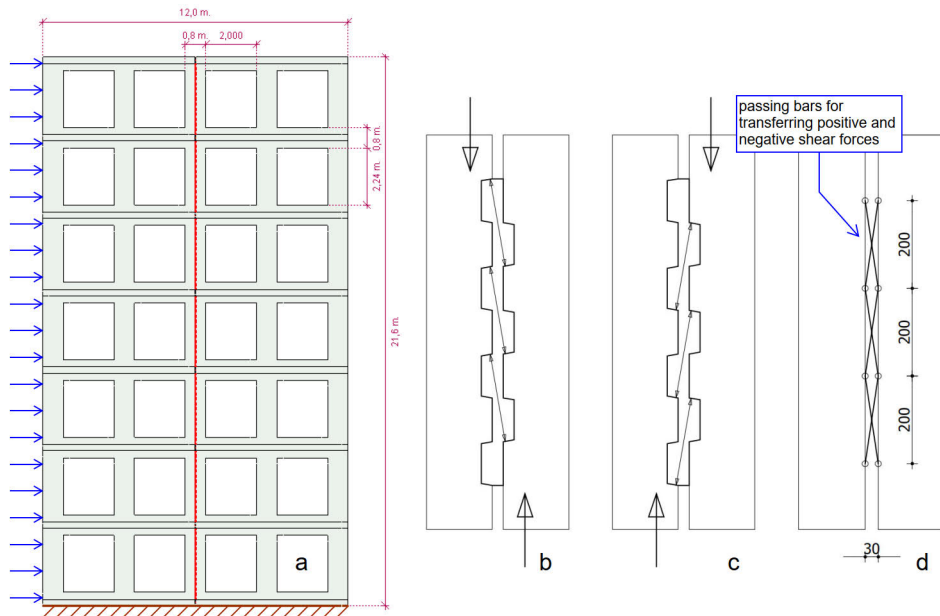acting passing bars to avoid mutual contact.

Figure 7.3: Precast concrete cantilever shear wall with openings (a) in which the Staggered shear key connection is modeled for positive as well as negative shear forces (b-d)

7.3.2   Behaviour of Staggered shear key connection in rigid frame

How the storey-high Staggered shear key connection behaves when modeled with the inclined compression struts in the rigid frame is displayed in figure 7.4. The shear forces are large in the middle of the columns per storey and reverse in sign around the slabs.

It can be that another distribution of shear forces was expected which needs to be explained. The functioning of the connection is partly dependent on the extent to which lateral resistance is offered. In the case of solid walls, the lateral resistance is equal over the height of the wall element as explained in the previous section. Then the distribution of shear forces over the height is uniform. With slender concrete columns, the lateral stiffness against horizontal displacements is less. In case of a very low lateral stiffness, it might be that the shear forces in the middle of the column are smaller and increase in the vicinity of the slabs. Contrary to this expectation, the figure shows that the shear forces are the greatest in the middle of the columns and reverse at the location of the slabs. This can be explained with the pictured distribution of compression forces (the red arrows in figure 7.5) that flow through the framed structure. The diagonal red force in the middle column indicates that the inclined truss elements transfer compression forces from the left side to the right side causing the highest forces to be transferred half way the column. The kink of the red forces just near the corners of the openings result in the blue compression forces for

in order to have equilibrium in the turning points. These blue forces are transferred via the inclined compression struts of the mortar connection and cause the reversal of the diagonal forces in the shear connection. From this it can be explained that the Staggered shear key connection transfers mainly the compression strut forces that are part of the main force distribution in such a rigid framed structure instead of the less dominant shear forces for joining the two cantilever shear walls to one large version.

Again, the way the structure is laterally loaded influences the horizontal forces in the slabs. The model in figure 7.4a is loaded only at the left side of the structure. It does not only cause that the resultant forces in the horizontal connection of the slab are still compression forces, but it also results in higher diagonal compression forces in the mortar filling of the connection. This can be observed from a comparison with the model results in figure 7.4b. Furthermore, it shows that the diagonal forces around the slabs are lower in the structure of figure 7.4b because no horizontal forces have to be passed on to the stack of wall elements right of the vertical mortar connection.
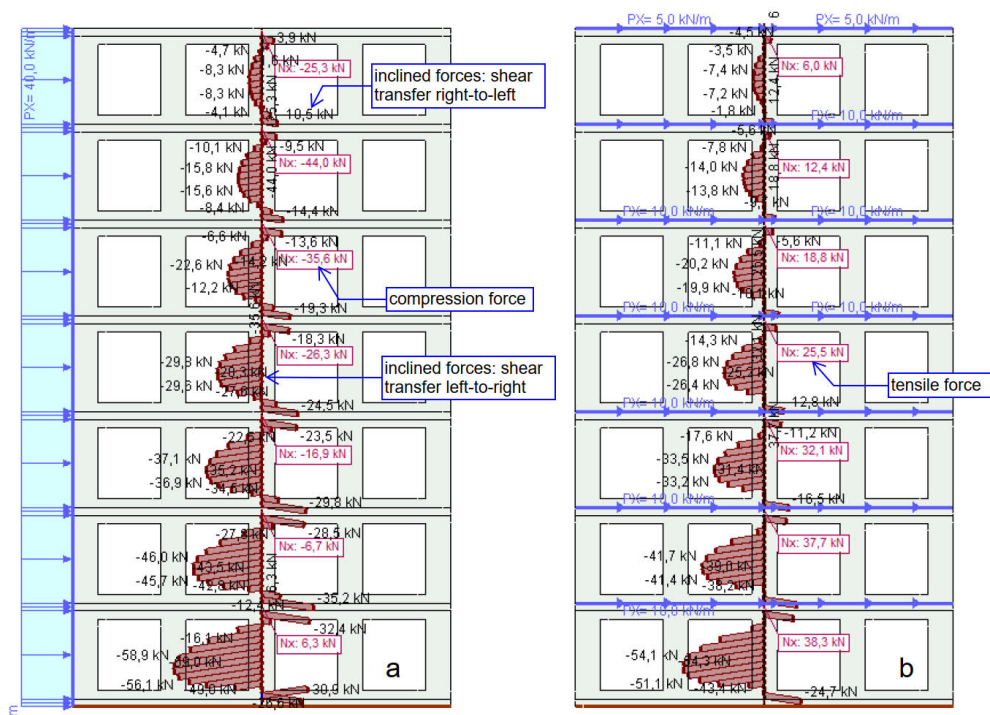
Figure 7.4: Connection behaviour of cantilever shear walls with lateral line load at the left side (a) and with a horizontal line loads along the slabs (b)
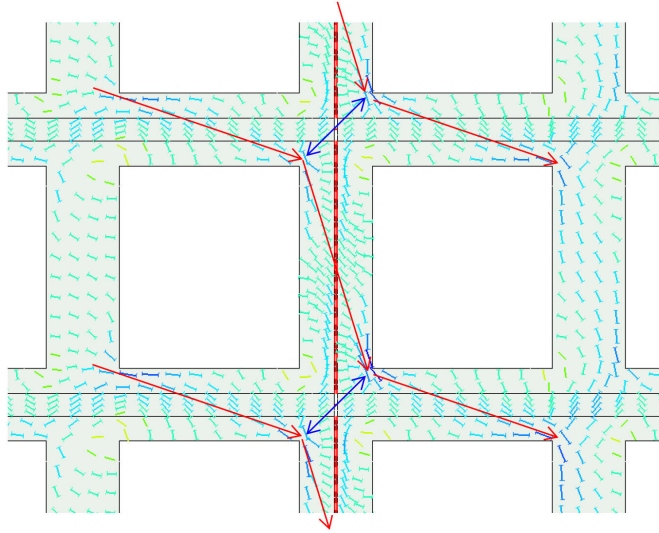
Figure 7.5: Compression struts as part of the internal force distribution in the
rigid frame of figure 7.4a

7.3.3 Transfer of lateral compression

An extra component must be added to the previously proposed compression strut model when it is applied as part of a complete interface model representing the Staggered shear key connection in e.g. cantilever shear walls. These are the horizontal truss elements (only compression) added every 200 mm according to figure 7.6. They are required for in the case the mortar filling is laterally compressed. They have to prevent that the inclined compression struts are unrealistically forced to transfer indirectly the lateral compression forces while they are passed directly through the mortar filling.
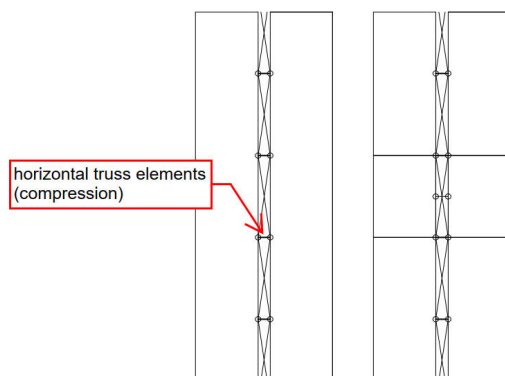
Figure 7.6: Modeling horizontal truss elements for the transfer of lateral compression forces in case they dominate the lateral dilation forces

7.4 Case studies with Staggered shear key connection

7.4.1 Cantilever shear wall

Figure 7.7a displays the previously discussed cantilever shear wall without window openings. How the Staggered shear key connection is composed in the seam between two precast concrete wall elements is shown in figure 7.8a. A 200 mm deep Staggered shear key connection within a wall thickness of 300 mm was chosen to make the connection covered inside the wall. This convered concept is explained in section 8.4. The covered appearance could be desirable for practical and aesthetic purposes. A deeper Staggered shear key connection with a higher shear capacity and a higher shear stiffness would fit into a 300 mm thick wall. However, with the selected depth of 200 mm, this case study considers the smallest version and the most conservative structural application.

Figure 7.8b shows how the shear keys and the slabs are modeled for this case study. The inclined compression struts have the same dimensions ($25x200 \text{ mm}^2$) as used earlier in this chapter. These inclined struts are also applied to the slabs. In this way, the absence of the transfer of shear forces via the slab has been dissolved. Again, this is a conservative approach because the slabs provide more shear capacity and shear stiffness than the applied inclined compression struts add. The horizontal connecting truss elements are modeled with a horizontal stiffness equal to what can be provided in tension by 2ø16 mm reinforcement bars embedded in a concrete slab. This amount of reinforcement is considered to be a minimum that is always present in slabs in practice. How the behaviour of the 2ø16 mm in the slabs is modeled with the horizontal strut element is explained in section F.3 of Appendix F. The numerical stiffness of the precast concrete wall membrane elements is set on 20.000 N/mm^2. Finally, both the horizontal and vertical stiffness of the line supports at the base of the cantilever shear wall are assumed to be 50.000 kN/m/m.
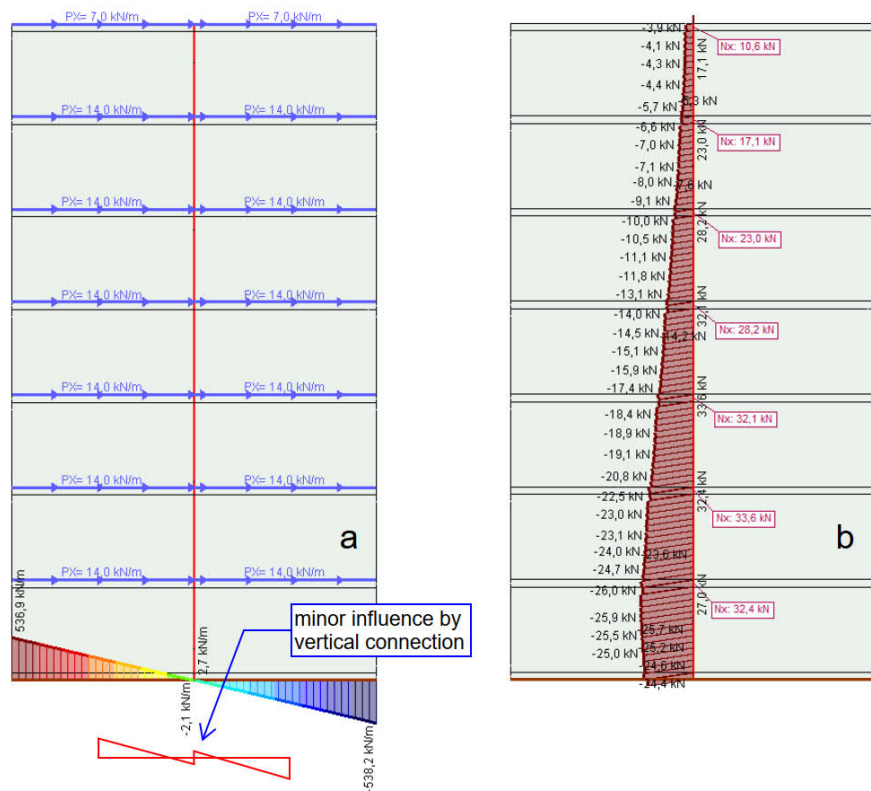
Figure 7.7: Case study cantilever shear wall with Staggered shear key connection: Lateral loads and vertical reaction forces (a) and an overview of shear forces and slab forces in SLS (b)

The lateral loads are set to a value that it results in a lateral deflection at the top of approximately $h_{csw}/500$ as shown in figure 7.9a. In this equation the term h_{csw} represents the height of the cantilever shear wall. This is the maximum permissible lateral deflection (21,6 m / 500 = 43,2 mm) prescribed in NEN-EN 1990 (1992) for the SLS of a building structure. As a result, the numerical model gives that the active forces in the inclined compression struts and the horizontal tensile trusses are the highest values that can arise in this shear wall because of the $h_{csw}/500$ limitation. The calculated inclined compression forces in the struts for the connection are displayed in figure 7.7b.

The Staggered shear key connection must have sufficient shear capacity V_{Rd} to transfer the active shear forces. It has to be noted that these forces have to be ULS forces. Since the lateral loads mostly have to be enlarged by a load factor of 1,5, the occurring ULS shear forces in the cantilever shear wall can be obtained by multiplying the SLS forces in figure 7.7b by 1,5. Then the largest SLS inclined compression force is 26,4 kN as displayed in the figure.

The shear force $V_{Ed;inclined}$ = 1,5 x 26,0 = 39,0 kN/shear key in the ULS. The (vertical) shear force V_{Ed} is slightly lower than the (inclined) force $V_{Ed;inclined}$ in the polygon of forces (diagonal:vertical = 202 mm:200 mm). This effect is neglected. The shear force $V_{Ed;inclined}$ is assumed to be equal to V_{Ed} = 39,0 kN/shear key (ULS). The shear capacity V_{Rd} must cover the shear force V_{Ed}. The shear capacity V_{Rd} can be calculated with the help of equation 6.9. This equation applies to a three keyed Staggered shear key connection. For a single keyed Staggered shear key connection this gives the equation[1]:

$$V_{Rd} \text{ [kN/shear key]} = \frac{1}{3}(524 - 138 \cdot \delta_{lateral}), \quad \delta_{lateral} < 2,0 \text{ mm} \qquad (7.1)$$
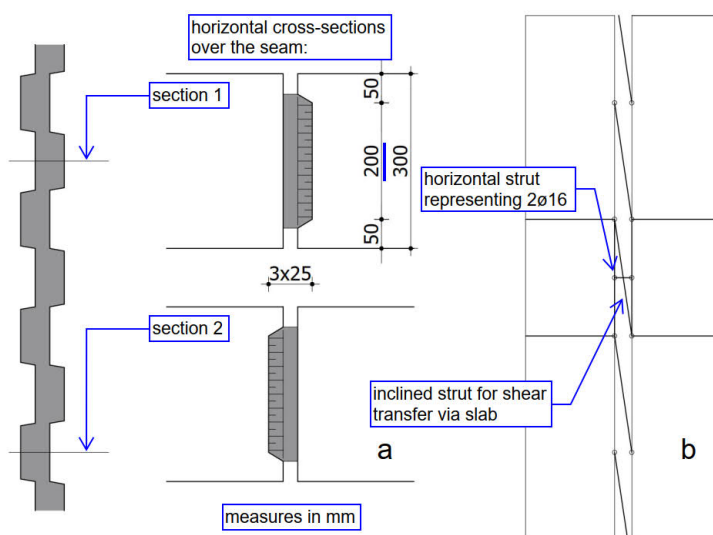
Figure 7.8: Lay-out of the Staggered shear key connection (a) and the way of modeling the slabs (b)

Figure 7.9a displays the lateral displacements for the Staggered shear key connection in the cantilever shear wall. The lateral displacements $\delta_{lateral}$ for the decisive shear force V_{Ed} is equal to the difference between the displacements at the right and the displacement at the left of the inclined compression strut, multiplied by 1,5 for verification in the ULS:

$$\delta_{lateral} = (7,2 - 6,9) \text{ x } 1,5 = 0,45 \text{ mm} < 2,0 \text{ mm}$$

For the shear capacity applies:

$$V_{Rd} = \tfrac{1}{3}(524 - 138 \cdot 0,45) = 154 \text{ kN/shear key}$$

[1]The equation applies to the used Tiksomortar K70 and concrete with strength grade C53/65.

By comparing the design shear capacity V_{Rd} to active shear force V_{Ed}, it can be concluded that only a quarter of the shear capacity is used for transferring the shear forces in this precast concrete cantilever shear wall. Apart from the shear forces, it has to be checked whether the tensile forces in the slabs can be taken by the 2ø16 mm reinforcement bars. The largest tensile force is 33,6 x 1,5 = 50,4 kN in the ULS (see figure 7.7b). The design capacity for a tensile force for the 2ø16 mm rebar is 2x 201 mm^2 x 435 N/mm^2 = 174 kN. This covers the active tensile forces.

A second point of concern is the effect of the shear stiffness of the Staggered shear key connection on the overall cantilever shear wall behaviour. It can be expected to have an effect on the force distribution and possibly result in an increase of the lateral displacements at the top. First, figure 7.7a displays the vertical forces at the base support of the shear wall. The kink in the usual linear distribution of vertical forces displays the influence of the reduced stiffness due to the connection when compared to a monolithic shear wall. The values for this kink are considered to be so small that they can be neglected. Also, the lateral displacements at the top of the precast concrete cantilever shear wall structure are compared with the monolithic concrete equivalent in order to investigate the influence of the connection shear stiffness on the lateral displacements of the shear wall (figure 7.9b). It can be observed from figure 7.9 that the lateral displacements of both shear walls are approximately equal to each other. Therefore, it can be concluded that, despite the reduced shear stiffness of the vertical connection, the lateral displacements have hardly increased and the force distribution have barely changed. For this cantilever shear wall, there is no significant difference in structural performance between this precast concrete version (with two stacks and one vertical connection) and a monolitic concrete version.
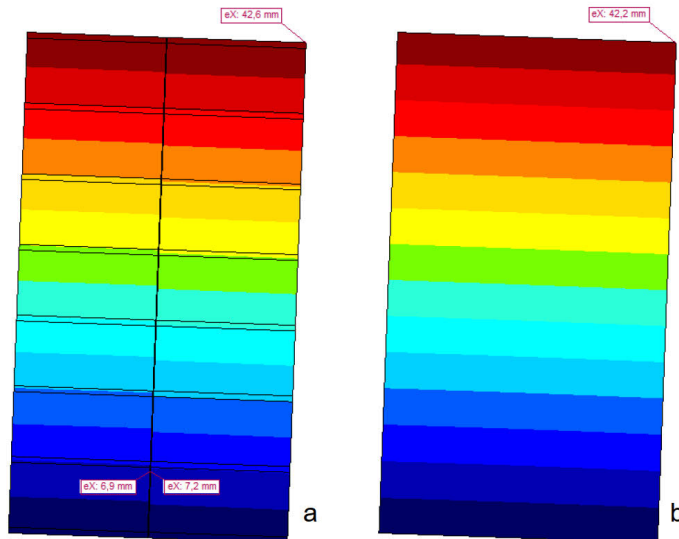
Figure 7.9: Lateral displacements of the Precast concrete cantilever shear wall (a) and the equivalent monolithic concrete cantilever shear wall (b)

7.4.2 Rigid frame

A similar analysis has been performed for the rigid frame version of the cantilever shear wall (see figure 7.10). The columns per storey at each side of the Staggered shear key connection can be considered as very small (400 mm wide at each side of the connection) and rather high (3,0 m). These columns are to be considered to have the minimum width for wall elements that can be made practically for such a rigid frame. The used numerical stiffness for the membrane elements representing these columns is $E_c = 9.000$ N/mm² assumed to represent cracked concrete beams and columns of a rigid framed structure.
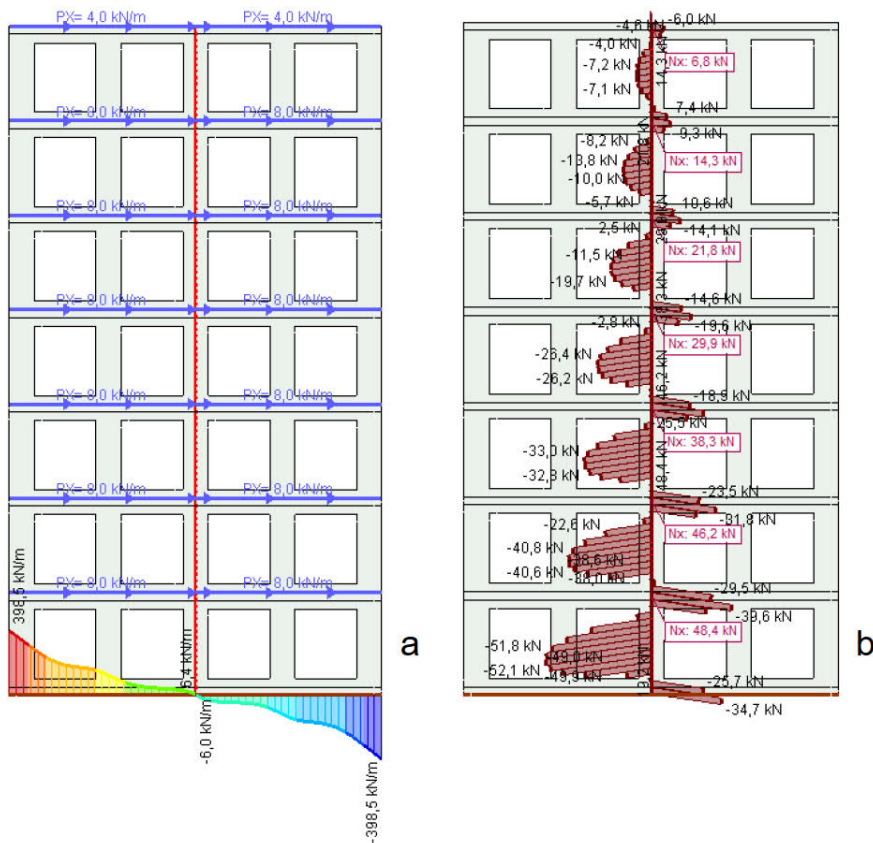
Figure 7.10: Case study cantilever shear wall with Staggered shear key connection: lateral loads and vertical reaction forces (a) and an overview of shear forces and slab forces (b)

The columns behave with a very low lateral stiffness k_h and because of that with significant lateral displacements $\delta_{lateral}$. Therefore, this rigid frame structure can be considered as one in which the Staggered shear key connection influences the overall force distribution and lateral displacements the most. Again, the lateral line loads

are set for the maximum permissible lateral displacements of $h_{csw}/500$ for getting the largest shear force V_{Ed}. The calculated inclined compression forces are displayed in figure 7.10b and the largest force equals V_{Ed} = 1,5 x 52 = 78 kN/shear key (ULS). The corresponding lateral displacement for this force is calculated to be $\delta_{lateral}$ = (5,6 - 4,5) x 1,5 = 1,65 mm < 2,0 mm in the ULS (figure 7.11). For the shear capacity applies:

$$V_{Rd} = \tfrac{1}{3}(524 - 138 \cdot 1,65) = 99 \text{ kN/shear key}$$

It turned out that the largest shear force V_{Ed} is 78% of the shear capacity V_{Rd} which means that the Staggered shear key connection is capable to transfer the largest shear forces in the framed precast concrete structure.

As a result of the lateral bending of the columns, a larger effect of the connection shear stiffness on the lateral displacements at the top of the rigid framed structure is expected. To verify that, figure 7.11 displays the lateral displacements at the top. The precast concrete structure displaces in lateral direction 44,6 mm compared to 41,6 mm for the monolithic concrete rigid frame. This is an increase of 7,2%. How the increase of the lateral displacements at the top of the framed structure should be interpreted, is discussed in next subsection. Finally, it can be noted that according to figure 7.10a no significant change in the distribution of the vertical reaction forces has arisen and the highest horizontal force representing the tyings in the slabs (1,5 x 49 kN = 73,5 kN in ULS) does not exceed the tensile capacity of the 2ø16 mm reinforcement bars (174 kN).

Figure 7.11: Lateral displacements of the Precast concrete rigid frame (a) and the equivalent monolithic concrete rigid frame (b)

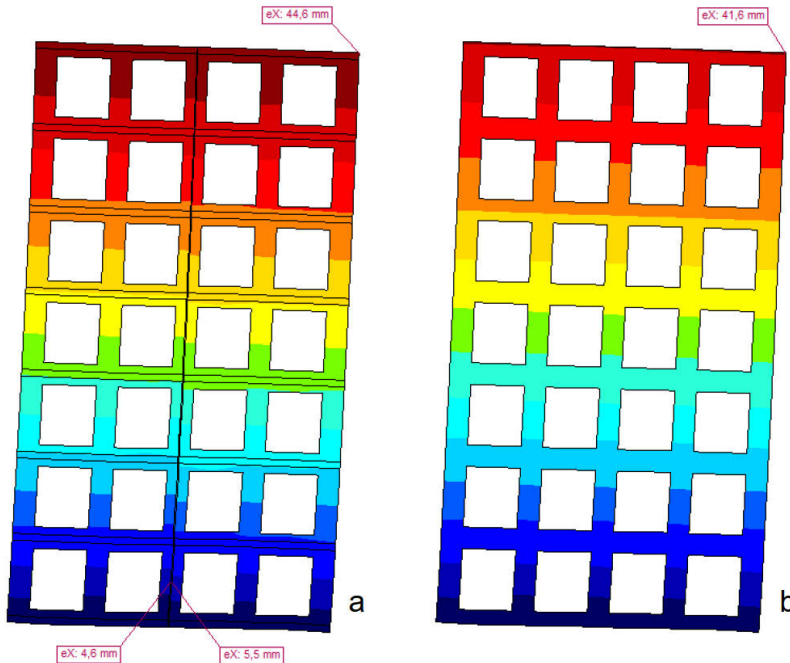### 7.4.3 Effect of the cantilever shear wall slenderness

To determine the effect of the vertical Staggered shear key connection on the lateral displacements of precast concrete shear wall structures, the two case studies presented in previous subsections have been selected. Less influence was expected for the case study with solid wall panels. Due to the slender columns near the vertical connection in the variant with openings, the influence would be greater. The increase turned out to be 7,2% for this version. Although it seems that this variant represents the most unfavorable application, it cannot be assumed that this is true. In another shear wall design, the reduced shear stiffness caused by the vertical connection could have a greater influence on the increased lateral displacements at the top. To determine the effect for such other shear wall designs, the findings of a study conducted by Van Keulen and Vambersky (2013) are used. It is a study into the effects that various connections, element lay-outs and the slenderness of the cantilever shear wall have on the increase in lateral deformations. By using this, it can be determined if more than the 7,2% increase could be expected for other rigid framed shear wall structures with the Staggered shear key connection.

According to Van Keulen and Vambersky (2013), the slenderness of a cantilever shear wall is the decisive design variable that determines how much the lateral deformations at the top are affected by the connections. The reason will be explained. These lateral deformations are the sum of bending and shear deformations. The shear stiffness of a vertical connection influences only the shear deformations. The contribution of the shear deformations to the total deformations decrease when the cantilever shear wall has a more slender shape. As a result, very slender structures deform in lateral direction almost only due to bending deformations while shear deformations are dominant in compact structures. From this it can be expected that the Staggered shear key connection affects less the increase of lateral displacements of a more slender version of the rigid frame. In that case the increase would be less than 7,2%. This is verified by adding five stories to the rigid frame model of figure 7.12a for evaluating a more slender version. Again, the lateral displacements at the top are forced to be approximatelly $h_{csw}/500 = 73,6$ mm as can be observed in figure 7.12b. The increase of lateral displacements at the top turned out to be 5,1%. This lower increase contradicts the possible intuition that due to the application of the connection the influence on the lateral displacements at the top of a cantilever shear wall is larger for a taller wall. However, this is not true because of the lower contribution of the shear deformations to the total deformations. The lower lateral increase of the lateral deformations at the top proves that the Staggered shear key connection has less effect than what was found for the previously analysed rigid frame structure.

The slender model provides shear forces V_{Ed} with smaller values than observed for the previously analysed framed structure. This is because the lateral displacement $h_{csw}/500$ is found with a lower total lateral load and that causes the lower shear forces. It makes clear that the shear forces in the Staggered shear key connections in taller shear walls are not larger, which may also be different than expected.

Figure 7.12: Results for very slender variant of rigid framed structure for the precast concrete version (a-b) and the monolitic version (c)

The effect that the Staggered shear key connection has in a more compact version of the firstly investigated framed structure is determined as well. This version (figure 7.13) was obtained by removing three stories and adding four vertically stacked wall elements next to it. This structure is loaded till the lateral displacement of approximated $h_{csw}/500 = 12,5$ m $/ 500 = 25$ mm. The model approximates larger shear forces $V_{Ed} = 1,5 \times 70$ kN $= 105$ kN/shear key (ULS) together with a lateral displacement of $\delta_{lateral} = 0,9$ mm x $1,5 = 1,35 < 2,0$ mm (ULS). This shear force does not exceed the shear capacity of $V_{Rd} = 112$ kN. The increase of lateral displacement at the top turned out to be 15,4%. This indicates a significant larger influence of the Staggered shear key connection on the lateral rigid frame displacements. It has to be noted that the absolute deformations of the more compact structures are usually very small and therefore less decisive than for slender structures.
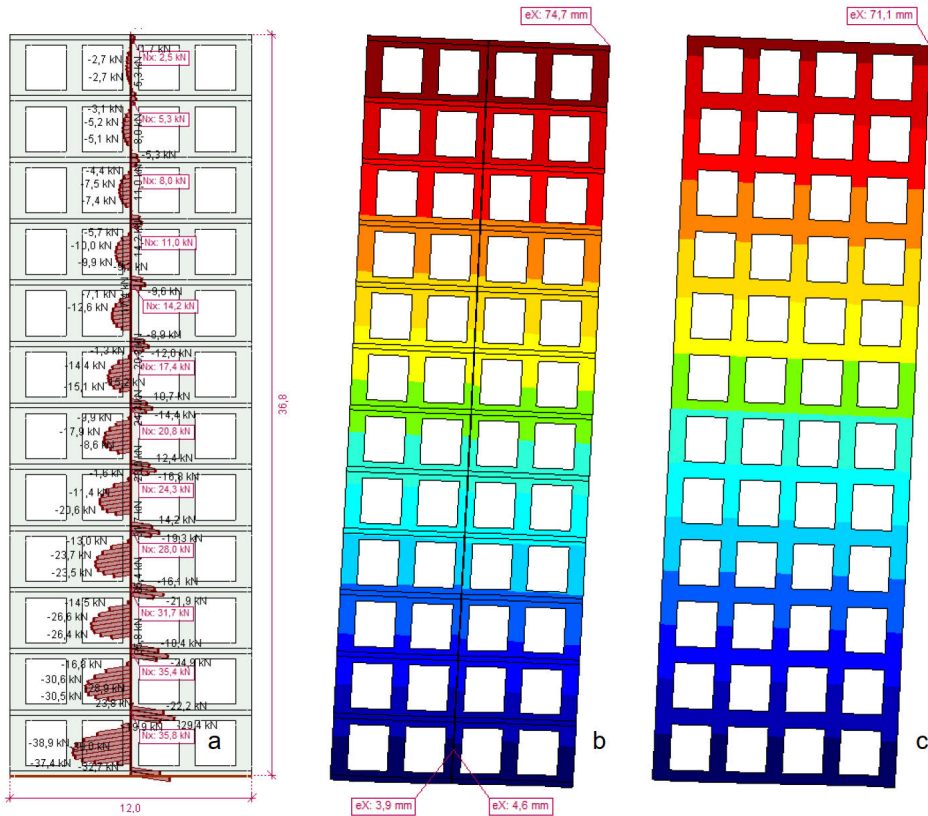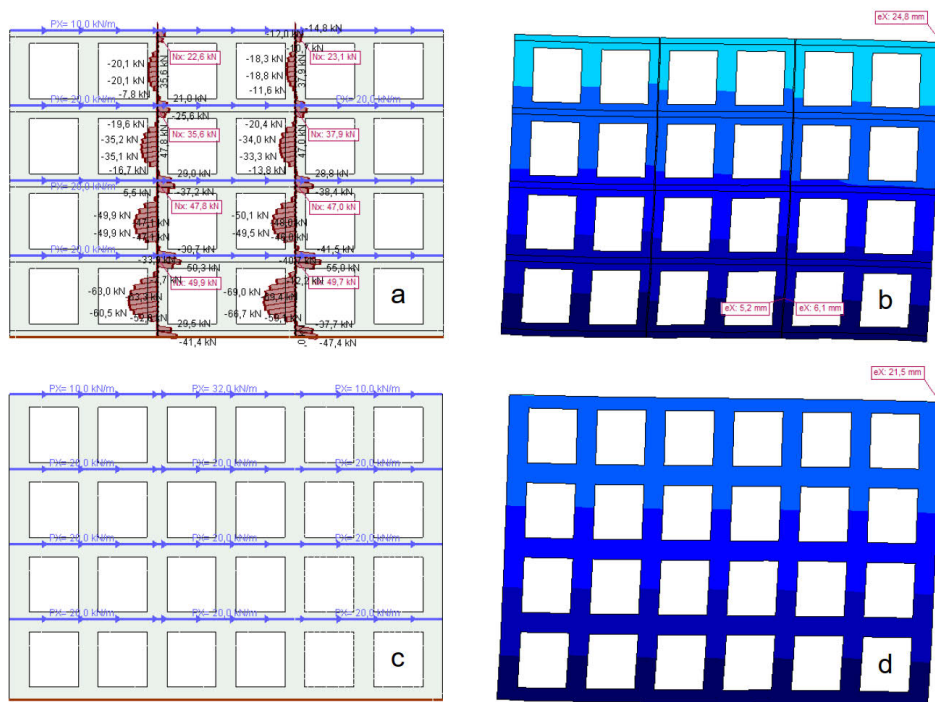
Figure 7.13: Results for compact variant of rigid framed structure for the precast
concrete version (a-b) and the monolitic version (c-d)

7.5   Conclusions

The storey-high application of the Staggered shear key connection as part of precast concrete cantilever shear walls is investigated in this chapter. The shear transfer mechanisms at the location of the slabs and the over the height of the precast concrete wall elements has been studied. The behaviour of the Staggered shear key connection is modeled with inclined compression struts. Horizontal tyings in the slabs are added for balancing the lateral dilation forces. The diagonal compresion struts represent the vertical connection shear behaviour.

   The massive wall elements without openings have a high stiffness against lateral displacements, resulting in an almost uniformly distributed transfer of shear forces over the height of the wall elements. It was expected that lateral forces have to be balanced by the horizontal tyings (tensile reinforcement) in the slabs. It turned out that the way the structure is loaded determines whether the tyings are loaded in tension. In case the lateral line load is applied only to the left side of the cantilever shear wall, the horizontal forces at the location of the slabs are still compression forces. The lateral dilation forces only lowered the compression forces. The alternative with lateral loads along the slabs represents a more realistic way of the loading of the cantilever

shear walls in practice. For this load, the numerical model resulted in tensile forces in the tyings (reinforcement in the slab) due to the dilation in de shear connection.

Window openings are added to the same cantilever shear wall in that case functioning as a rigid frame structure. Again, the functioning of the Staggered shear key connection is analysed. It demonstrates that the forces to be transferred via the storey-high vertical connection are dominated by the main compression forces that flow through the entire rigid framed structure. They cause the largest diagonal forces to arise half way the columns of the wall openings. Also, the diagonal forces reverse at the location of the slabs because of the equilibrium requirements for the leading force distribution inside the rigid framed structure.

Case studies with the Staggered shear key connection for the cantilever shear wall without and with openings are performed. The cross-sectional area and material stiffness of the inclined compression struts are taken from the physical smallest possible version of the mortar filling in order to verify its most conservative application in the cantilever shear walls. Also, the lateral stiffness provided by the tying reinforcement is taken rather low by modeling only 2ø16 mm reinforcement bars. The shear capacities are verified and the influence of the connection shear stiffness on the lateral displacements at the top of cantilever shear walls is considered. First, this is performed for the cantilever shear walls with seven floors. It turns out that for the conservative applications of the Staggered shear key connection, the active shear forces remain well below the available shear capacities. Furthermore, an increase of the lateral displacements at the top of the cantilever shear walls caused by the connection shear stiffness is expected. This effect is only found for the structure with wall openings. The increase of lateral displacements at the top turns out to be 7,2% only for the rigid framed version.

The research conducted by Van Keulen and Vambersky (2013) demonstrated that the slenderness of the precast concrete design dominates the influence of the connection shear stiffness on the lateral displacements at the top. In order to verify if the active shear forces and lateral displacements at the top can change significantly, the behaviour of a more slender and a more compact version of the rigid framed cantilever shear wall are analysed. It turns out that the active shear forces and the increase of lateral displacements at the top are lower for the more slender structure. The opposite is found for the compact version. The active shear forces in the Staggered shear key connection increase, but remain below its shear capacity. The lateral displacements of the compact structure increase with 15,4% indicating a significant larger influence. However, the absolute deformations are rather low and therefore, this increase does not block the application of the Staggered shear key connection in a compact precast concrete shear wall structure.

The investigation in this chapter demonstrates in detail how the Staggered shear key connection in a storey-high application with tyings in the slabs for cantilever shear walls behaves. Furthermore, from the case studies, it shows that its influence on the lateral displacements at the top is very limited.

Chapter 8

Retrospective View and Outlook

8.1 Overview of the research

The thixotropic properties of contemporary mortars allow the insertion of mortar in vertical seams by using a mortar pump without the need for traditional formwork. In such a seam, an easy to execute narrow vertical mortar connection for the transfer of shear forces can be created by simply adding a profile and possibly a roughening to the mortar-to-concrete interfaces. In this way a buildable and efficient continous vertical shear connection can be constructed, but can it also be taken into account as a structural connection for shear transfer in e.g. cantilever shear walls? Due to the absence of horizontal reinforcement like hairpins distributed over the height of the wall elements, the resistance against lateral dilation forces that result from the shear transfer, have to be taken by the concentrated tying reinforcement in the slabs. One of the things missing is an evaluation of the shear stiffness and the shear capacity of such a vertical connection. Therefore, the main objective of this research is to develop and model narrow vertical mortar connections that perform optimally for the transfer of shear forces in precast concrete shear wall structures with tying reinforcement in the slabs. They should transfer considerable shear forces in a reliable way and should behave with high shear stiffnesses. At the same time, the connections should preferably cause low dilation forces and should take full advantage of the lateral stiffnesses.

A literature review (chapter 2) is carried out to determine topics that are relevant for investigating the shear behaviour of profiled mortar connections. The results of earlier performed research are examined. This results in an overview of information on contemporary mortars, designs of profiled mortar connections, shear transfer mechanisms, variables that influence the connection behaviour, ways of modeling and the prediction of shear capacities. The next step is the development of mortar connections with five distinctive versions for the mortar-to-concrete interfaces (chapter 3). External actions provided by the surrounding precast concrete structure (e.g. lateral stiffness) that interfere with the connection behaviour are taken as

research variables. The effects that these variables have on the shear behaviour of the five mortar connections are investigated with the help of 33 physical shear tests (chapter 4). For performing these experiments, 600 mm high mortar connections are constructed in specimens from which during shear tests till failure the loads, forces and displacements are registred. The test results are reported and explained (chapter 5). The understanding of the shear behaviour of the connection requires a closer analyses of the test results (chapter 6). From these analyses, a compression strut modeling approach is proposed and applied to the Staggered shear key connection. This modeling method simulates the vertical and lateral displacements for a given shear force in the three-keyed specimen. The next step is to investigate the shear behaviour of the connection in the storey-high application of shear walls with and without window openings (chapter 7). The functioning of the compression strut modeling method is identified and tested for application in case studies.

8.2   Development of the mortar connections

The first objective of the research is to develop usable vertical shear connections for vertical seams. In a search the five mortar connections explained below are compiled for examination.

1. Because the **Aligned shear key connection** is usually applied in precast concrete shear wall structures, it is an obvious choice to adopt its concept for the first profiled mortar connection.

2. The same sized indentations of the previous connection are vertically shifted for creating the **Staggered shear key connection**. In this variant a slightly steeper inclined compression strut can develop and therefore it has possibly the potential to perform even better for the transfer of shear forces.

3. The **Aligned small shear key connection** is proposed for investigating the effect of more shear keys over the same 600 mm height. The 12 instead of 3 inclined compression struts could possibly provide more shear capacity. Also, the increased amount of contact surface between concrete and mortar could delay the instant of debonding in the interfaces.

4. It is known from previous research that a rough old-to-new concrete interface created by waterjetting provides a significant shear capacity and shear stiffness. To investigate the effect of an application with mortar instead of concrete, the **Plain waterjetted shear connection** is selected for examination.

5. The **Serrated waterjetted shear connection** is a combination of the rough waterjetted interface and a serration as a profile. This connection lay-out could possibly provide a high shear capacity and significant shear stiffness.

8.3   Conclusions

The shear test results show that the Aligned small shear key connection behaves with a lower secant shear stiffness compared to the other investigated connections. The Plain waterjetted shear connection transfers the shear forces while behaving with a significant high shear stiffness. However, possible unforeseen small lateral displacements by the surrouding precast concrete structure can easily cause debonding of the plain interfaces (brittle failure) which makes it questionable if this high shear stiffness can be maintained. Based on these observations it is concluded that both connections (Aligned small shear key connection and Plain waterjetted shear connection) are less suitable for application as vertical mortar connection. The remaining profiled mortar connections provide higher and more or less comparable secant shear stiffnesses which makes them equally suitable as vertical shear connection.

The analysis of the test results also reveals that the Staggered shear key connection and the Serrated waterjetted shear connection transfer the highest ultimate shear forces. This is true for the latter connection under the condition that the failure crack runs through the mortar filling and not only through the mortar-to-concrete interface. That the failure crack runs through the mortar filling cannot be guaranteed. This makes this connection less suitable as vertical mortar connection in shear walls. From these observations it can be concluded that the Staggered shear key connection is the best performing vertical mortar connection. It behaves with a significant high secant shear stiffness and provides the highest reproducable ultimate shear capacity with the least dependency on the lateral stiffness and lateral compression. It is determined that this performance is attributable to the functioning of the diagonal resultant force that develops steeper inside the mortar filling of this connection than in the mortar filling of the other profiled connections.

Either the Tiksomortar K70 or the Steel Fibre Reinforced Mortar (SFRM) can be applied as mortar filling. The investigation shows that for the Staggered shear key connection the SFRM causes the cracks to appear in the precast concrete L-elements instead of in the mortar filling. However, it does not lead to a significant improvement of the shear capacity or shear stiffness. Also, the pumping of SFRM via a hose requires additional handling and material that is not paid off. As a result the Tiksomortar K70 can be seen to be advantegeous for this application compared to the SFRM.

The shear behaviour of the Staggered shear key connection is simulated with a numerical modeling model. It turned out that the previously mentioned diagonal resultant force determines the stresses and displacements inside the Staggered shear key connection. The use of a diagonal bar model for simulating its behaviour is proposed. By schematizing such bars between two wall elements, a modeling method for the representation of the Staggered shear key connection in a precast concrete structure is created. This method is called the "inclined compression strut model" and its functioning is proven to be suitable via calibration on the shear test results. The compression struts are modeled with 1D truss elements. The inclination of the

truss element is based on the shape of the connection with a height of 200 mm and a width of 30 mm. For modeling the struts based on the dimensions of the connection a cross-sectional area of 25x200 mm^2 is used. To take into account the non-uniform stress distributions in the real mortar filling the linear behaviour (compression only) of the struts are set to a Young's modulus[1] of 9.000 N/mm^2.

The compression forces that arise in the inclined truss elements may not exceed the values that represent the shear capacity of the Staggered shear key connection. The analysis of the shear tests results shows that the shear capacity depends on the occurring lateral displacement $\delta_{lateral}$. In this thesis an equation[1] for predicting this shear capacity including the dependency on the lateral displacement is proposed. The design value of the shear capacity V_{Rd} for one shear key can be calculated with equation 8.1. So, in a structural analysis of a shear connection there is an interaction between the results of the analysis in terms of the lateral displacement $\delta_{lateral}$ [mm] and the capacity of the connection.

$$V_{Rd} \ [\text{kN/shear key}] = \frac{1}{3}(524 - 138 \cdot \delta_{lateral}), \ \ \delta_{lateral} < 2{,}0 \ \text{mm} \qquad (8.1)$$

The inclined compression strut model and the equation for prediction of the shear capacity apply to the three-keyed Staggered shear key connection. If they can be adopted for a storey-high version of this connection (which is defined as extrapolation step in this thesis) is investigated. The detailed analysis of the tests on the connection show that horizontal cracks separate the individual shear keys at rather low shear forces. As a result, it is found that most probably a minor structural interaction between the shear keys exists in reality. This allows that the Staggered shear key connection can be considered as a set of individually functioning compression struts irrespective of the number of shear keys that are placed in a row. It demonstrates the inclined compression strut model and the equation for prediction of the shear capacity can be used for a storey-high application of the Staggered shear key connection.

The case studies show that the storey-high Staggered shear key connection functions excellently when applied in cantilever shear walls. This holds true for shear walls with and without window openings. Despite the influence of the connection behaviour they demonstrate that for such commonly applied real precast concrete structures there are negligibly small differences in the force distributions and displacements compared to the monolitic concrete version of the same structure. The lateral displacements at the top only increase slightly in exceptional cases of cantilever shear wall designs and lateral loads. The shear capacity proved to be more than sufficient and the force distributions in the precast concrete wall elements hardly changed. As a result the application of the connection in a shear wall does not affect the required amount of reinforcement in it.

---

[1]The Youngs modulus and the equation apply to the used Tiksomortar K70 and concrete with strength grade C53/65.

8.4   Outlook for application in practice

By the research in this thesis for the storey-high Staggered shear key connection it
has been proven that it is a reliable shear connection for application in practice. Fig-
ure 8.1 displays the most obvious implementation of this connection in the concept
with tying reinforcement in the slabs.
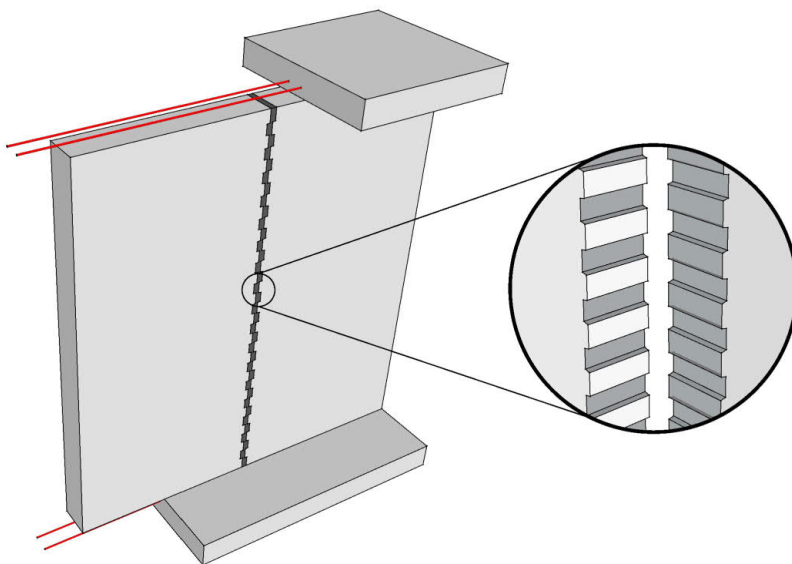
Figure 8.1: Drawing of the storey-high Staggered shear key connection with
concentrated tying in the slabs

For easthetic purposes, it may be preferable to avoid the visability of the connec-
tion plofiles at the wall element surface. If this is the case, figure 8.2 shows a variant
with the shear keys inside the vertical seam. It may be obvious that this version
provides a little less shear stiffness and shear capacity than the previous one. Since
the case studies showed the effect of the connection on the overall behaviour of the
cantilever shear wall is negligible, the covered version, as it can be named, provides
most likely a sufficient shear stiffness and shear capacity in many cases.
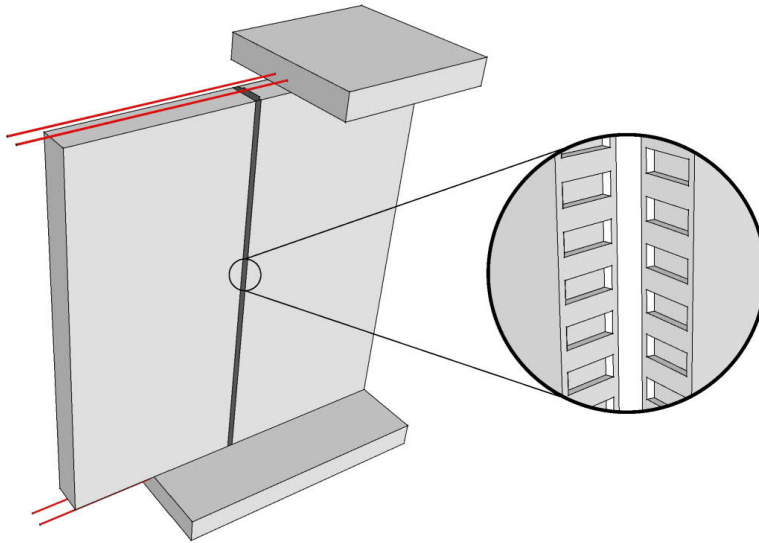
Figure 8.2: Drawing of the covered storey-high Staggered shear key connection
inside the vertical seam

The benefits of applying the vertical mortar connection in a cantilever shear wall can be explained with the help of figure 8.3. In figure 8.3a a version of a shear wall that is constructed in a real building is shown. The cooperation between the individual precast concrete wall elements is arranged with an interlocking lay-out of the wall elements. The vertical seams are considered structurally to be open seams, although they are filled with mortar for wall sealing purposes. The version with the Staggered shear key connection and tying reinforcement in the slabs is displayed in figure 8.3b. With the vertical mortar filling the seam functions structurally as vertical shear connection, while the sealing function is filled in in the same time. Both designs can be mutually compared. The first comparison applies to the repetition grade which influences the costs for element production. The design in figure 8.3a has 10 types of unique wall elements while design b requires 6 types. Furthermore, the second design (b) requires less projecting bars for assembling the same cantilever shear wall. It can be assessed that the version with the vertical mortar connection is the most economical version. Apart from the economical aspects, the second design provides a less complex design that is always preferred.

Figure 8.3: Precast concrete cantilever shear wall designs with traditional interlocking element lay-out (a) and a version with a vertical mortar connection (b)

The next example is the T-connection displayed in figure 8.4. It shows a storey-high vertical Staggered shear key connection between a structural façade wall element and an inner wall element that is perpendicularly to the façade positioned. The lateral dilation forces caused by the profiled mortar connection are balanced by hairpins in the slabs. These hairpins are installed around the vertical protruding bars for joining the "façade column" to the tying reinforcement. Nowadays, for this T-section example, the corbel connection from the inner wall into the façade column is frequently applied in precast concrete design. For many reasons, a disadvantage of this connection is that the façade columns must be constructed with resesses. Compared to this traditional corbel connection, the Staggered shear connection has the important advantage that the façade column can remain without the disturbing recess of a corbel.

Apart from the T-section, wall connections with a L-section shape are often present in buildings. The same design principles with hairpins and protruding bars discussed for the T-section connection apply to a L-shaped shear connection. It is envisioned that more applications where, based on the research in this thesis, the precast concrete industry can take advantage of the benefits of narrow vertical mortar connections.
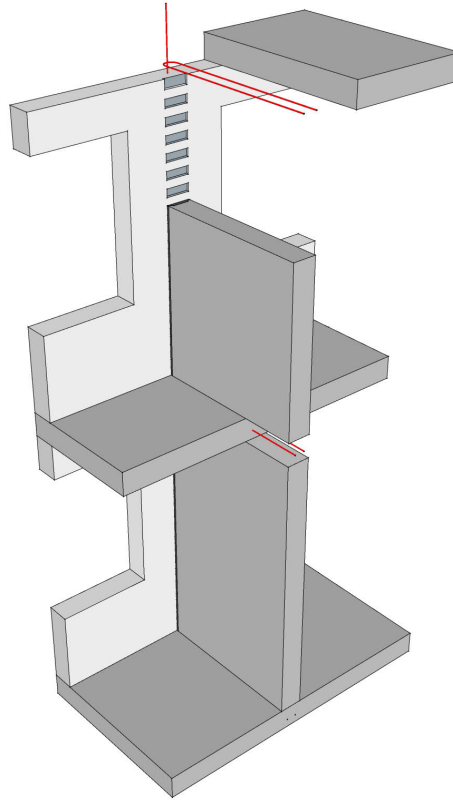

Figure 8.4: Application of the storey-high Staggered shear key connection in the version of a T-connection with hairpins in the slabs.

Bibliography

Abdul-Wahab, H. (1986). An experimental investigation of vertical castellated joints between large concrete panels. *The structural engineer*, 64B(4):93–99. 6, 33, 36, 37

Abdul-Wahab, H. (1992). Strength of vertical joints with steel fiber reinforced concrete in large panel structures. *ACI Structural Journal*, 89(4):367–374. 6, 26, 33, 41, 42, 64

Abdul-Wahab, H. and Sarsam, S. (1988). Strength of vertical plane joints between large, precast concrete panels. *The structural engineer*, 66(14):211–215. 24

Backler, A., Baylik, M., and Dill, M. (1973). Local behaviour of shear transfer and compression transfer joints, report 45: The behaviour of large panel structures. *Construction Industry Research and Information Association*. 6, 33

Beck, H., Mehlhorn, G., Stauder, W., and Schwing, H. (1973). Zusammenwirken von einzelnen fertigteilen als grossflachige scheibe. *Deutscher Ausschuss fur Stahlbeton, Inst. f. Massivbau, Techn. Hochschule Darmstad*, 224. 27

Bhatt, P. and Nelson, H. (1970). Strength and deformation of castellated vertical joints in shear walls. *Institute of structural engineering, University of Sheffield*. 6, 26, 33, 43

Birkeland, P. and Birkeland, H. (1966). Connections in precast concrete constructions. *Journal of the American Concrete Institute, ACI Proceedings*, 63(3):345–368. 19, 20

Chakrabarti, S., Nayak, G., and Paul, D. (1988). Shear characteristics of cast-in-place vertical joints in story-high precast wall assembly. *ACI Structural Journal*, (85-S4):30–45. 6, 33, 37, 39

Chatveera, B. and Nimityoungskul, P. (1994). Vertical shear strength of joints in prefabrprefab loadbearing walls. *Journal of the national research counsil of Thailand*, (26(1)):11–36. 6, 33, 39

Cholewicki, A. (1971). Loadbearing capacity and deformability of vertical joints in structural walls of large panel buildings. *Building Science*, 6:163–183. 6, 24, 26, 30, 32, 33, 39, 43, 44

Cugla (2015). Product sheet cuglacrete hechtprimer polymeer. Technical report. 66

Cugla (2016). Product sheet cuglaton tikso k70 mortar. Technical report. 63

CUR aanbeveling 24 (1991). Krimparme cementgebonden mortels. 14, 63, 67, 84, 88

Elliott, K. (2011). *Precast concrete structures*. Butterworth-Heinemann. 24, 27, 58

Engstrom, B. (1992). Ductility of tie connections in precast structures. *Chalmers University of Technology, Division of Concrete Structures, Publication 92:1, Goteborg.* 253

Eriksson, A., Karrholm, G., and Petersson, H. (1978). Ductile shear key joints in large panel structures. *Proceedings of the RILEM-CEB-CIB symposium mechanical & insulating properties of joints of precast reinforced concrete elements*, 1. 6, 31, 33, 35, 36

Espeche, A. and Leon, J. (2010). Estimation of bond strength envelopes for old-to-new concrete interfaces based on a cylinder splitting test. *Construction and Building Materials*, (25 (2011)):1222–1235. 28

Fauchart, J. and Cortini, P. (1972). Etude exprimentale de joints horizontaux entre panneaux prfabriqus pour murs de batiments. *Anales de l'Institut Technique du Batiment et des Travaux Publics.* 6, 33

fib bulletin 43 (2008). *Structural connections for precast concrete buildings, Guide to good practice, fib bulletin 43*. International Federation for Structural Concrete (fib). 24, 253, 254

fib bulletin 74 (2014). *Planning and design handbook, Manual - textbook, fib bulletin 74*. International Federation for Structural Concrete (fib). 8, 24, 44

fib Model Code 2010 (2013). *Model Code 2010*. International Federation for Structural Concrete (fib). 5, 6, 18, 23, 25, 137

Hansen and Olesen (1976). Results of danish shear tests on vertical wall joints, part 3 in "keyed shear joints". *Building Research and Practice, SBI-Report 97.* 6, 24, 27, 30, 33, 39, 45, 46, 47, 48, 49, 50, 54

Hansen, H. (1967). Mortar joints between concrete elements in shear walls. *Norges Byggforskningsinstitut, rapport 53.* 6, 33, 40, 41, 43

Hansen, K. (1974). Short description of shear tests on vertical joints. *Building Research and Practice, SBI-Report 97*, pages 20–33. 33, 34

Hansen, K., Kavyrchine, M., Melhorn, G., Olesen, S., Pume, D., and Schwing, H. (1974). Design of vertical keyed shear joints in large panel buildings. *Building Research and Practice, SBI-Report 97*, pages 5–19. 31, 39

Henry (2018). Dundeq system concrete surface profiles, tech-talk bulletin henry building envelope systems. Technical report. 19

Hobson, D. (2014). Fibre reinforced profiled mortar joints for precast concrete structures. Master's thesis, TU Delft. 64, 84

Hordijk, D., Bennenk, H., and Boer, S. d. (2005). Invloed opruwmethode op schuif-sterkte in aansluitvlakken. (3):72–76. 17

ICRI Technical Guideline (2013). Selecting and specifying concrete surface preparation for sealers, coatings, polymer overlays, and concrete repair. Technical Report No. 310.2R-2013, International Concrete Repair Institute. 18

Mattock, A. and Hawkins, N. (1972). Shear transfer in reinforced concrete - recent research. *Journal of the prestressed concrete institute*, 17(2):55–75. 6

Mehlhorn, G. and Schwing, H. (1977). Tragverhalten von aus fertigteilen zusam-mengesetzten scheiben. Technical report, Institut fur Massivbau, Technische Hochschule Darmstadt. 24, 27, 44, 45

Mehlhorn, G., Schwing, H., and Berg, K. (1977). Versuche zur schaubtragfahigkeit verzahnter fugen. Technical report, Institut fur Massivbau, Technische Hochschule Darmstadt. 6, 33

Menegotto, M. and Monti, G. (2005). Waved joint for seismic-resistant precast floor diaphragms. *Journal of structural engineering*, 131(10):1515–1525. 27

NEN-EN 12390-3 (2009). Testing hardened concrete - part 3: Compressive strength of test specimens. 84, 88

NEN-EN 12390-6 (2009). Testing hardened concrete - part 6: Tensile splitting strength of test specimens. 84, 88

NEN-EN 1990 (1992). Eurocode 1: Basis of structural design. 163, 180

NEN-EN 1992-1-1 (1992). Eurocode 2: Design of concrete structures - part 1-1: General rules and rules for buildings. 5, 6, 67, 84

Neppelenbroek, B. (2004). De voegmortel: onbekend maakt....... toch bemind! *Cement*, (6):44–47. 14

Olesen, S. (1975). Effects of vertical keyed shear joints on the design of reinforced concrete shear walls. *ACI, special publication*. 24

Randl, N. (2013). Design recommendations for interface shear transfer in fib model code 2010. *Structural concrete*, 14(3):230–241. 6, 17, 18, 20, 21, 22, 23

Rizkalla, S., Serette, R., Scott Heuvel, J., and Attiogbe, E. (1989). Multiple shear key connections for precast shear wall panels. *PCI Journal*, 34(2). 7, 28, 29, 31, 37, 38, 39, 40, 43, 54

Santos, P. and Julio, E. (2012). A state-of-the-art review on shear-friction. *Engineering Structures*, 45:435–448. 17

Santos, P. and Julio, E. (2013). A state-of-the-art review on roughness quantification methods for concrete surfaces. *Construction and Building Materials*, 38:912–923. 18

Santos, P. and Julio, E. (2014). Interface shear transfer on composite concrete members. *ACI Structural Journal*, pages 113–121. 20

Steinle, A., Bachman, H., and Tillmann, M. (2019). *Precast concrete structures*. Ernst & Sohn. 8, 24, 44

Straman, J. (1988). Geprefabriceerde stabiliteitsconstructies. Technical report, TU Delft. 33

Van, R. (2019). Application of vertical profiled mortar connections in precast concrete shear walls. Master's thesis, TU Delft. 32, 134

Van Keulen, D. (2013). Prefab betonverbindbeton met hoogwaardige mortelvoegen, beproeving en analyse van het afschuifgedrag, deel 1:inventariserende proeven fase 1. Technical report, TU Delft. 67, 68, 87, 212

Van Keulen, D. (2014). Prefab betonverbindbeton met hoogwaardige mortelvoegen, beproeving en analyse van het afschuifgedrag, deel 2: Proefresultaten fase 2. Technical report, TU Delft. 67, 87, 212

Van Keulen, D. (2015). Prefab betonverbindbeton met hoogwaardige mortelvoegen, beproeving en analyse van het afschuifgedrag, deel 3: Eindrapportage. Technical report, TU Delft. 67, 87, 212

Van Keulen, D. and Vambersky, J. (2013). Design and displacements of precast concrete shear wall structures. *Proceedings fib symposium Tel Aviv*. 185, 188

Winkler, P. (2014). Selecting and specifying concrete surface preparation for sealers, coatings, polymer overlays, and concrete repair. *Concrete Repair Bulletin*. 19

Zilch, K. and Reinecke, R. (2000). Capacity of shear joints between high-strength precast elements and normal-strength cast-in-place decks. *Proceedings fib International symposium on high performance concrete*. 20, 22, 23

List of symbols

Roman Upper Case

A	total cross-sectional area
A_c	cross-sectional area of the compression strut
B	width of the seam
D	height of the shear key
E_s	Young's modulus of steel
E_c	Young's modulus of concrete
F_d	reinforcement of deck joint
F_v	reinforcement of wall joint
$F_{friction}$	friction force
F_{strut}	compression strut force
$F\sigma_n$	lateral force in one horizontal external steel bar
$F\sigma_{n;A}$	lateral force in one horizontal external steel bars before starting the test
$F\sigma_{n;sum}$	summed lateral force of the four external steel bars
G	dead weight
H	horizontal force or height of the connection
$I.S.$	introduced shrinkage
$K2/3$	secant shear stiffness at a shear force of $0{,}67Q_u$
M	bending moment
N	tensile or compression force perpendicular to the connection
N_c	(axial) compression force
N_x	normal force in truss element according to numerical program

Q_c	shear force capacity at the instant of cracking
Q_u	ultimate shear force capacity
R_t	mean surface roughness
T	shear force
T_c	shear force in compressed interface
V	shear force
V_F	shear force
$V_{F;B}$	shear force at the instant of debonding
$V_{F;C}$	shear force at the instant of the diagonal cracks appearance
$V_{F;D}$	failure force for Aligned shear key connection
$V_{F;E}$	residual shear force
$V_{F;r}$	residual shear force
$V_{F;X}$	shear force for one of the principal stages (A till E)
$V_{F;u}$	ultimate shear force at the failure crack instant
V_{Ed}	design value of the shear force
$V_{Ed;inclined}$	design value of the inclined shear force
V_{Rd}	design value of the shear capacity

Roman Lower Case

b	width of the seam
d	depth of the shear key
f_c	concrete compressive strength (through cube tests 150x150x150 mm^3)
f_{ct}	concrete tensile splitting strength (through cube tests 150x150x150 mm^3)
f'_{mk}	mortar compressive strength (through prisms tests 40x40x80 mm^3)
f''_m	mortar flexural tensile strength (through prisms tests 40x40x160 mm^3)
h	height of the connection or height of the shear key
h_{csw}	height of the cantilever shear wall
h_1	increased height of the connection or height of the shear key indentation
h_2	height of the shear key

k	shear stiffness
$k_{con;1}$	initial shear stiffness (1)
$k_{con;2}$	initial shear stiffness (2)
k_v	shear stiffness
k_h	lateral stiffness
l_{strut}	length of the inclined compression strut
l_{bar}	length of the steel bar
n	number of shear keys
s	shear slip or shear displacament
t	panel thickness or depth of the shear key
w	slip opening

Greek Lower Case

α	angle of the inclined compression strut
β	angle of the sloped interface
δ	displacement
$\delta_{lateral}$	lateral displacement
δ_V	shear displacement
$\delta_{V;1}$	shear displacement as a result of shortening of the compression strut δ_{Nc}
$\delta_{V;2}$	shear displacement as a result of the lateral displacement $\delta\sigma_n$
δ_{Nc}	elastic shortening of the compression strut
$\delta\sigma_n$	lateral displacement
δ_{4xM16}	lengthening of steel bars M16
ϕ	diameter of steel bar
σ	normal stress
σ_s	tensile stress
σ_c	compressive stress
σ_x	horizontal prestress of wall joint
σ_n	initial compression

σ'_b	strength of the joint concrete
τ	shear stress
τ_c	shear stress at the instant of crack appearance in the joint concrete
$\tau_{deb;1}$	shear stress at the instant of debonding (1)
$\tau_{deb;2}$	shear stress at the instant of debonding (2)
$\tau_{(s)}$	shear stress as function of the shear displacements
τ_f	residual shear stress
τ_u	ultimate shear stress

Appendix A

Pump test

Vullingsproeven | Schaal: **1:10** | Getekend: **DvK** | Datum: **12-12-2012**

Figure A.1: Details of "Filling test"

Appendix B

Lay-out Specimens

ALGEMEEN

- geen instortvoorzieningen nabij kartels
- afstandhouders uitgevoerd in kunststof
- maattoleranties: NEN 2889 tabel 1
- oppervlaktebehandeling: NEN 6722 klasse A
- stortzijde vlinderen: [X]

BETON

- sterkteklasse beton: C53/65
- toeslagmateriaal: grind
- wapeningsstaven B500A
- milieuklasse: XC1
- watercementfactor <0,45
- ontkistingssterkte > 15 N/mm2
- cement: CEM III/A 52,5 N
- nominale korrel 16 mm

PROEFKUBUSSEN

- per stort 6 kubussen 150x150x150 maken
- mallen kunnen geleend worden van TU/e
- kubussen bij proefstuk bewaren

MAAT   MAAT
20

DET A
schaal 1:5

ELEMENT 16x UITVOEREN

VORMTEKENING

TEKENING T.B.V. PRODUCTIE BESTCON

INGENIEURSSTUDIO DCK

datum: 9-9-2017
schaal: 1:10
formaat: A3
get.: dck

Henry Dunantlaan 1 - 2992 KP Barendrecht - tel. 0180-890120 - www.studio-dck.nl - post@studio-dck.nl

PVC sparing ⌀25

demu 1988 M12-100, boutanker
voegprofiel

demu 1988 M16-140, boutanker
zwaartepunt

DET A
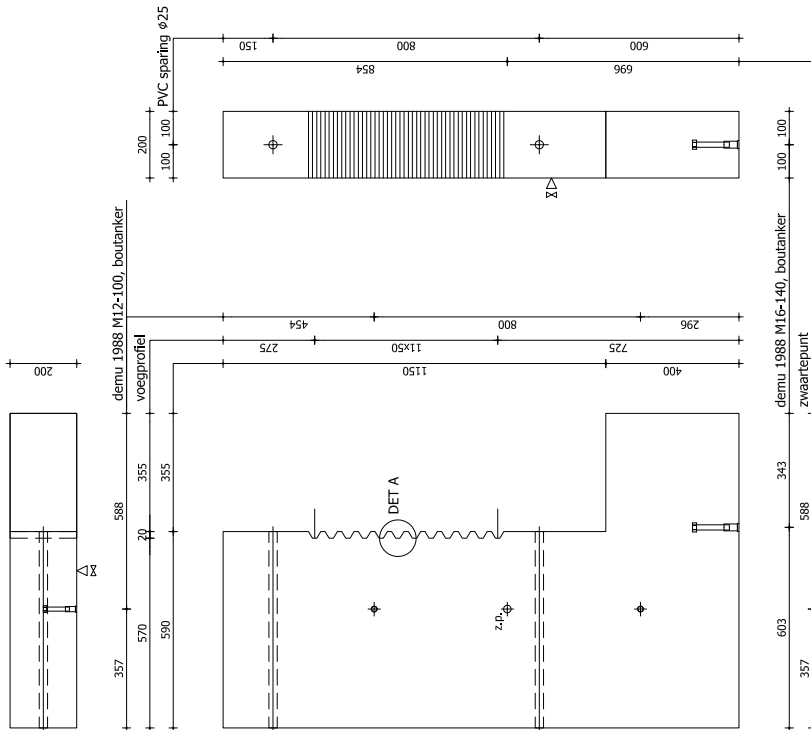
VOORAANZICHT = stortzijde
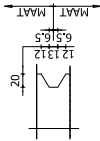
Inhoud: 0,2101 m3
gewicht: 525,25 kg

ALGEMEEN

- geen instortvoorzieningen nabij kartels
- afstandhouders uitgevoerd in kunststof
- maattoleranties: NEN 2889 tabel 1
- oppervlaktebehandeling: NEN 6722 klasse A
- stortzijde vlinderen: ∑▷

BETON

- sterkteklasse beton: C53/65
- toeslagmateriaal: grind
- wapeningsstaven B500A
- milieuklasse: XC1
- watercementfactor <0,45
- ontkistingssterkte > 15 N/mm2
- cement: CEM III/A 52,5 N
- nominale korrel 16 mm

PROEFKUBUSSEN

- per stort 6 kubussen 150x150x150 maken
- mallen kunnen geleend worden van TU/e
- kubussen bij proefstuk bewaren

WAPENINGSTEKENING

TEKENING T.B.V. PRODUCTIE BESTCON
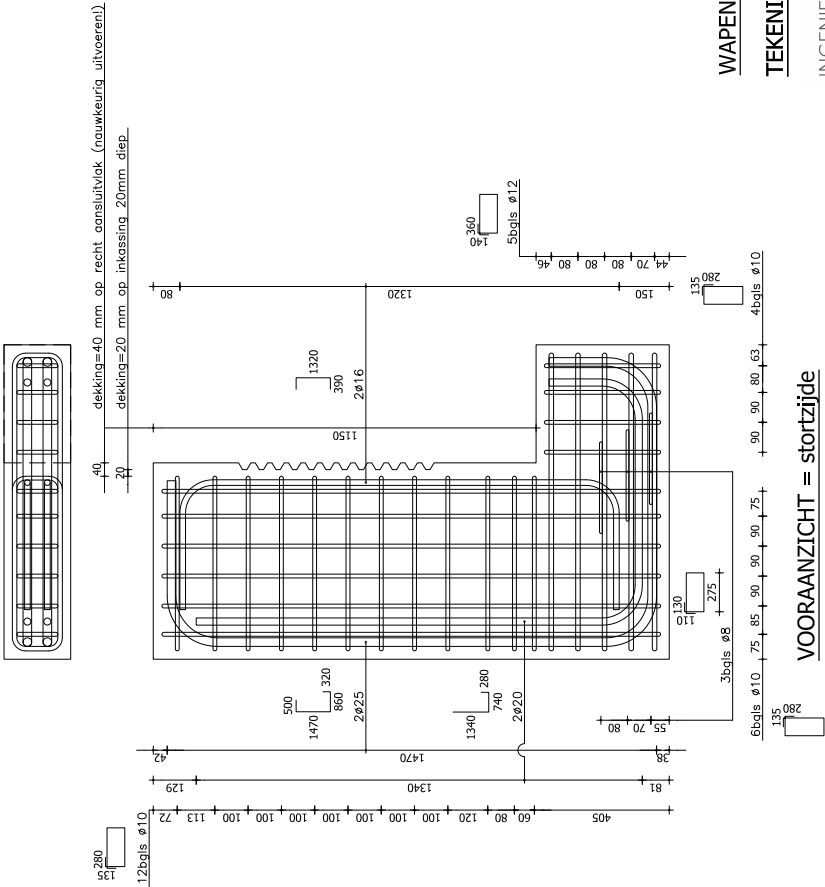
INGENIEURSSTUDIO DCK

datum: 9-9-2017
schaal: 1:10
formaat: A3
get.: dck

Henry Dunantlaan 1 - 2992 KP Barendrecht - tel. 0180-890120 - www.studio-dck.nl - post@studio-dck.nl

dekking=40 mm op recht aansluitvlak (nauwkeurig uitvoeren!)
dekking=20 mm op inkassing 20mm diep

VOORAANZICHT = stortzijde

5bgls ø12 — 360 / 140
4bgls ø10 — 280 / 135
2ø16 — 1320 / 390 / 1150
3bgls ø8
6bgls ø10 — 280 / 135 / 275 / 130 / 110
2ø25 — 1470 / 860 / 500 / 320
2ø20 — 1340 / 740 / 280
12bgls ø10 — 280 / 135

40 / 20 / 80 / 1320 / 150 / 46 80 80 80 70 44
90 80 63 / 90 90 75 / 90 90 90 / 55 70 80
1470 / 1340 / 42 / 38 / 129 / 81
405 / 72 113 100 100 100 100 100 100 120 80 60 120 80

PhD thesis		Shear tests	PhD thesis		Shear tests
Aligned shear key connection			**Plain waterjetted shear connection**		
Sp1-1	-	Sp1-9	Sp4-1	-	Sp2-11
Sp1-2	-	Sp1-10	Sp4-2	-	Sp2-12
Sp1-3	-	Sp1-11	Sp4-3	-	Sp2-13
Sp1-4	-	Sp1-12	Sp4-4	-	Sp2-14
			Sp4-5	-	Sp2-15
Staggered shear key connection					
Sp2-1	-	Sp2-1	**Serrated waterjetted shear connection**		
Sp2-2	-	Sp2-2	Sp5-1	-	Sp2-6
Sp2-3	-	Sp1-5	Sp5-2	-	Sp2-7
Sp2-4	-	Sp2-3	Sp5-3	-	Sp2-8
Sp2-5	-	Sp1-7	Sp5-4	-	Sp2-9
Sp2-6	-	Sp2-4	Sp5-5	-	Sp2-10
Sp2-7	-	Sp1-8	Sp5-6	-	Sp2-16
Sp2-8	-	Sp2-5			
Sp2-9	-	Sp1-6			
Aligned small shear key connection					
Sp3-1	-	Sp3-1			
Sp3-2	-	Sp3-2			
Sp3-3	-	Sp3-3			
Sp3-4	-	Sp3-4			
Sp3-5	-	Sp3-5			
Sp3-6	-	Sp3-6			
Sp3-7	-	Sp3-7			
Sp3-8	-	Sp3-8			
Sp3-9	-	Sp2-17			

Table B.1: Table with codings selected for this PhD thesis compared to the codings used for the same shear tests reported in Van Keulen (2013), Van Keulen (2014) and Van Keulen (2015).

Appendix C

Material tests

Precast concrete L-elements: Compressive strength (f_c) according to NEN-EN 12390-3, 2009							
Cubes 150x150x150	**Casting date**	**Testing date**	**Age**	**Cube 1**	**Cube 2**	**Cube 3**	**Mean**
Connection, Specimen			(days)	(N/mm^2)			
1. Aligned shear key							
Specimen 1-1 (Hurks 1)	28-5-2013	15-7-2013	48	83,6	84,7	78,8	**82,4**
Specimen 1-2 (Hurks 1)	29-5-2013	16-7-2013	48	85,2	83,2	82,7	**83,7**
Specimen 1-3 (Hurks 1)	30-5-2013	17-7-2013	48	87,2	87,5	86,9	**87,2**
Specimen 1-4 (Hurks 1)	3-6-2013	18-7-2013	45	83,9	85,6	80,1	**83,2**
2. Staggered shear key							
Specimen 2-1 (Hurks 2)	4-2-2014	28-3-2014	52	86,9	79,3	-	**83,1**
Specimen 2-2 (Hurks 2)	10-2-2014	8-4-2014	57	83,4	85,0	-	**84,2**
Specimen 2-3 (Hurks 1)	22-5-2013	5-7-2013	44	89,9	89,9	88,4	**89,4**
Specimen 2-4 (Hurks 2)	21-2-2014	8-4-2014	46	85,9	85,6	-	**85,8**
Specimen 2-5 (Hurks 1)	27-5-2013	12-7-2013	46	81,9	79,8	82,9	**81,5**
Specimen 2-6 (Hurks 2)	13-2-2014	23-4-2014	69	89,0	93,7	-	**91,4**
Specimen 2-7 (Hurks 1)	24-5-2013	11-7-2013	48	93,1	92,6	92,1	**92,6**
Specimen 2-8 (Hurks 2)	20-2-2014	9-4-2014	48	86,9	94,5	-	**90,7**
Specimen 2-9 (Hurks 1)	23-5-2013	9-7-2013	47	84,5	86,2	88,3	**86,3**
3. Aligned small shear key							
Specimen 3-1 (Bestcon)	11-10-2017	30-11-2017	50	88,4	94,1	91,2	**91,2**
Specimen 3-2 (Bestcon)	12-10-2017	1-12-2017	50	87,0	86,9	86,1	**86,7**
Specimen 3-3 (Bestcon)	13-10-2017	1-12-2017	49	92,7	93,6	95,8	**94,0**
Specimen 3-4 (Bestcon)	16-10-2017	4-12-2017	49	84,2	84	86,2	**84,8**
Specimen 3-5 (Bestcon)	17-10-2017	11-12-2017	55	84,9	84,2	90	**86,4**
Specimen 3-6 (Bestcon)	18-10-2017	11-12-2017	54	86,9	86,2	85,4	**86,2**
Specimen 3-7 (Bestcon)	19-10-2017	12-12-2017	54	-	-	87,8	**87,8**
Specimen 3-8 (Bestcon)	20-10-2017	12-12-2017	53	94,9	90,6	95,7	**93,7**
Specimen 3-9 (Hurks 2)	25-2-2014	23-4-2014	57	85,7	84,5	-	**85,1**
4. Plain waterjetted shear connection							
Specimen 4-1 (Hurks 2)	20-2-2014	9-4-2014	48	86,9	94,5	-	**90,7**
Specimen 4-2 (Hurks 2)	4-2-2014	11-4-2014	66	89,6	86,1	-	**87,9**
Specimen 4-3 (Hurks 2)	10-2-2014	11-4-2014	60	90,1	82,5	-	**86,3**
Specimen 4-4 (Hurks 2)	11-2-2014	25-4-2014	73	85,8	84,5	-	**85,2**
Specimen 4-5 (Hurks 2)	6-2-2014	25-4-2014	78	82,4	87,9	-	**85,2**
5. Serrated waterjetted shear connection							
Specimen 5-1 (Hurks 2)	21-2-2014	1-4-2014	39	83,6	74,5	-	**79,1**
Specimen 5-2 (Hurks 2)	5-2-2014	1-4-2014	55	89,3	83,2	-	**86,3**
Specimen 5-3 (Hurks 2)	4-2-2014	2-4-2014	57	90	84,8	-	**87,4**
Specimen 5-4 (Hurks 2)	24-2-2014	2-4-2014	37	81,8	78,0	-	**79,9**
Specimen 5-5 (Hurks 2)	20-2-2014	4-4-2014	43	87,4	-	-	**87,4**
Specimen 5-6 (Hurks 2)	11-2-2014	4-4-2014	52	80,2	86,4	-	**83,3**
Mean compressive strength μ (N/mm^2)							**86,5**
Standard deviation σ (N/mm2)							**3,75**

Table C.1: Compressive strength of the precast concrete L-elements

Precast concrete L-elements: Tensile splitting strength (f_{fct}) according to NEN-EN 12390-6, 2009							
Cubes 150x150x150	Casting date	Testing date	Age	Cube 1	Cube 2	Cube 3	Mean
Connection, Specimen			(days)	(N/mm^2)			
1. Aligned shear key							
Specimen 1-1 (Hurks 1)	28-5-2013	15-7-2013	48	4,4	4,6	4,6	**4,6**
Specimen 1-2 (Hurks 1)	29-5-2013	16-7-2013	48	4,7	4,4	4,4	**4,5**
Specimen 1-3 (Hurks 1)	30-5-2013	17-7-2013	48	4,5	6,1	5,2	**5,3**
Specimen 1-4 (Hurks 1)	3-6-2013	18-7-2013	45	4,9	4,8	4,3	**4,7**
2. Staggered shear key							
Specimen 2-1 (Hurks 2)	4-2-2014	28-3-2014	52	-	-	-	**-**
Specimen 2-2 (Hurks 2)	10-2-2014	8-4-2014	57	-	-	-	**-**
Specimen 2-3 (Hurks 1)	22-5-2013	5-7-2013	44	5,3	5,6	5,2	**5,4**
Specimen 2-4 (Hurks 2)	21-2-2014	8-4-2014	46	-	-	-	**-**
Specimen 2-5 (Hurks 1)	27-5-2013	12-7-2013	46	5,1	4,9	5,1	**5,0**
Specimen 2-6 (Hurks 2)	13-2-2014	23-4-2014	69	-	-	-	**-**
Specimen 2-7 (Hurks 1)	24-5-2013	11-7-2013	48	5,3	5,9	5,2	**5,5**
Specimen 2-8 (Hurks 2)	20-2-2014	9-4-2014	48	-	-	-	**-**
Specimen 2-9 (Hurks 1)	23-5-2013	9-7-2013	47	4,5	5,1	5,9	**5,2**
3. Aligned small shear key							
Specimen 3-1 (Bestcon)	11-10-2017	30-11-2017	50	5,1	5,0	5,3	**5,1**
Specimen 3-2 (Bestcon)	12-10-2017	1-12-2017	50	5,0	4,3	5,0	**4,8**
Specimen 3-3 (Bestcon)	13-10-2017	1-12-2017	49	5,0	4,9	4,4	**4,8**
Specimen 3-4 (Bestcon)	16-10-2017	4-12-2017	49	4,3	5,1	5,1	**4,8**
Specimen 3-5 (Bestcon)	17-10-2017	11-12-2017	55	5,0	4,4	5,2	**4,8**
Specimen 3-6 (Bestcon)	18-10-2017	11-12-2017	54	4,3	4,7	4,9	**4,6**
Specimen 3-7 (Bestcon)	19-10-2017	12-12-2017	54	5,1	5,1	4,6	**4,6**
Specimen 3-8 (Bestcon)	20-10-2017	12-12-2017	53	6,0	5,1	5,2	**5,4**
Specimen 3-9 (Hurks 2)	25-2-2014	23-4-2014	57	-	-	-	**-**
4. Plain waterjetted shear connection							
Specimen 4-1 (Hurks 2)	20-2-2014	9-4-2014	48	-	-	-	**-**
Specimen 4-2 (Hurks 2)	4-2-2014	11-4-2014	66	-	-	-	**-**
Specimen 4-3 (Hurks 2)	10-2-2014	11-4-2014	60	-	-	-	**-**
Specimen 4-4 (Hurks 2)	11-2-2014	25-4-2014	73	-	-	-	**-**
Specimen 4-5 (Hurks 2)	6-2-2014	25-4-2014	78	-	-	-	**-**
5. Serrated waterjetted shear connection							
Specimen 5-1 (Hurks 2)	21-2-2014	1-4-2014	39	-	-	-	**-**
Specimen 5-2 (Hurks 2)	5-2-2014	1-4-2014	55	-	-	-	**-**
Specimen 5-3 (Hurks 2)	4-2-2014	2-4-2014	57	-	-	-	**-**
Specimen 5-4 (Hurks 2)	24-2-2014	2-4-2014	37	-	-	-	**-**
Specimen 5-5 (Hurks 2)	20-2-2014	4-4-2014	43	-	-	-	**-**
Specimen 5-6 (Hurks 2)	11-2-2014	4-4-2014	52	-	-	-	**-**
Mean tensile strength μ (N/mm^2)							4,9
Standard deviation σ (N/mm2)							0,32

Table C.2: Tensile splitting strength of the precast concrete L-elements

Modulus of Elasticity (E_c)				Dimension prisms 100x100x400			
Connection, Specimen	Casting date	Testing date	Age (days)	Prism 1	Prism 2	Prism 3	Mean
						(N/mm^2)	
1. Aligned shear key							
Specimen 1-1 (Hurks 1)	28-5-2013	15-7-2013	48	31.537	32.522	31.980	**32.013**
Specimen 1-2 (Hurks 1)	29-5-2013	16-7-2013	48	32.582	32.896	33.201	**32.893**
Specimen 1-3 (Hurks 1)	30-5-2013	17-7-2013	48	33.193	33.985	32.307	**33.162**
Specimen 1-4 (Hurks 1)	3-6-2013	18-7-2013	45	31.499	31.610	31.870	**31.660**
2. Staggered shear key							
Specimen 2-1 (Hurks 2)	4-2-2014	28-3-2014	52	-	-	-	**-**
Specimen 2-2 (Hurks 2)	10-2-2014	8-4-2014	57	-	-	-	**-**
Specimen 2-3 (Hurks 1)	22-5-2013	5-7-2013	44	33.027	35.401	35.165	**34.531**
Specimen 2-4 (Hurks 2)	21-2-2014	8-4-2014	46	-	-	-	**-**
Specimen 2-5 (Hurks 1)	27-5-2013	12-7-2013	46	32.764	33.242	33.738	**33.248**
Specimen 2-6 (Hurks 2)	13-2-2014	23-4-2014	69	-	-	-	**-**
Specimen 2-7 (Hurks 1)	24-5-2013	11-7-2013	48	32.827	35.755	33.970	**34.184**
Specimen 2-8 (Hurks 2)	20-2-2014	9-4-2014	48	-	-	-	**-**
Specimen 2-9 (Hurks 1)	23-5-2013	9-7-2013	47	30.336	34.094	33.837	**32.756**
3. Aligned small shear key							
Specimen 3-1 (Bestcon)	11-10-2017	30-11-2017	50	-	-	-	**-**
Specimen 3-2 (Bestcon)	12-10-2017	1-12-2017	50	-	-	-	**-**
Specimen 3-3 (Bestcon)	13-10-2017	1-12-2017	49	-	-	-	**-**
Specimen 3-4 (Bestcon)	16-10-2017	4-12-2017	49	-	-	-	**-**
Specimen 3-5 (Bestcon)	17-10-2017	11-12-2017	55	-	-	-	**-**
Specimen 3-6 (Bestcon)	18-10-2017	11-12-2017	54	-	-	-	**-**
Specimen 3-7 (Bestcon)	19-10-2017	12-12-2017	54	-	-	-	**-**
Specimen 3-8 (Bestcon)	20-10-2017	12-12-2017	53	-	-	-	**-**
Specimen 3-9 (Hurks 2)	25-2-2014	23-4-2014	57	-	-	-	**-**
4. Plain waterjetted shear connection							
Specimen 4-1 (Hurks 2)	20-2-2014	9-4-2014	48	-	-	-	**-**
Specimen 4-2 (Hurks 2)	4-2-2014	11-4-2014	66	-	-	-	**-**
Specimen 4-3 (Hurks 2)	10-2-2014	11-4-2014	60	-	-	-	**-**
Specimen 4-4 (Hurks 2)	11-2-2014	25-4-2014	73	-	-	-	**-**
Specimen 4-5 (Hurks 2)	6-2-2014	25-4-2014	78	-	-	-	**-**
5. Serrated waterjetted shear connection							
Specimen 5-1 (Hurks 2)	21-2-2014	1-4-2014	39	-	-	-	**-**
Specimen 5-2 (Hurks 2)	5-2-2014	1-4-2014	55	-	-	-	**-**
Specimen 5-3 (Hurks 2)	4-2-2014	2-4-2014	57	-	-	-	**-**
Specimen 5-4 (Hurks 2)	24-2-2014	2-4-2014	37	-	-	-	**-**
Specimen 5-5 (Hurks 2)	20-2-2014	4-4-2014	43	-	-	-	**-**
Specimen 5-6 (Hurks 2)	11-2-2014	4-4-2014	52	-	-	-	**-**
Mean modulus of elasticity μ (N/mm^2)							33056
Standard deviation σ (N/mm2)							975

Table C.3: Modulus of elasticity of the precast concrete L-elements

Compressive strength and Flexural tensile strength according to CUR-aanbeveling 24 and ISO 679											
Dimension prisms	40x40x160										
Casting date	7-6-2013		Compressive strength f'$_{mk}$ (N/mm^2)				Flexural tensile strength f"$_m$ (N/mm^2)			
Connection, Specimen	Testing date	Age	Prism 1	Prism 2	Prism 3	Mean	Prism 1	Prism 2	Prism 3	Mean
1. Aligned shear key		(days)								
Specimen 1-1	15-7-2013	38	72,20	61,30	-	66,75	9,72	9,87	-	9,80
Specimen 1-2 (SFRM)	16-7-2013	39	93,20	94,80	90,30	92,77	13,30	13,18	11,54	12,67
Specimen 1-3	17-7-2013	40	81,30	-	-	81,30	8,81	-	-	8,81
Specimen 1-4 (SFRM)	18-7-2013	41	93,20	95,30	95,20	94,57	9,52	10,42	12,77	10,90
2. Staggered shear key										
Specimen 2-3	5-7-2013	28	78,90	79,40	-	79,15	11,81	11,73	-	11,77
Specimen 2-5	12-7-2013	35	73,60	70,80	-	72,20	8,84	10,04	-	9,44
Specimen 2-7	11-7-2013	34	75,20	73,30	-	74,25	8,84	9,51	-	9,18
Specimen 2-9 (SFRM)	9-7-2013	32	94,20	88,80	-	91,50	12,78	12,26	-	12,52
3. Remaining prisms										
Cuglaton Tikso K70	3-7-2013	26	76,90	77,20	-	77,05	11,14	13,05	-	12,10
Cuglaton Tikso K70	4-7-2013	27	74,00	74,90	-	74,45	7,98	8,33	-	8,16
Cuglaton Tikso K70 mortar										
Mean strengths μ (N/mm^2)						75,02				9,89
Standard deviation σ (N/mm2)						4,79				1,49
Steel Fibre Reinforce Mortar										
Mean strengths μ (N/mm^2)						92,94				12,03
Standard deviation σ (N/mm2)						1,54				0,98
All mortar mixtures are pressed through the hose into the prism moulds by means of a mortar pump.										

Table C.4: Material tests results for Tiksomortar K70 and Steel Fibre Reinforced Mortar

Appendix D

Shear behaviour of an example profiled mortar connection

D.1   Photos of shear test
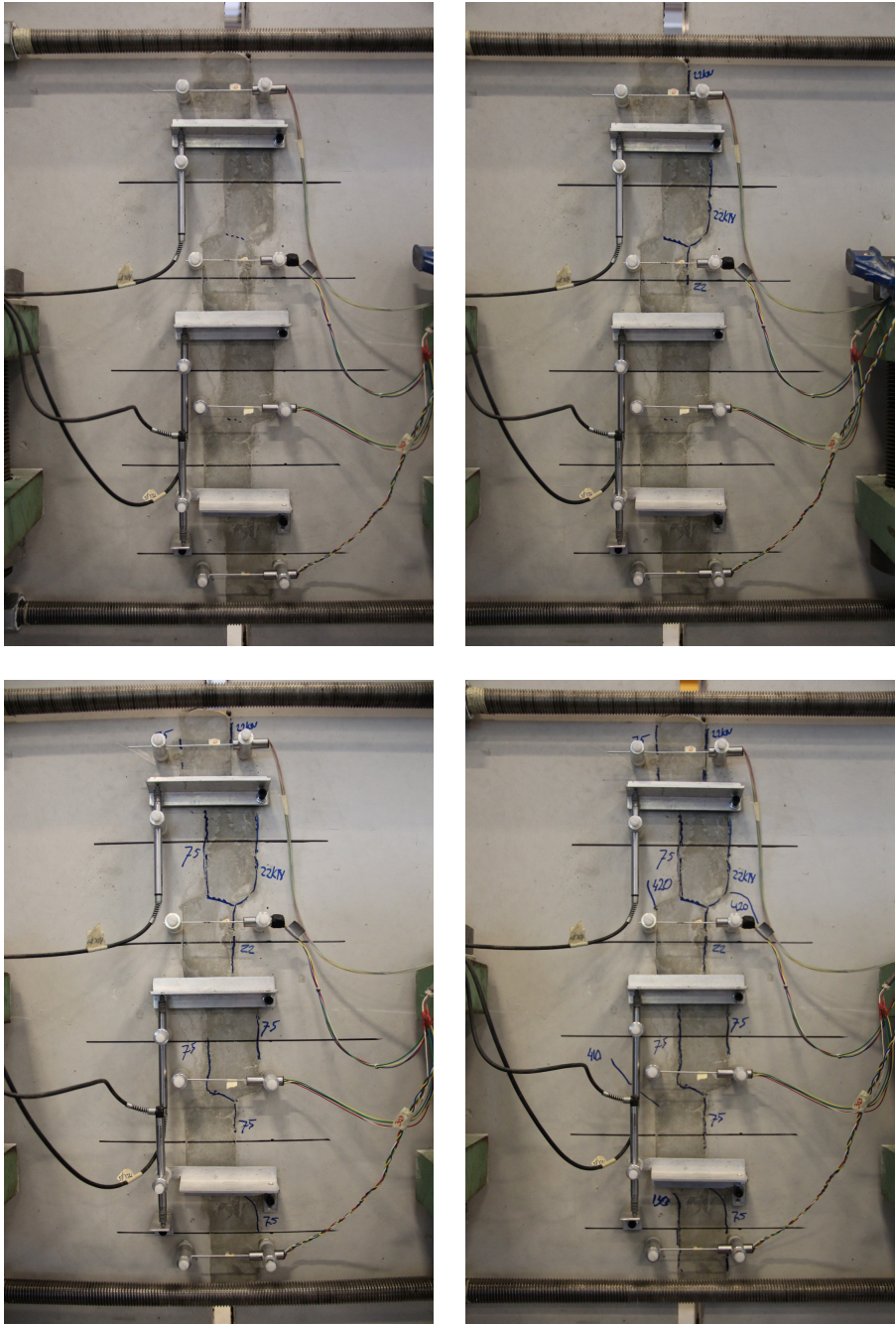
Figure D.1: Specimen 2-4: Shear load up to $V_{F;c}$ = 420 kN
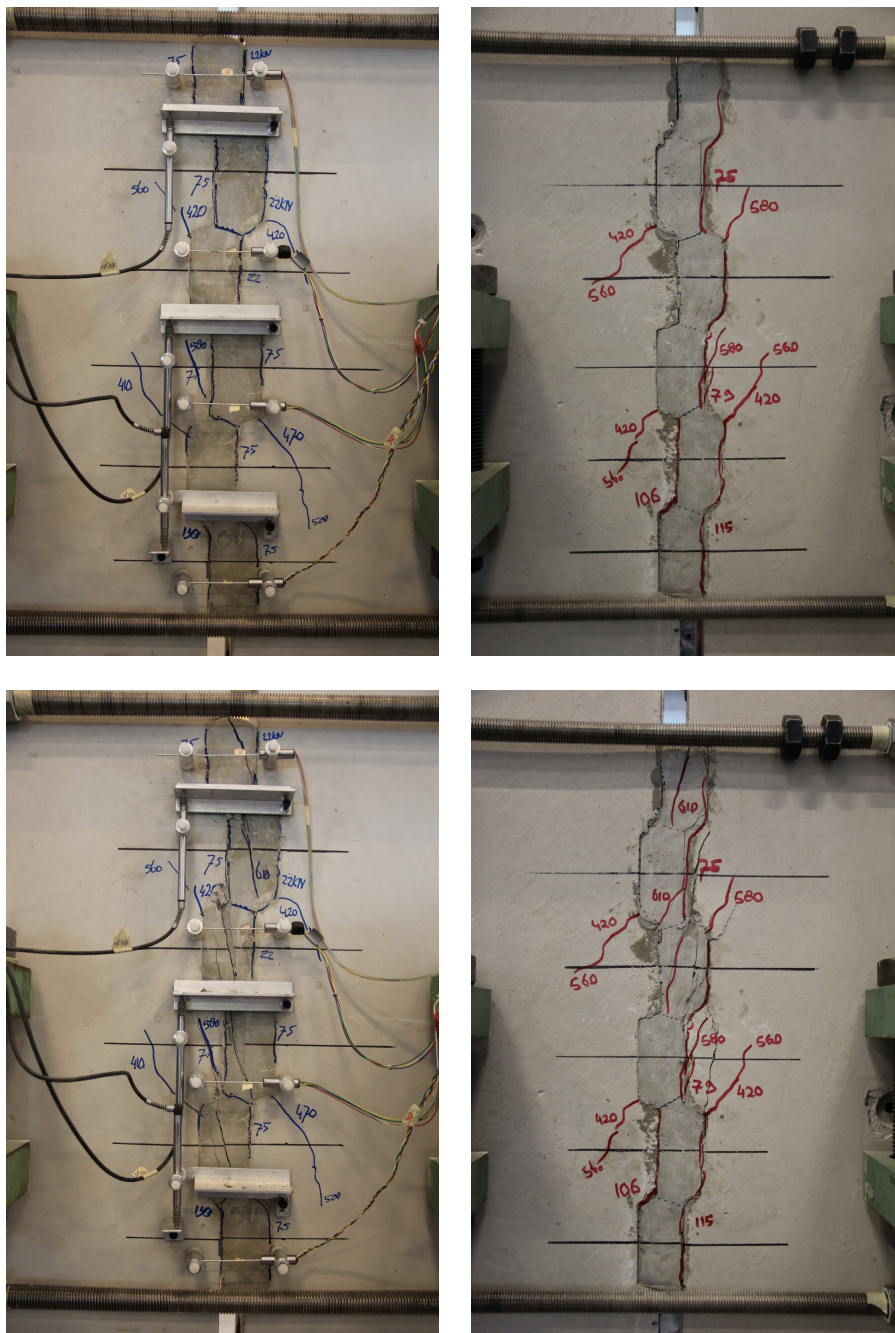
Figure D.2: Specimen 2-4: Shear load up to $V_{F;u}$ = 613,2 kN
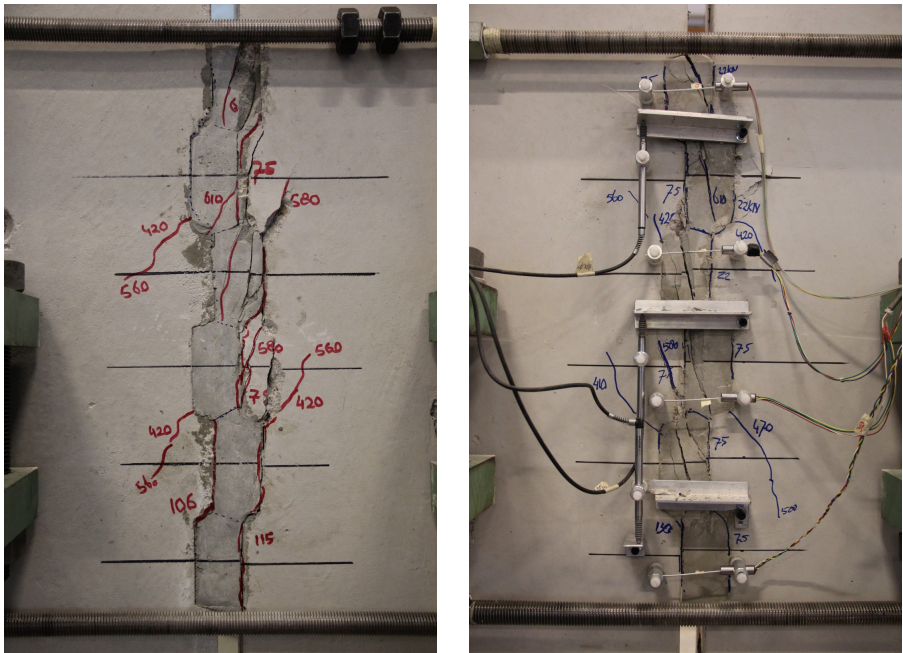
Figure D.3: Specimen 2-4: Residual shear load $V_{F;r}$ = 340 kN
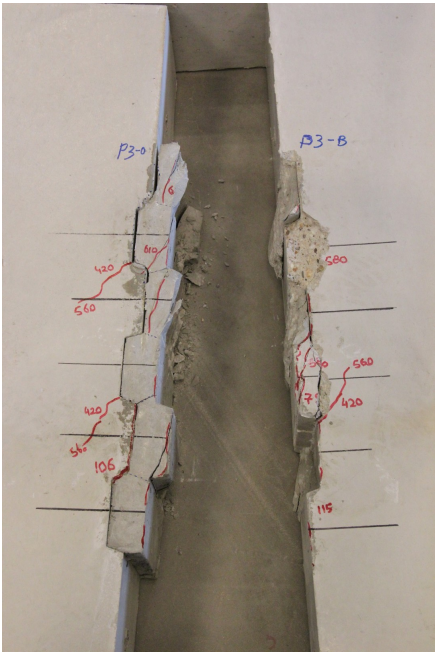
Figure D.4: Specimen 2-4: Dismantled mortar connection
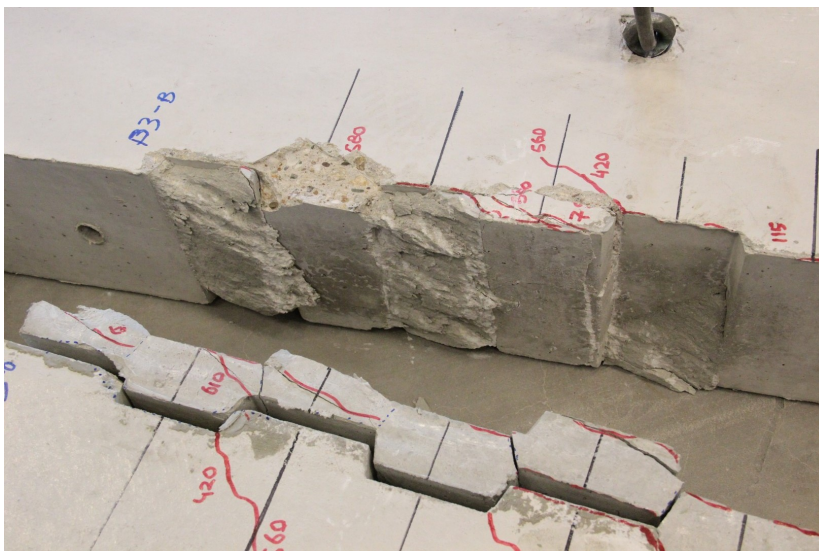
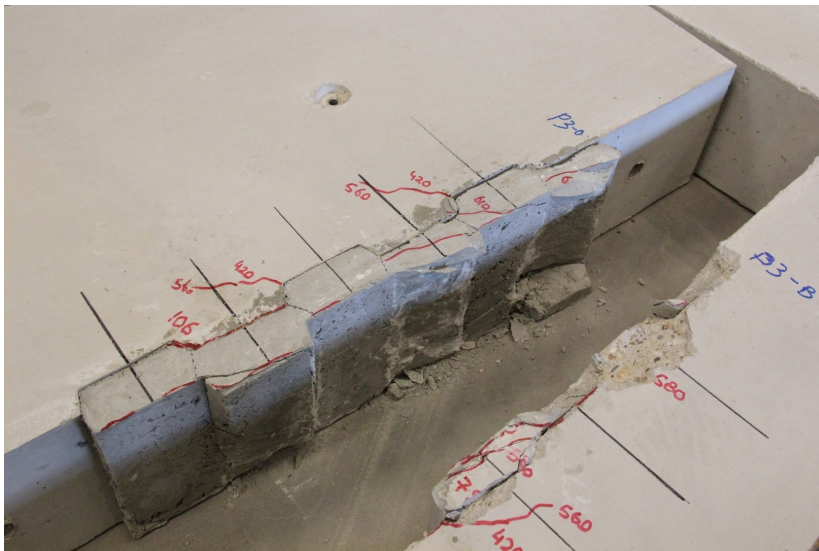Figure D.5: Specimen 2-4: Dismantled mortar connection

Appendix E

Photo's of cracked and dismantled mortar connections

E.1   Aligned shear key connection
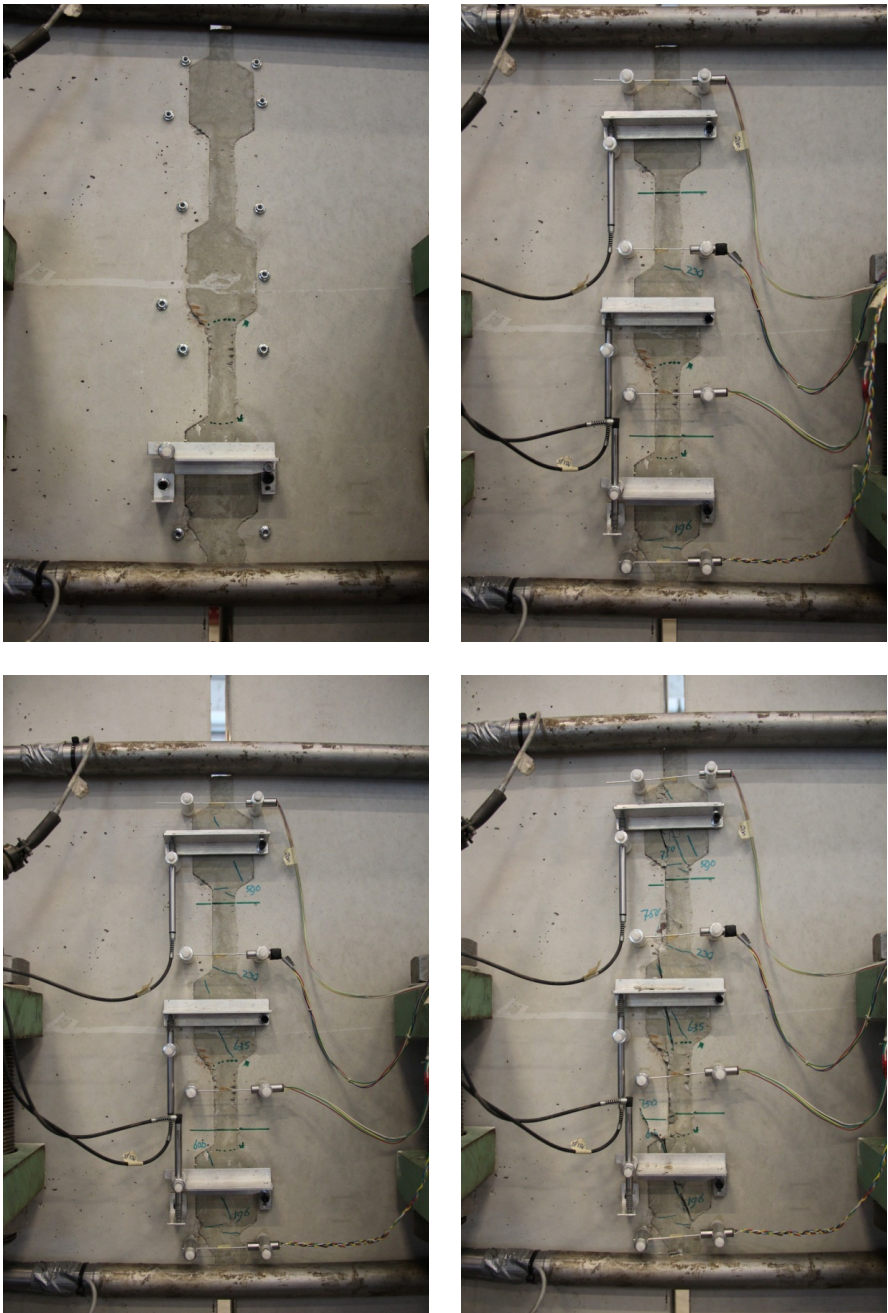
Figure E.1: Specimen 1-4: Crack formation during shear test
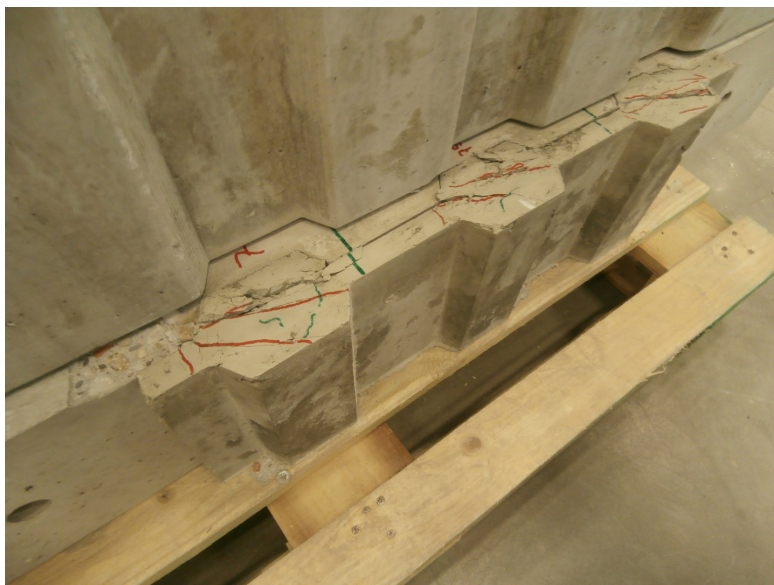
Figure E.2: Specimen 1-4: Dismantled specimen (Steel Fibre Reinforced Mortar)

Figure E.3: Specimen 1-3: Dismantled specimen (Tiksomortar k70)

E.2 Staggered shear key connection
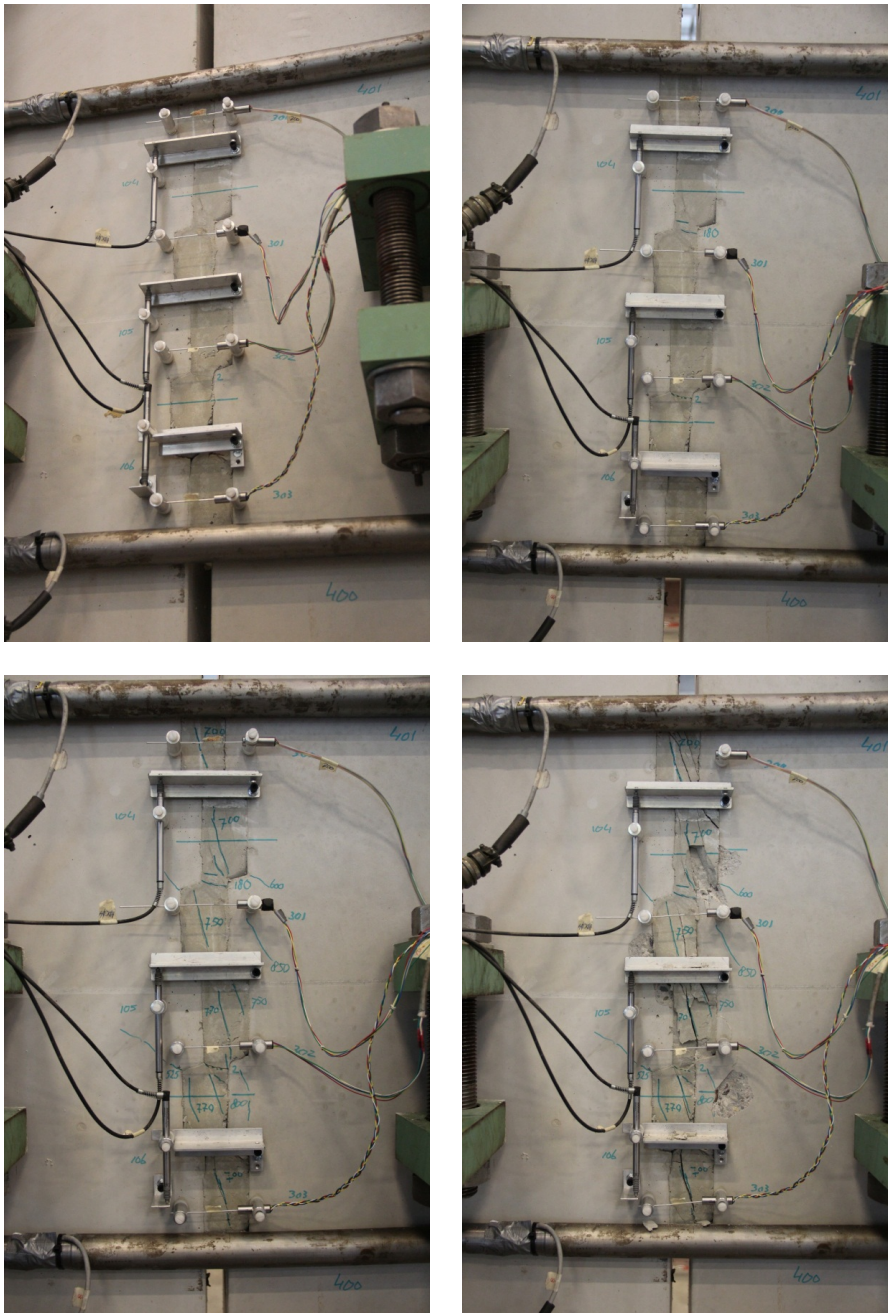
Figure E.4: Specimen 2-7: Crack formation during shear test

Figure E.5: Specimen 2-7: Dismantled specimen (Tiksomortar K70)

E.3 Aligned small shear key connection
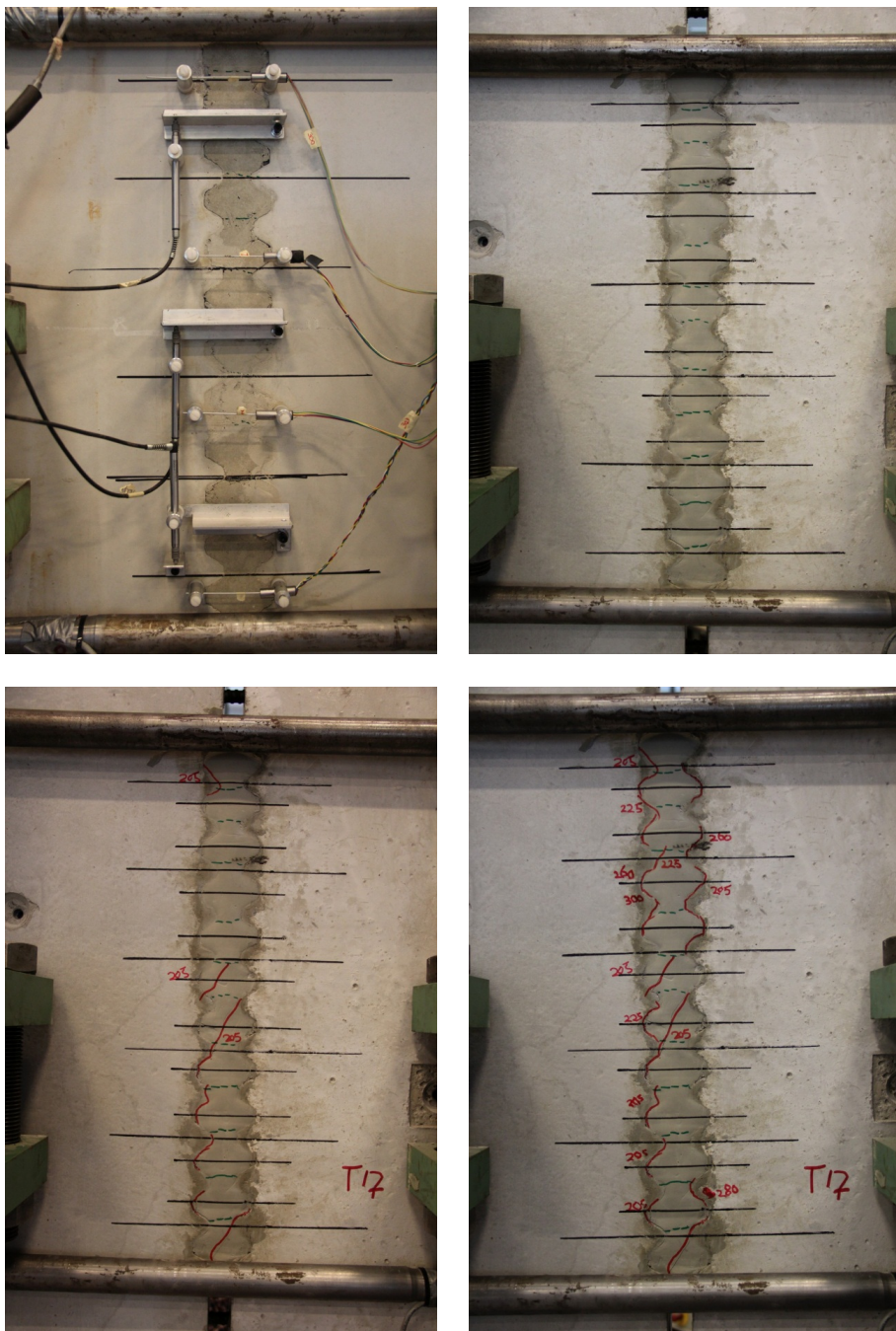
Figure E.6: Specimen 3-9: Crack formation during shear test

Figure E.7: Specimen 3-9: Crack formation during shear test
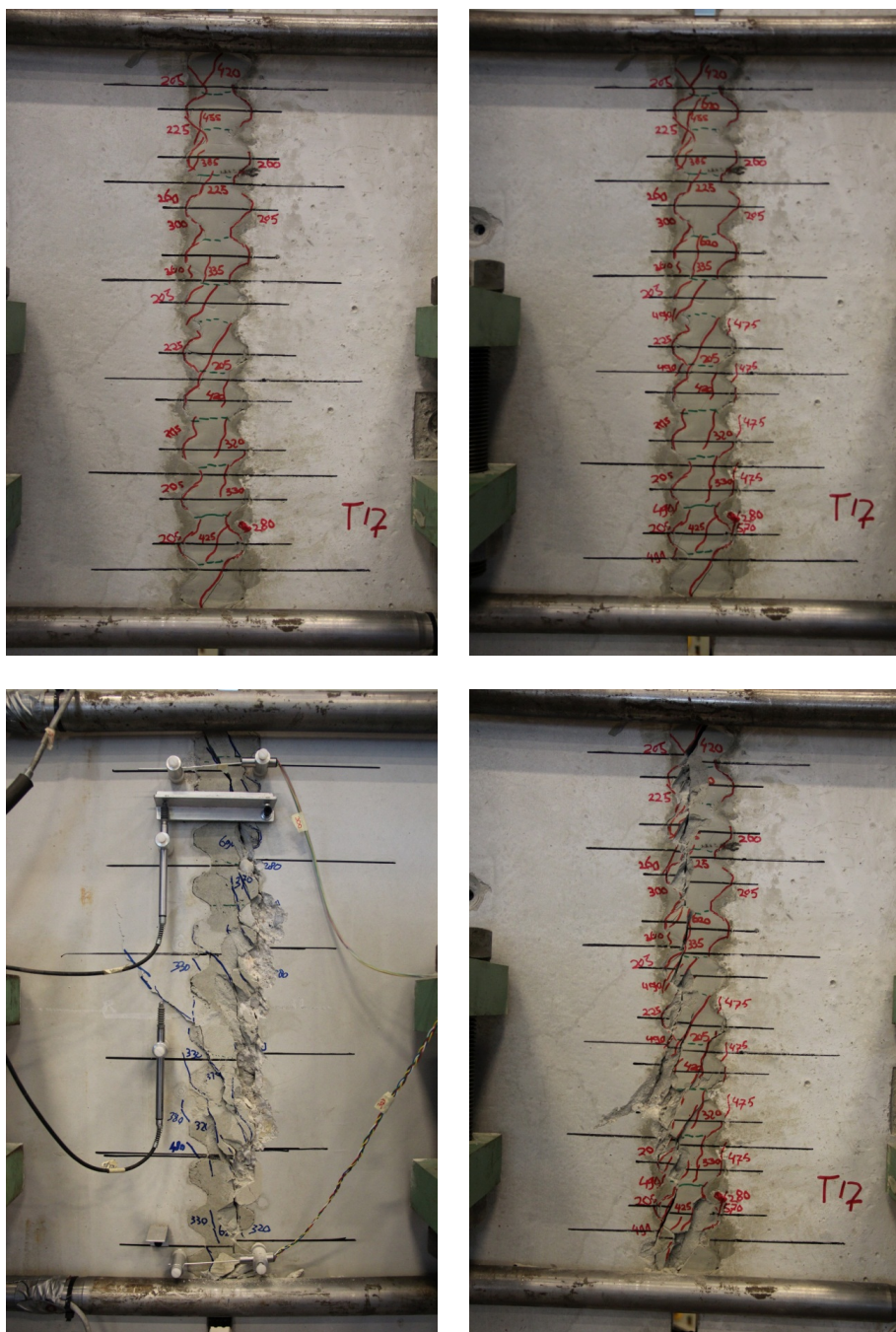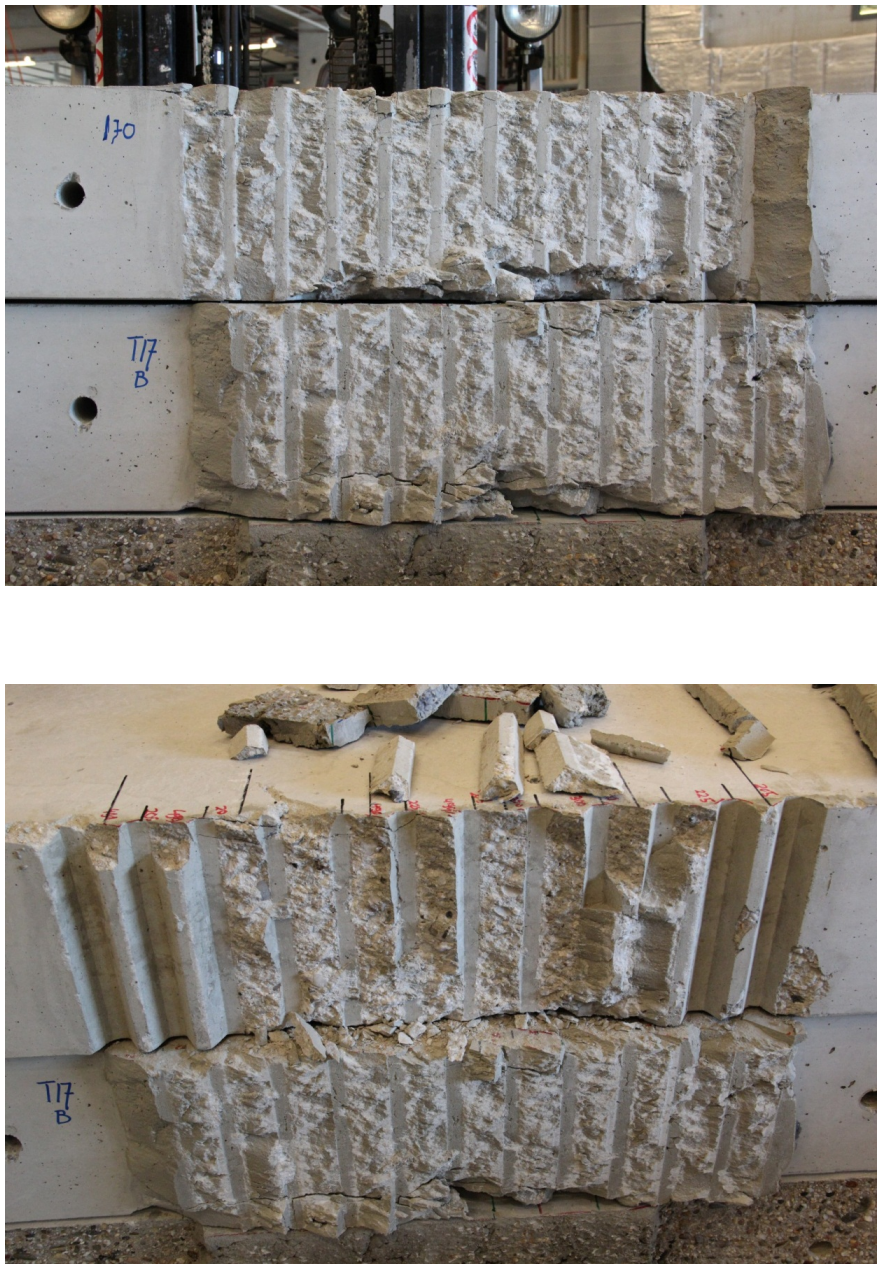
Figure E.8: Specimen 3-9: Dismantled specimen

Filling of specimens with Steel Fibre Reinforced Mortar

The next diagrams, table and photos in in this Appendix require the explanation of a shortcoming in the specimen before analysing the test results. Specimens 3-5 till 3-8 are filled with Steel Fibre Reinforced Mortar. The interspace between the two precast concrete elements should be completely filled. The photos in figures E.11 and E.12 show that the mortar filling is not complete for the specimens 3-6, 3-7 and 3-8. The filling of specimen 3-5 is considered full as can be observed on the photo. This is the reason for only incorporating the test results of specimen 3-5 in the diagram and table in subsection 5.8.2.

The incomplete filling is observed after taking the specimens from the table in the concrete factory where the mortar is inserted. This could not be observed earlier since the specimen layed on one side on the table. The cause of this incomplete filling has to be attributed to using a too dry mortar. The mortar pump is unable to press the fibre reinforced mortar to the lower section of the mortar filling. This is not observed during inserting the mortar in the specimen.
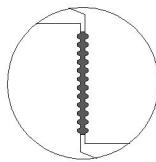
The recovery of the mortar filling is considered before performing the actual shear test. The first option is to remove and refill the connection with new mortar. However, the suitability of the bonding agent would be questionable. It provides additional bonding in the mortar-to-concrete interface of the connection. This bonding had to be broken and could damage the surface of the precast concrete surface. However, applying new bonding agent on a probably damaged precast concrete surface provides questionable test results. It has been decided not to do this type adjustment of the specimen.

Another type of repair for the specimens 3-6, 3-7 and 3-8 has been applied. The existing mortar is maintained in the connection and the open volumes at the back are filled with steel fibre reinforced mortar on a surface of new bonding agent. The result is that the mortar-to-concrete interfaces remained as before. The interface properties of the repaired specimens are equal to specimens with bonding agent without mortar filling problems.

The repair of specimens 3-6, 3-7 and 3-8 influences the shear behaviour of the connection. It turned out that bonding between old and new mortar filling in the old-to-new mortar interface breaks at point B of the diagram. The old and new mortar are seperated from that point on in the diagram. The contribution to transferring shear forces of the newer mortar terminates after point B. However, the connection continuous to transfer shear forces. The photos in the figures E.11 and E.12 display a reduced area of the profile mortar connection where mortar filling is able to transfer shear forces. A reduction of the mortar filling surface can be observed and measured from these photos. The linear reductions are 68% for specimen 3-6, 61% for specimen 3-7 and 55% with regard to a 100% filled profiled mortar connection.
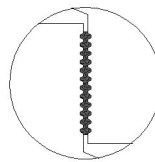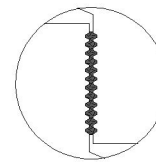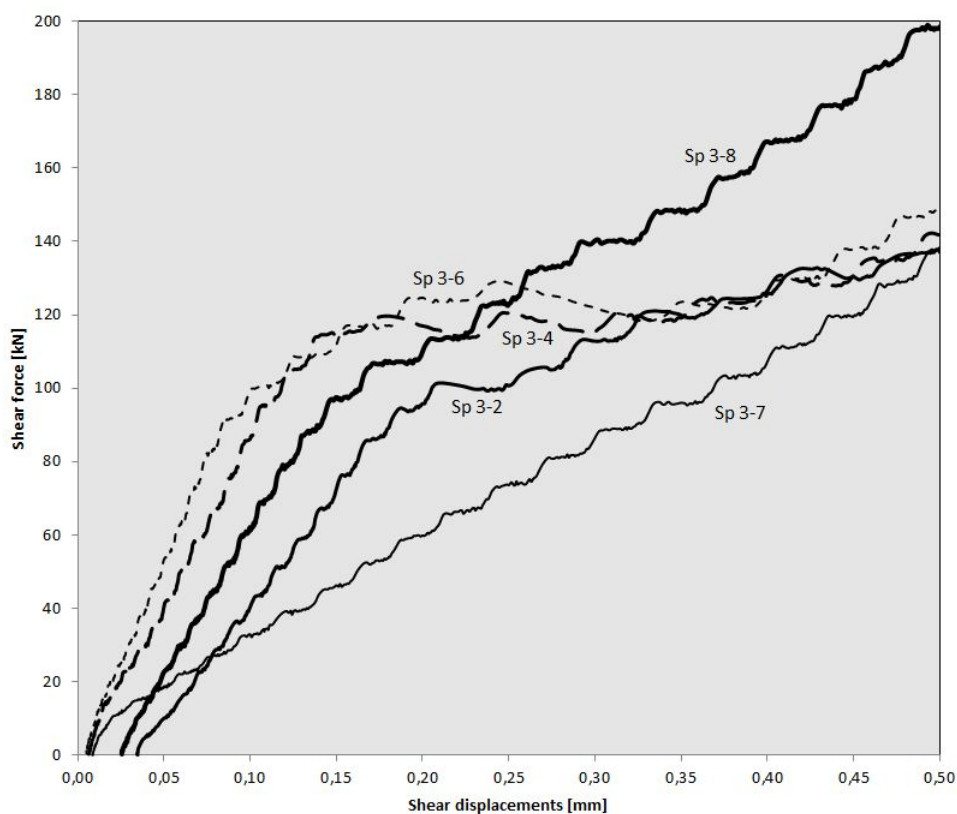
Figure E.9: Diagram for "Aligned small shear key" connection, (results for connections 3-6 till 3-8 belong to specimens with incomplete mortar filling)

Shear force $V_{F;X}$	$V_{F;B}$	$V_{F;C}$	$V_{F;D}$	$V_{F;E}$
Connection	[kN]	[kN]	[kN]	[kN]
3-2	100	–	381	≈ 304
3-4	123	115	291	≈ 271
3-6	129	118	259	≈ 291
3-7	–	–	429	≈ 500
3-8	105	–	396	≈ 416

Table E.1: Shear forces $V_{F;X}$ of Aligned small shear key connection, (results for connections 3-6 till 3-8 belong to specimens with incomplete mortar filling)

Figure E.10: Enlarged diagram for Aligned small shear key connection, (results for connections 3-6 till 3-8 belong to specimens with incomplete mortar filling)

Figure E.11: Dismantled specimen: Specimen 3-5 (top) and 3-6 (bottom)

Figure E.12: Dismantled specimen: Specimen 3-7 (top) and 3-8 (bottom)

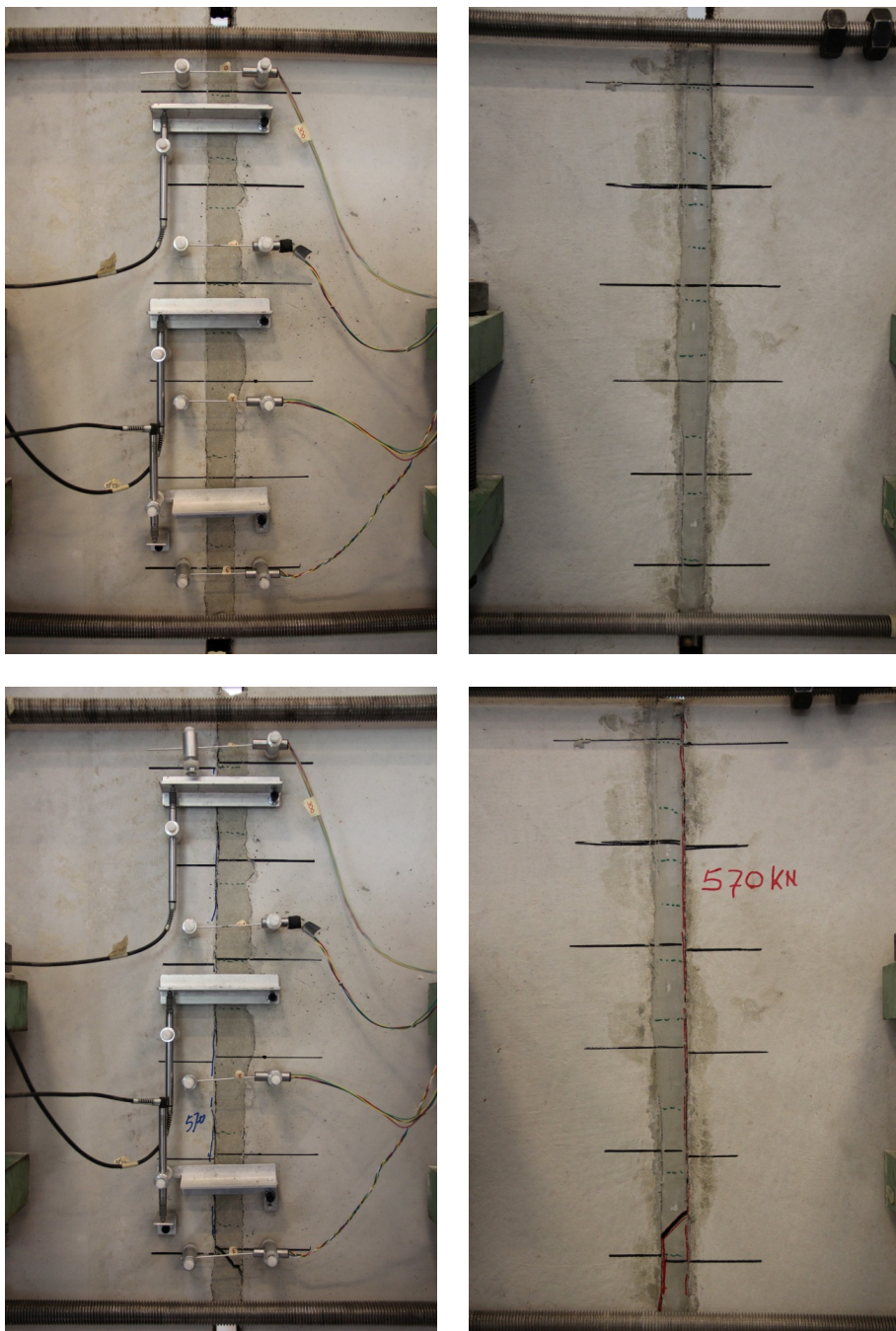# E.4 Plain waterjetted shear key connection

Figure E.13: Specimen 4-5: Crack formation during shear test

Figure E.14: Specimen 4-5: Dismantled specimen

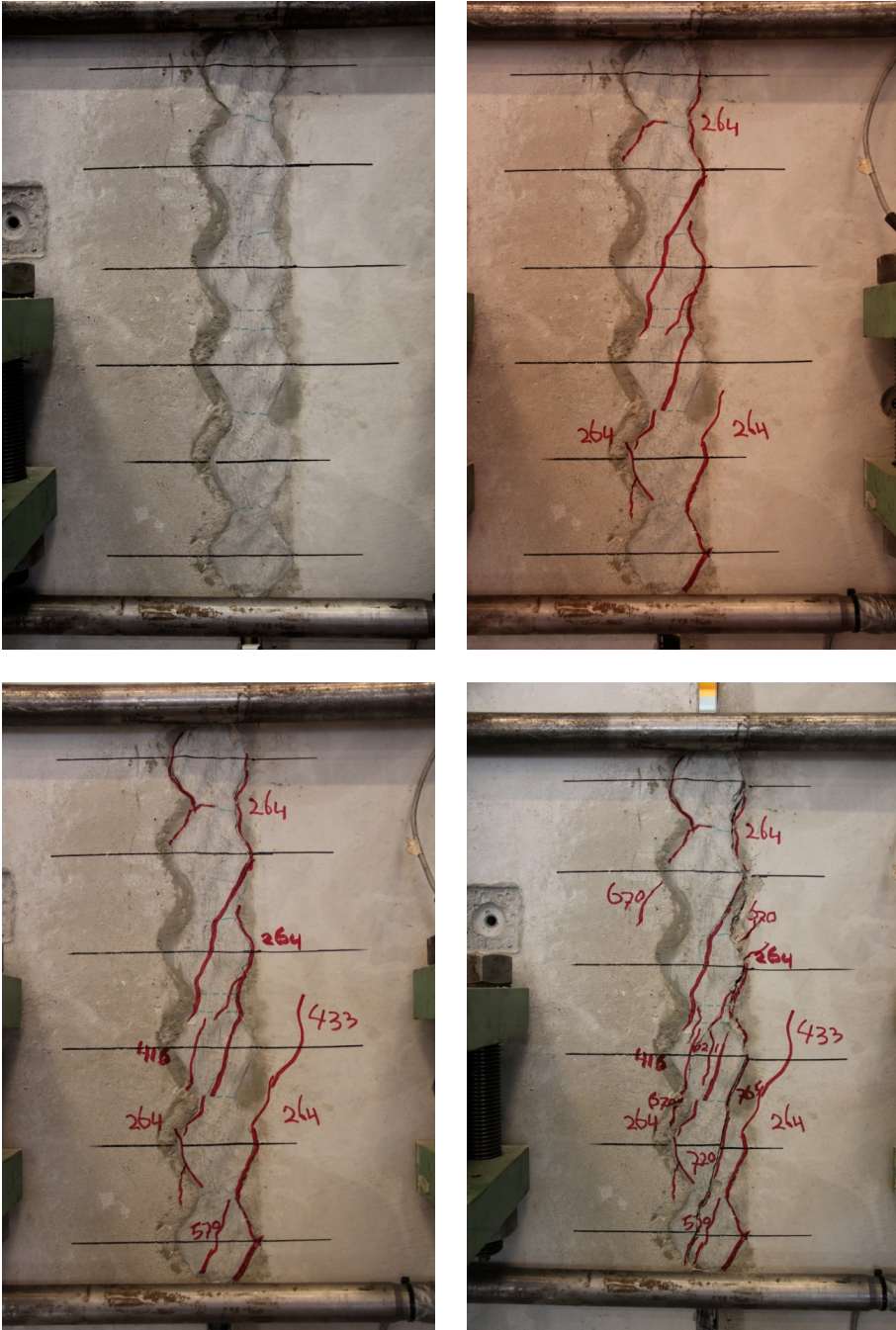## E.5   Serrated waterjetted shear key connection

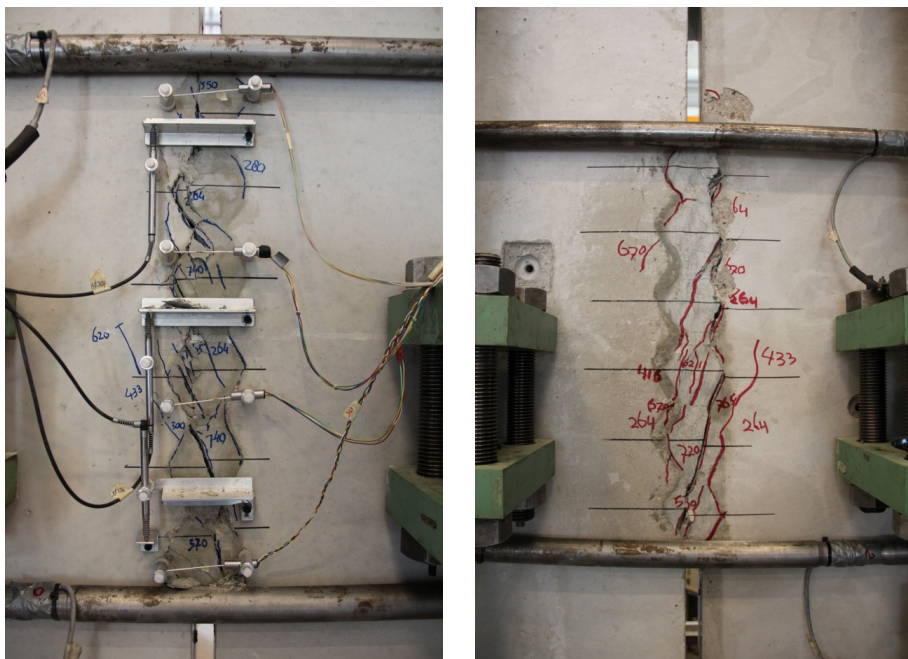Figure E.15: Specimen 5-3: Crack formation during shear test

Figure E.16: Specimen 5-3: Crack formation during shear test

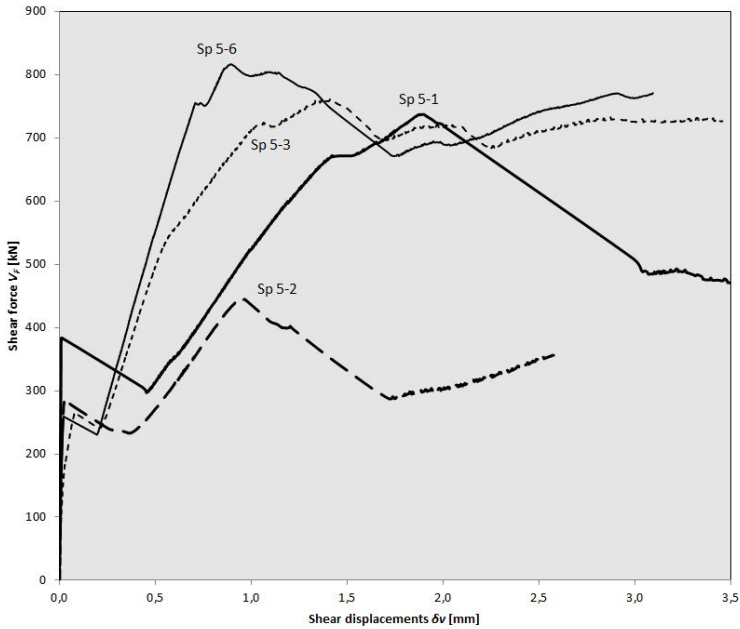Figure E.17: Specimen 5-3: Dismantled specimen

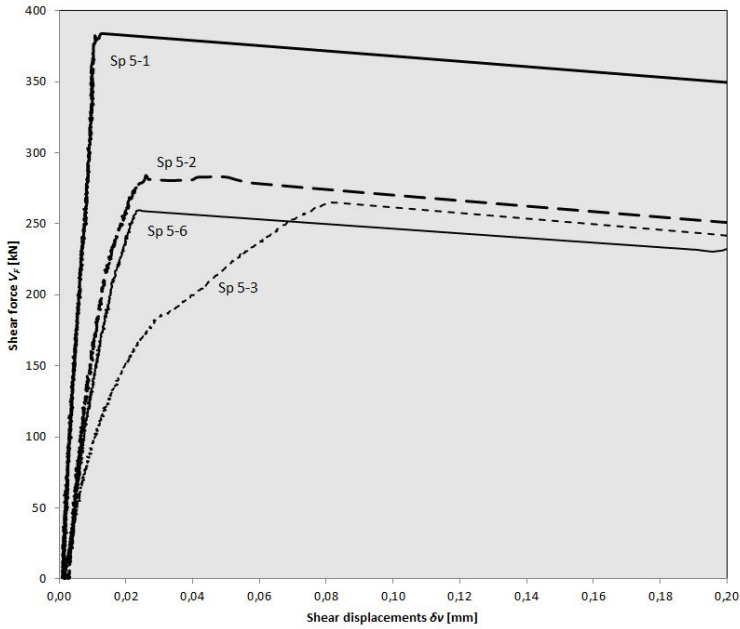Figure E.18: Diagram for Serrated waterjetted shear key connection

Figure E.19: Enlarged diagram for Serrated waterjetted shear key connection

Appendix F

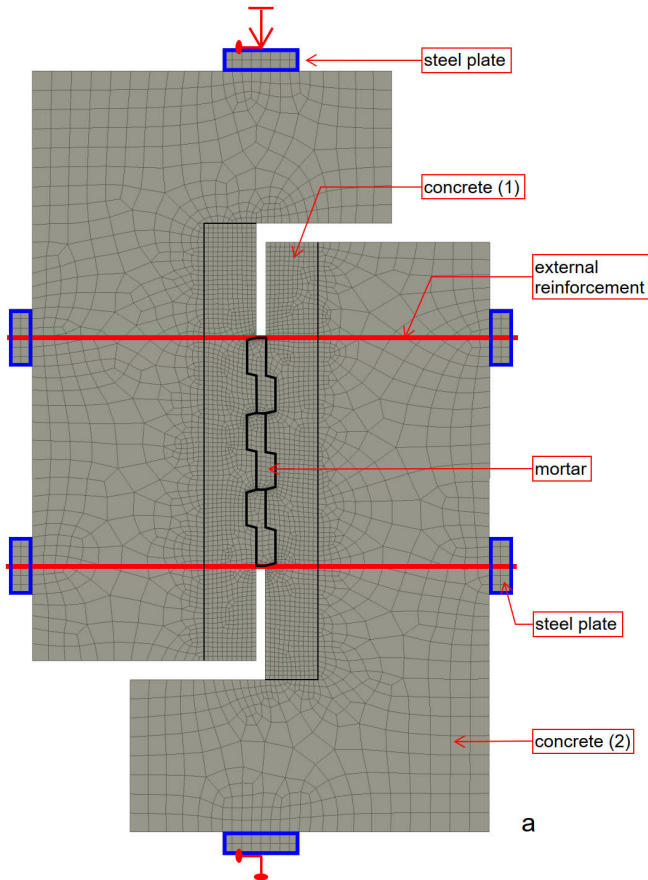# Properties numerical models

F.1   Membrane specimen model

Figure F.1: ″Membrane″ specimen model

Mortar	ATENA material model	CC3DNonLinCementitious2
	MC Strength type (Model Code)	Cubic-Mean
	MC Strength value	70 N/mm^2 (K70)
	MC Safety Format	Mean
	Youngs modulus-E	27.500 N/mm^2
	Tension strength-FC	4,15 N/mm^2
	Compression strength-FC	-60,7 N/mm^2
	Fracture energy-GF	1,53x10^{-4} MN/m
	Geometrical Non-linearity	NONLINEAR
	Idealisation	PLANE STRESS
	Element Thickness	0,2 m

Reinforced	ATENA material model	CCCombinedMaterial
Concrete (1)		CC3DNonLinCementitious2
	MC Strength type	Cubic-Mean
	MC Strength value	67,0 MPa (C55/67)
	MC Safety Format	Mean
	Youngs modulus-E	34.500 N/mm^2
	Tension strength-FC	4,07 N/mm^2
	Compression strength-FC	-57,1 N/mm^2
	Fracture energy-GF	1,52x10^{-4} MN/m
	Geometrical Non-linearity	NONLINEAR
	Idealisation	PLANE STRESS
	Element Thickness	0,2 m
		CCSmeared Reinforcement
	Youngs modulus-E	200.000 N/mm^2
	Reinforcing ratio p=As/Ac	0,01
	Yield strength YS	550 N/mm^2
	Element Thickness	0,2 m
Concrete (2)	ATENA material model	CC3DElastIsotropic
	Youngs modulus-E	34.500 MPa (table C.3)
	Geometrical Non-linearity	NONLINEAR
	Idealisation	PLANE STRESS
	Element Thickness	0,2 m
External	ATENA material model	CCReinforcement
Cable	Youngs modulus-E	Steel bars 2x2 M16: 105.000 N/mm^2
	(Calibrated)	Steel bars 2x2 M24: 40.000 N/mm^2
		Steel bars 2x2 M38: 42.500 N/mm^2
	Yield strength YS	275 N/mm^2
	Geometrical Non-linearity	LINEAR
	Geom Type	CABLE
	Active Anchor	BOTH
	Friction / Cohesion / Radius	0,0 / 0,0 MN/m / 0,0 m
Steel plates	ATENA material model	CC3DElastIsotropic
	Youngs modulus-E	210.000 N/mm^2
	Geometrical Non-linearity	NONLINEAR
	Idealisation	PLANE STRESS
	Element Thickness	0,2 m
Interfaces	ATENA material model	CC2DInterface
	Normal Stiffness-K$_{NN}$	3,00E+05
	Tangential Stiffness-K$_{TT}$	1,50E+05
	Cohesion	1,0 MPa
	Friction Coeficient	0,1
	Tension Strength-FT	0,0 N/mm^2
	Min Norm Stiffness-K$_{NN;min}$	1,00E+04
	Min Tang Stiffness-K$_{TT;min}$	1,00E+04

Table F.1: Material properties Membrane specimen models

F.2   Compression strut specimen model

	Model properties	
Compression	Finite elements	Truss (Compression only)
strut	Cross-section-A	25x200 mm^2
	Youngs modulus-E	9.000 N/mm^2
	Geometrical Non-linearity	LINEAR
Concrete	Finite elements	Membrane
	Youngs modulus-E	34.500 N/mm^2
	Geometrical Non-linearity	LINEAR
	Idealisation	PLANE STRESS
	Element Thickness	0,2 m
External Cable	Finite elements	Truss (Tension only)
	Youngs modulus-E	Steel bars 4xM16: 105.000 N/mm^2
	(Calibrated)	Steel bars 4xM24: 60.000 N/mm^2
		Steel bars 4xM38: 42.500 N/mm^2
	Geometrical Non-linearity	LINEAR
Steel plates	Finite elements	Membrane
	Youngs modulus-E	210.000 N/mm^2
	Geometrical Non-linearity	LINEAR
	Idealisation	PLANE STRESS
	Element Thickness	0,2 m

Table F.2: Material properties Compression strut specimen model

F.3 Modeling tying reinforcement in the slabs

The way the lateral dilation forces are balanced via the slabs is explained with the help of figure F.2. To exclude the transfer of shear forces via the bending capacity of the slabs, an assumed imaginary vertical crack is displayed in figure F.2a. This crack opens horizontally as soon as lateral tensile forces are transferred via the two reinforcement bars. The width of the vertical crack increases as the tensile force increases as a result of pullout behaviour of the reinforcement bars. The crack width can be equated to the pullout displacements of the embedded reinforcement in the left ($S_{end;1}$) and right ($S_{end;2}$) part of the slab.
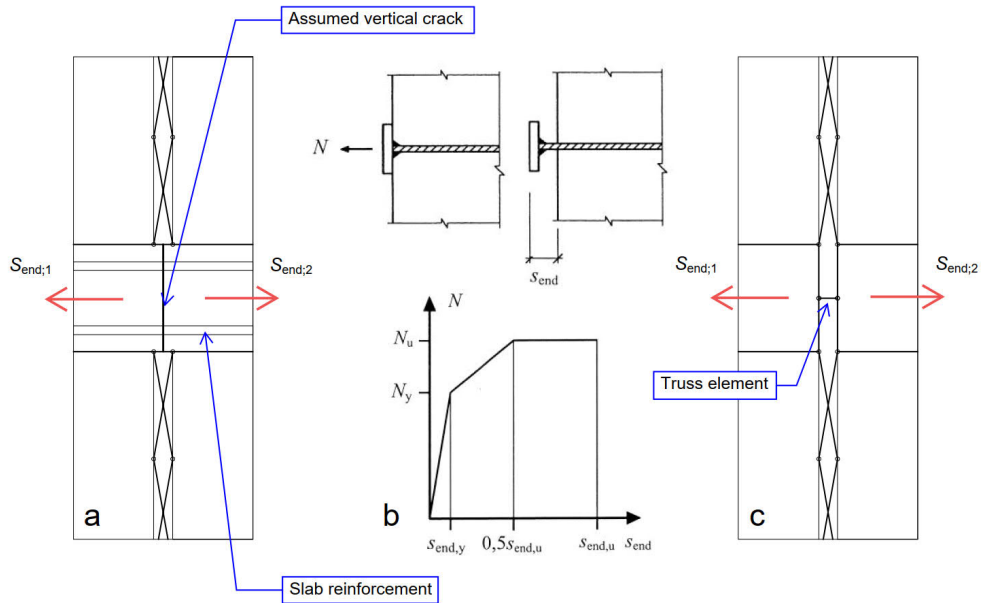

Figure F.2: Modeling tying reinforcement in the slabs

Engstrom (1992) performed pullout test on anchor bars embedded in concrete and studied the "end-slip response" as displayed in figure F.2b. The embedded anchor bar is pulled out with an end-slip (S_{end}) as a result of the imposed tensile force N. An idealised tri-linear tensile force versus end-slip relationship is proposed where N_y is defined as the yield capacity of the steel bars. According to this research, the end-slip ($S_{end,y}$) for the yield capacity N_y can be predicted by using the equation (see *fib* bulletin 43 (2008)):

$$S_{end,y} = 0,288 \left(\frac{\phi \cdot \sigma_s^2}{\tau_{b,max} \cdot E_s} \right)^{0,714} + \frac{\sigma_s}{E_s} \cdot 2\phi \qquad \text{(F.1)}$$

where:
	$S_{end,y}$	end-slip at yielding	mm
	ϕ	diameter anchor bar	mm
	σ_s	steel stress at yielding (f_y)	N/mm^2
	$\tau_{b,max}$	average bond stress for good bonding	N/mm^2
	E_s	Young modulus steel anchor bar	N/mm^2

The truss element displayed in figure F.2c has to be modeled with the tensile behaviour of the embedded reinforcement bars. The lengthening of this truss element can be modeled with Hooke's law. For the application of this law, the corresponding equation can be used:

$$E_{tr} = \sigma_{y;tr} \cdot \frac{l_{tr}}{\Delta l_{tr}} \qquad \text{(F.2)}$$

and

$$\Delta l_{tr} = S_{end;1} + S_{end;2} \qquad \text{(F.3)}$$

where:
	E_{tr}	Young modulus of truss element	N/mm^2
	$\sigma_{y;tr}$	steel stress at yielding	N/mm^2
	l_{tr}	length of truss element	mm
	Δl_{tr}	lengthening of truss element	mm
	$S_{end;1}$	pullout left part of the slab	mm
	$S_{end;2}$	pullout right part of the slab	mm

For the assumed 2ø16 mm reinforcement bars applied to the concept displayed in figure F.2, the truss element properties are determined below. The cross-sectional area of the two bars is equal to 402 mm^2 which is set for the truss element. The steel stress at yielding ($\sigma_{y;tr}$) is assumed 500 N/mm^2. The average bond stress for good bonding ($\tau_{b,max}$) is equal to 15,0 N/mm^2 according to *fib* bulletin 43 (2008). The end-slip for one reinforcement bar is calculated with equation F.1:

$$S_{end,1} = S_{end;2} = 0,288 \left(\frac{16 \cdot 500^2}{15,0 \cdot 200.000} \right)^{0,714} + \frac{500}{200.000} \cdot 2 \cdot 16 = 0,434 \, \text{mm}$$

With the help of equation F.3, the lengthening of the truss element as a result of the pullout from both parts of the slabs can be determined:

$$\Delta l_{tr} = 0,434 + 0,434 = 0,868 \, \text{mm}$$

The length of the truss elements (l_{tr}) is equal to 30 mm. The stiffness (E_{tr}) of the truss element can be obtained by equation F.2:

$$E_{tr} = 500 \cdot \frac{30}{0,868} = 17.280 \, \text{N/mm}^2$$

This calculation method can be used for acquiring the truss element properties for different sets of tying reinforcement at the location of the slabs. Table F.3 displays the values for a number of reinforcement configurations that can be used for modeling the 30 mm long truss element. This table demonstrates the increasing axial stiffness (EA_{tr}) for the truss element with more tying reinforcement at the location of the slabs.

slab reinforcement	A_{tr} [mm^2]	E_{tr} [N/mm^2]	EA_{tr}
2ø12 mm	226	21.550 N/mm^2	4,87·10^6
4ø12 mm	452	21.550 N/mm^2	9,74·10^6
2ø16 mm	402	17.280 N/mm^2	6,95·10^6
4ø16 mm	804	17.280 N/mm^2	13,89·10^6
2ø20 mm	628	14.560 N/mm^2	9,14·10^6
4ø20 mm	1256	14.560 N/mm^2	18,29·10^6

Table F.3: Cross-sectional area (A_{tr}), stiffness (E_{tr}) and axial stiffness (EA_{tr}) for different sets of reinforcement to be used for a 30 long truss element representing the tensile behaviour of the given tying reinforcement at the location of the slabs